# Interfacially Active Magnetic Nanoparticles for Efficient Oil/Water Separation from Oil-in-Water or Water-in-Oil Emulsions

by

Xiao He

A thesis submitted in partial fulfillment of the requirements for the degree of

Doctor of Philosophy

in

Materials Engineering

Department of Chemical and Materials Engineering
University of Alberta

# Abstract

The emulsions, either oil-in-water (O/W) or water-in-oil (W/O) emulsions, are inevitably formed during the industrial production processes and the daily household activities. The O/W emulsions such as crude oil-in-water emulsions or oily wastewaters generated from the industrial fields, oil spills or domestic sewages can contaminate valuable freshwater resources, harm human health, and destruct the marine ecological systems. The W/O emulsions such as water-in-crude oil emulsions from the extraction of bitumen or crude oil could cause damages to the downstream processing equipment or poison the catalyst during the refinery process due to the presence of harmful salts in the emulsified water phase. Therefore, the oil/water separation of such emulsions prior to their discharge or downstream processing is essential if not required. However, natural emulsion stabilizers such as asphaltenes in the crude oil, oil impurities in the cooking oil or detergent contained in the wastewaters could significantly enhance the stability of those undesirable emulsions, causing difficulties in desired oil/water separation. There are significant drawbacks to the current oil/water separation strategies. Researchers are therefore motivated to find more effective methods for the efficient oil/water separation.

In this thesis, a series of magnetically responsive and interfacially active nanoparticles (nanoparticles with uniform or asymmetric surface wettability) were designed and applied to the efficient oil/water separation. With their desirable interfacial activities, such nanoparticles could effectively deposit onto the oil-water interface, tagging the target oil or water droplets. With the introduction of an external magnetic field, the nanoparticle-tagged droplets could be attracted and transported to the desired locations, achieving effective oil/water separation. Characterization using FE-SEM, TEM, zeta potential measurements, thermogravimetric analysis (TGA), and Fourier-transform infrared spectroscopy (FTIR) confirmed the successful synthesis of the nanoparticles with uniform and asymmetric surface properties. The results from interfacial property measurements of interfacial tension, interfacial pressure-area ($\pi$-$A$) isotherm, crumpling ratio and coalescence time confirmed the effective deposition (anchoring) of such nanoparticles at the oil-water interface and demonstrated the satisfying interfacial activities of the synthesized nanoparticles. Based on the results of interfacial property measurements, the synthesized Janus nanoparticles exhibited superior interfacial activities including further lowering of the oil-water interfacial tension, prevention of the emulsified droplets from coalescence, and quicker and firmer deposition onto the target oil-water interface, making the oil-water interface more rigid as compared with the nanoparticles of uniform surface wettability. The synthesized nanoparticles could achieve effective oil/water separation from either O/W or W/O emulsions with the Janus nanoparticles of superior interfacial activities exhibiting higher oil/water separation efficiency. Furthermore, the synthesized nanoparticles of uniform or asymmetric surface wettability could be recycled and reused by retaining high oil/water separation efficiency without complex regeneration. With their satisfying interfacial activities, high oil/water separation efficiency and exceptional recyclability, such magnetically responsive and interfacially active nanoparticles have promising applications to efficient oil/water separation of water-in-crude oil emulsions from crude oil-related extraction processes, or oil-in-water emulsions as encountered in oil spills in the marine system and oily wastewaters from industrial production processes and daily household activities.

# Preface

This thesis is composed of a series of papers that have either been published in journals, submitted for consideration of publication, or in preparation. Below is a statement of contributions to co-authored papers contained in this thesis:

- Chapter 1. *Introduction.* This section is an original work by Xiao He.
- Chapter 2. *Literature Review.* This section is an original work by Xiao He.
- Chapter 3. *Experimental.* This section is an original work by Xiao He.
- Chapter 4. *Adsorption-Based Synthesis of Magnetically Responsive and Interfacially Active Janus Nanoparticles using Cellulosic Materials.* A version of this section has been published as **X. He**, C. Liang, Q. Liu and Z. Xu, Magnetically Responsive Janus Nanoparticles Synthesized using Cellulosic Materials for Enhanced Phase Separation in Oily Wastewaters and Water-in-crude Oil Emulsions. *Chemical Engineering Journal*, 2019, 122045. X. He was responsible for designing and performing the experiments, collecting and analyzing the data, and writing the entire paper. C. Liang helped with revising the introduction of the paper. Q. Liu and Z. Xu contributed to the discussion on experimental data and paper editing.
- Chapter 5. *Treatment of Oily Wastewaters using Magnetic Janus Nanoparticles of Asymmetric Surface Wettability.* A version of this section has been submitted as **X. He**, Q. Liu and Z. Xu, Treatment of Oily Wastewaters using Magnetic Janus Nanoparticles of Asymmetric Surface Wettability, submitted. X. He was responsible for designing and performing the experiments, collecting and analyzing the data, and writing the entire paper. Q. Liu and Z. Xu contributed to data analysis and paper editing.

- Chapter 6. *Removal of Emulsified Process Water from Crude Oil Emulsions using Magnetic Janus Nanoparticles.* A version of this section is in preparation: **X. He**, Q. Liu and Z. Xu, Removal of Emulsified Process Water from Crude Oil Emulsions using Magnetic Janus Nanoparticles, in preparation. X. He was responsible for designing and performing the experiments, collecting and analyzing the data, and writing the entire paper. Q. Liu and Z. Xu contributed to data analysis and paper editing.
- Chapter 7. Conclusions and Future Perspectives of the Work. This section is an original work by Xiao He.

Other co-authored publications not listed as thesis chapters are as follows:

- C. Liang, **X. He**, Q. Liu and Z. Xu, Adsorption-Based Synthesis of Magnetically Responsive and Interfacially Active Composite Nanoparticles for Dewatering of Water-in-Diluted Bitumen Emulsions, *Energy & Fuels,* **2018**, 32(8), pp 8078-8089. X. He was responsible for performing some of the experiments, collecting and analyzing the data and writing roughly 50% of the paper. C. Liang was equally responsible for designing and performing other parts of the experiments, analyzing the data, and writing the discussion and experimental section of the paper. Q. Liu and Z. Xu contributed to data analysis and paper editing.
- T. Yue, Z. Niu, H. Tao, **X. He**, W. Sun, Y. Hu and Z. Xu, Green Recycling of Goethite and Gypsum Residues in Hydrometallurgy with α-$Fe_3O_4$ and γ-$Fe_2O_3$ Nanoparticles: Application, Characterization, and DFT Calculation. *ACS Sustainable Chemistry & Engineering,* **2019**, 7(7), 6821-6829. X. He was responsible for collecting and analyzing the data of magnetization measurements.

- Z. Niu, R. Manica, Z. Li, **X. He**, J. Sjoblom, and Z. Xu, Interfacial properties pertinent to W/O and O/W emulsion systems prepared using polyaromatic compounds. *Colloids and Surfaces A: Physicochemical and Engineering Aspects,* **2019**, 575, 283-291. X. He was responsible for a part of experiments using Langmuir mini trough.

# Acknowledgments

I would like to express my gratitude and appreciation to:

- My supervisors, Prof. Zhenghe Xu and Prof. Qingxia Liu for their great guidance, patience, support, and supervision in my research.
- Mr. James Skwarok, Ms. Jie Ru and Ms. Ni Yang for their help in locating supplies, instrument training and technical help.
- Ms. Lisa Carreiro and Ms. Lily Laser for administrative assistance.
- All the members and friends in the group, in particular, Dr. Chen Liang, Dr. Zhenzhen Lu and Dr. Zuoli Li for their help in sharing research experience.
- NSERC Industrial Chair Program in Oil Sands Engineering for financial support.

Finally, I would like to express my deepest gratitude to my father, my mother and my girlfriend. Without their support and everlasting love, I cannot go pass through these stressful years. Because of them, I know the responsibilities I have on my shoulder. Thank you and I love you! It is to them that I dedicate this work.

# Table of Contents

# List of Tables

# List of Figures

# List of Abbreviations

| | |
|---|---|
| W/O | water-in-oil |
| O/W | oil-in-water |
| O/W/O | oil-in-water-in-oil |
| W/O/W | water-in-oil-in-water |
| cmc | critical micelle concentration |
| HLB | hydrophilic-lipophilic balance |
| SAGD | steam-assisted gravity drainage |
| TGA | thermogravimetric analysis |
| TEM | transmission electron microscope |
| SEM | scanning electron microscope |
| FE-SEM | field emission scanning electron microscope |
| QCMD | quartz crystal microbalance with dissipation monitoring |
| L-B | Langmuir-Blodgett technique |
| FTIR | Fourier-transform infrared spectroscopy |
| EO | ethylene oxide |
| PO | propylene oxide |
| CMC | sodium carboxymethyl cellulose |
| EC | ethyl cellulose |
| DS | degree substitution |
| BIT | bitumen |

# Chapter 1 Introduction

## 1.1 Background

With the increasing demand and consumption of oil in the industrial field and the daily household activities, growing volumes of oil-in-water (O/W) and water-in-oil (W/O) emulsions are generated along with the extraction processes of crude oil from nature, upgrading and refining processes and daily activities of human beings. For instance, oil spills are now considered as global challenges and the spillage of crude oil often arises from the leak of petroleum pipeline, the shipwreck of tankers during transportation and the natural oil seeps on the ruptured seafloor. The large volumes of oily wastewaters are engendered in various industrial production processes and domestic sewages. The W/O emulsions such as water-in-crude oil emulsions are often formed during the recovery of bitumen or crude oil from oil sands using warm water, followed by the dilution and centrifuging processes. Like a coin has two sides, the ever-increasing generation of such emulsions not only indicates the prosperous development of human civilization but also raises noticeable environmental issues and economic losses in the meantime. The discharge of such emulsions into the freshwater and marine systems can cause severe contaminations to the water resources. Besides, with the presence of the emulsions in the aqueous system, a thick oil slick could float on the water surface to isolate the aqueous phase from the atmosphere, leading to the oxygen-poor condition of the aqueous phase and therefore destructing the aqueous life forms. The evaporation of hydrocarbon contents from the emulsions can result in air pollution and the percolation of the oil into the soil can pollute the valuable underground water resources. In the aspect of possible economic losses, salts such as chlorides and sulfides are contained in the W/O emulsions formed in the recovery or extraction processes of crude oil contain. It should be noted that such salts are harsh hazards to the downstream processing equipment in the industrial field because they can give rise to severe corrosion to the refinery equipment and serious poisoning to the catalytical processes. Furthermore, the direct discharge of the O/W and W/O emulsions is energy wasting because crude oil and cooking oil contained in the emulsions can be used for producing renewable energy sources if appropriately treated. Therefore, to eliminate the hazards of O/W and W/O emulsions to the environment and the economy, and utilize the energy to a maximum extent, the oil/water separation of these emulsions is urgently and critically required prior to their discharge or downstream processing. As shown in **Table 1-1**, current strategies regarding the oil/water separation of the O/W and W/O emulsions include skimming,[1-5] oil sorption,[6-10] electrocoagulation,[11-17] filtration,[18-27] flotation,[28-33] biological treatment,[34-37] chemical demulsifiers,[38-43] thermal treatment,[44] electrostatic demulsification and microwave radiation.[45-51] However, there are potential drawbacks in these techniques such as the high consumption of energy, the relatively low oil/water separation efficiency, the secondary pollution from demulsifiers, and the complicated recycling and regeneration for subsequent applications. Considering these drawbacks of the technologies, it is necessary to develop a new method that generates no secondary hazards, requires low labor-intensity and shows robust applicability to treating different O/W or W/O emulsions. Recently, methods based on using magnetically responsive and interfacially active nanoparticles have attracted considerable interests due to its less labor-intensity, high output and efficiency, low economic consumption and promising recyclability. The surfaces of these nanoparticles are modified uniformly by different functional materials such as polyvinylpyrrolidone,[52-53] PDMAEMA,[54] polyelectrolytes,[55] ethyl cellulose (EC),[56-58] etc. With their satisfying interfacial activities, such nanoparticles can anchor at the oil-water interfaces and then the nanoparticle-tagged droplets can be attracted and transported to the desired locations under the introduced magnetic field, achieving satisfactory oil/water separation.

In reality, however, the stability of the O/W and W/O emulsions under realistic conditions is often enhanced by other interfacially active components such as asphaltenes in crude oils, and natural and/or synthetic surfactants in the emulsion systems. As a result, the enhanced stability of the emulsions makes it harder for the nanoparticles of uniform surface modification to anchor securely at the oil-water interface. Moreover, the insufficient interfacial activities of the nanoparticles could cause their easy desorption from the oil-water interface under the external magnetic field, leading to inefficient control of the emulsion droplets and hence ineffective oil/water separation. Therefore, nanoparticles of stronger interfacial activities are highly desirable in oil/water separation of the O/W and W/O emulsions. Janus nanoparticles of asymmetric surface properties have attracted public interests due to their stronger interfacial activities. With part of nanoparticle surfaces being hydrophilic and another part being hydrophobic, the Janus nanoparticles of asymmetric surface properties show better interfacial behaviors, including lower oil-water interfacial tension, firmer anchoring at the oil-water interface and higher required desorption energy from the interface as compared with the nanoparticles of uniform surface wettability. With their superior interfacial activities, such Janus nanoparticles can more securely tag the emulsified emulsion droplets, leading to better control of the Janus nanoparticle-tagged emulsion droplets under the external magnetic field and therefore more promising oil/water separation than the nanoparticles of uniform surface wettability. However, the Janus nanoparticles reported for oil/water separation of O/W emulsions are not effective to deal with the W/O emulsions such as water-in-crude oil emulsions due to the lack of functional materials for effectively breaking the asphaltene film which is one of main contributions to the incredible stability of the water-in-crude oil emulsions. Furthermore, the materials used in synthesizing the magnetically responsive and interfacially active nanoparticles are not biodegradable which could cause secondary pollution to the emulsions. Consequently, it is necessary to synthesize a new series of Janus nanoparticles using environmentally friendly and biodegradable materials for the effective oil/water separation of the W/O and O/W emulsions.

**Table 1-1.** Current technologies for treating O/W or W/O emulsions.

| Technology | Advantages | Disadvantages | References |
|---|---|---|---|
| Skimming | Large scaled-up treatment | Time-consuming;<br>Energy-consuming;<br>Low oil removing efficiency;<br>High cost | 1-5 |
| Oil sorption | Easy operation;<br>Low cost;<br>High oil removing efficiency | Low reusability;<br>Possible secondary hazards | 6-10 |
| Flotation | Quick oil removal;<br>Production of fewer sludges;<br>High separation Efficiency | Manufacturing and repairing problems of the device;<br>High energy consumption | 11-17 |
| Membrane filtration | Little pollution;<br>Low consumption of energy;<br>High separation efficiency | Easy fouling;<br>Thermal instability;<br>Easy corrosion;<br>No scaled-up treatment | 18-27 |
| Coagulation | High oil/water separation;<br>No secondary hazards;<br>Environmental friendliness;<br>Quick oil/water separation | Low selection;<br>Requirement of conductive wastewater;<br>High energy consumption;<br>Manufacturing and repairing problems of device | 28-33 |
| Biological treatment | Little pollution | Long-period treatment | 34-37 |
| Thermal treatment | High generality | High energy consumption | 44, 51 |
| Chemical demulsifier | Low consumption of energy;<br>High dewatering efficiency;<br>Low labor-intensity | Unrecyclability;<br>Generation of secondary hazards;<br>Slow settling of water droplets | 38-43 |
| Electrostatic demulsification | No secondary hazards | Formation of burdensome water droplets | 48-51 |
| Microwave radiation | Relatively less consumption of energy;<br>Good controllability;<br>High heating efficiency;<br>No secondary hazards | Strict requirements for the salt concentrations and conductivity of W/O emulsions | 45-47, 51 |

## 1.2 Objectives and Thesis Scope

The main objectives of the work are as follows:

1) To synthesize magnetic Janus nanoparticles using environmentally friendly and biodegradable materials for the efficient and effective oil/water separation of the W/O and O/W emulsions.

2) To compare the interfacial activities between the nanoparticles of Janus and uniform surface wettabilities in the O/W and W/O emulsion systems.

3) To compare the oil/water separation efficiencies of the nanoparticles of Janus and uniform surface wettabilities for treating O/W and W/O emulsions.

The first part of the thesis focuses on the synthesis and characterization of magnetic Janus nanoparticles (M-Janus nanoparticles) synthesized from cellulosic materials. In this part, quartz crystal microbalance with dissipation monitoring (QCM-D) was applied to measure the interaction between the cellulosic materials (ethyl cellulose and carboxymethyl cellulose) between the bare iron oxide nanoparticle surfaces, which was the focus of synthesizing M-Janus nanoparticles. Zeta potential measurements and thermogravimetric analysis (TGA) were used to confirm the adsorption of cellulosic materials on the M-Janus nanoparticle surfaces. Characterization methods such as Fourier-transform infrared spectroscopy (FTIR), FE-SEM and TEM were applied to confirm the synthesis of M-Janus nanoparticles. The results from interfacial tension measurements, interfacial pressure-area ($\pi$-$A$) isotherms measurements, coalescence time and crumpling ratio measurements showed stronger interfacial activities of the synthesized M-Janus nanoparticles of asymmetric surface wettabilities at the clean toluene-water interface than the nanoparticles of uniform surface wettability (M-CMC-EC nanoparticles) reported previously.

In the second part, a comparison between the interfacial activities of M-Janus nanoparticles and M-CMC-EC nanoparticles in different oily wastewater systems was comprehensively investigated. Despite the other interfacially components such as asphaltenes, natural and/or synthetic surfactants and remaining detergents in the studied oily wastewaters, the M-Janus nanoparticles could still anchor at the oil-water interface and exhibited better interfacial behaviors such as lower oil-water interfacial tension and firmer deposition at the oil-water interface than M-CMC-EC nanoparticles. The M-Janus nanoparticles were capable of removing/recovering waste oil from different oily wastewaters. The oil recovered as such was of high quality (water content: ~1.6 wt%) for subsequent refining. Moreover, the M-Janus nanoparticles could be recycled and reused at a high oil removal/recovery efficiency in the subsequent applications without complex regeneration. The results show that M-Janus nanoparticles of asymmetric surface properties are more promising candidates for oil remediation from various types of oily wastewaters than M-CMC-EC nanoparticles of uniform surface properties.

In the last part, the M-Janus and M-CMC-EC nanoparticles were applied to the dewatering of the process water-in-crude oil emulsions. The M-Janus nanoparticles of asymmetric surface wettabilities showed better interfacial performances at the diluted bitumen-process water interface than M-CMC-EC nanoparticles of uniform surface wettability. With the addition of 0.75 wt% M-Janus nanoparticles, around 90 % of process water was removed from the diluted bitumen emulsions, in contrast to 80 % of water removal obtained with the addition of M-CMC-EC nanoparticles at the same dosage. The M-Janus nanoparticles showed robust dewatering ability to the diluted bitumen emulsions of different initial water contents (2.5 wt% ~ 20 wt%). After dewatering the diluted bitumen emulsion, the M-Janus nanoparticles could be recycled and reused for the subsequent dewatering process with facile regeneration. Besides, the recycled M-Janus nanoparticles could still retain high dewatering efficiency and excellent interfacial activities at least for six cycles. The superior interfacial activities, high dewatering efficiency, exceptional recyclability are contributed to the promising potential of M-Janus nanoparticles for dewatering efficiently the process water-in-diluted bitumen emulsions.

### 1.3 Merit and Impact of Research

The major contribution of this thesis research to the fields of science and engineering is the design and synthesis of novel magnetic Janus nanoparticle using cellulosic materials for effective and efficient oil/water separation of W/O and O/W emulsions. The two kinds of cellulosic materials of contrasting wettability were coated directly onto the opposite sides of the Janus nanoparticle surfaces without complex chemical reaction, achieving facile synthesis and generating no secondary hazards. By applying various characterization methods such as interfacial tension measurements, interfacial pressure-area isotherms measurements, and coalescence time measurements, the interfacial behaviors between the Janus nanoparticles and nanoparticles of uniform surface properties in the O/W and W/O emulsions were comprehensively investigated, improving our understanding of the differences between the interfacial activities of the Janus nanoparticles and nanoparticles of uniform surface wettability at various oil-water interfaces. The Janus nanoparticles designed in this study could be produced on a large scale, showing the potential of their application to the oil/water separation in the industrial field. With their excellent interfacial activities, high oil/water separating efficiency, good recyclability and facile regeneration for subsequent applications, the nanoparticles of Janus nature are more promising candidates for treating the oily wastewaters from industrial processes and domestic sewages, the oil spills in marine systems and the water-in-crude oil emulsions in petroleum-related industries than the nanoparticles of uniform surface modification.

## 1.4 Thesis Structure

This thesis has been structured as a compilation of papers. Chapters 4-6 are research papers either published, submitted to scientific journals or in preparation. The key content of each chapter is shown as follows:

**Chapter 1** provides the overall introduction of the thesis, including the background, objectives and thesis scope.

**Chapter 2** presents a comprehensive literature review on the current experimental and theoretical synthesis of interfacially active nanoparticles and their applications to the O/W and W/O emulsions.

**Chapter 3** introduces an overview of materials, instruments and experimental protocols used in the current investigates.

**Chapter 4** illustrates the adsorption-based synthesis of magnetically responsive and interfacially active Janus nanoparticles using cellulosic materials. The concept and detailed synthesis procedures of M-Janus nanoparticles were described, and characterization of the physicochemical properties and interfacial activities of the synthesized Janus nanoparticles were comprehensively investigated. A version of this chapter has been published in:

X. He, C. Liang, Q. Liu and Z. Xu, Magnetically Responsive Janus Nanoparticles Synthesized using Cellulosic Materials for Enhanced Phase Separation in Oily Wastewaters and Water-in-crude Oil Emulsions. *Chemical Engineering Journal*, 2019, 122045.

**Chapter 5** discusses the comparison between the interfacial properties and application of M-Janus nanoparticles and M-CMC-EC nanoparticles in different oily wastewaters. A thorough comparison between the interfacial behaviors and oil/water separating performance of the nanoparticles of

Janus and uniform surface wettability in mimetically realistic oily wastewater systems was comprehensively investigated. A version of this chapter has been submitted as:

X. He, Q. Liu and Z. Xu, Treatment of Oily Wastewaters using Magnetic Janus Nanoparticles of Asymmetric Surface Wettability.

**Chapter 6** presents the application of M-Janus nanoparticles and M-CMC-EC nanoparticles to dewatering the water-in-crude oil emulsions. A comparison between the interfacial activities and the dewatering efficiency of M-Janus nanoparticles and M-CMC-EC nanoparticles in the process water-in-crude oil emulsions were thoroughly investigated. A version of this chapter has been prepared as:

X. He, Q. Liu and Z. Xu, Removal of Emulsified Process Water from Crude Oil Emulsions using Magnetic Janus nanoparticles, in preparation.

# Chapter 2 Literature Review

## 2.1 Concept of Emulsion

An emulsion is traditionally defined as a dispersed, opaque, heterogeneous system composed of two immiscible liquid phases (usually ‘oil’ and ‘water’) with one phase being referred to as the emulsified phase and another as the continuous phase.[59] Typically, to classify the emulsions by the emulsified and continuous phase, most emulsions can be divided into two types: (1) water-in-oil (W/O) emulsion where oil droplets well dispersed in continuous aqueous phase and (2) oil-in-water (O/W) emulsion where emulsified water droplets are dispersed in continuous oil phase.[60] The oil-in-water emulsions and water-in-oil emulsions can be distinguished using the dilution method. The W/O emulsion can be easily diluted and dispersed in the added oil phase, while an O/W emulsion will form large blobs with the addition of excess oil.

In addition to the two basic types of emulsion (W/O emulsion and O/W emulsion), there are particular dispersion systems such as (1) foam (air-in-water emulsion), (2) “Dry water” (water-in-air emulsion), (3) W/O/W (water-in-oil-in-water) complex multiple emulsion and (4) O/W/O (oil-in-water-in-oil) complex multiple emulsion, which are not limited to liquid (organic and aqueous) phases or simple emulsion structures.[61]

As for the size of emulsion droplets, emulsified droplet size generally varies from 1 μm to over 10 μm, which is larger than most colloidal particles on the upper end. Noteworthy, some emulsions can have even smaller emulsified droplet size, approximately 1 to 100 nm, and these emulsions are referred to as micro-emulsions, which are isotropic and thermodynamically stable systems.

## 2.2 Emulsion Stability

Generally, it is thermodynamically unfavorable for the formation of an emulsion because a large increase of interfacial areas would be generated along with the emulsification process, leading to an increase in total system energy. The change of Gibbs free energy for the formation of an emulsion is illustrated in **Equation 2-1**:[62]

$$\Delta G = \gamma \Delta A - T \Delta S \qquad (2\text{-}1)$$

where $\Delta G$ is the Gibbs free energy change from a system with two separated phases to an emulsion system, $\gamma$ is the interfacial tension of the interface between two immiscible liquids, $\Delta A$ is the increased interfacial area, $T$ is the temperature in Kelvin of the system and $\Delta S$ the change of system entropy.

In most cases, $\gamma \Delta A >> T \Delta S$, which means that the total Gibbs free energy change of the system is always positive, and the formation of an emulsion from a phase-separated system is nonspontaneous and thermodynamically unstable. According to the equation (1), there are two methods to favor the formation of emulsion: (1) lower the interfacial tension between the two immiscible liquids and (2) increase the entropy of the emulsion. The increase in configurational entropy can be achieved by the dilution effect and resulting dispersion of the globules which is commonly seen in the formation of the microemulsion.[63] For lowering the interfacial tension, the most common method is the addition of the stabilizers into the emulsion. The emulsifiers are interfacially active and can be adsorbed onto the interface between two immiscible phases. They can dramatically decrease the interfacial tension of the interface, and thus remarkably slow down or even stop the phase separation process. An effective emulsifier can create a barrier between the emulsified droplets to prevent them from coagulation, flocculation or coalescence. In summary, there are typically two kinds of emulsifiers in stabilizing emulsions: surfactant and solid particles, which we will discuss in detail below.

### 2.2.1 Stabilization of Emulsions by Surfactants

The term "surfactant" comes from the words "surface-active agent" and refers to the chemicals which are interfacially active at air-water interfaces or oil-water interfaces.[60] To anchor effectively at the liquid-liquid interface, the surfactants are required to be intrinsically amphiphilic. In most cases, surfactants are composed of a water-loving (hydrophilic) head and a water-hating (hydrophobic) long tail. A typical structure of the amphiphilic surfactant (sodium dodecyl sulfate) is shown in **Figure 2-1**. The amphiphilic surfactants have affinities for both of the aqueous phase and oil phase, and therefore they are partially soluble in water and organic solvent. Depending on the intrinsic nature of the water-loving head, there are three kinds of surfactants: anionic, cationic and non-ionic, according to the charges on the active part of the surfactants. In the presence of amphiphilic surfactants at the interface, the interfacial tension of the air-water interface or oil-water interface could decrease significantly, leading to a favorable formation of emulsios.

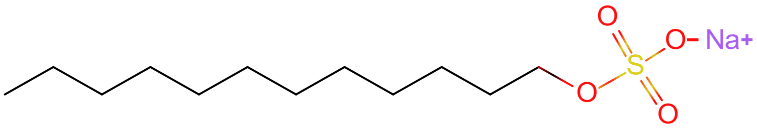

**Figure 2-1.** Typical structure of an amphiphilic surfactant. Sodium dodecyl sulfate molecule is used as an example.[60]

Although all the amphiphilic surfactants are composed of a hydrophilic head and a hydrophobic tail, they can only stabilize certain categories of emulsions according to their intrinsic amphiphilicity, which can be described as an empirical scale of hydrophilic-lipophilic balance (HLB).[60] HLB is a value which can define the degree of hydrophobicity or hydrophilicity of the surfactant. High HLB value means that the hydrophilic polar head prevails the hydrophobic tail, while low HLB indicates a more hydrophobic property of the surfactant. HLB can be calculated from the ratio of the surfactant solubility in water and oil (partition coefficient) or calculated from the **Equation 2-2** using hydrophilic and hydrophobic (lipophilic) group number:

$$\text{HLB}=7 + \Sigma\ (\text{hydrophilic group members}) + \Sigma\ (\text{lipophilic group numbers}) \qquad (2\text{-}2)$$

For emulsions stabilized by surfactants, the emulsified droplets are always prevented from coalescence, contact or flocculation by the electrostatic barrier and steric barrier created by the adsorbed surfactant at the liquid-liquid interface. For the amphiphilic ionic surfactants with proper HLB value, they can effectively stabilize the emulsions with the electrostatic repulsive force. Like anionic surfactants such as sodium dodecyl sulfate (SDS), sodium oleate, and sodium bis (2-ethylhexyl) sulfosuccinate or the cationic surfactants such as alkylamine hydrochloride and alkyl trimethyl ammonium salts, with the polar head pointing out, they can generate the surface charges on the emulsified droplet surfaces. As for the water-in-oil (W/O) emulsions, the amphiphilic surfactants would be adsorbed at the water/oil interface with their hydrophobic hydrocarbon tail facing the continuous organic phase and the hydrophilic polar head immersing in the water phase, charging the emulsion droplets and generating the electrostatic repulsion. For the case of oil-in-water (O/W) emulsions, the orientation of the surfactants is reversed when compared with the situation in W/O emulsions. With the facing-outward charged hydrophilic polar head, the emulsion droplets are prevented from coalescence with electrostatic repulsive forces generated by the emulsion droplet surface charges. According to the calculated number of an amphiphilic surfactant, we can know the exact emulsion type that the surfactant is favorable of forming. The relation between the different HLB values and their corresponding emulsion types are listed in **Table 2-1**.

**Table 2-1.** HLB values of surfactants and their corresponding applications.[60]

| HLB Range | Application | Solubility in Water | Example |
|---|---|---|---|
| 1 - 4 | N/A | Insoluble | Fatty Alcohols |
| 3 - 6 | W/O Emulsifiers | Poorly Soluble | Fatty Acids |
| 7 - 9 | Hydrotropes<br>Demulsifiers | Unstably Dispersed | Span 20 (sorbitan monolaurate) |
| 8 - 18 | O/W Emulsifiers | Stable | Tween 60 (polyoxyethylene sorbitan oleate) |
| > 15 | Wetting Agents, Detergents | Clear Solution | Soaps (HLB ~ 20)<br>SDS (HLB = 40) |

### 2.2.2 Stabilization of Emulsions by Particles

Without the stabilization of emulsions by amphiphilic surfactants, the emulsions can also be stabilized by solid particles. In this case, the solid particles can act as "solid surfactant" and anchor securely at the emulsion droplet surfaces.[64] The mechanism of emulsion stabilization enhanced by the small solid particles results from the steric barrier created by the firmly-anchored particle at the emulsion droplet surface, preventing a close droplet-to-droplet contact. It is worth noting that in order to locate at the oil-water interface, the particles cannot be completely wetted by either phase of the emulsion. Otherwise, the emulsions would end up with destabilization.

Typically, the emulsion stabilized by the solid particles only is called "Pickering" emulsion. The term "Pickering" was named after S.U. Pickering, who discovered the specific emulsions stabilized by the solid particles other than amphiphilic surfactant.[65] The type of Pickering emulsions (O/W or W/O) is determined by the wettability of the solid stabilizers partitioned at the oil/water interface.

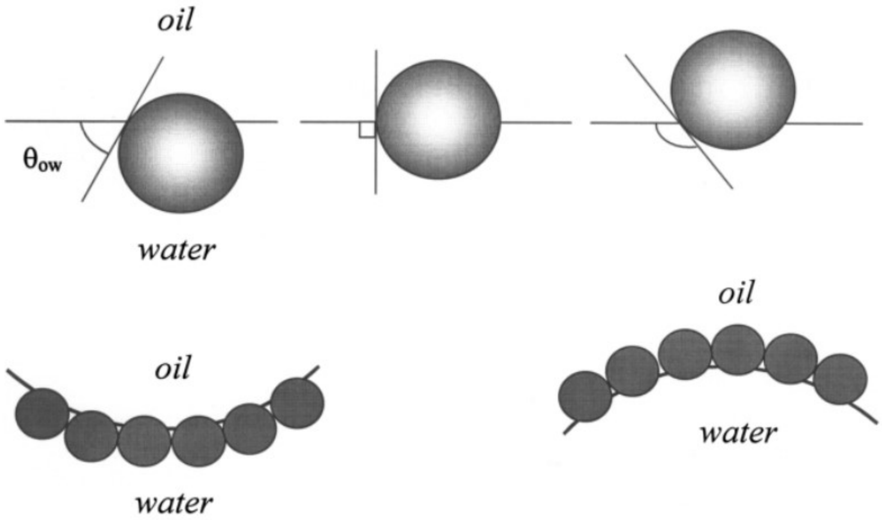

**Figure 2-2.** Upper row shows three particles with different surface wettabilities (from left to right: more hydrophilic, amphiphilic, more hydrophobic), lower row shows O/W Pickering emulsions stabilized by more hydrophilic particles and W/O Pickering emulsions stabilized by more hydrophobic particles.[66]

The wettability of particle surfaces can be determined by the many factors such as surface roughness, the zeta potential of the particles, and, most importantly, the hydrophilicity/hydrophobicity of the particle surfaces. As shown in **Figure 2-2**, by controlling the contact angle of the particles at the oil/water interface, the most part of the particles would be immersed at either water phase (contact angle < 90º) or oil phase (contact angle > 90º), resulting in O/W or W/O Pickering emulsions.

The most significant difference in the mechanism of solid particles and surfactants in stabilizing emulsions is the origin of their energy source. The surfactant can lower the interfacial tension of the oil/water interface after its adsorption, as described by Gibbs' law. While the solid particles can lower the total free energy of the system by locating at the interface. During the adsorbing process of particles onto the water/oil interface, part of water/oil was replaced by the occupation of the solid particles, resulting in the loss of energy. As particular emulsion systems, Pickering emulsions with particles adsorbed at the interface of two immiscible phases show remarkable stability, mostly due to the steric barrier created between the emulsified droplets and the high desorption energy required for the particles detaching from the interface.[67-69] The high desorption energy of the particle partitioned at the oil/water interface contributes mainly to the secure partition of the particles at the interface. The total energy $E$ required to remove the particle from the interface is given by **Equation 2-3**:[64]

$$E = \pi r^2 \Upsilon_{o/w} \, ( 1 \, \pm \cos \theta)^2 \tag{2-3}$$

where r represents the radius of the particles adsorbed at the oil/water interface, $\Upsilon_{o/w}$ is the interfacial tension of the pure water and pure oil, $\theta$ is the contact angle of the particle formed at the oil/water interface. The $\pm$ sign represents the particles detaching from the interface into the oil phase (positive, "+") or aqueous phase (negative, "-"). As shown in **Figure 2-3**, when $\theta$ approaches 0º or 180º, the particle is completely wetted or unwetted, which means that the particle cannot be adsorbed at the oil-water interface. For $\theta$ < 90º (hydrophilic), the particles are more eager to go to the aqueous phase and for $\theta$ > 90º (hydrophobic), the particles more like going to the organic phase. The $E$ reaches maximum value when $\theta$ equals 90º, which is three orders of magnitude higher than the desorption energy of the surfactant when the particle has a radius of 10 nm.[70] Once the particles requires high energy to desorb from the oil-water interface, such particles can be seen irreversibly adsorbed at the oil/water interface, resulting in forming stable Pickering emulsions.

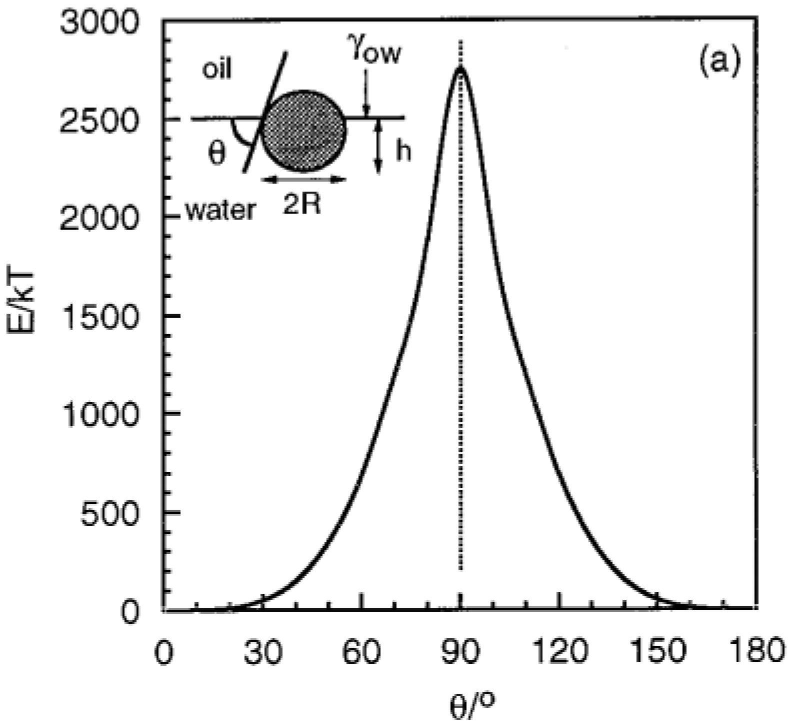

**Figure 2-3.** Energy *E* required for a solid spherical particle with a radius of 10 nm and a contact angle $\theta$ to desorb from a planar oil/water interface.[68]

The adsorbed particle layer at the emulsion droplet surfaces mainly acts against coalescence. Such a particle layer is rigid and has excellent mechanical strength, which comes from the aggregation of solid particles and the interactions between the particles. When two emulsion droplets get closer, the emulsified phase would not contact due to the protection of the adsorbed particle layer and therefore against coalescence. The solid particles also contribute to preventing emulsion droplets from coagulation. As an example, when the charged particles are adsorbed at emulsion droplet surfaces, such particle layer can generate obvious electrostatic repulsion between the emulsion droplets as ionic surfactants do, leading to less chance for the emulsion droplets contacting with each other.[71-72] Also, the formation of "bridge" between the particle-stabilized emulsion droplets keeps the emulsified droplets apart and prevents them from coalescence as well.[73-74]

### 2.2.3 Interactions between Emulsion Droplets

The interactions between emulsions droplets play essential roles in many phenomena and practical applications such as stability of emulsions, mineral processing, oil recovery from oily wastewaters, utilization of detergents, etc. There are several kinds of forces such as van der Waals force, electrostatic force and steric force that contribute to the synergic interactions between the emulsion droplets.

#### 2.2.3.1 Van Der Waals Force

Generally, the van der Waals force is a kind of attractive force between atoms or molecules, and there are three types: (1) dipole-dipole (Keesom) interaction, (2) dipole-induced dipole (Debye) interaction and (3) dispersive (London) interaction.[75] It is worth noting that the Debye and Keesom interaction forces are related to directions of atoms or molecules, which means that such attractions could be canceled due to the difference between the directions of the dipoles. As for London interactions, it results from the random fluctuations of the electrons in the molecules (atoms).[76] With the electron fluctuations, a temporary dipole is generated in a molecule and it would induce another dipole in another molecule, leading to an overall attraction between these two molecules.

For two spherical emulsion droplets with the same radius a at a separation distance H, the van der Waals attraction energy $V_{\text{s-s}}$ can be calculated by **Equation 2-4**:[60]

$$V_{\text{s-s}} = \frac{-\mathrm{Aa}}{12\mathrm{H}} \tag{2-4}$$

where A is the effective Hamaker constant and its value depends on the London dispersion constant β and the number of atoms per unit volume $q$. With such an attractive interaction, the flocculation of emulsion droplets is super-fast if no repulsions forces exist. To against the flocculation and keep the stability of the emulsion, it is necessary to have repulsive interactions between the emulsion droplets.

### 2.2.3.2 Electrostatic Force

When ionic surfactants are adsorbed at emulsions droplets surfaces, the surfactant-stabilized emulsion droplets can gain surface charges, and we should take into account the electrostatic force generated between the charged emulsion droplets. When two charged emulsion droplets approach each other, their electric double layers would overlap with each other, leading to electrostatic interaction. The strength of their electrostatic interactions is related to their surface potential, which decreases first linearly to the stern potential and then exponentially with the increase of their distance $H$. The potential energy of the electrostatic interactions between two charged spherical emulsion droplets can be expressed as **Equation 2-5**:[60]

$$V_{EDL} = \frac{64n_0KT}{\kappa^2} tanh^2(\frac{ze\psi_0}{4KT})\exp(-\kappa H) \tag{2-5}$$

where $\psi_0$ is the surface potential of the emulsion droplet, $\kappa$ is a constant depending on the composition of the electrolyte and ambient temperature. For the cases of emulsions droplets with small surface potentials ($\psi_0 < 25\ mV$), their surface charge $\sigma_0$ can be expressed as $\sigma_0 = \varepsilon\kappa\psi_0$ and we can substitute such $\sigma_0$ into **Equation 2-5** and get the potential energy of the electrostatic interactions between two emulsion droplets of radius a with low surface charge density as **Equation 2-6**:[60]

$$V_{EDL} = \frac{2\pi\sigma^2 a}{\kappa^2\varepsilon}\exp(-\kappa H) \tag{2-6}$$

Based on the DLVO theory, the energy of an emulsion system $E_{total}$ is the net worth of the attractive can der Waals energy $E_{vdW}$ and the energy $E_{DLVO}$ of the repulsive force generated by the overlapped electric double layers of the emulsion droplets (**Equation 2-7**):[60]

$$E_{total} = E_{vdW} + E_{EDL} = -\frac{A}{12H}a + \frac{64n_0KT}{\kappa^2}tanh^2(\frac{ze\psi_0}{4KT})\exp(-\kappa H) \qquad (2\text{-}7)$$

The $E_{vdW}$ is always negative due to the attractive van der Waals force and the $E_{EDL}$ is usually positive because of the repulsive electrostatic forces. The total energy $E_{total}$ varies depending on the distance between the two charged emulsion droplets. As an example, the change of total energy for two spherical emulsion droplets of surface potential to be 15 mV in 0.001 M KCL solution at 25 °C is illustrated in **Figure 2-4**.

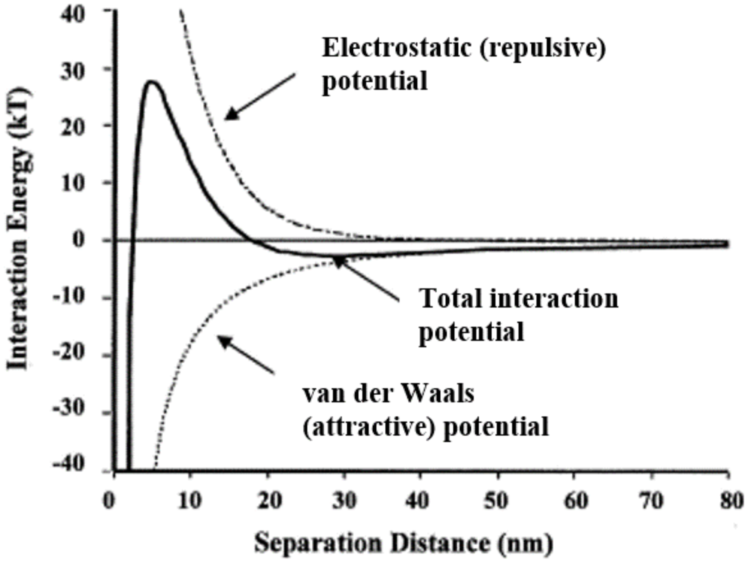

**Figure 2-4**. Schematic illustration of interaction energy of two emulsion droplets versus distance.[77]

We can know that at large distances, the total interaction for these two emulsion droplets is negative. Such a phenomenon could lead to an overall attractive force between the two charged emulsion droplets. The interaction energy would decrease continuously until reaching a minimum value of ~ -1.5 $\kappa$T at a distance of ~ 45 nm. If two droplets want to contact with each other, they have to surpass the energy barrier shown as a peak in **Figure 2-4**. Once surpass the barrier, the emulsion droplets could form flocs and aggregates, leading to the subsequent coalescence if possible.

#### 2.2.3.3 Other Forces

Different from the electrostatic forces which are generated by the overlap of the electric double layers, the steric barrier is not created by the surface charges on the emulsion droplet surfaces. The stabilization induced by the steric barrier is attributed to the physical obstacle formed by the adsorption of the neutral components at the emulsion droplet surfaces such as polymeric materials and colloids.[78] With the occupation of such materials at the liquid-liquid interface, the emulsified droplets cannot get contacted, leading to the less chance of coalescence of the emulsion droplets and hence the enhanced stability of the emulsion. Typically, the steric barrier cannot be achieved by the sole surfactant molecule but the aggregates of the interfacially active polymers and even small particles. The big polymeric surfactant usually has much more molecular weight than the surfactant mentioned in the electrostatic interaction section because the polymeric surfactants are polymerized from tons of monomers with the same structure. The occupation of the polymeric surfactants at the liquid-liquid interface can have a vital impact on the emulsion stability.

Take a W/O emulsion as an example, when a polymeric surfactant is located at the interface, the long chain of the surfactant may form train, loops or tails and the loops or tails should be hydrophobic and therefore kind of dehydrated, as shown in **Figure 2-5**. If the emulsion droplets approach, the loops and tails part of the surfactant would be hydrated, leading to an increase of total energy of the emulsion system. Such increased system energy results in the interference of the coalescence of the droplets and therefore enhance the emulsion stability.[79] Moreover, the facing-outward loops and tails can create space between the emulsion droplets, preventing the contact of the droplets and resulting in more stable emulsions.

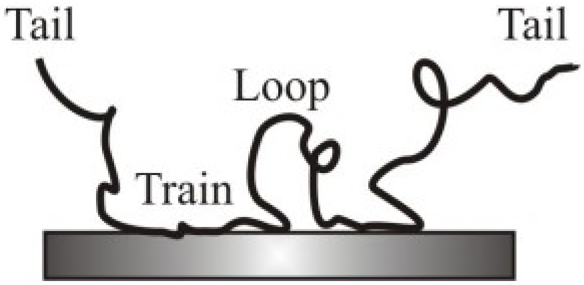

**Figure 2-5.** Possible configuration of a polymeric surfactant adsorbed on particle surfaces.[80]

There are many factors affecting the degree of steric stabilization by polymeric materials. With a thick adsorbed polymer layer at the liquid-liquid interface, there would be a long distance between the emulsion droplets, leading to the weaker van der Waals force between the droplets and thus lowering the tendency for droplets approaching. Also, the solvency of the polymer in the medium would affect the morphology of the surfactant at the interface. The steric barrier would decrease along with the hydration of the loops and tails of the surfactant.

However, it is worth noting that the addition of the polymer can also destabilize the emulsion, resulting from the polymer bridging mechanism. Such a phenomenon often occurs when a single polymeric surfactant molecule adsorbs at more than one emulsion droplet, leading to the flocculation of the emulsion droplets.[81] When it comes to the bridging effect of the polymeric surfactants, we need to talk about how the morphology of the polymer at the interface affects the emulsion stability. To make a perfect steric barrier instead of realizing the bridging effect, there should be no polymer-free surface that is necessary for bridging effect taking place or the morphology of the surfactant at the interface to compress polymer strings or loops. With proper charge density, the polymer is flexible at the interface and create the possibility for the effective bridging between the particles. While higher or lower charge density would lead to a stiffer or more collapsed polymer at the interface, both leading to weak bridging effect and decent steric repulsion between the emulsion droplets, respectively. We should note that when an ionic polymer has high charge density, it would be stiff due to the intramolecular repulsion and be adsorbed at the interface at the same time, leading to minimal anchoring points for bridging effect and resulting in a stronger steric barrier.

There is another non-DLVO interaction named hydration effect, which always exists between two hydrophilic surfaces.[82] Due to hydrophilicity of the surfaces, water molecules could form hydrogen bonding with the oxygen atoms at the oxide surface. When such two hydrophilic colloids get closer, the repulsive force stems from the requirement of removing the hydrating water molecules from the hydrophilic surfaces, leading to an increase in the system energy. Such hydrating effects can also be considered as a specific "steric effect" between the colloids.

The last non-DLVO interaction is hydrophobic interaction.[83] For a colloid without any polar groups or hydrogen bonding atoms, it cannot form hydrogen bonding with the surrounding water molecules. When the colloids approach, the water molecules between such colloids can only form hydrogen bonding with other water molecules within the gaps between the colloids. Such limitation could lead to an attractive force between the non-polar colloids, which is induced by an entropic factor. As an example, in the application of flotation, tiny air bubbles can attach to the hydrophobic force.

### 2.3 Stable Emulsions under Realistic Conditions

As discussed above, surfactants and particles can act as effective stabilizers for stabilizing O/W or W/O emulsions. Under different realistic conditions, there are many natural and/or synthetic surfactants, fine particles and clays acting as stabilizers, resulting in various types of stable emulsions.

It is undisputed that the emulsions stabilized by natural and/or synthetic surfactants, particles, and proteins have many applications such as cosmetics, drug delivery, oil/water separation, and enzyme immobilization.[84] However, increasing problems also arise, which will be discussed in detail as follows.

#### 2.3.1 Problem Description of Oil-in-Water Emulsions (Oily Wastewaters)

With the prosperous industrial development and ever-increasing population, the consumption of oils, including mineral oil, heavy oil, and edible oil, is increasing rapidly in every aspect of industrial processing and human activities.[85] Meanwhile, large volumes of oil-in-water emulsions (oily wastewaters) are generated during the heavy industrial process and daily household activities. Due to the lag of the faulty management of various management on treating such oily wastewaters, tons of oily wastewaters have been directly discharged into the natural environment, resulting in severe pollution and harsh environmental issues.[86-87] For example, if the oily wastewaters are discharged into the aqueous systems, the floating oil on the water surface would form a thick film which can isolate the aqueous phase from the atmosphere, leading to an oxygen-poor condition in the aqueous phase and hence threatening the living organisms in the water.[88-90] In 2010, an explosion at the Deepwater Horizon oil drilling rig caused the severest and largest oil spill in United States history.[91] Such oil spills also lead to widespread influence, including the reduction of fisheries output, the hindered plant photosynthesis and impaired growth of the crops.[92-93]

Moreover, the evaporation of oil into the air and the percolation of oil into the soil can lead to severe air and serious land pollution.[94]

### 2.3.2 Conventional Treatment of Oily Wastewaters

There are two main kinds of oily wastewaters for treatment: domestic oily wastewaters generated from daily household activities and industrial oily wastewaters generated from heavy industrial processes. The purposes for treating such oily wastewaters are: 1) removing a large volume of oil or dissolved organic components, and 2) removing the mixed components such as suspended particles and fines, sulfide, and ammonia.[95] The specific methods for treating oily wastewaters are discussed as follows.

#### 2.3.2.1 Membrane Filtration Technology

The membrane can be seen as a barrier that separates two immiscible liquid phases and constrains the transport of different organic or chemicals at a selective level. [96] As shown in **Figure 2-6**, a typical membrane can be designed as symmetric or asymmetric in structure, homogeneous or heterogeneous (Janus) in wettability, and liquid or solid in membrane type. Also, due to the difference in the pressure which drives the separation process, the membrane separation technology can be divided into three kinds: microfiltration, nanofiltration and reverse osmosis. The pressure required for microfiltration is the lowest among these three membrane separation technologies. The nanofiltration membranes are used to separate or retain small compounds and ions, which have a smaller extent than the components retained using reverse osmosis filtration. As a consequent, the osmotic pressure is lower than the pressure required for nanofiltration membranes.[97]

Treating oily wastewaters using membrane has now been considered as an alternative method to other conventional industrial methods such as centrifugation, extraction, distillation, flocculation, and coagulation.[98-99] Compared with these conventional methods, separation of oil/water using membrane shows numerous advantages, including excellent selectivity, long-term reusability, low cost, and high flexibility.[100] When the oil/water mixture is driven through the membrane, the rejection surface of the membrane could reject the organic solvent or aqueous phase of the oil/water mixture, and only selected liquid phase could go through the membrane,[101-102] achieving the successful oil/water separation. However, the drawbacks of membrane filtration technology are also obvious. For the hydrophobic and oleophilic membranes, they are always used in energy-intensive oil/water separation because they are not suitable for separating oily wastewaters under driving by gravity. In another aspect, though the hydrophilic and oleophobic membranes are suitable for treating oily wastewaters by gravity-driven, they are not capable of treating oil/water mixtures because their in-air oleophobicity could turn into underwater oleophilicity, leading to both transport of oil and water through the membrane.[103-104] Another drawback is the easy fouling for the oleophilic membrane. The fouling issues resulting from the formation of a cake layer of the materials at the rejection surface of the membrane could cause significant loss in the transmembrane flux, leading to a low oil/water separation efficiency.[105]

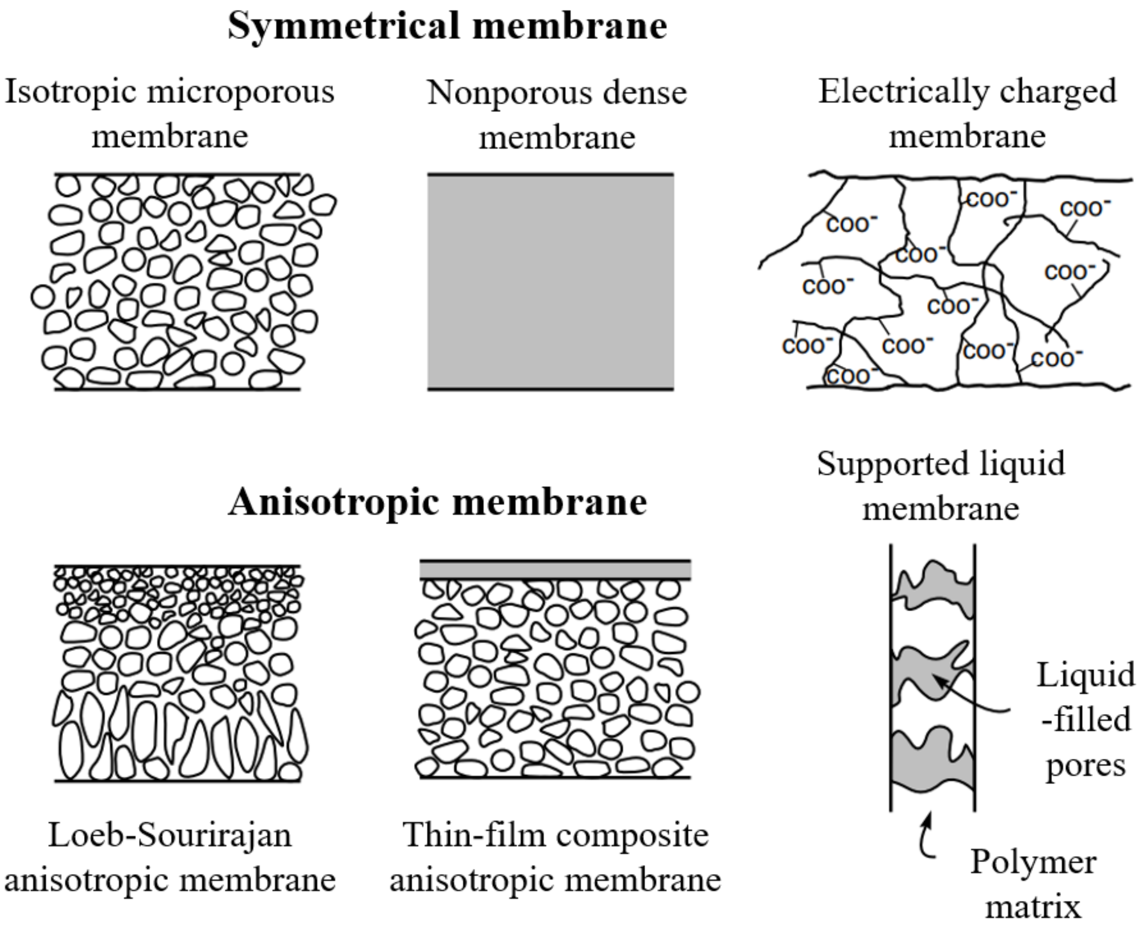

**Figure 2-6.** Schematic illustration of different types of membranes.[106]

### 2.3.2.2 Flotation Technology

Flotation has been considered as an accelerated separation technique in which an aqueous phase containing numerous fine bubbles are injected into the oily wastewater.[107] Due to the hydrophobic force between the fine bubbles and small oil droplets, the fine bubbles can attach themselves to the oil droplets. The bubble-tagged oil droplets become lighter because of the increased density difference between the oil/bubble agglomerations and aqueous phase, leading to the flotation of the oil droplets and hence the separation of oil from oily wastewaters.[108] The flotation technique has great potential due to the little produced sludge, relatively high separation efficiency, and large capacity.[107] However, there are still downsides in the treatment of oily wastewaters using flotation. In order to inject fine bubbles into the water, the bubble generator should be turned on for a long time, and the manufacturing and repairing problems of the device require intensive labor work and high cost. Moreover, the attachment of fine bubbles onto the oil droplet surfaces depend on the surface characteristics of the bubbles and oil droplets, which should be properly understood prior to applying the flotation technique to particular oily wastewater. As a result, many types of research should be conducted to improve flotation technology, including investigating the interfacial behavior of the flotation agents, designing novel and efficient flotation cells and devices.

#### 2.3.2.3 Coagulation Technology

In coagulation, emulsified oil droplets get together and become concentrated in the oily wastewaters under the external electric field.[109] Due to its capability of destabilizing and aggregating emulsified colloids and oil droplets, coagulation technology is widely used in treating oily wastewaters.[110] Generally, many mechanisms can contribute to effective coagulation of oil droplets and colloids, including neutralization of their surface charge by adsorption of charged species and/or compression of electrical double layers, inter-colloids/droplets bridging, sweep coagulation and ionic layer compression.[111] The well-dispersed oil droplets in oily wastewaters can be coagulated by adding coagulants into the oily wastewater systems and then removed from the wastewater systems, leading to effective oil/water separation. However, the realistic conditions of the oily wastewaters are complex and there are a lot of experiments should be done prior to selecting an effective coagulant for treating the oily wastewaters.[112]

Recently, a more advanced technology named electro-coagulation has been explored for treating oily wastewaters.[113] Such technology combines the advantages and functions of traditional coagulation technique, flotation method, and electrochemistry.[114] Compared with conventional coagulation, electrocoagulation shows numerous advantages such as simple equipment, facile operation, no addition of chemicals, the capability of removing the smallest colloidal particles, and more clear and colorless water after treatment. However, the downsides of electrocoagulation are still noticeable. One of the most critical factors for effective electrocoagulation is the high conductivity of oily wastewater. Such drawback has seriously restricted the wide applications of electrocoagulation in many practical situations.[115]

#### 2.3.2.4 Biological Treatment

The purpose of treating oily wastewaters using biological technology is to make use of the microbial metabolism to turn organic pollutants into harmless components.[116-117] With the help of biological treatment, there are generally two methods for treating oily wastewaters: activated sludge and biological filter.[118-120] During the treatment, activated sludge is always poured in an aeration tank, and then the microbial agents are added into the tank. Such agents can adsorb and concentrate on the surface of the sludge to decompose the organic components.[121] As for the biological filter, the micro-organisms are placed and attached to the filter. After that, the aimed oily wastewaters will go through the filter surface while the microorganisms will decompose the organic pollutants in the wastewaters.[122]

Due to the complete decomposition of organic components by microbial metabolism, the biological treatment can effectively treat the oily wastewaters containing hazardous organic agents. However, the total duration for treating oily wastewaters is relatively long when compared with other oil/water separation methods discussed above. Moreover, biotechnology is the key to the biological treatment process and the selection of a particular micro-organism according to the pollutants in the oily wastewaters is also noteworthy.

#### 2.3.2.5 Skimming

Skimming refers to various types of equipment that are used to remove the floating oil physically from the water surface. Such a technique is commonly observed in treating floating oil spills. During the skimming process, an oleophilic skimmer is used to adsorb oil to the rotating surface of the skimmer. After adsorption, the skimmer is then lifted and transfer the attached oil spills to an oil removal device such as roller and scraper. For large scale clean-up application of oil spills, skimming technique is very time-consuming and expensive.[123]

To improve the oil removal efficiency, the methods such as changing the shape of the recovery unit and changing the surface geometry of the skimmer have been applied to the new skimming technology. The main contribution of changing the shape and surface geometry is to increase the surface area of the skimmer. By increasing the area, more oil spills can be attached to the skimmer in one cycle, leading to higher oil removing efficiency.[124]

### 2.3.3 Water-in-Crude Oil Emulsions

The formation of water-in-crude oil emulsions occurs inevitably in petroleum-related industries. Although such emulsions are thermodynamically unstable, they are often stabilized by the natural surfactants, wax, and solids, leading to incredible stability of water-in-crude oil emulsions.[125] It is worth noting that the emulsified water droplets in the crude oil emulsions contain harsh salts such as chloride and sulfide salts which can poison the refinery catalysts and corrode the distillation columns.[126] Therefore, the emulsified aqueous phase must be removed from the crude oil emulsions to recover "clean" crude oil prior to their downstream processing. Typically, as discussed above, the emulsions are extremely stable due to the stabilization by various interfacially active components in the crude oil. Destabilization of water-in-crude oil emulsions is a necessary step before removing water from the emulsion. To effectively destabilize the water-in-crude oil emulsions, we have to be clear about the stabilization mechanism of such emulsions. Though the water-in-crude oil emulsions are stabilized by various interfacially active components such as asphaltenes, wax, resins, fines and clays, the asphaltenes in crude oil are one of the main contributors to the stability of the water-in-crude oil emulsions. Based on this reason, we will mainly focus on the stabilization of water-in-crude oil by asphaltenes.

#### 2.3.3.1 Stabilization of Water-in-Crude Oil Emulsions by Asphaltenes

Asphaltene is known as the fraction of crude oil with a complex chemical structure that is insoluble in straight-chain alkanes but soluble in toluene. The molecular structure of asphaltene is built on fused aromatic rings with saturated substituents and groups such as amine, hydroxyl, and sulfur-containing functional groups which make asphaltene amphiphilic.[127] Actually, asphaltene should be described as a kind of chemical mixture other than a specific family. With its structural complexity and uncertainty, asphaltene exhibits many states of molecules varying from a single unit to asphaltene aggregation, and it is hard to give a typical asphaltene molecule. However, known as the heaviest, most polar and surface-active components of crude oil, all the asphaltene molecules are contributed to the formation of stable O/W and W/O emulsions in the petroleum-related industry, hindering the oil production and interfering industry processing. It is necessary to fully understand the physicochemical properties, the interfacial behavior of asphaltene as well as the mechanism of asphaltene in stabilizing the W/O or O/W emulsion during the process and the effective ways to achieve oil/water separation of asphaltene-stabilized crude oil emulsions.

According to the results of the elemental composition analysis, the asphaltene molecules consist of C (carbon), H (hydrogen), N (Nitrogen), and S (sulfur) along with the trace amounts of Va (vanadium) and Ni (nickel).[128] The amounts of carbon and hydrogen are around 82 % and 8.1%, respectively, with a fairly constant hydrogen-to-carbon ratio (H/C) of 1.15.[129] Based on the results from vapor pressure osmometry (VPO) and gel permeation chromatography (GPC), the molecular weight of asphaltenes at 3000 Da to 10000 Da are much higher than the recent results of 750 Da which was analyzed by modern analytical techniques, leading to the different understanding on the asphaltene molecular structure and the molecular models.[130] The asphaltenes in crude oil are regarded as the colloidal-sized aggregates. With highly polar resins acting as peptizing agents, asphaltene attracts the resins together and resins, which act as a protective layer.[131] Under the protection and stabilization of reins, the asphaltenes are believed to dispersed in crude oil as a suspension.

As discussed above, the estimated asphaltene molecular weight affects the understanding of the molecular structure and molecular model of asphaltene. As shown in **Figure 2-7**, there are two conventional models showing the probable structure of asphaltenes molecule: archipelago model and island or like-your-hand model. The main difference between these two models is the asphaltene molecular mass.[132-133] Based on the molecular mass estimations of VPO and GPC, the molecular weight of asphaltene is several thousand. According to this result, Strausz *et al.* introduced the archipelago model.[133] In this model, the asphaltene molecule has a loose and flexible architecture and the aromatic and naphthenic rings are bonded together (**Figure 2-7a**). These bonded rings are connected with the core of asphaltene molecules via the bridges of alkyl chains, sulfur, -C-O- and -O-. After Several years, Groenzin and Mullins came up with an island-like or hand-like model of asphaltene molecule structure in 2007 (**Figure 2-7b**).[134] The island-like model has a much smaller weight mass of 500 Da to 1500 Da with an average molecular weight of 750 Da, as compared with the weight of the archipelago model. This model was also confirmed and supported by the later optical absorption and fluorescence studies.[135] This model indicates that the small aggregates, so-called nano-aggregates, are formed by asphaltene by the Van der Waals attraction between them at low concentrations and the larger aggregation would form at higher concentration, which contributes to the stabilization of emulsion system.

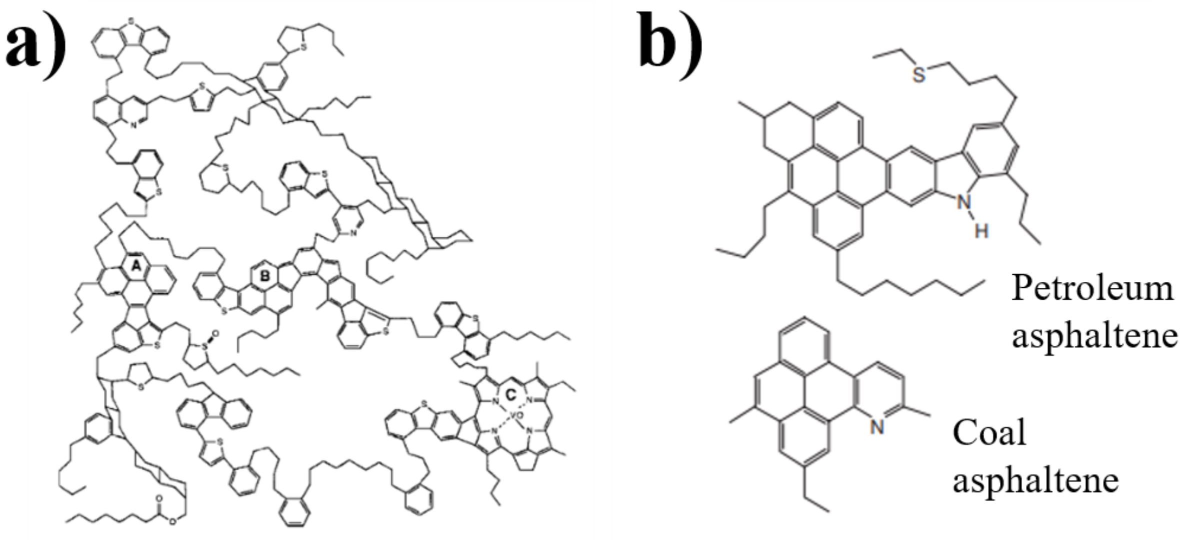

**Figure 2-7.** a) Hypothetical 'archipelago' asphaltene molecular structure where A, B and C represent aromatic clusters, and b) proposed molecular structures for coal and petroleum asphaltenes.[133-134]

### 2.3.3.2 Interfacial Behavior of Asphaltenes

Consisting of polycyclic aromatic hydrocarbon rings and polar parts, asphaltene can effectively adsorb at the water/oil interfaces, changing the interfacial properties such as the interfacial tension, rigidity, and elasticity of the interface and therefore leading to the formation of extremely stable crude oil emulsions.[136] Especially the nano-aggregates, clusters, and precipitation of the asphaltene at the water/oil interface are considered as irreversible adsorption due to their surface-active property. The asphaltene aggregates adsorbed at the crude oil-water interface can create strong steric barriers between the emulsified water droplets. The hydrophilic heads of the asphaltenes have natural affinities for the aqueous phase while the hydrophobic tails mainly stay in the crude oil phase. As a result, when dispersed water droplets approach each other, the adsorbed asphaltene would prevent the water droplets from contacting, resulting in little chance for the coalescence of the water droplets.

Stabilization of water droplets by asphaltenes also results from the Marangoni effect.[137] Such an effect can stabilize water-in-crude oil emulsions by slowing or preventing the drainage of the interfacial film between two water droplets. When the water droplets approach, their surfaces are deformable and eventually become parallel, followed by the drainage of the interfacial film between the water droplet surfaces. However, the outward flow results in a relatively lower concentration of the surfactants in the middle of the film as compared with the continuous bulk phase, leading to an interfacial tension gradient between the water droplets. The difference in the concentrations of surfactants could generate a diffusion tendency which has an opposing direction against the previous outward flow, preventing the drainage of the film between the water droplets. Due to the Marangoni effect, the emulsified water droplets are less possible to contact each other and therefore less possibility of coalescence.

The third mechanism is the low interfacial tension of the oil-water interface in the presence of the asphaltenes. The adsorption of asphaltene onto the oil/water interface is a kinetic process. As shown in **Figure 2-8**, the dynamic interfacial tension of the water/oil interface decreases with the timeline, suggesting the kinetic adsorption of asphaltene onto the oil/water interface.

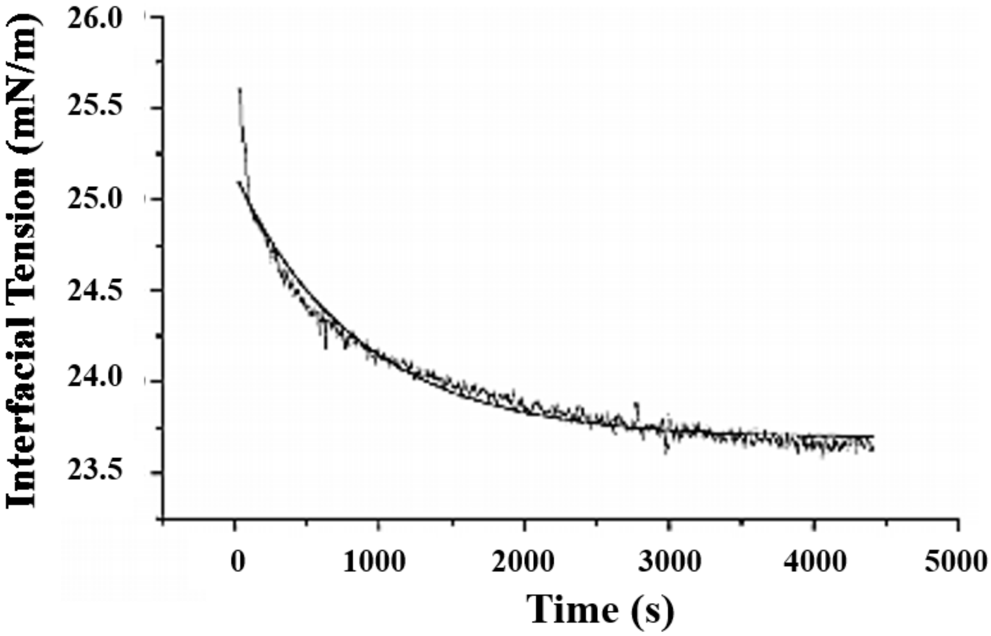

**Figure 2-8.** Dynamic interfacial tension of water and 3 wt% asphaltene solutions in toluene.[138]

The last mechanism for stabilizing water droplets comes from the formation of the interfacial film with high mechanical strength. The adsorbed asphaltenes at the oil-water interface would form a consolidated and rigid skin that can effectively resist the coalescence of water droplets. As shown in **Figure 2-9**, the water droplets stabilized by the interfacial film show obvious crumpling behavior during the contracting process, demonstrating the rigidity of the interfacial film.

Although other factors such as viscosity of continuous crude oil phase and size of dispersed water droplets can also affect the stabilization of water-in-crude oil emulsions, the stabilization by the asphaltenes at the oil-water interface has more prominent effects as compared with these factors. Therefore, we are more focused on the stabilization mechanism and destabilization of water-in-crude oil emulsions by investigating the interfacial behaviors of asphaltenes.

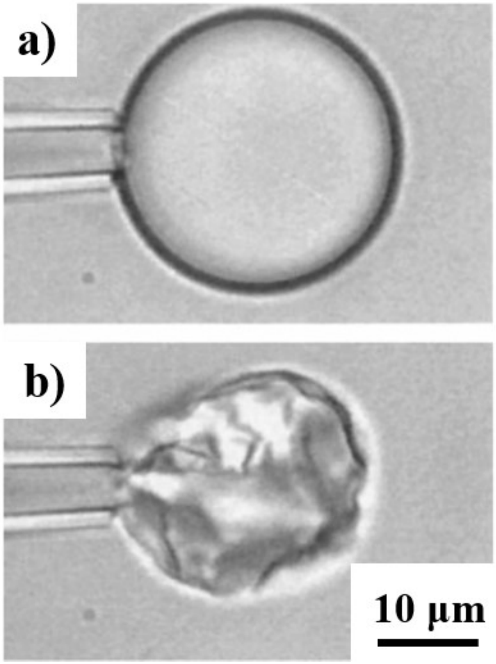

**Figure 2-9.** Contraction of a water droplet generated in diluted crude oil.[139]

### 2.3.4 Demulsification of Water-in-Crude Oil Emulsions

During petroleum production, the primary processing for treating water-in-crude oil emulsions is to separate water from the crude oil emulsions, which is known as demulsification of water-in-crude oil emulsions. Typically, conventional thermal treatment has been used to increase the temperature of the crude oil emulsions, lower the viscosity of the emulsions, weaken the strength of the interfacial film and accelerate the coalescence and flocculation of the water droplets. The coalesced, or flocculated water droplets could lead to quick oil-water separation. Another physical method to assist the dewatering of the crude oil emulsions is centrifugation. However, such methods are labor-intensive and energy-intensive, resulting in a heavy financial burden on the industries. Moreover, there is only 2 - 4 wt% water in the crude oil emulsions and emulsified water droplets are in the form of tiny droplets of several micrometers in sizes.[127] Dewatering by conventional heating and physical methods cannot completely remove all the tiny water droplets from the crude oil emulsion. Consequently, researchers have been motivated to explore more efficient and effective methods for dewatering the water-in-crude oil emulsions.

#### 2.3.4.1 Chemical Demulsifiers

Demulsification using chemical surfactants has been considered as a convenient and economical technique to break the stable water-in-crude oil emulsions. Generally, the chemical demulsifiers are amphiphilic compounds which are interfacially active. Such demulsifiers can disturb the stability of the water-in-crude oil emulsions by changing the interfacial tension of the oil-water interface, decreasing the mechanical strength of the interfacial film, reducing the thickness and elasticity of the interfacial regions and flocculating the dispersed water droplets.[140-142] The demulsifiers are usually oil-soluble and they can anchor at the crude oil-water interface through the organic phase (also, there are still a few reports showing the demulsification of water-in-crude oil emulsions using water-soluble demulsifier).[143] By anchoring at the crude oil-water interface, the long hydrocarbon tails of the demulsifiers are extended in the organic phase, bridging the water droplets and resulting in flocculation of the water droplets.

In practical demulsification, the commercial demulsifiers are mostly polymeric surfactants. There are typically two kinds of demulsifiers used for treating water-in-crude oil emulsions: low-molecular-weight polymeric demulsifiers and high-molecular-weight polymeric demulsifiers.[41] The polymeric demulsifiers with low-molecular-weight have high interfacial activities, and they can adsorb irreversibly at the oil-water interface, rupturing the interfacial film and leading to the coalescence of the water droplets.[144] As for the demulsifiers with high-molecular-weight, they often destroy the stability of the water-in-crude oil emulsions by flocculating water droplets based on the bridging effect.[39] Recently, more and more reports showed that the polymeric demulsifiers with intermediate molecular weights (7500-15000 Da) such as polymerized polyols, EO/PO copolymers, and alkylphenol formaldehyde resins modified with EO/PO have excellent ability on breaking the water-in-crude oil emulsions.[145-147] Such polymeric demulsifiers with intermediate molecular weights can effectively break stable water-in-crude oil emulsions due to the flocculation and coalescence of the water droplets. Later on, Feng *et al.* reported a novel demulsifier, named ethylcellulose (EC), for dewatering water-in-crude oil emulsions.[41] The ethylcellulose can effectively break the rigid interfacial film and replace the asphaltene aggregates at the crude oil-water interface. Meanwhile, the ethylcellulose can flocculate the dispersed water droplets, leading to the agglomeration of water droplets and therefore resulting in quick separation of water from crude oil emulsions.

The chemical demulsifiers show high efficiency in removing emulsified water droplets from water-in-crude oil emulsion by flocculation and coalescence of the water droplets. However, the drawback of this technique is still noticeable. The chemical demulsifier could generate secondary pollution to crude oil emulsions. Even though some demulsifiers such as ethylcellulose are biodegradable and non-toxic, they cannot be recycled after the dewatering process, leading to their poor reusability and sustainability.

#### 2.3.4.2 Microwave Treatment

Based on the fact that conventional methods such as heat and chemical demulsifiers for demulsifying water-in-crude oil emulsions are considered as expensiveness, high consumption of energy and/or pollution to the crude oil phase, microwave treatment has been applied as an alternative demulsification method for efficiently dewater the water-in-diluted bitumen emulsions.[148] The microwave treatment was first patented in 1986.[149] As a novel technique for treating the water-in-crude oil emulsions, microwave demulsification combines many upsides, including selective provision of energy to activate the aqueous, indigenous surfactants and interfacial films components, no generation of secondary pollution, no chemical additives, high penetration power, and fast dewatering.[150-152]

The mechanism of microwave treatment for the water-in-crude oil emulsions are as follows: 1) reducing significantly the viscosity of the crude oil phase, which favors the contact of emulsified water droplets;[150, 153] 2) reducing the stability of the emulsified water droplets as a result of microwave-induced rotation of water molecules, which can decrease the surface charge of the water droplets and break the hydrogen bonding between the water molecules and the surfactants and 3) reducing the thickness of the interfacial film by the expansion of the water droplets, which results from the increased internal pressure during the microwave radiation.[154-155]

Although dewatering crude oil emulsions using microwave treatment has been shown to be effective in various applications, including oil extraction from underground, upgrading, and refining, such technique is still not used commercially due to the lack of understandings of microwave radiation by end-users in industry, high set-up expense, and uncertain potential.[156]

#### 2.3.4.3 Electrostatic Demulsification

Dehydration of crude oil emulsions using electrical method has been reported in a large number of patents and widely used in the petroleum industry.[157-159] Generally speaking, the application of an electrical field to the water-in-crude oil emulsions can accelerate the motion of water droplets in crude oil emulsions, promote contact between the water droplets and assist drop-drop coalescence.[160]

There are many mechanisms contributing to the effective dewatering of water-in-crude oil emulsions based on electrostatic demulsification. 1) 3-Stage process/mechanism. The water droplets in an applied electrical field would approach each other, leading to the drainage of the interfacial film of the continuous phase.[161] At the high shear rate, the rupture of the interfacial film could easily happen under disturbance when the film reaches a specific thickness, leading to the coalescence of water droplets.[162] 2) Dipole coalescence. When water droplets are under an external electric field, such electric field can induce charges of opposite signs on the surface of two water droplets, resulting attractive force between the water droplets.[163] If the two water droplets are close enough, the van der Waals attraction could play an important role in assisting the contact of water droplets, helping their coalescence. 3) Electrophoresis. Such a mechanism refers to the motion of charged water droplets under the influence of an electric field. The electrophoresis could result in frequent contact between the water droplets, which favors the coalescence of emulsified water droplets. 4) Dielectrophoresis. Different from "electrophoresis", dielectrophoresis refers to the motion of matter caused by polarization effects under a non-uniform electric field.[164] However, in practical applications, the contribution of dielectrophoresis to the coalescence of water droplets is smaller as compared with electrophoresis, due to the relatively low velocity of water droplets in a non-uniform electric field.[165]

The electrostatic demulsification has shown to be an effective method for dewatering the water-in-crude oil emulsions, but its efficiency is influenced by many factors such as oil phase viscosity, size of the dispersed water droplets and the strength of the applied electric field.[166]

## 2.4 Oil/Water Separation using Magnetically Responsive and Interfacially Active Nanoparticles

### 2.4.1 Introduction

As discussed above, there are still drawbacks in the current technologies for oil/water separation, including the high capital cost, relatively low efficiency, unavailability of large scale-up, easy fouling, poor recyclability, and unsustainability. Such drawbacks inspired researchers to find more efficient oil/water separation methods based on magnetically responsive and interfacially active nanoparticles. Generally, magnetic nanoparticles with excellent interfacial activities can stay securely at the liquid-liquid interface or air-water interface. By tagging emulsified droplets (oil droplets or water droplets), such droplets can be transported and removed to the desired locations under the external magnetic field, achieving the oil/water separation.

For oil/water separation using magnetically responsive and interfacially active nanoparticles, the synergic actions of high magnetic responsiveness and satisfying interfacial activities contribute to the efficiency of oil/water separation.

### 2.4.2 Interfacial Activities of Nanoparticles

The excellent interfacial activities of nanoparticles can ensure their secure anchoring at the liquid-liquid interface, leading to the formation of stable Pickering emulsions. The stable Pickering emulsion achieved by the magnetic nanoparticles is an essential prerequisite for the subsequent oil/water separation. In the past years, design and synthesis of interfacially active nanoparticles which were used as stabilizers in the Pickering emulsions have been widely investigated to achieve irreversible adsorption of particles at the oil-water interface and make stable Pickering emulsions at high efficiency and low cost.[167-171] The types of particles used as the stabilizers are custom-designed according to different situations. The materials for the particles include calcium carbonate, barium sulfate, carbon particles, magnetite or maghemite particles, nanocrystals, bacteria or polymerized materials and all these materials show great potentials for effectively stabilizing emulsions.[172] With further functionalization on the particle surfaces, the synthesized particles can be used as solid stabilizers with multiple functions.

The homogeneously surface-modified particles have uniform surface properties such as wettability (hydrophilic or hydrophobic), surface charge (positively charged or negatively charged), stimulus-responsive property (carbon dioxide, light or thermal-responsive). Generally, there is no specific control during the synthesizing process or surface-modification process, leading to the synthesis of homogeneously surface-modified particles.

To make particle interfacially active, interfacially active materials are often coated or grafted onto the particle surfaces with the specific chemical bonding such as a covalent bond or hydrogen bond.[173] Moreover, with the different modification ratio of the materials on the particle surfaces, the surface wettability can be adjusted to either more hydrophilic or more hydrophobic. B.P. Binks *et al.* successfully change the wettability of the silica particles by adjusting the SiOH ratio on the silica particle surfaces to use the particles as stabilizers for stabilizing oil-in-water emulsions, water-in-oil emulsions and even water-in-air emulsions which were also known as dry water.[61] Furthermore, they also concluded the relationship between the wettability of particle surface and fluid/fluid ratio with the emulsions types (W/O or O/W), as shown in **Figure 2-10**.

However, the homogeneous particles sometimes cannot perform well in stabilizing the emulsion due to not high required desorption energy to detach from the interface, leading to their easy desorption from the oil-water interface and hence the destabilization of the emulsion. Compared with the interfacially active particles of uniform surface wettability, a novel particle, called the "Janus" particle, combines two opposite surface wettabilities in a single particle, presenting a heterogeneously modified surface.

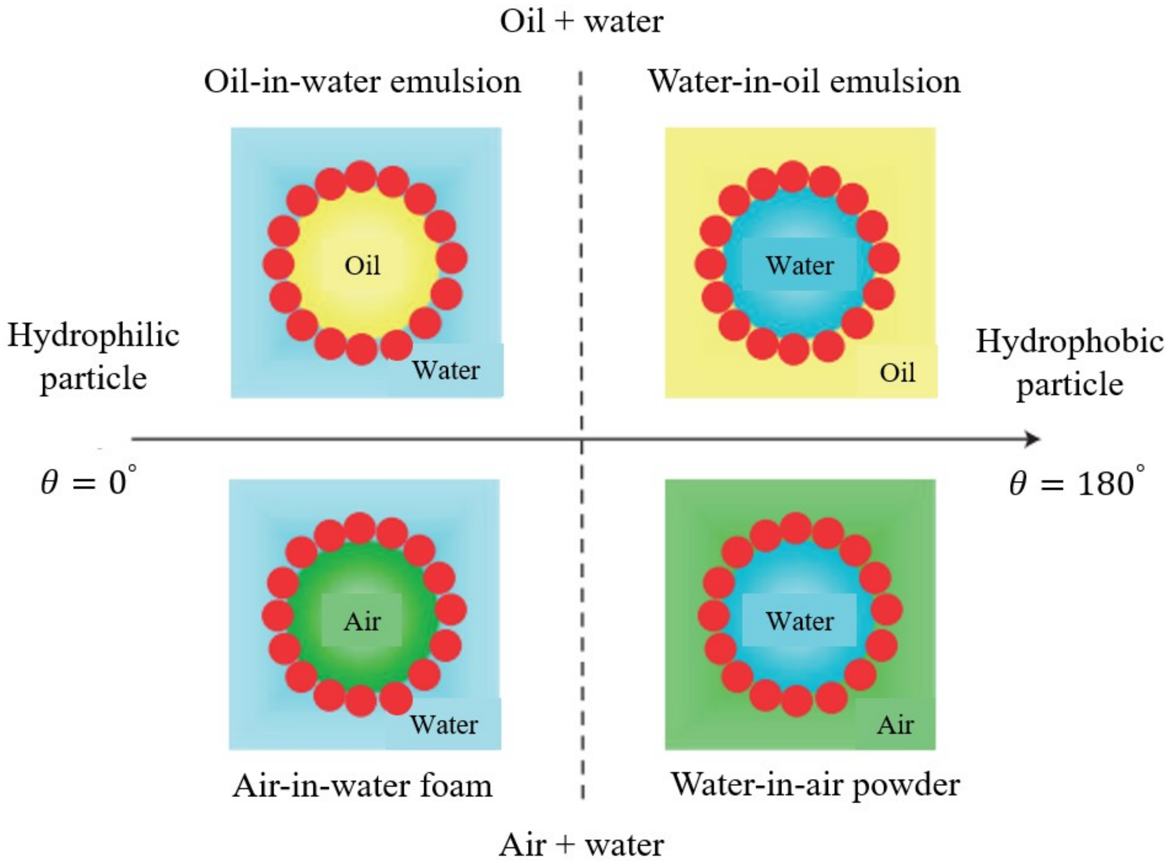

**Figure 2-10.** Inversion of different types of emulsions by either changing particle wettability at a fixed fluid/fluid ratio or by varying fluid/fluid ratio at fixed particle wettability. The particle wettability is described by the contact angle $\theta$.[61]

As shown in **Figure 2-11**, the boundary dividing the polar surface region and the apolar surface region is denoted by parameter $\alpha$. The particle would be considered as a homogeneous particle when α equals 0º or 180º. According to the work of Ondarcuhu *et al.*,[174] the total free energy for the Janus particle locating at the planar oil/water interface can be described as a function of the angle $\beta$:[175]

For $\beta \leqslant \alpha$ , $E(\beta) = 2\pi R^2 \left[\gamma(AO)(1 + cos\alpha) + \gamma(PO)(cos\,\beta - cos\alpha) + \gamma(PW)(1 - cos\beta) - \frac{1}{2}\gamma(OW)(sin^2\beta)\right]$

For $\alpha \leqslant \beta$, $E(\beta) = 2\pi R^2 \left[\gamma(AO)(1 + cos\beta) + \gamma(AW)(cos\,\alpha - cos\beta) + \gamma(PW)(1 - cos\alpha) - \frac{1}{2}\gamma(OW)(sin^2\beta)\right]$

where R is the radius of the Janus particles and $\gamma(AO)$, $\gamma(PO)$, $\gamma(OW)$, $\gamma(AW)$ and $\gamma(PW)$ are the interfacial tensions of the apolar/oil, polar/oil, oil/water, apolar/water, and polar/water. From the Young-Laplace equation, we can get:[175]

$$\cos\theta_A = \frac{\gamma(AW) - \gamma(AO)}{\gamma(OW)}$$

$$\cos\theta_P = \frac{\gamma(PW) - \gamma(PO)}{\gamma(OW)}$$

where $\theta_A$ and $\theta_P$ are the contact angles of the apolar surface region and the polar surface region of the Janus particle, respectively. For a concrete case, one spherical Janus particle with a radius of 10 nm, α of 90° and the interfacial tension of the oil/water is 36 mN/m as a constant. With the introduction of the equation: $\theta_{Average} = \frac{\theta_A\,(1+\cos\alpha)+\theta_P(1-\cos\alpha)}{2}$ ,[175] the energy ($\kappa$T) required for the Janus particle desorbing from the oil/water interface as a function of the average contact angle is shown in **Figure 2-12**.

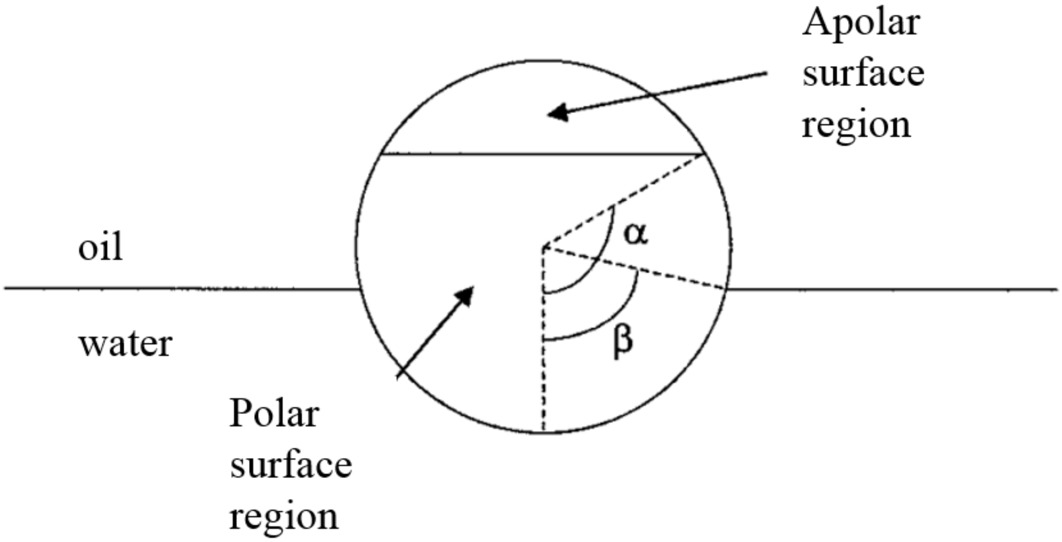

**Figure 2-11.** Schematic illustration of a Janus particle adsorbed at oil-water interface. Parameter $\alpha$ represents the relative areas of polar or apolar region of a Janus particle and parameter $\beta$ represents the depth of a Janus particle immersed in an aqueous phase.[175]

For this case, the amphiphilicity and the resulting desorption energy of the Janus particle are adjusted by changing $\Delta\theta$ (defined as $\Delta\theta = \frac{\theta_A - \theta_P}{2}$). When $\Delta\theta$ equals 0, this case represents a homogeneous particle with no amphiphilicity, leading to the lowest desorption energy required as compared with other kinds of Janus particles with different $\Delta\theta$. In **Figure 2-12**, it should be noted that with increasing $\Delta\theta$ as well as amphiphilicity of the Janus particle, the required desorption energy increases remarkably, further indicating that the Janus particles can be more stably adsorbed at the liquid-liquid interface and therefore are more effective in stabilizing emulsions. In summary, the required desorption energy of the amphiphilic Janus particles is much higher than the homogeneous particles and it is expected that the amphiphilic Janus particles can be used as more efficient stabilizers in stabilizing emulsions as compared with particles of uniform surface wettability.

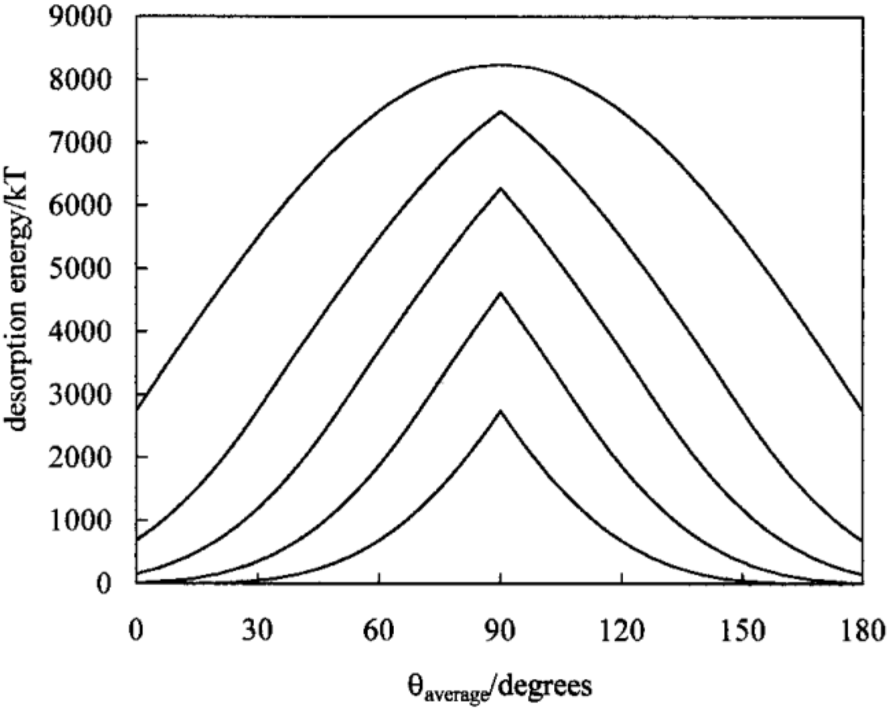

**Figure 2-12.** Variation of energy for a Janus particle with a radius of 10 nm and α of 90° detaching from a planar oil-water interface. The different curves refer to $\Delta\theta$ of 0 (the homogeneous particle), 20, 40, 60 and 90° (from the bottom up).[175]

For example, we can quantitatively evaluate the energy change for a single nanoparticle of uniform or asymmetric surface wettability adsorbing from the aqueous phase onto the oil-water interface. The adsorption of one nanoparticle of uniform or asymmetric surface wettability (**Figure 2-13**) onto the oil-water interface would lead to a decrease of total energy in the emulsion system. We assume that the two kinds of nanoparticles (radius equals 10 nm) are adsorbed onto a toluene-water interface ($\gamma_{OW}$ = 36 mJ/m$^2$) from the aqueous phase (half surface of the Janus nanoparticle shown in **Figure 2-13** is hydrophilic, and the other half is hydrophobic).

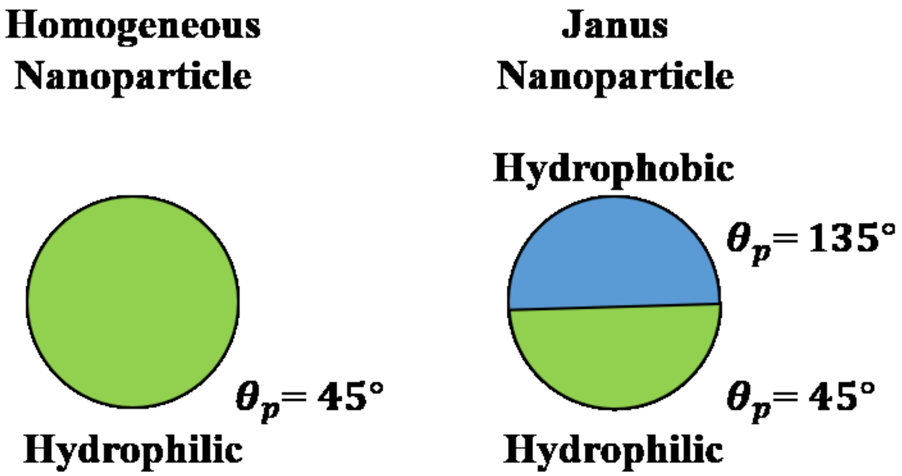

**Figure 2-13.** Schematic illustration of nanoparticles of asymmetric or uniform surface wettability.

The change of total system energy $\Delta G_{HP}$ due to the adsorption of single homogeneous nanoparticle from the aqueous phase onto the toluene-water interface can be calculated:

$$\Delta G_{HP} = 2\pi R^2(1-\cos\theta_P)(\gamma_{PO}-\gamma_{PW}) - \pi(R\sin\theta_P)^2\gamma_{OW}$$

where R is the radius of the nanoparticle, $\theta_P$ is the contact angle (measured in water) of homogenous nanoparticle surface, $\gamma_{PO}$ is the interfacial tension of toluene and hydrophilic nanoparticle surface, $\gamma_{PW}$ is the interfacial tension of water and hydrophilic nanoparticle surface and $\gamma_{OW}$ is the interfacial tension of toluene and water. We can obtain $\Delta G_{HP}$ for the adsorption of a single homogeneous nanoparticle from aqueous phase onto the toluene-water interface to be -9.7 x $10^{-19}$ J for the total system energy. For the total energy change $\Delta G_{JP}$ resulting from the adsorption of a single Janus nanoparticle from aqueous phase onto the oil-water interface, $\Delta G_{JP}$ can be calculated as:

$$\Delta G_{JP} = 2\pi R^2(\gamma_{AO}-\gamma_{AW}) - \pi R^2\gamma_{OW}$$

where $\gamma_{AO}$ is the interfacial tension of toluene and hydrophobic Janus nanoparticle surface, and $\gamma_{AW}$ is the interfacial tension of water and hydrophobic Janus nanoparticle surface. We can obtain $\Delta G_{JP}$ for a single Janus nanoparticle to adsorb from aqueous phase onto the toluene-water interface to be -2.73 x $10^{-17}$ J. Based on this quantitative evaluation of free energy change for a homogeneous nanoparticle and Janus nanoparticle to adsorb from aqueous phase onto a toluene-water interface, the Janus nanoparticles can make oil-water interface more stable by further lowering the total free energy of the system than the homogeneous nanoparticles, suggesting a better stabilization of oil-water interface by Janus nanoparticles than homogeneous nanoparticles.

### 2.4.3 The Origin of Magnetism

As effective tools to process oil/water separation, the interfacially active nanoparticles should have desired magnetic responsiveness for oil/water separation and the recyclability after oil/water separation. With high magnetic responsiveness, the nanoparticle-tagged oil or water droplets could be efficiently and quickly removed from the continuous phase, resulting in efficient oil/water separation. Moreover, under the external magnetic field, the responded magnetic forces could lead to subsequent recycling of the nanoparticles after oil/water separation. Therefore, to achieve high performance of the magnetically responsive and interfacially active nanoparticles on oil/water separation and recycling, the satisfying property of magnetic responsiveness is critically necessary to the nanoparticles.

Every atom contains electron(s) and quark(s). Due to the charge they have (one electron has charge of -1e and one quark has charge of - $\frac{2}{3}$ e), the electrons and quarks could be seen as “mini-magnet”, which are also named as intrinsic magnetic moments. When we discuss the magnetism at a level of an atom, it is worth noting that the magnetic moment of the nuclei is negligible as compared with the intrinsic magnetic moments of an electron. However, electrons keep moving in orbital motions and self-spinning around a nucleus and only two electrons with opposite directions of self-spinning can occupy one orbit at the same time. As a result, two paired electrons cannot show the magnetism and only unpaired electrons can generate magnetism. There are three types of magnetism: 1) ferromagnetism. This kind of material has paralleled magnetic moments and shows magnetic responsiveness under the external magnetic field; 2) paramagnetism. The directions of magnetic moments in paramagnetic materials are random and no macroscopic magnetization appears. And only small magnetization would be shown when the external magnetic field is applied; 3) anti-ferromagnetism. Actually, most of the materials in this world have ferromagnetism but this property was covered by other magnetic properties.[176]

For synthesizing magnetically responsive nanoparticles, the magnetite ($Fe_3O_4$) nanoparticles are often used as cores or affinities to prove the synthesized interfacially active nanoparticles with magnetic responsiveness. The bare magnetite ($Fe_3O_4$) nanoparticles are ferromagnetic due to the parallelization of the intrinsic magnetic domain. However, when the ferromagnetic particles have nano-sizes, the magnetic moments in the particles can be thermally fluctuated and therefore turn into paramagnetic nanoparticles even at room temperature. Such interesting properties can contribute to the desirable properties of synthesized nanoparticles, including the satisfactory magnetic responsiveness under an external magnetic field, and no aggregation during storage and without the external magnetic field.

### 2.4.4 Oil/Water Separation using Magnetically Responsive and Interfacially Active Nanoparticles of Uniform Surface Wettability

The nanoparticle surfaces are modified with interfacially active materials to show excellent interfacial activities at the oil-water interface. According to different emulsion systems (W/O or

O/W emulsions), the nanoparticle surfaces should be adjusted to be relatively hydrophobic or hydrophilic to be effective Pickering emulsion stabilizers. For example, Mirshahghassemi *et al*. reported magnetic nanoparticles with surface modification by polyvinylpyrrolidone (PVP) for removing oil from oily wastewaters, achieving the removal of over 99% crude oil from seawater environment.[52-53] Later on, magnetic nanoparticles modified with expanded perlite,[177] polymerizations of dimethyl amino ethyl methacrylate (PDMAEMA),[54] poly(vinyl alcohol),[178] chitosan,[179] triethoxy(phenyl)silane,[180] and cellulose crystals have been reported to assist oil remediation by removing oil droplets from bulk seawater.[181]

As for dealing with W/O emulsions, especially water-in-crude oil emulsions, it is not insufficient for nanoparticles with satisfying interfacial activities to remove water from water-in-crude oil emulsion. Due to the presence of the interfacial film covering water droplet surfaces, it is hard for nanoparticles to anchor at water droplet surfaces. To solve this problem, the nanoparticles are often coated with functional materials, which can effectively break the interfacial film to create the anchoring site for the nanoparticles. In 2012, Peng *et al.* reported interfacially active nanoparticles with a coating of ethyl cellulose (M-EC nanoparticles).[57-58] EC is known as biodegradable cellulosic material for effectively disturbing and breaking the rigid asphaltene film.[41-43, 127] With the EC on the iron oxide nanoparticle surfaces, the M-EC nanoparticles can not only break the asphaltene film but also anchor at the water droplets surface due to the hydrophobicity of ethyl cellulose. Later on, nanoparticles with uniform surface modification by oleic acid,[182] polyelectrolytes,[55] and polyvinylpyrrolidone were reported for treating crude oil emulsions.[183]

Although these nanoparticles can treat crude oil-related emulsions, they may desorb from the emulsified droplet surface under the external magnetic field, leading to possible low efficiency of oil/water separation.[184] A weak magnetic field can avoid the desorption of the nanoparticles from the oil-water interface, but the oil/water separating process is inefficient due to the feeble responded magnetic forces. Consequently, we need to apply nanoparticles with superior interfacial activities to process more efficient oil/water separation.

### 2.4.5 Oil/Water Separation using Magnetic Janus Nanoparticles of Asymmetric Surface Wettability

Janus particles have attracted considerable interests on account of their asymmetric structures or the opposing surface properties combined in one individual particle.[185] With such unique characteristics, the Janus particle can feature excellent and even extraordinary properties. For example, the amphiphilic or biwettable Janus particle can effectively deposit at the oil-water interface with their hydrophobic part in the oil phase while the hydrophilic part in the aqueous phase, exhibiting excellent interfacial activity.[186-187] Moreover, due to their asymmetric surface properties, the desorption energy of Janus nanoparticles required to detach the oil-water interface is much higher than the nanoparticles of uniform surface properties. Compared with the particles with uniform and homogeneous surface wettability, biwettable Janus particles possess better interfacial properties including more effective emulsion stabilizers and higher required desorption energy from the oil-water interface.[188-189] As a result, magnetic Janus nanoparticles are anticipated to have better performance on oil/water separation.

Ali *et al.* synthesized P(MMA-AA-DVB)/$Fe_3O_4$ Janus particles as effective demulsifiers for breaking heavy oil and water emulsion.[190-191] Song *et al.* reported the novel hydrophilic/hydrophobic magnetic Janus particles for efficient oil/water separation.[192] Such Janus particles showed excellent performance on removing oil from oil/water mixtures and also exhibited high adsorption energy at the oil-water interface.

It is worth noting that, under realistic conditions, the oil-water interfaces of the oily wastewater systems and water-in-crude oil emulsions are stabilized by various interfacially active components such as synthetic surfactants (detergent), natural surfactant (asphaltenes), particles and clays. Moreover, the conditions of the ambient environment can enhance the interfacial behavior of the interfacially active components at the oil-water interfaces, leading to more stable W/O or O/W emulsions and hence more difficult for interfacially active nanoparticles in anchoring securely at oil-water interfaces.[193] As a result, the Janus nanoparticles of asymmetric surface wettability are anticipated to have better performance on oil/water separation as compared with the interfacially active nanoparticles of uniform surface wettability, which is one of the main focuses in this thesis.

# Chapter 3 Experimental

## 3.1 Materials

### 3.1.1 Chemical Received without Purification

Purchased chemicals, reagents and other materials used in the experiments are all listed in **Table 3-1**. The deionized water (> 18.0 MΩ • cm) was supplied from Thermo Fisher Barnstead Nanopure ultrapure water purification system, and tap water was used whenever required. The process water supplied by Aucura of pH 8.9 contains 25 ppm $Mg^{2+}$, 41 ppm $Ca^{2+}$, 79 ppm $SO_4^{2-}$, 527 ppm $Na^+$, 22 ppm $K^+$, 407 ppm $Cl^-$, and 793 ppm $HCO_3^-$. The composition of synthetic seawater was listed in **Table 3-2**.

**Table 3-1.** Chemical compounds and reagents used in experiments.

| Chemicals | Supplier | Notes |
|---|---|---|
| Iron Oxide Nanoparticle | Sigma Aldrich | 50 – 100 nm |
| Carboxymethyl Cellulose | Sigma Aldrich | MW: 250,000 g/mol<br>DS: 0.7 |
| Ethyl Cellulose | Sigma Aldrich | Ethoxy Content: 42 wt% |
| Paraffin Wax | Sigma Aldrich | Melting Point: 56 - 61°C |
| Toluene | Fisher Scientific | ACS Grade |
| Ethanol | Fisher Scientific | ACS Grade |
| Acetone | Fisher Scientific | ACS Grade |
| Heavy Naphtha | Champion Technology | Petroleum Reformate |
| Bitumen | Syncrude | Vacuum Distillation Feed Bitumen |
| Detergent | Superstore Market | DAWN, 700 mL |
| Cooking Oil | Organic Biologique | Extra Virgin Olive Oil, 500 mL |

**Table 3-2.** Composition of synthetic seawater.[194]

| Synthetic seawater | | | | | | | |
|---|---|---|---|---|---|---|---|
| Salt | NaCl | $MgCl_2$ | $MgSO_4$ | $CaCl_2$ | KCl | $NaHCO_3$ | Total |
| g/L | 24.95 | 2.58 | 3.21 | 1.15 | 0.74 | 0.20 | 32.83 |

### 3.1.2 Prepared Chemicals

*Diluted crude oil.* 50 g naphtha-diluted bitumen was prepared by mixing heavy naphtha and bitumen with a mass ratio of 0.65 ($m_{naphtha}/m_{bitumen}$), as typically used in the oilsands industrial field. The obtained mixture was put on the shaker for 12 h at 120 cycles/min.

*Process water-in-crude oil emulsion.* The process water-in-diluted bitumen emulsion was prepared by mixing 50 g diluted bitumen and 2.63 g process water using a homogenizer (VWR 250 Homogenizer) running at 30,000 rpm for 3min.

*Oily wastewaters (experimental condition).* The two kinds of oily wastewaters were prepared using an ultrasonic bath to emulsify 1) 1 ml toluene (dyed using Sudan III) with 9 ml SDS aqueous ($C_{SDS}$ = 0.04 mg/ml) solution and 2) 1 ml naphtha-diluted bitumen with 9 ml DI water for 30 min, respectively.

*Oily wastewaters (mimetically realistic condition).* The diluted crude oil (2 mg/mL crude oil in toluene) and the pure cooking oil were used as waste oil in the oil removal/recovery test. The oily wastewaters were prepared by emulsifying oil (diluted crude oil or pure cooking oil) in water (synthetic seawater or tap water without or with 0.04 mg/mL detergent) at a volume ratio of 1:9 ($v_{oil}/v_{water}$) using an ultrasonic bath for 30 min.

### 3.2 Instrumentation and Experimental Protocols

*Preparation of M-CMC-EC nanoparticles*. The bare iron oxide nanoparticles (200 mg) were first dispersed in a diluted (1.0 wt%) CMC aqueous solution (100 mL) using an ultrasonic Dismembrator (Fisher Model 500) operating at 40% amplitude for 15 min. The obtained nanoparticles were denoted as M-CMC nanoparticles. The M-CMC nanoparticles formed as such were collected by a strong hand magnet and then washed with deionized water, followed by drying in a vacuum oven at 75ºC for 12 h. The suspension of the M-CMC nanoparticles (200 mg) in 1.0 wt% EC-in toluene solution (100 mL) was then prepared using the same procedures mentioned above. The resulting M-CMC-EC nanoparticles were collected using a hand magnet and washed with pure toluene three times, followed by drying in a vacuum oven at 75ºC for 12 h.

*Preparation of M-Janus nanoparticles*. The M-CMC-EC (200 mg) nanoparticles were dispersed in paraffin wax (1 g) at 60ºC. The mixture was then emulsified in deionized water (50 mL) using a homogenizer (VWR 250 Homogenizer) at a speed of 22,000 rpm for 3 min, resulting in the formation of stable wax-in-water Pickering emulsions. Due to hydrophobic forces between the M-CMC-EC nanoparticles exposed in the aqueous phase, additional M-CMC-EC nanoparticles could migrate to the nanoparticle layer at the wax-water interface, leading to multilayer deposition in the form of aggregates. A desirable amount of CMC aqueous solution was then added into the Pickering emulsion, followed by vigorously mixing using Vortex Mixer for 3 min. Since the M-CMC-EC nanoparticles which are in the aggregates of M-CMC-EC nanoparticles formed at the wax-water interface during this process are almost fully exposed to the aqueous phase, the surfaces of such nanoparticles are not protected by the wax from the adsorption of CMC, making these nanoparticles hydrophilic or water wettable (most likely as M-CMC-EC-CMC nanoparticles) and hence highly dispersed in the aqueous phase. The collected nanoparticles were dried in a vacuum oven at 75ºC for 12 h and then used to form a toluene-in-water Pickering emulsion. Only M-Janus nanoparticles migrated to the toluene-water interface and the hydrophilic M-CMC-EC-CMC-like nanoparticles remained in the aqueous phase. After the creaming of the emulsion, the stable toluene droplets stabilized by M-Janus nanoparticles were carefully collected using a micropipette, followed by washing with acetone and toluene. The final M-Janus nanoparticles are obtained after drying in a vacuum oven at 75ºC for 12 h.

*Preparation of M-CMC-EC-CMC nanoparticles*. The M-CMC-EC-CMC nanoparticles were synthesized by dispersing M-CMC-EC nanoparticles (200 mg) in 1 wt% CMC/Water solution (100 mL) using Ultrasonic Dismembrator and then collected by the hand magnet, followed by washing with DI water three times. The nanoparticles obtained as such were dried in a vacuum oven at 75 ºC for 12 h.

*Quartz crystal microbalance with dissipation monitoring.* The adsorption of CMC and EC adsorbed on iron oxide sensor surface was investigated by quartz crystal microbalance with dissipation monitoring (Biolin Scientific, USA). QCM-D sensors with iron oxide coatings ($Fe_3O_4$; QSX 326) were purchased from Q-Sense (Biolin Scientific, USA) The cleanliness of sensor surface was determined by a frequency change less than 1 Hz when dry air flowed through the sensor surface for initial 5 min. For each separate experiment, solutions (50 mL) were prepared and flew over the sensor surface at a 0.2 μL/min rate. DI water or toluene was also required to flow over the sensor surface before and after the adsorption of CMC or EC respectively to obtain a stable baseline. Adsorption time varies from one measurement to another, depending on the solution conditions.

*Field-emission scanning electron microscope (FE-SEM).* FE-SEM was used to determine the state of dispersion and size of synthesized nanoparticles. During the measurement, FE-SEM was operated at 5 kV with a working distance of 6.5 mm and an amplification of 20,000.

*Transmission electron microscope.* The morphologies of the studied nanoparticles were characterized using JEOL JEM-ARM200CF S/TEM (Narwhal).

*Zeta potential measurement.* The zeta potentials of particles were determined using Zetasizer Nano (Nano ZS) and particle suspensions in 1 mM KCl solution of pH of 4.5 at room temperature. The cell was first rinsed with DI water and subsequently with particle suspension three times.

*Thermogravimetric analysis.* The thermogravimetric analysis was performed using a Thermo Gravimetric Analyzer (TA Instrument Q-500). Samples were placed in a platinum pan and heated at a rate of 10 $^{o}$C/min from room temperature to 800$^{o}$C under the protection of the nitrogen atmosphere.

*Fourier-transform infrared spectroscopy.* FTIR spectrometer (Cary – 670 Agilent technologies) was used to determine the infrared spectra of celluloses and synthesized particles with an attenuated total reflection (ATR) sampling accessory. The spectra of samples were collected from a wavenumber range 4000 to 550 cm$^{-1}$ at a spectral resolution of 4 cm$^{-1}$.

*Magnetization saturation measurement.* The magnetization property of the M-Janus nanoparticles was characterized using a Quantum Design PPMS magnetometer. The measurement was conducted at room temperature with an applied magnetic field between -4 and 4 Tesla.

*Coalescence time measurement.* The coalescence time of two toluene droplets with a diameter around 2 mm in the toluene phase was measured by a house-built Induction Timer. Toluene (100 mL) containing studied nanoparticles (10 mg) concentration was used as emulsified phase. The toluene droplet was generated and suspended from the tip of the capillary and then brought onto the hydrophobic substrate which was located at the bottom of the chamber. Another toluene droplet was then generated and suspended in the same way. The central points of the two toluene droplets were adjusted to be aligned and the vertical separation between the two centers was set at 175 μm. The measurements started after 30 min equilibrium. During the measurement, the upper toluene droplet moved downwards by 187.5 μm and the two droplets were made in contact with an overlap distance of 12.5 μm. For each experiment, 120 s is the maximum duration for one experiment. If the coalescence was not observed over this contact period, the coalescence time was considered to be greater than 120 s or the droplets stable against coalescence

*Interfacial tension measurement.* The interfacial tension of toluene-water interface adsorbed with M-Janus or M-CMC-EC nanoparticles were measured by pendant drop method using a Theta Optical (T200 Biolin Scientific). Studied nanoparticles were first dispersed in toluene (0.5 mg mL$^{-1}$) using an ultrasonic bath for 15 min. A toluene droplet containing dispersed nanoparticles with volume around 20 μL was then generated in the aqueous phase. The interfacial tension was measured at room temperature for 600 s once toluene droplets contacted with the aqueous phase. After interfacial tension measurement, a contraction force was introduced to decrease the volume of the particle-containing toluene droplets. The morphology change of toluene droplets was recorded using a high-speed camera at 30 frames per second rate.

*Interfacial pressure-area (π-A) isotherms measurement.* An interfacial Langmuir trough (KSV, Finland) was used to obtain interfacial pressure-area isotherms. Two symmetrical barriers were used to compress the oil-water interface or air-water interface. Before each experiment, barriers and mini-trough were cleaned multiple times with toluene, acetone, and water until the surface pressure changed less than 0.2 mN/m under full compression of the air-water interface with a compression rate of 30 mm/min, which were considered clean. For each experiment, DI water (120 mL) was loaded into the lower part of the compartment by pipetting, followed by placing a toluene phase (100 mL) containing different concentrations of particles on the top of the water phase. The oil-water interface was left for 30min to allow the particles to diffuse homogeneously to the oil-water interface. To transfer the nanoparticles from the oil-water interface to the substrate surface using Langmuir-Blodgett technology for SEM imaging, silicon wafers purchased from Nanofab (University of Alberta) were used as substrate. Prior to their use, they were cleaned by Expanded Tabletop Plasma Cleaner (Sigma-Aldrich). After cleaning, silicon wafers were cut to small pieces of 1 x 3 $cm^2$ used in Langmuir-Blodgett deposition.

*Dewatering process water-in-diluted crude oil emulsion.* A required amount (100 mg) of M-Janus nanoparticles were first dispersed in a tiny amount of heavy naphtha and then added into the water-in-diluted bitumen emulsions, followed by vigorous mixing using a Vortex Mixer (Thermo Fisher Scientific, MAXI MIX Plus) for 3 min. A strong hand magnet was put at the bottom of the vial for 30 min at room temperature. After settling process, the water contents at 1.0 cm from the top surface and at 0.5 cm from the bottom of the emulsions were immediately measured with Karl Fischer titrator (Cou-Lo 2000) at ambient temperature, respectively.

*Removing/Recovering oil from oily wastewater.* In each test, 150 mg M-Janus nanoparticles were first dispersed in a tiny amount of seawater or tap water and then added into the prepared oily wastewaters. The M-Janus nanoparticles together with the oily wastewaters were then vigorously mixed using a Vortex Mixer (Thermo Fisher Scientific, MAXI MIX Plus) for 3 min. A strong hand magnet was then put at the side of the wastewaters for 30 min to remove/recover the waste oil from the oily wastewaters.

The total carbon contents of the oily wastewaters before and after the introduction of the strong hand magnet were measured using TOC-L. The removal or recovery efficiency ($E_{oil}$) of oil from the oily wastewaters using M-Janus nanoparticles or M-CMC-EC nanoparticles was calculated using **Equation 3-1**:

$$E_{oil}(\%) = 100 * (C_o - C_r)/C_o \tag{3-1}$$

where $C_o$ is the original carbon content of the freshly prepared oily wastewaters and $C_r$ is the carbon content of the water after oil removal by the hand magnet. The carbon content of the detergent in the oily wastewaters was not considered because the dosage of the detergent was negligible when compared with the content of cooking oil in the oily wastewaters. The microscopy images of the oil droplets in the oily wastewaters before and after the introduction of the external magnetic field were obtained using a Zeiss optical microscope (Carl-Zeiss, Axioskop 40). To evaluate the quality of the recovered oil, the water content of the oil-rich phase was measured using a Karl Fischer titrator (Cou-Lo 2000) after oil removal/recovery.

*Recycling test.* To investigate the reusability of the spent M-Janus nanoparticles, the nanoparticles were collected using a strong hand magnet after the oil removal/recovery test, followed by simple washing with toluene and acetone three times. After drying of the M-Janus nanoparticles recycled as such in a vacuum oven at 75°C for 12 h, the interfacial properties of the recycled M-Janus nanoparticles were investigated by measuring the interfacial tension of toluene droplets in the suspension of M-Janus nanoparticles using the Theta Optical Tensiometer (T200 Biolin Sci). The M-Janus nanoparticles regenerated as such were then applied to the subsequent oil/water separation tests for evaluating their reusability.

# Chapter 4 Adsorption-Based Synthesis of Magnetically Responsive and Interfacially Active Janus Nanoparticles using Cellulosic Materials

X. He, C. Liang, Q. Liu and Z. Xu, Magnetically Responsive Janus Nanoparticles Synthesized using Cellulosic Materials for Enhanced Phase Separation in Oily Wastewaters and Water-in-crude Oil Emulsions. *Chemical Engineering Journal*, 2019, 122045.

A new class of magnetically responsive Janus (M-Janus) nanoparticles was designed and synthesized by sequential adsorption of cellulosic materials: hydrophobic ethyl cellulose (EC) and hydrophilic carboxymethyl cellulose (CMC) on the opposite sides of magnetite ($Fe_3O_4$) nanoparticles. The adsorption study using quartz crystal microbalance with dissipation monitoring (QCM-D) proved the concept of the proposed synthesis of magnetically responsive (M-Janus) nanoparticles. The adsorption of EC and CMC on magnetite nanoparticles was confirmed by zeta-potential measurements, thermogravimetric analysis (TGA), characterization using Fourier transform infrared spectroscopy (FTIR) and TEM. The surface wettabilities of the opposite sides on the M-Janus nanoparticles were investigated by measuring contact angles of nanoparticle surfaces deposited from the oil-water interfaces using the Langmuir-Blodgett method. SEM images revealed an excellent dispersion of M-Janus nanoparticles in both aqueous and organic phases. The results from the coalescence time and crumpling ratio measurement of particles-stabilized oil droplets along with the interfacial pressure-area isotherms demonstrated stronger interfacial activities of M-Janus nanoparticles and a stiffer interface with adsorbed M-Janus nanoparticles as compared with the interfaces stabilized by conventional interfacially-active nanoparticles. The microscopy images confirmed the deposition of M-Janus nanoparticles at the emulsion droplet surface during the demulsification process. The M-Janus nanoparticles not only exhibited excellent capability and high efficiency in separating emulsified water from water-in-crude oil emulsions and the oil from oily wastewaters under an external magnetic field, but also retained high interfacial activity and hence desirable separation efficiency after five-cycle applications. Because of the environmentally friendly and biodegradable cellulosic materials used in the synthesis, the M-Janus nanoparticle can process effective oil/water phase separation without causing further pollution to the continuous phase.

## 4.1 Introduction

Formation of emulsions is inevitable in various situations such as the water-in-crude oil (W/O) emulsions (water content < 5 wt%) in the petroleum-related industry and the oily wastewaters (O/W) in daily life.[85, 195] Typically, those emulsions are undesirable and even detrimental. For instance, the emulsified water phase in the crude oil emulsions can cause problems and damage the equipment of crude oil production because the dissolved salt in the aqueous phase can poison refinery catalyst and cause severe corrosions of the process equipment; while stable oil droplets in oily wastewaters can easily cause pollution on water resource.[86-87, 196-198] Therefore, the oil-water phase separation of such emulsions is necessary to remove undesirable phase in advance of the further process. Unfortunately, the oil-water phase separation of these emulsions is a well-known challenging issue due to the inherent high stability of the emulsions, resulting from the adsorption/assembly at the oil-water interface of interfacially active components such as asphaltenes in the crude oil and/or surfactants in the oily wastewaters.

Recently, various techniques have been reported for treating oily wastewaters, including oil sorption,[199-201] filtration,[86, 100, 197, 202-203] electrocoagulation,[87, 112, 204] solvent extraction[205] and coalescers.[206-207] However, each of these techniques bears inherent drawbacks, such as high cost of raw materials, low efficiency, and high energy cost in the treatment, and complicated procedures for equipment set-up.[177, 208-209] As for dewatering of the water-in-crude oil emulsions, the key point is to disturb and destroy the rigid asphaltene film, which often forms at the oil-water interface and prevents the water droplets from coalescing. In general, heating and chemical treatment are used to destabilize the water-in-crude oil emulsions. However, these methods consume too much energy, and the residual chemicals are hardly recyclable and often an environmental liability.[210] Up to date, studies regarding destabilization of water-in-crude oil emulsions have been focused mainly on breaking the elastic interfacial films using chemical demulsifiers to accelerate the coalescence of the water droplets.[211-212] Zhang *et al.* reported a commercial copolymer: ethylene oxide (EO)/propylene oxide (PO) demulsifier to soften the rigid asphaltene film.[213] Later on, an interfacially active polymer ethyl cellulose (EC) was reported by Feng *et al.* to effectively demulsify the water-in-diluted bitumen emulsions by disrupting the asphaltene film and reducing asphaltene aggregation.[127] Although asphaltene film can be destroyed by such polymeric demulsifiers, following oil-water phase separation still relied on gravitational settling, which was inefficient due to the small difference in density between water and oil phase as well as the high viscosity of the bitumen. Furthermore, conventional demulsifiers were not able to be recycled after demulsification, leading to the high cost of their applications. It is therefore highly desirable to develop a new class of demulsifiers that is not only efficient but also reusable for oil-water phase separation in the treatment of oily wastewaters and water-in-crude oil emulsions.

Recently, the magnetically responsive and interfacially active particles have attracted considerable attentions.[214-219] With the firm adsorption of such particles at the oil-water interface, undesirable phases such as the waste oil droplets in the oily wastewaters or the emulsified aqueous phase in the water-in-crude oil emulsions can be attracted, gathered and eventually removed under the external magnetic field, leaving a clean and purified phase for the further processing. For example, Mirshahghassemi *et al.* designed polymer-coated iron oxide nanoparticles to effectively collect and remove waste oil from water systems.[52] Xu *et al.* reported a kind of magnetic nanoparticles grafted with expanded perlite to adsorb oil spills from the oily wastewaters.[177] Specifically, to dewater the water-in-crude oil emulsions, functional materials such as EO/PO copolymer, ethyl cellulose, polyelectrolyte are necessarily required to effectively disrupt or disturb the asphaltene film.[42, 55, 195] The particles modified with those materials can tag the water droplets and such tagged droplets can be effectively removed under the external magnetic field. Peng *et al.* firstly reported a novel magnetic iron oxide nanoparticle grafted with interfacially active polymer ethyl cellulose (EC) using an esterification reaction.[58, 220] The magnetic iron oxide nanoparticles grafted with EC showed excellent performance in destroying aged asphaltene film and dewatering the water-in-crude oil emulsions. Later on, Pensini *et al.* reported the adsorption of hydrophilic carboxymethyl cellulose (CMC) on iron oxide substrate, which revealed the potential of CMC to be used as a connective material.[221] Recently, we investigated the strong interactions of carboxymethyl cellulose (CMC) with bare iron oxide nanoparticles and CMC with EC, which led to magnetic iron oxide nanoparticles fully covered with EC (M-CMC-EC) using convenient procedures.[56] In the procedures, the CMC was used as a bridge to directly link iron oxide particles with EC, leading to the formation of M-CMC-EC nanoparticles with EC wholly coated on the nanoparticle surfaces.[56] According to the discussions above, these magnetic nanoparticles are interfacially active, induced by homogeneous surface coatings of nanoparticles. However, such particles are sometimes found inefficient and ineffective due to the possible desorption of the particles from the interface under the influence of external magnetic force, leading to insufficient efficiency of demulsification.[222-223] Therefore, magnetic particles as demulsifiers with stronger interfacial activity are more desirable in phase separating the oily wastewaters and the water-in-crude oil emulsions under an external magnetic field.

Janus-type particles are individual particles with two opposite surface properties in one single particle such as hydrophilicity or hydrophobicity,[185, 224] negatively charged surface or positively charged surface.[225] For example, a spherical particle can have one side with hydrophilicity while another is hydrophobic. Compared with homogeneously surface-modified particles, biwettable Janus particles have better interfacial activities with stronger pinning to stabilize emulsions. They are also more difficult to desorb from the oil-water interface.[188-189] Various of Janus particles have been applied for phase separating either oily wastewaters or water-in-crude oil emulsions.[189, 191, 226] However, such Janus particles applied to the oily wastewaters are not very effective to deal with the water-in-crude oil emulsions due to the lack of functional materials for effectively disturbing or destroying asphaltene film.[189] Also, the particles workable for dewatering the water-in-crude oil emulsions are usually hard to effectively adsorbed to the oil-water interface of oily wastewaters due to the high hydrophilicity of the particles.[191, 226] Based on our previous work, EC and CMC can both attach onto iron oxide surface while having opposite wettability and EC can effectively disturb the asphaltene film. The biwettable Janus nanoparticles can be synthesized by coating hydrophilic CMC and hydrophobic EC at opposite sides of the particle surfaces. With their unique biwettability, such Janus nanoparticles are expected to have stronger interfacial properties, leading to more efficient removal of emulsified oil droplets under the external magnetic fields, as compared with M-CMC-EC nanoparticles of homogeneous wettability. Also, due to the coating of functional material EC, the interfacially active Janus nanoparticles can be applied to effectively phase separate not only the oily wastewaters but also the water-in-crude oil emulsions under an external magnetic field. Furthermore, due to the biodegradability and environmental friendliness of the cellulosic materials, such Janus nanoparticles would not cause pollution to the demulsified emulsion systems.

In this study, we report a novel magnetically responsive and interfacially active Janus (M-Janus) nanoparticle with hydrophobic EC and hydrophilic CMC coated on the opposite sides of the nanoparticle surface. Compared with the previously reported EC wholly-coated magnetic nanoparticles,[56] better interfacial properties of the M-Janus nanoparticles were investigated by measuring coalescence time using induction timer, interfacial pressure-area isotherms (π-A) using Langmuir trough and dynamic interfacial tension change of the M-Janus nanoparticles adsorbed oil-water interface. M-Janus nanoparticles were applied to effectively phase separate both of the water-in-crude oil emulsions and the oily wastewaters under an external magnetic field. The quick and efficient phase separation of such emulsions suggests potential applications of M-Janus nanoparticles to dewatering of water-in-crude oil emulsions in the heavy oil industry and removal of undesirable oil phases from the oily wastewaters. Furthermore, owing to the biocompatibility and biodegradability of the cellulosic materials used in synthesizing M-Janus nanoparticles, the M-Janus nanoparticles can effectively deal with the oily wastewaters and the water-in-crude oil emulsions without polluting the continues phase.

## 4.2 Concept of Synthesizing M-Janus Nanoparticles

As shown in **Scheme 4-1**, iron oxide nanoparticles (M) are first coated (Step I) with hydrophilic CMC by adsorption in aqueous phase through the electrostatic force and hydrogen bonding between deprotonated carboxyl groups on CMC and positively charged magnetite nanoparticle surfaces on magnetite nanoparticles to form highly dispersed and interfacially inactive hydrophilic M-CMC nanoparticles. Hydrophobic (water-insoluble) EC is then adsorbed on M-CMC nanoparticles (Step II) from EC-in-toluene solution through hydrogen bonds between EC and preadsorbed CMC to form interfacially active M-CMC-EC nanoparticles, as demonstrated in our previous study.[56] The M-CMC-EC nanoparticles have been shown to effectively stabilize oil-in-water (O/W) emulsions, which provides a practical avenue to synthesize magnetically responsive Janus particles by the Pickering emulsion method as shown in Step III. In this case, the interfacially active M-CMC-EC nanoparticles dispersed in the liquid wax phase at a slightly elevated temperature are used to form wax-in-water Pickering emulsions. After cooling the Pickering emulsion to solidify the wax droplets with M-CMC-EC nanoparticles at the wax-water interface, a desired amount of CMC is added into the emulsion (suspension) to allow the CMC adsorb from its aqueous solutions onto M-CMC-EC nanoparticle surfaces which are in contact with aqueous phase (Step III in **Scheme 4-1**). The wax particles along with hydrophilic or water wettable nanoparticles are separated from their suspension by a strong hand magnet, followed by dissolving the wax by toluene and washing also with toluene. In order to separate hydrophilic nanoparticles from M-Janus nanoparticles, the particles collected as such are used to make toluene-in-water Pickering emulsions. Only M-Janus nanoparticles could remain at the toluene-water interface with the hydrophilic nanoparticles remaining in the aqueous phase. After the creaming of the emulsions, the emulsified toluene droplets are carefully collected using a micropipette. After washing of collected droplets with acetone and toluene, we thus obtain M-Janus nanoparticles as designed. The magnetically responsive M-Janus nanoparticles synthesized as such are anticipated to have excellent interfacial properties and can effectively phase separate the oily wastewaters and the water-in-crude oil emulsions. The physicochemical properties and interfacial activities of the synthesized Janus nanoparticles are comprehensively investigated as shown below.

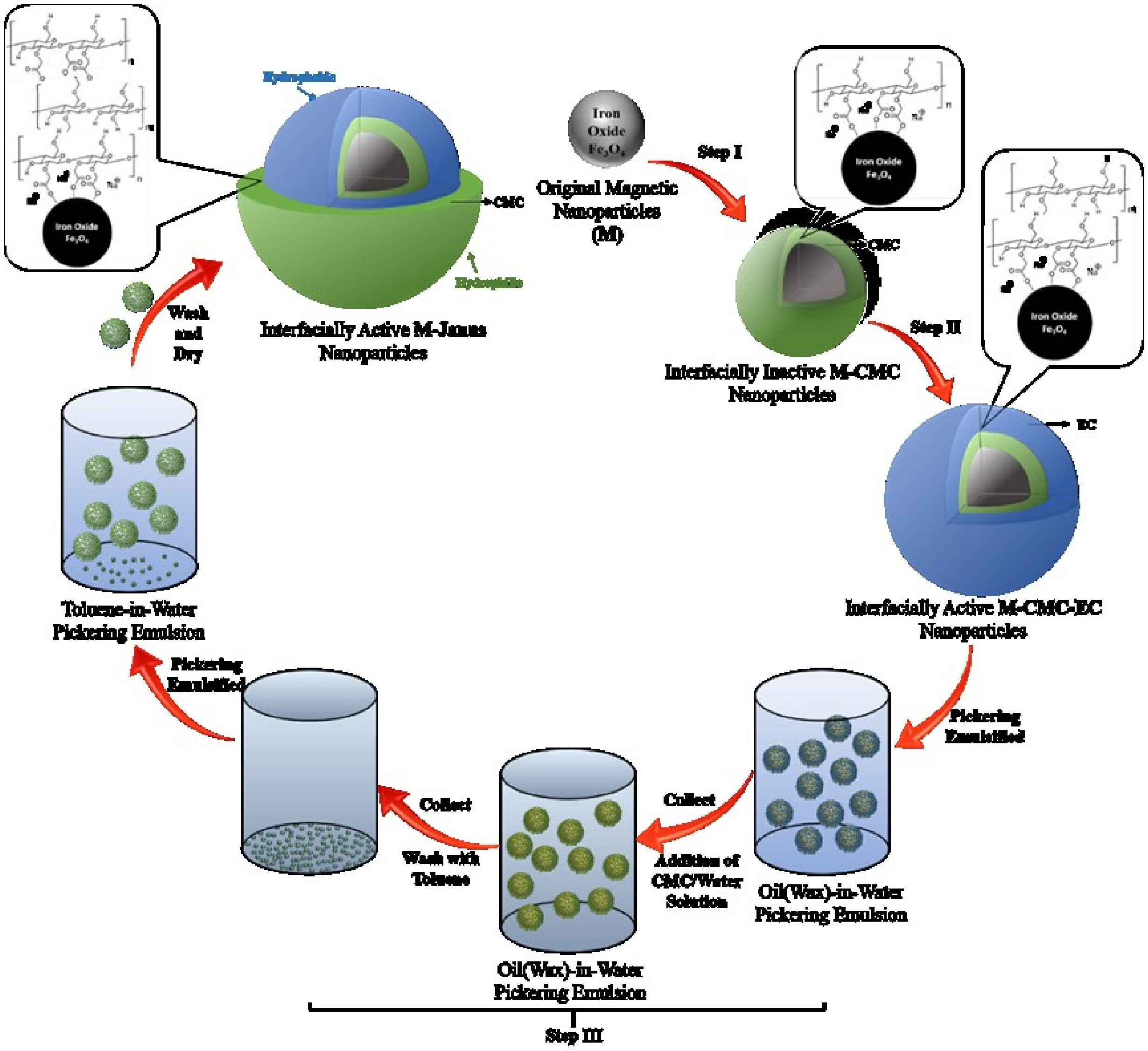

**Scheme 4-1.** Synthesis procedures of M-Janus nanoparticles

## 4.3 Results and Discussion

### 4.3.1. Evaluation and Quantitative Analysis of EC/CMC Adsorption on Iron Oxide Surface by QCM-D Studies and Wettability Measurements

To confirm the feasibility of our synthesis, QCM-D was used to investigate the sequential adsorption of EC and CMC on the iron oxide surface which is mentioned in the concept of synthesizing M-Janus nanoparticles. In this set of studies, pure deionized water was used to flow through the bare iron oxide sensor surface. After establishing a stable baseline (Adsorbing Process I) as shown in **Figure 4-2**, the flowing liquid was switched to a dilute (1.0 wt%) CMC aqueous solution at point A. In response, a significant and sharp decrease in frequency by 19.5 Hz was observed, accompanied by an increase in dissipation by 24.6 x $10^{-6}$. After reaching a dynamic adsorption equilibrium indicated by a stable frequency, the adsorbed CMC layer was washed with pure deionized water starting at point B. A significant and rapid increase by 17.5 Hz in frequency accompanied by a decrease in dissipation by 23.9 x $10^{-6}$ was observed, indicating significant desorption of loosely bound CMC from the sensor surface. Despite such significant desorption of CMC, an overall decrease in frequency by 2 Hz and an overall increase in dissipation by 0.7 x $10^{-6}$ in Adsorbing Process II were observed. The decrease in the frequency demonstrates the stable adsorption of CMC on the bare iron oxide surface, although in a small amount. The thickness and mass of the adsorbed CMC layer shown in **Table 4-1** indicate a thin CMC layer adsorbed irreversibly on the bare iron oxide sensor surface. Such thin layer adsorption of CMC on the iron oxide sensor surface possibly results from water being a perfect solvent for CMC, thus interaction between CMC and water molecule overwhelming the intermolecular forces of CMC (**Figure 4-3**). The contact angle of water decreased from 5.03 ± 0.17° on bare iron oxide surface to 1.81 ± 0.15° on CMC-adsorbed iron oxide surface, further confirming the irreversible adsorption of hydrophilic CMC on the iron oxide sensor surface. In Adsorbing Process III, toluene used as a new background medium was first injected to develop new baselines of frequency and dissipation. At point C, toluene was switched to 1 wt% EC/toluene solution, which led to a much more significant reduction in frequency by 158 Hz and an increase in dissipation by 15 x $10^{-6}$. It is evident that a significant amount of EC was adsorbed onto the CMC-primed iron oxide sensor surface. The remarkable changes in frequency and dissipation suggest a thick and massive EC layer adsorbed on the CMC-primed iron oxide sensor due to the abundant hydroxyl groups on EC which bind strongly with CMC on the iron oxide sensor surface through multiple hydrogen bonds. Once switching to toluene at point D, the adsorbed EC layer became more swollen by trapping toluene in the EC layer as indicated by the continuous increase in dissipation and the decrease in frequency. In the case of EC-CMC-coated iron oxide sensor surfaces (Inset iii, **Figure 4-2**), the contact angle was measured to be 61.17 ± 3.61°, which was consistent with the literature value for surfaces fully covered by EC.[227] To imitate the Step III in the synthesis procedure, the EC-CMC-iron oxide sensor surface was first coated with molten wax, leading to a contact angle of 112.56 ± 0.24° (**Figure 4-1a**). Then the contact angle decreased back to 58.80 ± 3.93° after washing with toluene to remove wax (**Figure 4-1b**), suggesting unchanged surface wettability of the EC-coated surface by wax coating and its removal. After drying by nitrogen gas, EC-CMC-coated iron oxide sensor was first washed with deionized water, then a dilute (1.0 wt%) CMC aqueous solution at point E, and deionized water again at point F (Adsorbing Process IV). There was apparent adsorption of CMC on EC-CMC-coated iron oxide surface which was indicated by an overall decrease in frequency by 18 Hz. It is interesting to note that the water drop on the CMC-EC-CMC-iron oxide sensor still had a contact angle of 19.41 ± 1.16° despite excellent hydrophilicity of the adsorbed CMC layer. This finding indicates an incomplete layer of CMC adsorbed on the EC-CMC-coated iron oxide sensor surface and therefore a limited exposure of the interfacially active EC layer.

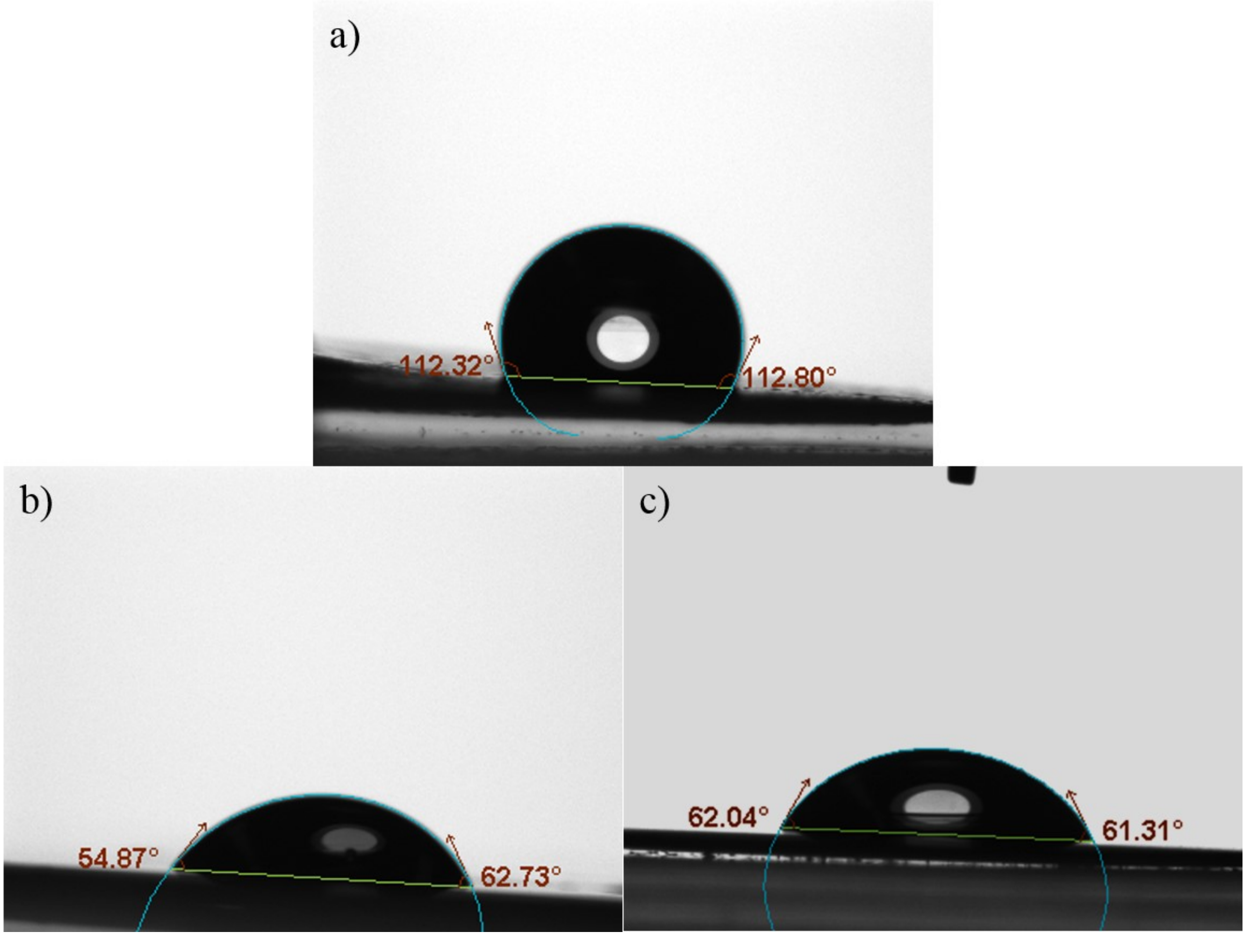

**Figure 4-1.** Contact angles of water droplets on a) wax-coated EC-CMC-iron oxide sensor surface, b) EC-CMC-iron oxide sensor surface after dissolving wax, and c) EC-iron oxide sensor surface.

The amount of EC and CMC adsorbed on the substrates was calculated by applying either the Sauerbrey equation or the viscoelastic model, depending on the ratio of dissipation change to frequency change ($\Delta D\ \Delta F^{-1}$).[228-230] The amount of CMC adsorbed was calculated to be 41 ± 6.1 ng $cm^{-2}$ on the bare iron oxide surface and dramatically increased to 260 ± 11 ng $cm^{-2}$ on the EC-CMC-iron oxide surface. Compared with direct adsorption of CMC layer on iron oxide, the CMC was adsorbed at a much higher amount and more strongly bound on the EC-CMC-coated iron oxide surfaces, indicating more stable adsorption of CMC on iron oxide surface enhanced by the pre-coated EC layer via multiple hydrogen bonds according to the FTIR results shown later.

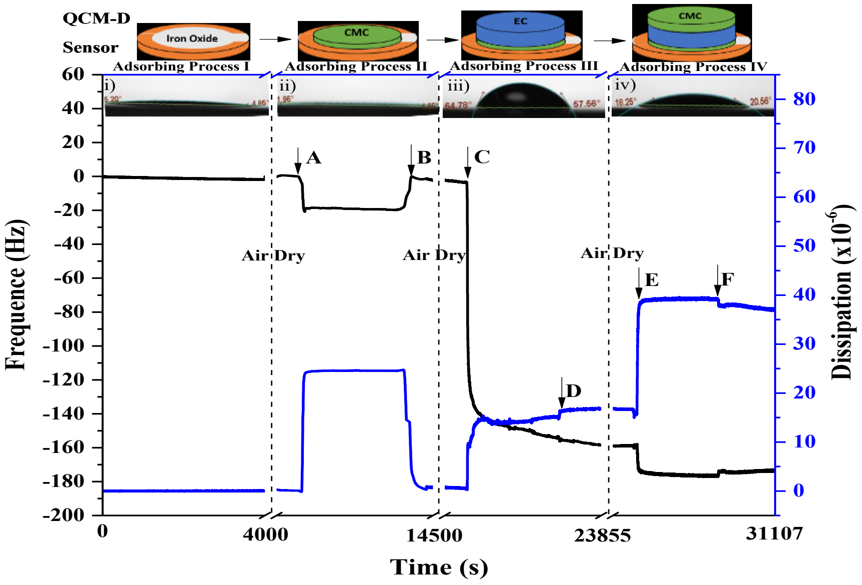

**Figure 4-2.** Change in frequency and dissipation of QCM-D sensor. The breaks and dash lines indicate sensors being taken out and dried by air. Bare iron oxide sensor surface was first run through by DI water to get a baseline (Process I); CMC was allowed to adsorb onto sensor surface by pumping a 1.0 wt% CMC aqueous solution (A) through the cell and then an enormous amount of DI water (B) was pumped through the cell to remove loosely bounded CMC on sensor surface (Process II); EC was allowed to adsorb onto CMC-adsorbed sensor surface by pumping a 1.0 wt% EC/toluene solution (C) through the cell (Process III) and then an enormous amount of toluene was pumped through the cell to remove loosely bounded EC on CMC-adsorbed sensor surface (D); in Process IV, CMC was allowed to adsorb onto EC-CMC-adsorbed sensor surface by pumping a 1.0 wt% CMC/water solution (E) through the cell and then loosely bounded CMC was removed from sensor surface by exceeding DI water (F). The insets i) to iv) show contact angles of water droplets on bare iron oxide sensor surface and cellulose-adsorbed iron oxide sensor surfaces obtained after each adsorbing process: i) bare iron oxide sensor surface, ii) CMC-adsorbed iron oxide sensor surface, iii) EC-CMC-adsorbed iron oxide sensor surface and iv) CMC-EC-CMC-adsorbed iron oxide sensor surface.

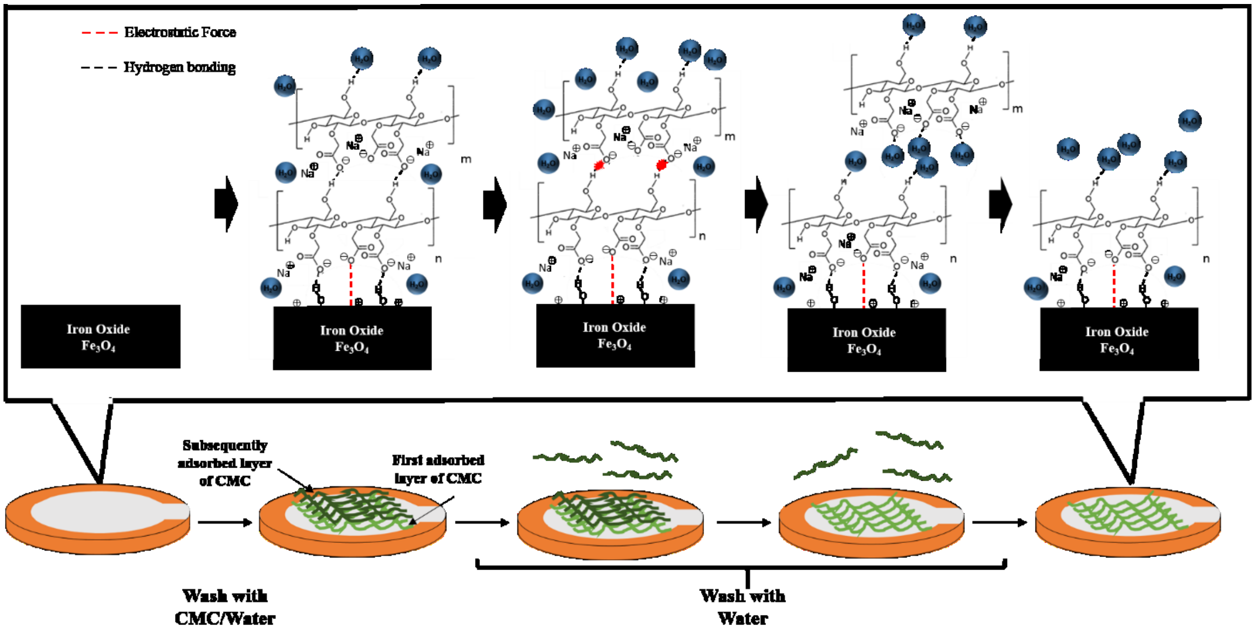

**Figure 4-3.** Schematic illustration of single CMC layer adsorbed on iron oxide sensor surface via hydrogen bonding and attractive electrostatic force.

The enhanced adsorption of EC on CMC-iron oxide surfaces was also observed. With a tiny amount of CMC adsorbed on bare iron oxide sensor surfaces, the adsorption of EC increased from 1990 ± 120 ng cm$^{-2}$ on bare iron oxide sensor surface to 2600 ± 240 ng cm$^{-2}$ on CMC-iron oxide sensor surface (**Figure 4-4**). Meanwhile, the thickness of the adsorbed EC layer remained the same for both cases, suggesting a more compact structure of EC layer on CMC-iron oxide surfaces than on bare iron oxide surfaces and strong adsorption by multiple binding through hydrogen bonds between EC and CMC. In Adsorbing Process IV, CMC remained more on the EC-CMC-coated sensor surfaces after washing with DI water as compared with a small amount of CMC remained on bare iron oxide surfaces, confirming the strong interactions between the celluloses and ensuring the successful CMC coating on M-CMC-EC nanoparticle surfaces in Step III.

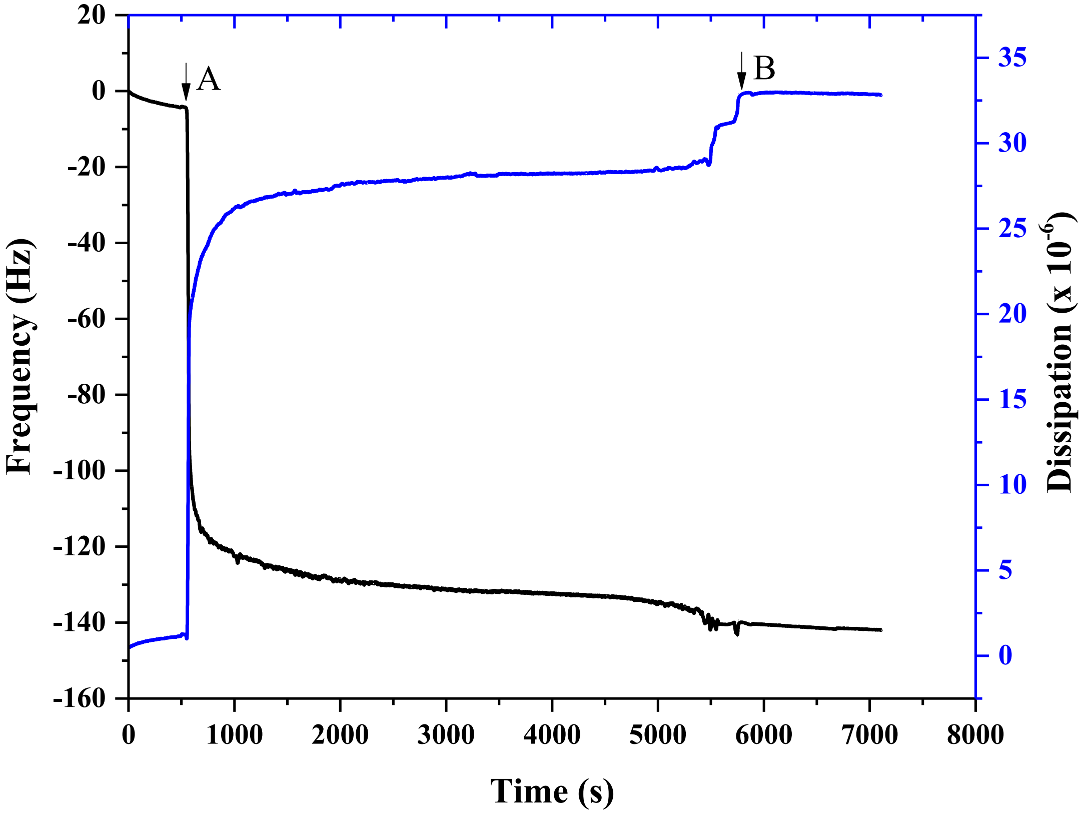

**Figure 4-4.** Change in frequency and dissipation of the QCM-D sensor. Bare iron oxide sensor surface was first cleaned by toluene to get a baseline and then EC was allowed to adsorb onto bare iron oxide sensor surface by pumping a 1 wt% EC/toluene solution (A) through the cell. To remove loosely bounded EC on sensor surface, toluene was again pumped (B) through the cell.

### 4.3.2 Characterization of M-Janus Nanoparticles

#### 4.3.2.1 Physicochemical and Colloidal Properties of Magnetic M-Janus Nanoparticles

The morphology and structure of bare iron oxide nanoparticles, M-CMC nanoparticles, M-CMC-EC nanoparticles, and M-Janus nanoparticles were characterized using a transmission electron microscope with the corresponding micrographs being shown in **Figure 4-5 a-d**. Compared with the bare iron oxide nanoparticles (**Figure 4-5a**), no visible cellulose films were observed on the M-CMC nanoparticle surfaces (**Figure 4-5b**). Such observation is reasonable as the CMC on bare iron oxide surface is ultra-thin as revealed by the QCM-D results. After the massive adsorption of EC onto the M-CMC nanoparticle surfaces, a thin and homogeneous layer with a thickness of 2.35 ± 0.39 nm was observed on the M-CMC-EC nanoparticle surfaces (**Figure 4-5c**), confirming the adsorption of EC layer. It is interesting to note that the thickness of the EC layer shown in the TEM image is thinner than the thickness determined using *in situ* QCM-D method. The smaller value in the thickness of EC film determined from TEM than from *in situ* QCM-D is a result of film shrinking after drying out the organic solvent trapped in the swelling EC film. Such change corresponds well with the results from TGA measurement (**Table 4-2** and **4-3**). In **Figure 4-5d**, the cellulose films on the M-Janus nanoparticle surfaces were found heterogenous, indicated by an asymmetric thickness of the adsorbed layer on the opposite sides of the M-Janus nanoparticles, which results from the adsorption of CMC on the partially exposed M-CMC-EC nanoparticle as described in Step III of the synthesis procedure.

**Figure 4-6** shows the scanning electron microscopy (SEM) images of bare iron oxide nanoparticles, M-CMC nanoparticles, M-CMC-EC nanoparticles, and M-Janus nanoparticles in either aqueous phase or organic phase. As shown in **Figure 4-6a**, bare iron oxide nanoparticles formed agglomerations in the aqueous phase due to insufficient electrostatic forces between the particles despite the positive surface charge of 21.8 mV.[231] After the adsorption of CMC on the iron oxide nanoparticle surfaces, M-CMC nanoparticles became highly dispersed in the aqueous phase as shown in **Figure 4-6b** as a result of the strong electrostatic repulsive force enhanced by the adsorbed CMC layers, as indicated by a negative zeta potential of -45.6 mV. However, severe aggregations of M-CMC nanoparticles were observed in the organic phase, as shown in **Figure 4-**

**6c**. The formation of such aggregates results from van der Waals forces since there is no electrostatic repulsion and only a negligible steric repulsion between hydrophilic CMC in the organic solvent. With the subsequent adsorption of EC on the M-CMC nanoparticle surfaces, M-CMC-EC nanoparticles became highly dispersed again in the organic phase due most likely to steric repulsion between highly solvated chains of EC in the good solvent of toluene as reported in early studies (**Figure 4-6d**).[56]

**Table 4-1.** Amount of ethyl cellulose and carboxymethyl cellulose adsorbed on iron oxide sensor surfaces.

| Sequence of Adsorption[a] | Thickness of Adsorbed Layer (nm) | Mass of Adsorbed Layer (ng cm$^{-2}$) | Contact Angle (degree)[b,c] |
|---|---|---|---|
| 1 wt% CMC/Water | < 1.0 | 41 ± 6.1 | 1.81 ± 0.15° |
| 1 wt% EC/Toluene | 21 ± 2.0 | 1990 ± 120 | 61.68 ± 0.37° |
| 1 wt% CMC/Water + | < 1.0 | 41 ± 6.1 | 1.81 ± 0.15° |
| 1 wt% EC/Toluene + | 19 ± 4.7 | 2600 ± 240 | 61.17 ± 3.61° |
| 1 wt% CMC/Water | 3.0 ± 1.1 | 260 ± 11 | 19.41 ± 1.16° |
| Wax on EC-coated surface<br>+<br>Wax Dissolving | N/A | N/A | 112.56 ± 0.24°<br>58.80 ± 3.39° |

[a] Ethanol was used to transition from organic solution to aqueous solution and from aqueous solution to organic solution

[b] The water droplet on the bare iron oxide surface had a contact angle of 5.03 ± 0.17°

[c] The image of the water droplet on EC-iron oxide surface is shown in **Figure 4-1c**

**Table 4-2.** Specific surface area of bare iron oxide nanoparticles and synthesized nanoparticles determined using BET method.

| Sample | BET (m$^2$ g$^{-1}$) |
|---|---|
| M | 16.28 |
| M-CMC | 15.78 |
| M-CMC-EC | 15.55 |
| M-Janus | 14.39 |
| M-CMC-EC-CMC | 13.33 |

**Table 4-3.** Adsorption density (ADcal) calculated from TGA results and determined using QCM-D method ($AD_{QCM\text{-}D}$) of the cellulosic materials on studied nanoparticle surfaces.

| Adsorbed Cellulose Films | QCM-D | M | M-CMC | M-CMC-EC | M-Janus | M-CMC-EC-CMC |
|---|---|---|---|---|---|---|
| | $AD_{QCM\text{-}D}$ ($10^{-5}$g m$^{-2}$) | $AD_{cal}$ ($10^{-5}$g m$^{-2}$) | $AD_{cal}$ ($10^{-5}$g m$^{-2}$) | $AD_{cal}$ ($10^{-5}$g m$^{-2}$) | $AD_{cal}$ ($10^{-5}$g m$^{-2}$) | $AD_{cal}$ ($10^{-5}$g m$^{-2}$) |
| CMC$^{1st}$ | 41 ± 6.1 | N/A | 38.7 ± 23.3 | 38.7 ± 23.3 | 38.7 ± 23.3 | 38.7 ± 23.3 |
| EC | 2600 ± 240 | N/A | N/A | 325.1 ± 22.8 | 325.1 ± 22.8 | 325.1 ± 22.8 |
| CMC$^{2nd}$ | 260 ± 11 | N/A | N/A | N/A | N/A | 222.6 ± 50.8 |

In contrast, M-CMC-EC nanoparticles became severely aggregated in the aqueous phase as shown in **Figure 4-6e**, due most likely to attractive hydrophobic forces between hydrophobic EC layers on M-CMC nanoparticles despite electrostatic repulsion between the charged surfaces of -21.5 mV.[232-233] The negative surface charge stems from the ionization of hydroxyl groups on EC, compounded by limited carboxylic groups of CMC that were not fully shielded by incomplete coverage of EC. Since this zeta potential value is similar to the zeta potential value of -18.3 mV for M-EC nanoparticles, the negative surface charge could be considered to arise mainly from the ionization of hydroxyl groups on EC, compounded by limited carboxylic groups of CMC that were not fully shielded by incomplete coverage of EC. The small difference in zeta potentials between M-CMC-EC nanoparticles and M-EC nanoparticles could be attributed to a less amount of EC and hence less amount of hydroxyl groups on M-EC nanoparticles than on M-CMC-EC nanoparticles as revealed in the QCM-D results. In our QCM-D study, EC was shown to be adsorbed on bare iron oxide surfaces at a much less amount than on CMC-primed iron oxide surfaces, translating to a less amount of hydroxyl ions on M-EC nanoparticles and therefore presenting a less negative zeta potential of the M-EC nanoparticles. Due to the coating of the EC layer, the M-EC nanoparticles and the M-CMC-EC nanoparticles exhibited similar dispersion. (**Figures 4-7a** and **4-7b**). M-Janus nanoparticles had an intermediate negative zeta potential of -31.1 mV which is between the zeta potential values of M-CMC nanoparticles (-45.6 mV) and M-CMC-EC nanoparticles (-21.5 mV), suggesting a successful but partial coating of CMC on M-CMC-EC nanoparticle surfaces (~50%). Compared with the M-CMC-EC nanoparticles, M-Janus nanoparticles exhibited improved dispersion in both the aqueous phase and organic phase due to the steric repulsion and sufficient electrostatic repulsion provided by EC and CMC, respectively (**Figures 4-6g** and **4-6h**). The satisfied dispersion of M-Janus nanoparticles in either organic or aqueous phase allows the formation of a single-particle layer at the oil-water interface, leading to better interfacial properties which are shown later by the measured coalescence time and interfacial pressure-area isotherms. To further confirm the formation of M-Janus nanoparticles, the zeta potential of M-CMC-EC-CMC nanoparticles was measured to be -39.6 mV, which is close to the zeta potential of M-CMC nanoparticles. Furthermore, both M-CMC and M-CMC-EC-CMC nanoparticles were highly aggregated in the organic solvent as shown in **Figures 4-7c** and **Figure 4-7d**, respectively, in contrast to good dispersion of M-Janus nanoparticles. The results of zeta potential measurement described here provide direct evidence on the successful coating of cellulosic materials on the particle surfaces in each synthesis step as described in **Scheme 4-1** and revealed by QCM-D experiments.

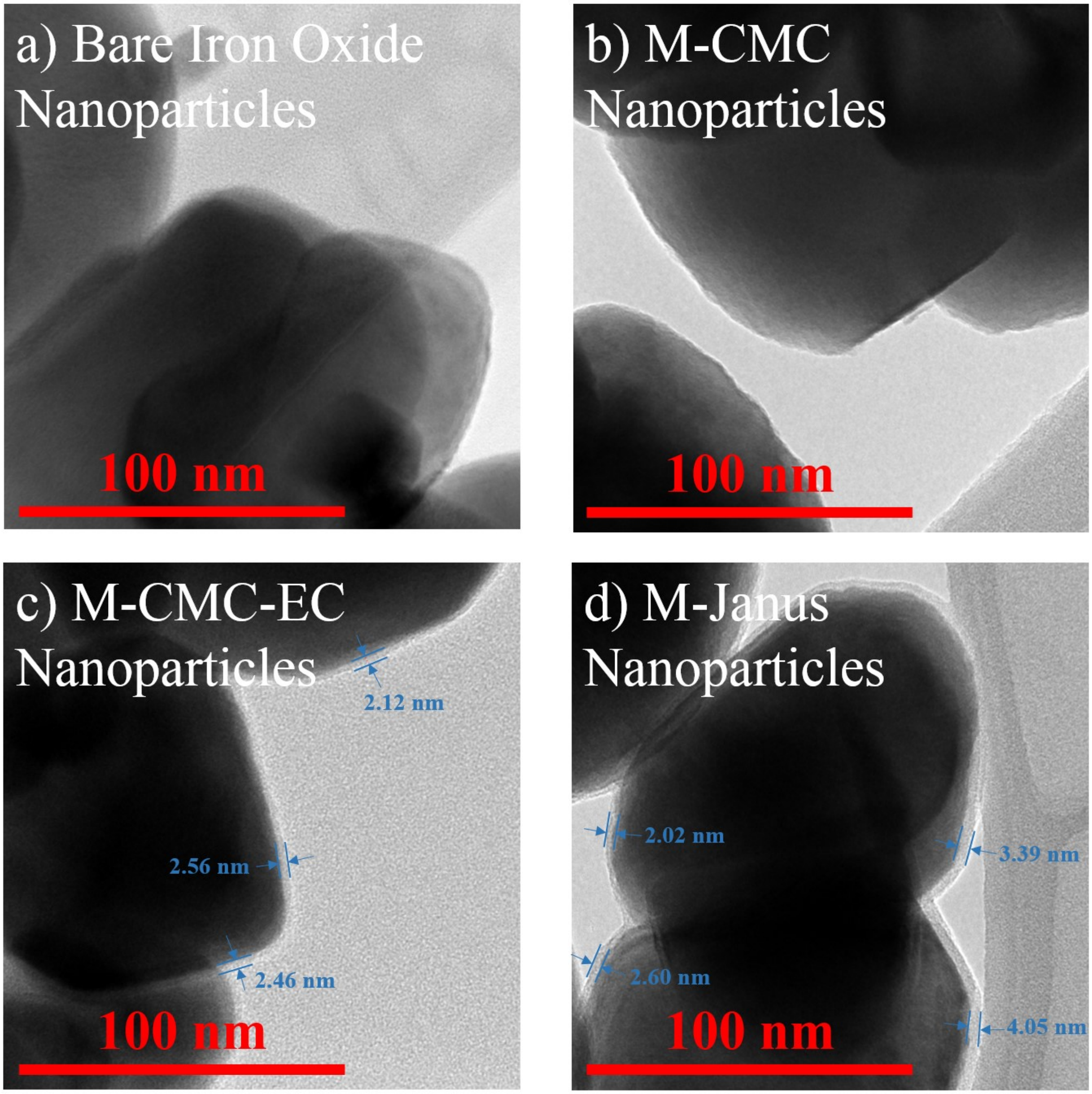

**Figure 4-5.** Transmission electron microscopy images of different nanoparticles synthesized in each synthesizing stage: a) bare iron oxide (M) nanoparticles, b) M-CMC nanoparticles, c) M-CMC-EC nanoparticles, and d) M-Janus nanoparticles.

The amount of cellulosic materials coated on magnetite nanoparticles was determined by thermogravimetric analysis (TGA). The results are shown in **Figure 4-8a** and **Table 4-4**. There is a 0.30 ± 0.24% weight loss from the bare iron oxide nanoparticles, possibly due to the removal of associated water.[234] The M-CMC nanoparticles only had a total weight loss of 0.93 ± 0.15 %, in which only 0.63 ± 0.39% of the weight loss resulted from the adsorbed CMC on the M-CMC nanoparticle surfaces. This result indicates a limited amount of CMC adsorbed directly on iron oxide nanoparticles, which agrees well with the results of QCM-D studies. The M-CMC-EC nanoparticles showed a much higher weight loss of 6.06 ± 0.21%, confirming successful adsorption of EC on CMC-primed nanoparticle surfaces. With subsequent adsorption of CMC on M-CMC-EC nanoparticles, M-Janus nanoparticles had a weight loss of 7.80 ± 0.29%, indicating a weight loss of 1.74 ± 0.50% for subsequent adsorption of CMC in the case of M-Janus nanoparticles. In contrast, a total weight loss of 9.52 ± 0.19 % was observed for M-CMC-EC-CMC nanoparticles, with the total amount of CMC on M-CMC-EC-CMC being 4.09 ± 0.79%. This result confirms not only the enhanced coating of CMC on EC surfaces but also the partial coating of CMC for the case of M-Janus nanoparticles.

It is interesting to note that the adsorption density calculated from TGA results (**Table 4-2** and **4-3**) is smaller than the value determined using *in situ* QCM-D due to the mass solvent trapped in the adsorbed cellulose films that was not involved in the TAG measurement QCM-D. The similar observations that mass of solvent trapped in the cellulose film varies from the adsorbed layer structure, leading to the difference between the QCM-D results and the results calculated from surface plasmon resonance (SPR) were reported in open literature.[235-236] For pure cellulosic materials, almost complete decomposition of EC was observed at around 330 $^{\circ}$C while the continuous decomposition of CMC was observed during the heating, confirming the weight loss of synthesized nanoparticles from the decomposition of cellulosic materials.

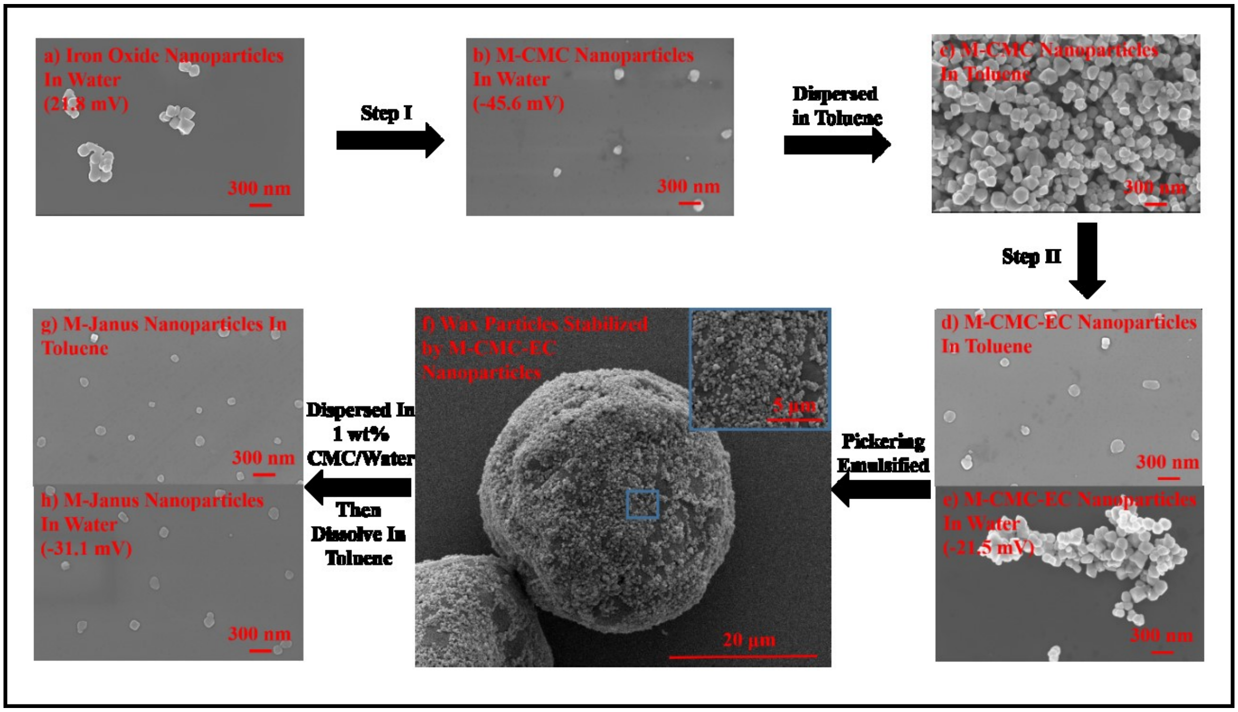

**Figure 4-6.** Field-emission scanning electron microscopy images of nanoparticles in each synthesizing stage: iron oxide nanoparticles in water (a); M-CMC nanoparticles in water (b) and in toluene (c); M-CMC-EC nanoparticles in toluene (d) and in water (e); wax spheres stabilized by M-CMC-EC nanoparticles (f); and M-Janus nanoparticles in toluene (g) and in water (h).

**Table 4-4.** Total weight loss of nanoparticles with and without adsorption of different cellulosic materials (CMC and/or EC).

| Property [a] | M | M-CMC | M-CMC-EC | M-Janus | M-CMC-EC-CMC |
|---|---|---|---|---|---|
| Weight Loss (wt%) | 0.30 ± 0.24 | 0.93 ± 0.15 | 6.06 ± 0.21 | 7.80 ± 0.29 | 9.52 ± 0.19 |
| CMC content (wt%) | N/A | 0.63 ± 0.39 | 0.63 ± 0.39 | 2.37 ± 0.89 | 4.09 ± 0.79 |
| EC content (wt%) | N/A | N/A | 5.13 ± 0.36 | 5.13 ± 0.36 | 5.13 ± 0.36 |

[a] Estimated using thermogravimetric analysis;

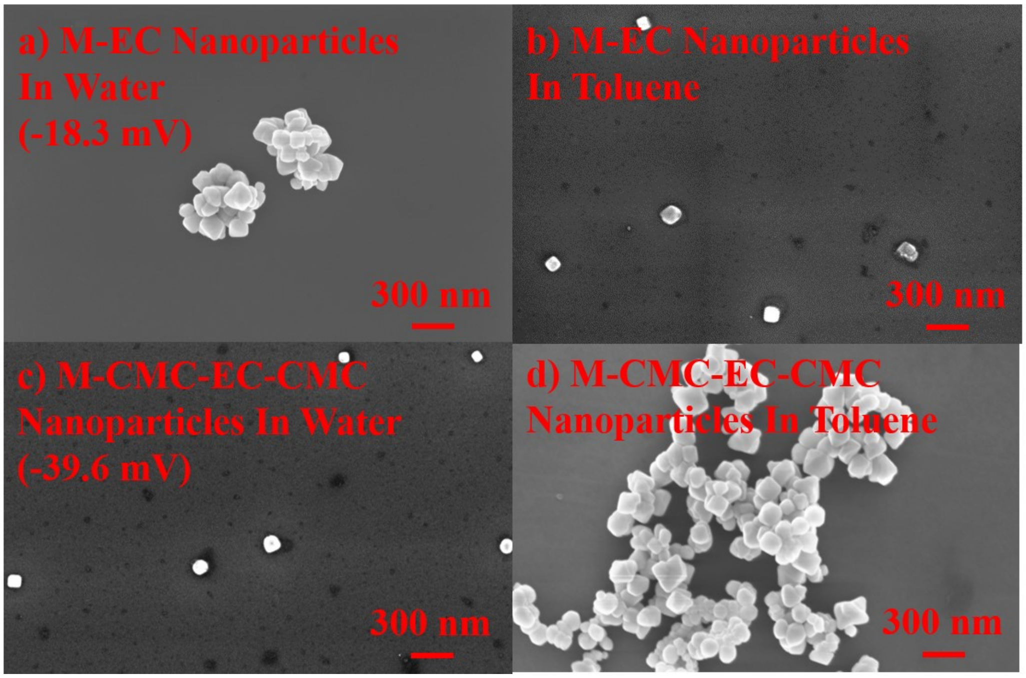

**Figure 4-7.** Field-emission scanning electron microscopy images: M-EC nanoparticles in water (a) and toluene (b); M-CMC-EC-CMC nanoparticles in water (c) and toluene (d). The zeta potentials of synthesized nanoparticles are shown inside the microscopy images.

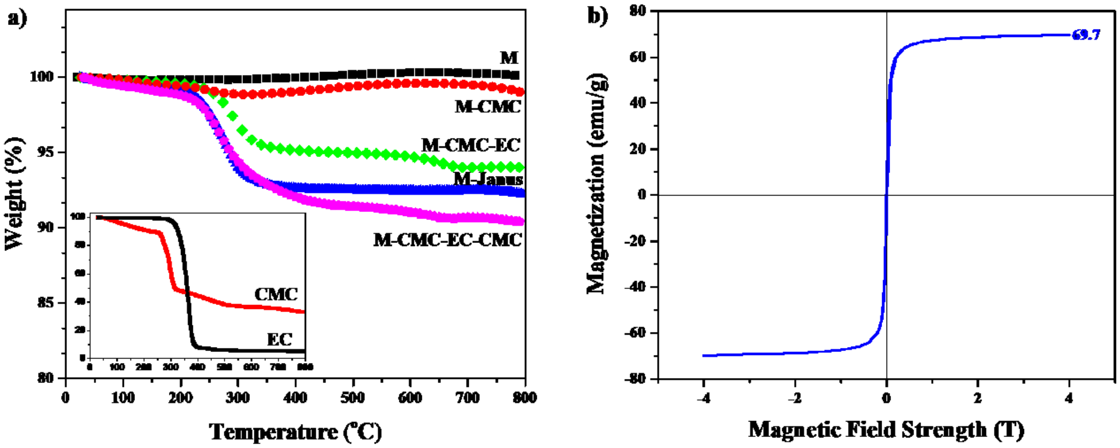

**Figure 4-8.** a) Weight loss of cellulose on iron oxide heated at a rate of 10 °C/min in 60 ml/min nitrogen flow. The inset shows the weight loss of pure celluloses during heating process. b) Magnetization hysteresis loop of M-Janus nanoparticles.

The high saturation magnetization of the M-Janus nanoparticles is essential to achieve efficient separation of the oily wastewaters and the water-in-crude oil emulsions using magnetically responsive Janus nanoparticles under an external magnetic field. As shown in **Figure 4-8b**, the M-Janus nanoparticles had a saturation magnetization of 69.7 emu/g, which is sufficiently strong to be collected using a strong hand magnet. Compared with previously reported M-CMC-EC nanoparticles which had a saturation magnetization of 71 emu/g,[56] the M-Janus nanoparticles showed a smaller saturation magnetization, resulting from the non-magnetic CMC coated on the M-CMC-EC nanoparticle surfaces and therefore confirming the results of QCM-D and TGA measurement.

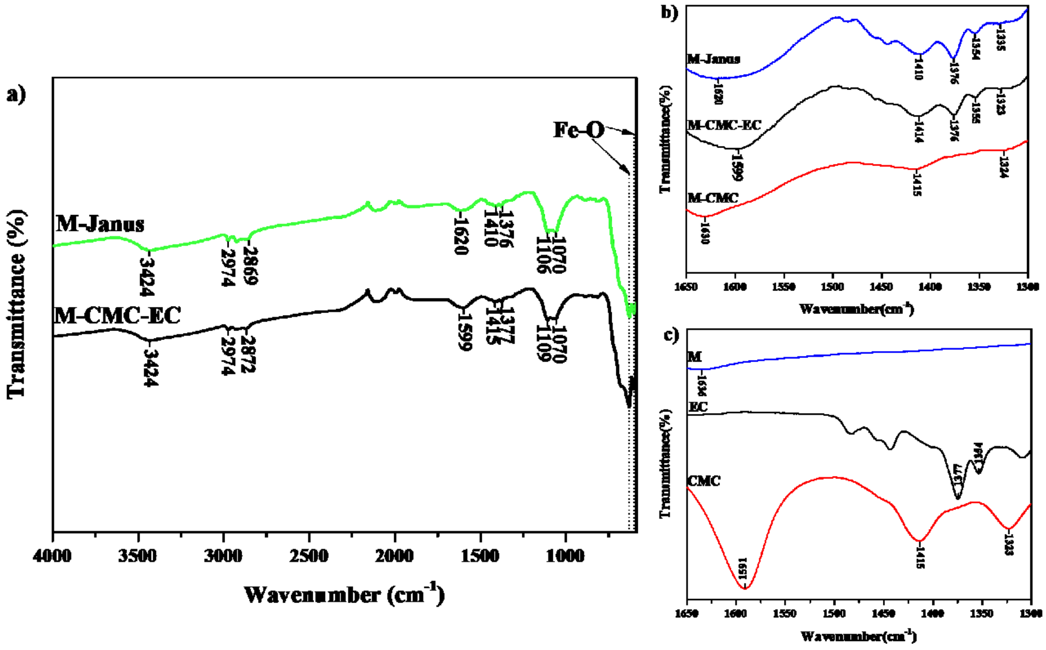

**Figure 4-9.** a) FTIR spectra of M-Janus nanoparticles, and M-CMC-EC nanoparticles; b) narrow scan FTIR spectra of M-Janus nanoparticles, M-CMC-EC nanoparticles, M-CMC nanoparticles indicating the coating of celluloses on synthesized nanoparticle surfaces; c) narrow scan FTIR spectra of raw materials used for synthesizing M-Janus nanoparticles with M representing original magnetite ($Fe_3O_4$) nanoparticles.

The characteristic peaks of Fe-O were observed on the spectra (**Figure 4-9a**) for both M-Janus and M-CMC-EC nanoparticles, as shown by the bands at 630 cm$^{-1}$ and 600 cm$^{-1}$. For the spectrum of pure CMC (**Figure 4-9c**), the existence of carboxyl groups on CMC is proved by the strong peak at 1591 cm$^{-1}$, which is a characteristic peak of –COOH functional group. Furthermore, bands at 1415 cm$^{-1}$ and 1323 cm$^{-1}$ are attributed to the in-plane stretching vibration of –OH groups and stretching vibration of C-H on CMC, respectively. As shown in **Figure 4-9b**, weak bands at 1415 cm$^{-1}$ and 1324 cm$^{-1}$ were observed in the spectrum of M-CMC nanoparticles, indicating the successful coating of CMC onto iron oxide nanoparticles. Meanwhile, the previous band at 1591 cm$^{-1}$ disappeared in the spectrum of M-CMC nanoparticles, accompanied by the appearance of a new band at 1630 cm$^{-1}$. Such phenomena result from the binding of carboxyl groups on CMC with iron oxide nanoparticle surfaces. The bands at 1376 cm$^{-1}$ and 1355 cm$^{-1}$ in the spectrum of M-CMC-EC nanoparticles and the bands at 1376 cm$^{-1}$ and 1354 cm$^{-1}$ in the spectrum of M-Janus nanoparticles confirm the successful grafting of EC on these two kinds of nanoparticles. Compared with the spectrum of M-CMC nanoparticles, the characteristic peak of –COOH functional groups shifted from 1630 cm$^{-1}$ to 1599 cm$^{-1}$ in the spectrum of M-CMC-EC nanoparticles, resulting from the hydrogen bonds between EC and M-CMC nanoparticles. It is obvious to find that the original band at 1599 cm$^{-1}$ in M-CMC-EC nanoparticle's spectrum disappeared after coating CMC onto M-CMC-EC nanoparticles, accompanied by the appearance of the band at 1620 cm$^{-1}$ in M-Janus nanoparticle's spectrum, confirming the formation of hydrogen bonds between the CMC and EC sequentially adsorbed on iron oxide in the M-CMC-EC nanoparticles.

#### 4.3.2.2 Interfacial Properties of M-Janus Nanoparticles

The interfacial properties of the nanoparticles obtained in each synthesis step were investigated by measuring the coalescence time of particle-loaded droplets using a house-built induction timer.

The results in **Table 4-5** show the immediate coalescence of toluene droplets in the aqueous phase. Similar situations were observed for toluene droplets containing well-dispersed bare iron oxide nanoparticles or M-CMC nanoparticles, indicating the interfacial inactive nature of those nanoparticles. Interestingly, despite the hydrophilic CMC layer coated on the nanoparticle surfaces, the M-CMC-EC-CMC nanoparticles showed a negligible increase in the coalescence time by 1.2 ± 0.7 s, as shown in **Figure 4-10** as well as **Table 4-5**. This finding suggests a weak interfacial activity of the M-CMC-EC-CMC nanoparticles, resulting from partial exposure of interfacially active EC layer beneath the incomplete coating of CMC on M-CMC-EC particles. For M-CMC-EC nanoparticles, a coalescence time of 19.2 ± 5.23 s was observed as shown in **Figure 4-10**, indicating the interfacial activity of M-CMC-EC nanoparticles as anticipated. In contrast, the coalescence time of toluene droplets stabilized by the M-Janus nanoparticles increased dramatically to 65.1 ± 4.60 s as shown in **Figure 4-10**, indicating a much stronger interfacial activity of M-Janus nanoparticles as compared with M-CMC-EC nanoparticles as highly desired for our objectives. The results clearly show that M-CMC-EC-CMC nanoparticles, M-CMC nanoparticles, and bare iron oxide nanoparticles cannot act as stabilizers for O/W Pickering emulsions due to their nature of inactive interfacial properties. Compared with those interfacially inactive nanoparticles, the interfacially active M-CMC-EC nanoparticles and M-Janus nanoparticles could effectively partition at the oil-water interface and stabilize the oil droplets in the aqueous phase due to the coating of interfacially active EC on the nanoparticle surfaces. In particular, the M-Janus nanoparticles with their unique Janus structure and superior interfacial activity remarkably increased the coalescence time of the emulsified toluene droplets, resulting from the more stable occupation of such nanoparticles at the oil-water interface.

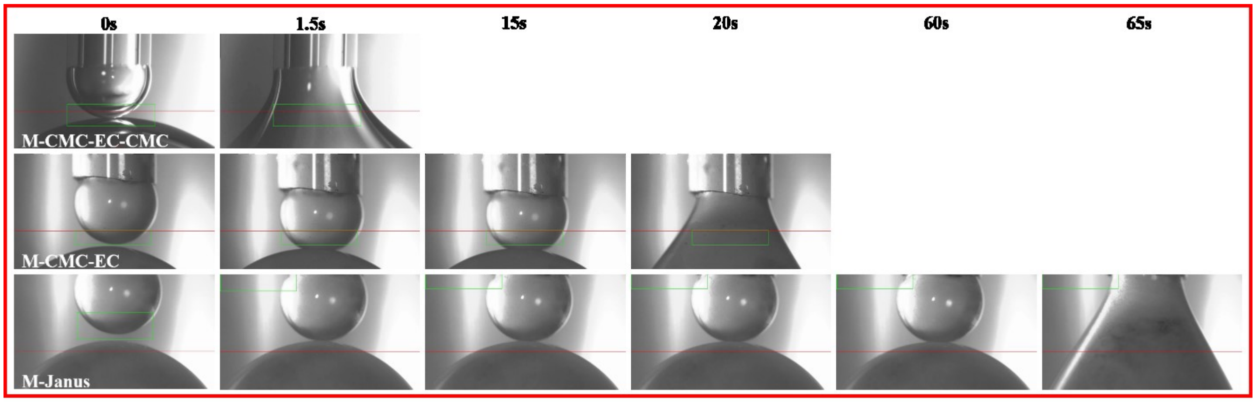

**Figure 4-10.** Snapshots for the coalescence process of toluene droplets stabilized by M-CMC-EC-CMC nanoparticles, M-CMC-EC nanoparticles or M-Janus nanoparticles in aqueous phase.

**Table 4-5.** Coalescence time of toluene droplets stabilized by different synthesized nanoparticles in aqueous phase.

| Particles | Coalescence Time (s) |
|---|---|
| Iron oxide nanoparticles | 0 |
| M-CMC nanoparticles | 0 |
| M-CMC-EC nanoparticles | 19.20 ± 4.71 |
| M-Janus nanoparticles | 65.10 ± 4.60 |
| M-CMC-EC-CMC nanoparticles | 1.20 ± 0.70 |

To reveal the mechanism of M-CMC-EC nanoparticles and M-Janus nanoparticles in stabilizing the emulsified oil droplets, a Theta Optical Tensiometer (T200 Biolin Scientific) combined with pendent drop method were used to measure the interfacial tension and the crumpling ratio of the particle-stabilized toluene droplet suspended in the aqueous phase.[237] The toluene droplets containing either dispersed M-Janus nanoparticles or M-CMC-EC nanoparticles were used as the drop phase while pure deionized water was used as the continuous phase. The crumpling behavior measurement was introduced right after the interfacial tension measurement by continuously contracting the volume of the toluene droplet. The continuous contraction would result in an poorly compressible toluene-water interface due to the particle network at the interface, which could be visualized by the visible crumpling.[238]

A crumpling ratio (CR) (**Equation 4-1**)was introduced to evaluate the degree of crumpling behavior. A higher crumpling ratio indicates a more rigid and poorly compressible toluene-water interface:

$$CR = \frac{A_c}{A_i} = \frac{\pi {r_c}^2}{\pi {r_i}^2} = \frac{{r_c}^2}{{r_i}^2} \tag{4-1}$$

In **Equation 4-1**, $A_c$ and $r_c$ are the projected area and radius of the droplet right before the visible crumpling while $A_i$ and $r_i$ are the projected area and radius of the initial droplet, respectively. **Figure 4-11a** shows the dynamic interfacial tension of the toluene-water interface. The interfacial tension of the clean toluene-water interface was 37.4 mN $m^{-1}$. With the adsorption of M-CMC-EC nanoparticles or M-Janus nanoparticles at the toluene-water interface, the dynamic interfacial tension decreased sharply at first and stabilized finally at 15.92 mN $m^{-1}$ and 13.09 mN $m^{-1}$, respectively. This finding indicates the adsorption of interfacially active nanoparticles at the toluene-water interface and suggests a stronger interfacial activity of M-Janus nanoparticles as compared with M-CMC-EC nanoparticles. Interestingly, when compared with the M-CMC-EC nanoparticles, a more rapid decrease in dynamic interfacial tension was observed for the case of M-Janus nanoparticles, indicating stronger adsorption of M-Janus nanoparticles than M-CMC-EC nanoparticles at the toluene-water interface. During the contracting process, the crumpling behaviors of the particle-stabilized toluene droplets were visualized for both cases, indicating the formation of rigid skins on the droplets stabilized by the interfacially active nanoparticles. By analyzing the contracting process frame by frame, the crumpling ratio of M-Janus nanoparticle-stabilized toluene droplet was calculated to be 0.18 ± 0.03 which is much higher than the case of

M-CMC-EC nanoparticles (0.11 ± 0.02), suggesting a more rigid and poorer compressible interface with the adsorption of M-Janus nanoparticles. The more rigid toluene droplet loaded with M-Janus nanoparticles led to a longer coalescence time as shown in the coalescence time measurement.

To further understand the interfacial activity of the synthesized nanoparticles, the Langmuir-Blodgett technique was applied to study the M-CMC-EC nanoparticles, the M-CMC-EC-CMC nanoparticles and the M-Janus nanoparticles at the toluene-water interface. As shown in Figure **4-11b**, a baseline of pure deionized water and pure toluene was set to confirm that the interfacial pressure of the clean toluene-water interface is independent of the change in the interfacial area. With the adsorption of studied nanoparticles at the interface, slight increase in the interfacial pressure at full trough area was observed except for the case of M-CMC-EC-CMC nanoparticles, indicating that the amount of the interfacially active nanoparticles adsorbed at the toluene-water interface is sufficient to affect the interfacial pressure and that the M-CMC-EC-CMC nanoparticles are interfacially inactive. The pressure-area isotherms in **Figure 4-11b** show that the interface adsorbed with the M-Janus nanoparticles features the highest interfacial pressure as compared with other nanoparticles, suggesting the strongest interfacial activity of the M-Janus nanoparticles among the studied nanoparticles. For the toluene-water interface partitioned with M-Janus nanoparticles of lower particle concentrations, more compressed interfacial pressure-area isotherms of such toluene-water interfaces were observed, as shown in **Figure 4-11c**.

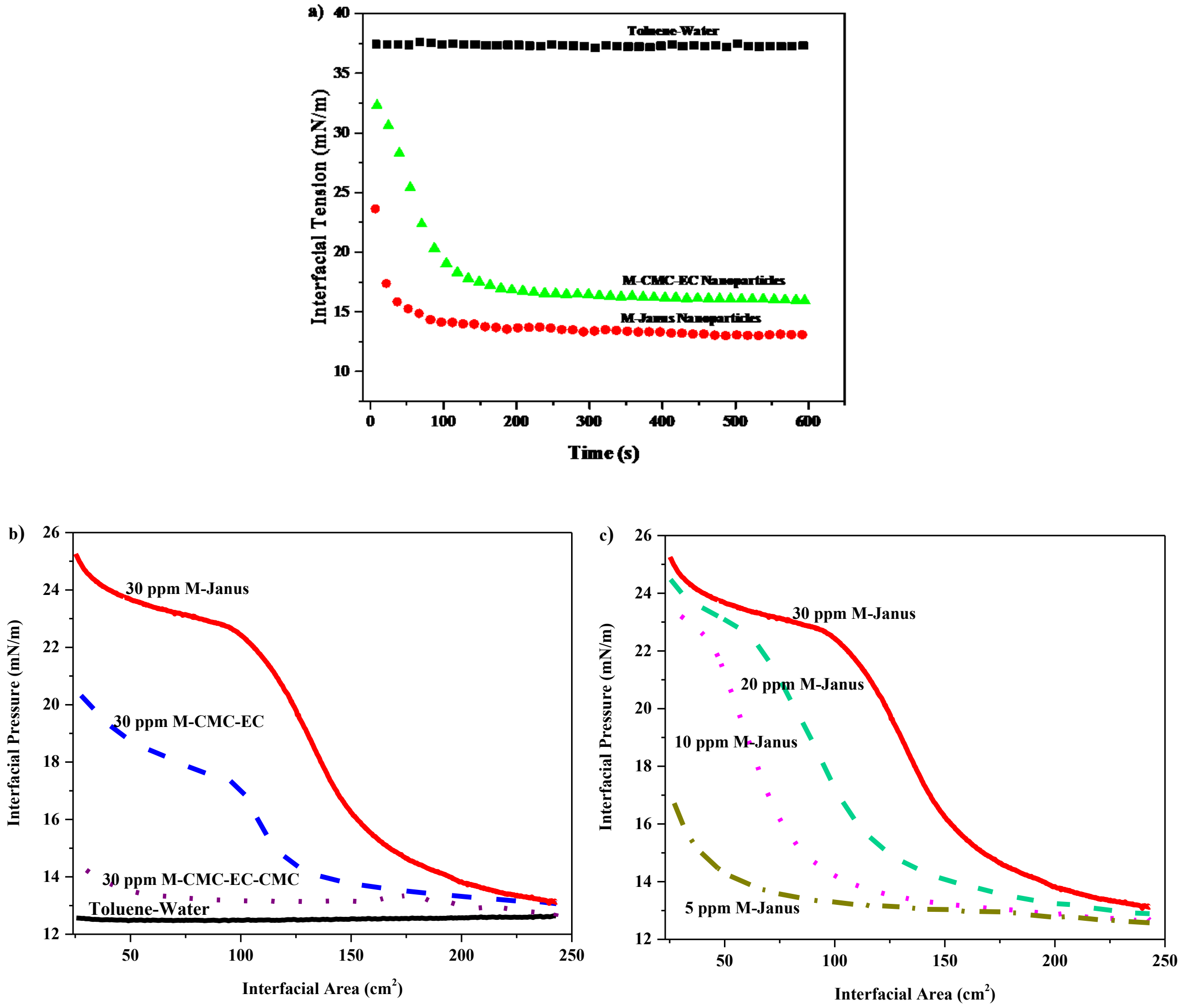

**Figure 4-11.** a) Dynamic interfacial tension of toluene-water interfaces adsorbed with interfacially active nanoparticles; b) interfacial pressure-area isotherms of 30 ppm M-Janus nanoparticles, 30 ppm M-CMC-EC nanoparticles or 30 ppm M-CMC-EC-CMC nanoparticles at toluene-water interface; and c) interfacial pressure-area isotherms of M-Janus nanoparticles at different particle concentrations.

At full trough area ($\pi$ = 13.2 mN/m), the M-Janus nanoparticles with a diameter around 145 nm (**Figure 4-12**) were well and loosely dispersed at the toluene-water interface and slow increase of interfacial pressure isotherm was observed due to weak particle interactions, as shown in Figure **4-13a**. Compared with the case of full tough area, the M-Janus nanoparticles were observed to be more closely partitioned at the toluene-water interface upon further compression (π = 15.5 mN/m), as shown in **Figure 4-13b**, leading to stronger interactions of particles at the interface and a more rapid increase in the interfacial pressure. The interfacial pressure kept rapidly increasing until buckling behavior of the toluene-water interface dominated (π = 22.2 mN/m), as indicated by the inflection point and the subsequent slower increase in the interfacial pressure shown in the curve. At maximum compression (π = 25.0 mN/m), the slightly sharper increase of the interfacial pressure was observed, resulting from the folding of the nanoparticle-stabilized toluene-water interface and the eventual formation of thick and overlapped particle layers, as shown in **Figure 4-13c**.

To reveal the difference in wettability of the M-Janus nanoparticles on opposite sides, the M-Janus nanoparticles (30 ppm) or the M-CMC-EC nanoparticles (30 ppm) were transferred from toluene-water interfaces to a silica wafer using Langmuir-Blodgett deposition method at an interfacial-pressure of 18 mN/m or 15.5 mN/m, respectively. As shown in **Figure 4-14a**, the deposition of M-Janus nanoparticles on hydrophilic silica wafer by pulling method increased the contact angle of a water droplet from 6.90º ± 0.69º to 56.87º ± 0.40º, indicating a strong hydrophobicity of the hydrophobic surface coated with EC. In order to compare and clearly show the different wettabilities at the opposite sides of the M-Janus nanoparticle surfaces, we transferred the second layer of M-Janus nanoparticles by dipping the particle-deposited wafer obtained using the pull method from oil-phase into the aqueous phase. The contact angle of a water droplet on this surface decreased from 56.87º ± 0.40º to 23.09º ± 0.23º, resulting from the exposure of hydrophilic surfaces on M-Janus nanoparticles. This finding clearly demonstrates surfaces of contrast wettability on M-Janus nanoparticles as anticipated. With the deposition of M-CMC-EC nanoparticles onto the hydrophilic silica wafer (**Figure 4-14b**) using pulling method, the contact angle of the water droplet increased from 5.33º ± 0.18º to 55.85º ± 0.91º as anticipated.

Interestingly, after the dipping of the surface through the oil phase into the aqueous phase, the contact angle of water on this second layer of M-CMC-EC nanoparticles even increased although only slightly from 55.85º ± 0.91º to 61.18º ± 2.26º, due most likely to the increase in the surface roughness of deposited M-CMC-EC layer in the dipping process.

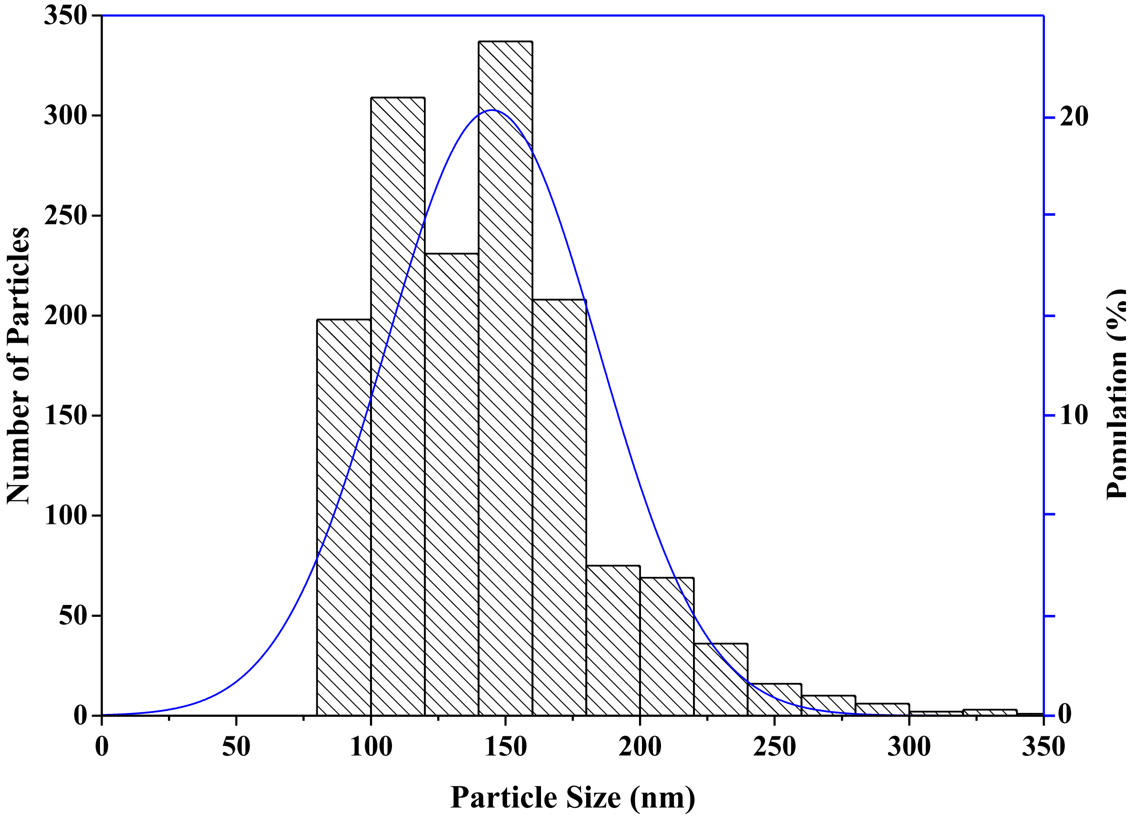

**Figure 4-12.** Size distribution of 30 ppm M-Janus nanoparticles adsorbed at clean toluene-water interface of full trough area (analyzed using commercial imaging analysis software ImageJ).

Based on the characterization results, a new class of novel magnetically responsive Janus (M-Janus) nanoparticles was synthesized by coating with hydrophobic ethyl cellulose (EC) and hydrophilic carboxymethyl cellulose (CMC) on the opposite sides of iron oxide nanoparticle surfaces using a simple and controlled adsorbing process. Due to the steric repulsion and electrostatic repulsive force created by coated celluloses on the nanoparticle surfaces, M-Janus nanoparticles have excellent dispersion in either organic phase or aqueous phase. Compared with M-CMC-EC nanoparticles, M-Janus nanoparticles exhibited stronger interfacial activities, including the prevention of the emulsified phase from coalescing, quick adsorption of M-Janus nanoparticles onto the oil-water interface, lower interfacial tension, and more rigid oil-water interfaces. With their superior interfacial activity and stable occupation at the oil-water interface, the M-Janus nanoparticles are expected to exhibit excellent performance in phase separating both of the oily wastewaters and the water-in-diluted bitumen emulsions.

### 4.3.3 Application of M-Janus Nanoparticles to Oil/Water Separation of Oily Wastewaters and Water-in-Diluted Bitumen Emulsions

As an example, the applications of the magnetically responsive and interfacially active M-Janus nanoparticles to remove the dispersed emulsion phase from oily wastewaters and water-in-crude oil emulsions by external magnetic forces are shown below. As shown in **Figure 4-15**, the surfactant-stabilized oily wastewater was prepared by mixing toluene (dyed using Sudan III) and SDS/water ($C_{SDS}$=0.04 mg/ml) solution at 1:9 volume ratio using the ultrasonic bath, followed by vigorous shaking with Vortex Mixer for 3 min. Tiny oil droplets were observed in the SDS-stabilized emulsion (**Figure 4-15a**) and no distinct phase separation was observed after 30 min settling, suggesting high stability of surfactant-stabilized oily droplets in wastewater if not properly treated. With the addition of M-Janus nanoparticles into the emulsion, followed by vigorous mixing using Vortex Mixer for 3 min, such emulsion rapidly showed clear phase separation in 5 min. This phenomenon may result from that the solvated cellulosic chain on the M-Janus nanoparticles caused the flocculation of particle-stabilized oil droplets, which led to quick phase separation of the emulsion.[239] Under the external magnetic field, the M-Janus nanoparticle-tagged toluene droplets were attracted and gathered at the side of the vial, leaving the clear aqueous phase (**Figure 4-15b**). As shown in **Figure 4-15c**, the dark rim of the droplets indicates the deposition of the M-Janus nanoparticles at the oil-water interface. When compared with the previous SDS-stabilized toluene-in-water emulsion, the size of most emulsion droplets increased to around 50 μm, suggesting the enhanced coalescence of toluene droplets assisted by the adsorption of biwettable M-Janus nanoparticles at the oil-water interface with the external magnetic field. By measuring the carbon content in the emulsions using TOC before and after the phase separation, the M-Janus nanoparticles had a higher phase separation efficiency of 92.76 ± 2.57 % than the case of the M-CMC-EC nanoparticles which had phase separation efficiency of 85.22 ± 1.69 %, indicating more effective and efficient phase separation of the surfactant-stabilized oily wastewaters using M-Janus nanoparticles. Another oily wastewater emulsion (diluted bitumen-in-water emulsion) was prepared using the same method shown above. As shown in **Figure 4-16**, the diluted bitumen-in-water emulsion was stable due to the interfacially active materials such as asphaltene in the bitumen. With the addition of the M-Janus nanoparticles and following vigorous shaking, the oil droplets of larger sizes were observed, coupled with the occupation of the Janus nanoparticles at the oil-water interface (**Figure 4-16c**), suggesting the strong interfacial activity of the M-Janus nanoparticles to occupy the oil-water interface and their potential ability to deal with the oil spills in the environment.

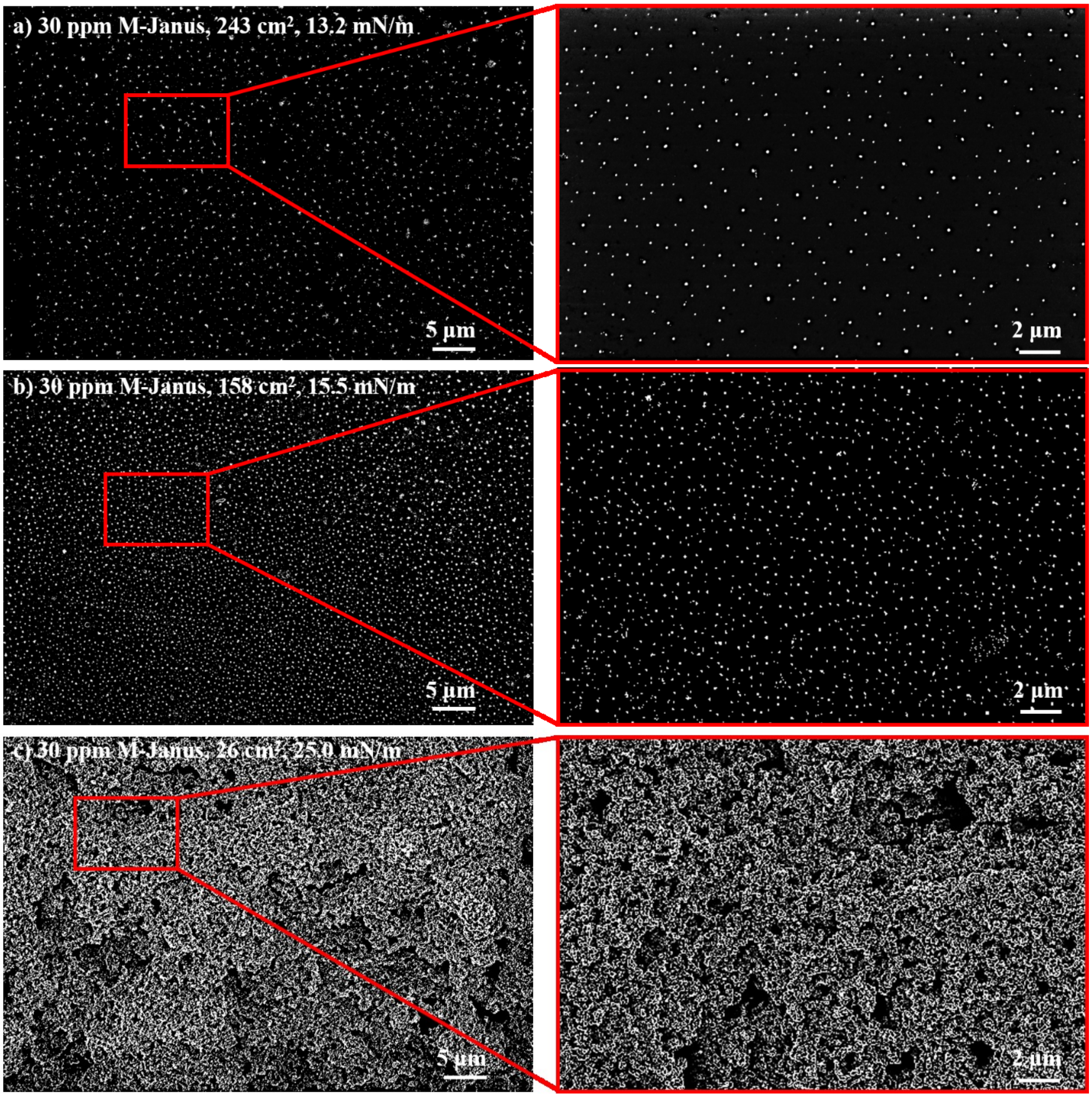

**Figure 4-13.** a-c) Micrographs of M-Janus nanoparticles transferred from toluene-water interface using Langmuir-Blodgett technique. Trough area and film interfacial pressure during deposition are provided in each micrograph.

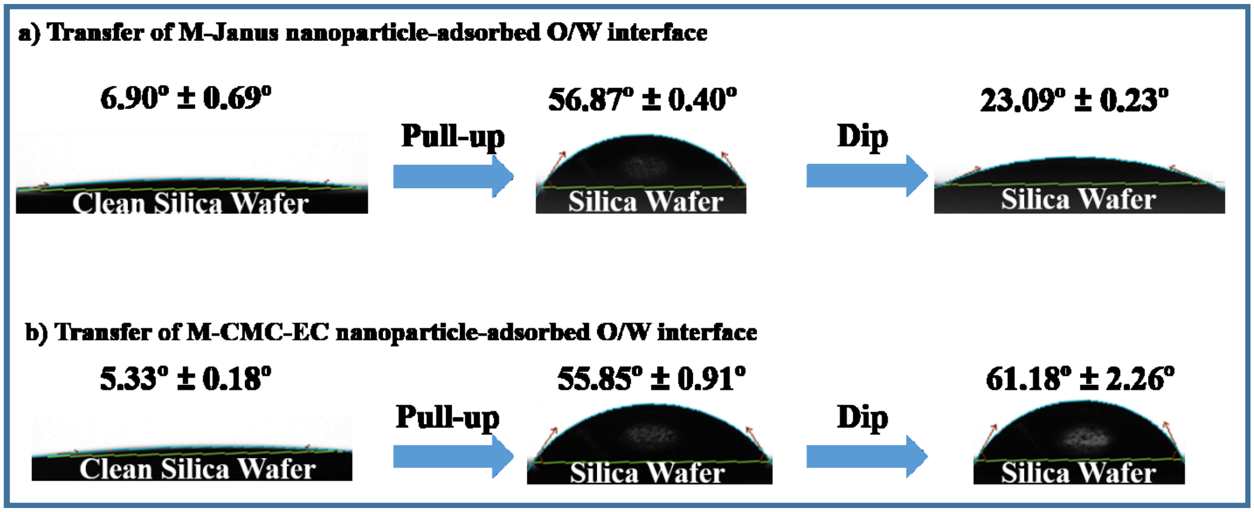

**Figure 4-14.** Contact angles of water droplets on silica wafers with M-Janus nanoparticles (a) or M-CMC-EC nanoparticles (b), obtained by pulling (Pull-up) or dipping (Dip) of a wafer using Langmuir-Blodgett deposition method.

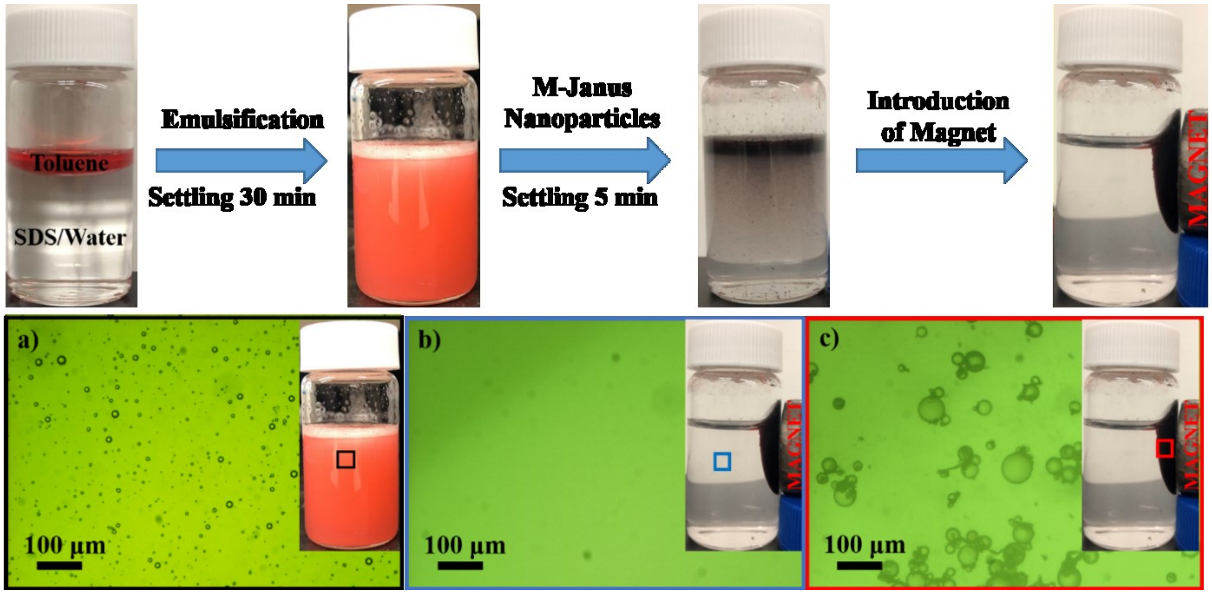

**Figure 4-15.** Micrographs showing oil/water separation process of SDS-stabilized toluene-in-water emulsions with addition of M-Janus nanoparticles under external magnetic field: a) stable tiny toluene droplets before oil/water separation; b) clear water phase after oil/water separation and c) M-Janus nanoparticle-tagged toluene droplets after oil/water separation. The scale bars in figure are 100 µm.

In order to investigate the dewatering ability of M-Janus nanoparticles to the water-in-diluted bitumen emulsions, the micrographs of emulsified water droplets were taken from different positions of the vial before and after the dewatering process. After 2 h settling, fine water droplets with diameters around 10 μm were observed at the top and bottom of the vial. The morphology and size of the water droplets at different positions of the vial were similar, suggesting high stability of the water-in-diluted bitumen emulsions, as shown in **Figures 4-17a** and **4-17b**. With the addition of M-Janus nanoparticles and following settling a strong hand magnet for 30 min, obvious water droplets with sizes larger than 100 μm appeared at the bottom (**Figure 4-17d**). Meanwhile, the clear upper phase without apparent water droplets was discovered as shown in **Figure 4-17c**. Such phenomena indicate the enhanced coalescence of asphaltene-stabilized water droplets with the addition of M-Janus nanoparticles and more effective water removal from the water-in-diluted bitumen emulsions by such M-Janus nanoparticles in the external magnetic field. The water content at the top phase decreased from 5.39 ± 0.17 % to 0.26 ± 0.02 % after the dewatering process, showing a 95 % water removal efficiency which is higher than the case of the M-CMC-EC nanoparticles.[56]

As shown by the results presented above, the M-Janus nanoparticles can efficiently separate the dispersed phase from both of the water-in-crude oil emulsions and the oily wastewaters under an external magnetic field. The key features of such magnetic nanoparticles for their sustainable applications are their reusability and stability. The reusability of the M-Janus nanoparticles was investigated by conducting a series of recycling tests and the stability of the nanoparticles was studied by measuring the dynamic interfacial tensions of the water-toluene interfaces with the adsorption of recycled M-Janus nanoparticles after each dewatering or oil removal test. As shown in **Figure 4-18**, the M-Janus nanoparticles showed a nearly constant dewatering efficiency of 95 %

for the water-in-diluted bitumen emulsion (a) and over 90 % removal of oil for the SDS-stabilized toluene-in-water emulsions (b) in all 5 cycles. Such results indicate the excellent recyclability and reusability of the M-Janus nanoparticles in the dewatering from water-in-crude oil emulsions or oil removal from oily wastewater by magnetic separation. Furthermore, the M-Janus nanoparticles recycled remained effective in lowering the interfacial tension of the water-toluene interface, demonstrating the stable interfacial activity of the M-Janus nanoparticles after reuse and recycling.

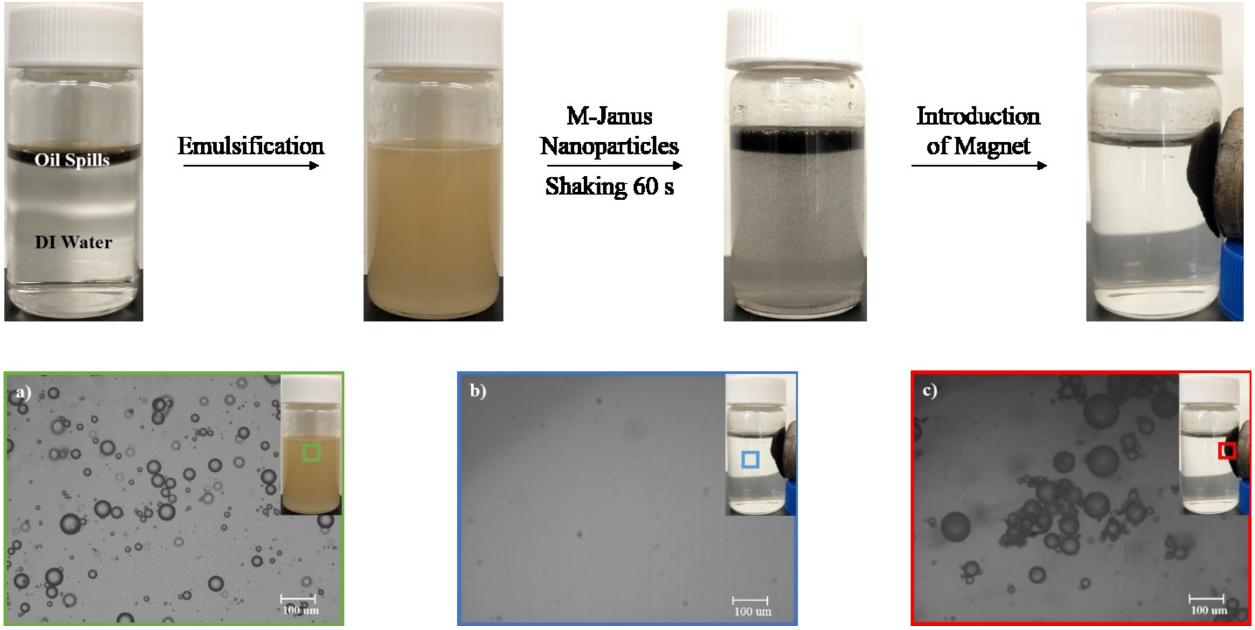

**Figure 4-16.** Micrographs showing oil/water separation process of diluted bitumen-in-water emulsions with addition of M-Janus nanoparticles under external magnetic field: a) stable tiny diluted bitumen droplets before oil/water separation; b) clear water phase after oil/water separation and c) M-Janus nanoparticle-tagged toluene droplets after oil/water separation. The scale bars in figure are 100 μm.

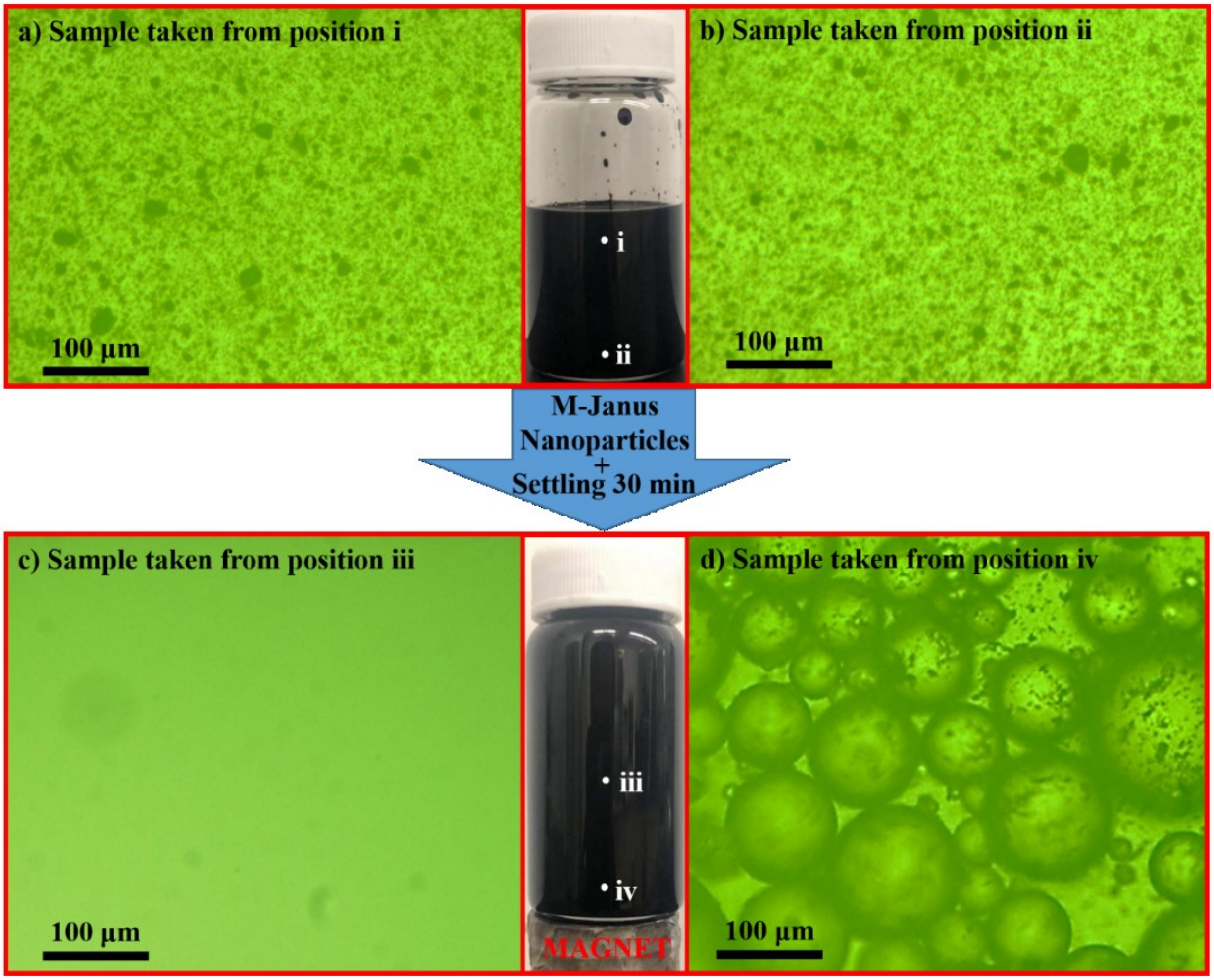

**Figure 4-17.** Micrographs of water droplets in water-in-diluted bitumen emulsions at different positions in the vial before dewatering (a and b) and after dewatering (c and d) using M-Janus nanoparticles after settling on a hand magnet for 30 min. The scale bars in figure are 100 µm.

Here, we demonstrate the efficient separation of emulsified oil from surfactant-stabilized oil-in-water emulsions, oil spills in water and the water-in-diluted bitumen emulsions assisted with the addition of M-Janus nanoparticles under the external magnetic field. The stable dewatering or oil removal efficiency of the M-Janus nanoparticles in the recycling test clearly demonstrates the recyclability and reusability of such magnetically responsive and interfacially active Janus nanoparticles. The results of interfacial tension measurement suggest that the M-Janus nanoparticles could retain high interfacial activity simple washing of spent particles. Our studies show the promising applications of M-Janus nanoparticles to separating dispersed phase from both the oily wastewaters and the water-in-crude oil emulsions in the environmental science and the petroleum-related industrial field.

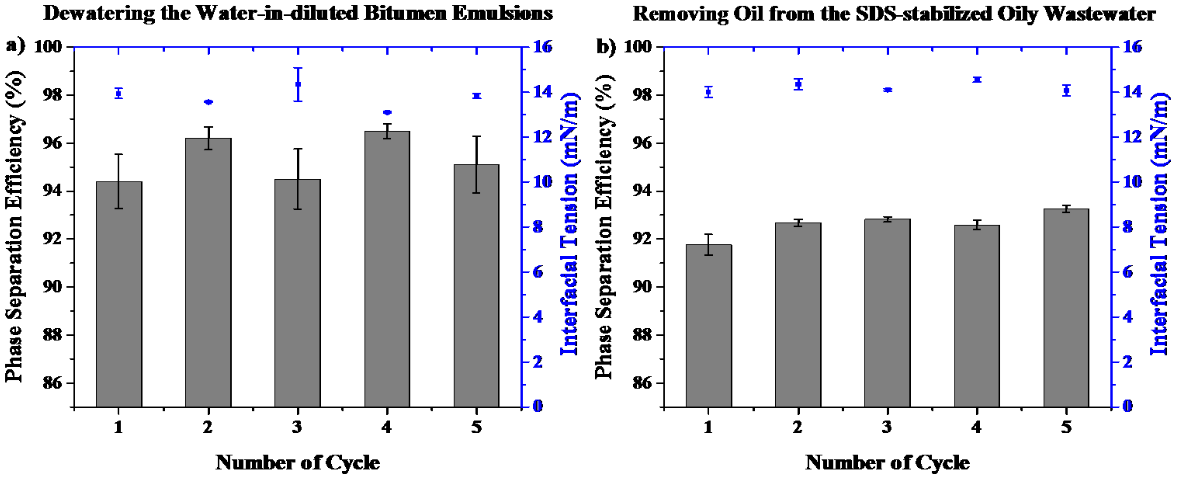

**Figure 4-18.** Phase separation efficiency of dispersed phase from diluted bitumen emulsions (a) and SDS-stabilized oily wastewaters (b) using recycled M-Janus nanoparticles, and corresponding interfacial properties after each reuse cycle and regeneration.

## 4.4 Conclusions

The magnetically responsive Janus nanoparticles were successfully designed and synthesized by consecutive adsorption of hydrophilic CMC and hydrophobic EC onto iron oxide nanoparticles under well-controlled condition. The results from the coalescence time and the crumpling ratio measurement of particle-stabilized droplets along with the interfacial pressure-area isotherms indicate superior interfacial activities of the M-Janus nanoparticles and more stable oil-water interfaces with the adsorption of the M-Janus nanoparticles as compared with the adsorption of conventional interfacially active nanoparticles such as M-CMC-EC nanoparticles. As an example of potential applications, M-Janus nanoparticles were applied to efficiently phase separate the oily wastewaters and the water-in-crude oil emulsions under the external magnetic field. The remaining carbon content in the oily wastewaters and the remaining water content in the diluted bitumen emulsions was less than the case of phase separation using the M-CMC-EC nanoparticles, suggesting the higher dewatering/oil removing efficiency of the M-Janus nanoparticles. The results of recycling test show the desirable reusability and stability of the M-Janus nanoparticles after reuse for several cycles. We anticipate that the magnetically responsive and interfacially active Janus nanoparticles have promising applications to the cleaning of oil spills and removal of oil from household oily wastewaters as well as the removal of undesirable water phase from the crude oil emulsions in the petroleum industrial process. Furthermore, owing to the excellent interfacial properties of the M-Janus nanoparticles as well as the biocompatibility and biodegradability of the cellulosic materials on the particle surfaces, such M-Janus nanoparticle-stabilized Pickering emulsions with high stability show the potential applications to the transit of food-grade ingredient in food science and biomedical materials delivery in biotechnology assisted with an external magnetic field.

# Chapter 5 Treatment of Oily Wastewaters using Magnetic Janus Nanoparticles of Asymmetric Surface Wettability

X. He, Q. Liu and Z. Xu, Treatment of Oily Wastewaters using Magnetic Janus Nanoparticles Synthesized from Cellulosic Materials, submitted.

Efficient treatment of large volumes of oily wastewaters and sludges is a global challenge. The oil in discharged oily wastewaters can cause potential environmental hazards if not treated properly. Due to their excellent interfacial activity, magnetic Janus nanoparticles are considered to be a great vehicle to develop a viable technology for treating large volumes of various types of oily wastewaters and sludges. In this study, a new class of magnetic Janus nanoparticles synthesized using natural cellulosic materials, called M-Janus nanoparticles, were applied to removal or recovery of crude oil or waste cooking oil from oily wastewaters. The M-Janus nanoparticles of superior interfacial activities could anchor securely at the oil-water interface of emulsified oil droplets despite the presence of other interfacially active components such as asphaltenes, natural and/or synthetic surfactants in cooking oil and remaining detergents in the studied oily wastewaters. Compared with the interfacially active nanoparticles of uniform surface properties reported previously, the M-Janus nanoparticles showed stronger interfacial activities such as lower oil-water interfacial tension and firmer deposition at the oil-water interface of the different oily wastewater systems. With the tagging of emulsified oil droplets by M-Janus nanoparticles, followed by magnetic separation, an oil removal or recovery efficiency of greater than 91% was achieved for different oily wastewaters. The oil recovered as such contained less than 1.6 wt% of water, showing its high quality for the subsequent oil refining. Furthermore, the M-Janus nanoparticles could be recycled and reused at a high oil recovery and removal efficiency in the subsequent applications without complex regeneration. The superior interfacial activity, high efficiency and exceptional robustness of M-Janus nanoparticles make them an excellent candidate for treating various types of oily wastewaters such as oil spills in seawater, produced wastewater in the oil field or domestic sewage of waste cooking oils.

## 5.1 Introduction

The consumption of various types of oils in industrial processes and daily household activities is snowballing with the prosperous industrial development and ever-growing population.[84] The inevitable generation of large volumes of oily wastewaters from various industrial processes and domestic sewages raises ever-increasing concerns on oil-related environmental hazards and pollutions.[240] Furthermore, the discharge of oily wastewaters containing reusable oil such as crude oil and cooking oil could lead to the loss of energy resources if not recovered as a usable and economical source of energy.[241-242] To minimize the negative impact of the oily wastewaters on our environment and maximize the utilization of limited oil resources, oil removal/recovery from oily wastewaters are therefore of great environmental and socio-economic importance.

Removing or recovering oil from discharged oily wastewaters is now a global challenge because the oil droplets of micro-sizes are extremely stable, resulting from the stabilization by natural and/or synthetic surfactants in the oily wastewaters.[243] Due to the limited difference in densities between oil and water, the oily wastewaters are not readily stratified if not properly treated. Current strategies for treating oily wastewaters or oil spills include sorption,[199, 201, 244-245] membrane filtration,[202, 246-251] electrocoagulation,[87, 112, 204] biological oxidations and chemical-induced coalescence.[206-207, 252-253] Despite their industrial applications, each method suffers inherent drawbacks such as the high cost of raw materials for some oil sorbents, easy fouling in filtration membranes, unsatisfying oil/water separation efficiency and high energy consumption. Compared with the methods mentioned above, technologies based on magnetically responsive and interfacially active nanoparticles for treating oily wastewaters have attracted increasing public interests because of their robustness and low cost, high throughput and efficiency, and less labor-intensity of operations. In recent years, a variety of interfacially active and magnetically responsive nanoparticles with uniform surface modification by polyvinylpyrrolidone,[52] poly(2-dimethylaminoethyl methacrylate) (PDMAEMA),[54] polyelectrolytes and ethyl cellulose (EC) have been reported to assist removal/recovery of oil from oily wastewaters. [55-58] With their active interfacial behaviors, the nanoparticles can anchor at the oil-water interface and tag the oil droplets, leading to the formation of nanoparticle-stabilized oily wastewaters.[254-255] The tagging of waste oil droplets by these interfacially active magnetic nanoparticles makes the tagged oil droplets to be effectively attracted to the desired locations under an external magnetic field, achieving efficient removal or recovery of the waste oil from the oily wastewaters

It is worth noting that the interfacially active components in oily wastewaters could significantly enhance the stability of the emulsified oil droplets, depending on the different ambient environments.[193] The high concentration of salts in seawater, for example, could greatly enhance the interfacial activities of interfacially active components such as asphaltenes and/or natural surfactants in the crude oil, leading to more stable oil spills in the marine system and hence more challenging to treat oil spills.[256] For the domestic sewage, the spent cooking oil is one of the primary waste sources as household sewage.[257] The waste cooking oil is stabilized as emulsion droplets due to the presence of surface-active impurities such as detergents used in dishwashing or home cleaning.[258] The enhanced stability of such oily wastewaters would inevitably cause greater difficulties to the tag of the emulsified oil droplets by the interfacially active magnetic nanoparticles of uniform surface properties.

Janus particles of asymmetric surface wettability have attracted considerable interests.[185] Compared with the particles of uniform surface wettability, Janus particles of asymmetric surface wettability were found to be more effective emulsion stabilizers, leading to higher desorption energy of these particles from an oil-water interface.[188-189, 259-260] Early studies showed a significant improvement in the anchoring of interfacially active particles if the particles were made of Janus characteristics, leading to a much stronger tagging of emulsified oil droplets and hence more efficient removal or recovery of oil from oily wastewaters.[186-187] On this basis, we designed a new class of M-Janus nanoparticles synthesized by controlled adsorption of two natural cellulosic materials of opposing solubilities: a uniform adsorption of oil-soluble (hydrophobic) ethyl cellulose (EC), followed by the adsorption of water-soluble (hydrophilic) carboxymethyl cellulose (CMC) on a controlled area of the magnetite nanoparticle surfaces.[194] Compared with the M-CMC-EC nanoparticles of uniform surface modification by EC,[56] M-Janus nanoparticles synthesized as such showed a much stronger interfacial activity and firmer anchoring at the toluene-water interface, leading to a more stable toluene-in-water Pickering emulsion. Due to their superior interfacial activities, we anticipate a more efficient removal/recovery of oil from the oily wastewaters by M-Janus nanoparticles than by M-CMC-EC nanoparticles of uniform surface modifications.[259] To prove this hypothesis, we applied the M-Janus nanoparticles to the removal and recovery of oil from oily wastewaters. First, we investigated the interfacial activities of M-Janus nanoparticles in the complex oily wastewaters (crude oil-in-water emulsions and cooking oil-in-water emulsions stabilized by synthetic surfactants). Compared with the M-CMC-EC nanoparticles reported previously, the M-Janus nanoparticles were found to deposit more effectively at the oil-water interface of the oily wastewaters, leading to a firmer deposition at the interfaces. The efficient removal and recovery of oil from oily wastewaters using M-Janus nanoparticles were demonstrated for four types of oily wastewaters (crude oil in synthetic seawater, crude oil in tap water, cooking oil in synthetic seawater and cooking oil in detergent-containing tap water) to show the robust and wide applicability of M-Janus nanoparticles for treating different types of oily wastewaters. Finally, the recyclability of M-Janus nanoparticles from the recovered oil-rich phase was investigated, demonstrating a significant reduction in operating cost and production of secondary hazardous. This study clearly shows the great potentials of M-Janus nanoparticles of asymmetric surface wettability for treating challenging oily wastewaters and recovering valuable oil resources than the M-CMC-EC nanoparticles of uniform surface wettability.

## 5.2 Results and Discussion

### 5.2.1 Field Emission Scanning Electron Microscopy (FE-SEM) Imaging

As shown in **Figure 5-1**, the M-CMC-EC nanoparticles with homogeneous EC coating formed agglomerates in the aqueous phase (**Figures 5-1a** and **5-1b**), resulting from the attractive hydrophobic force between the water-insoluble EC layers on the M-CMC-EC nanoparticle surfaces. In contrast, the M-Janus nanoparticles were highly dispersed in the aqueous phase (**Figure 5-1c and Figure 5-1d**), due most likely to the hydrophilic CMC partially-coated subsequently on the M-CMC-EC nanoparticle surfaces. The abundant carboxyl groups of the hydrophilic CMC can generate strong electrostatic repulsive forces in the aqueous environment, leading to well-dispersed M-Janus nanoparticles.[194] The measurement of particle size distribution could further demonstrate the better dispersion of M-Janus nanoparticles in the aqueous solution. After 15 min settling, the M-Janus nanoparticles still showed an average diameter of 183 nm, in contrast to an average diameter of 1042 nm for M-CMC-EC nanoparticles (**Figure 5-2**). Such results again demonstrate that the suspension of M-Janus nanoparticles could have a better dispersion and stability than the suspension of M-CMC-EC nanoparticles in the aqueous solution due to stronger electrostatic repulsive forces between the M-Janus nanoparticles than that between M-CMC-EC nanoparticles. It is worth noting that the M-Janus nanoparticles had an average size of 223 nm in synthetic seawater (**Figure 5-3**), which is indeed slightly larger than the average size of 183 nm (**Figure 5-2**) for M-Janus nanoparticles in DI water, showing limited aggregation. Despite weak electrostatic repulsion in high electrolyte (synthetic seawater) solutions, the limited aggregation of M-Janus nanoparticles in synthetic seawater could be attributed to the steric repulsion of exposed CMC on M-Janus nanoparticles. The M-Janus nanoparticles with sizes between 100 - 200 nm were observed in the microscopic view, which were comparable with the average size of 167 nm analyzed using the commercial ImageJ software (**Figure 5-4**). The excellent dispersion state of the interfacially active M-Janus nanoparticles in the aqueous phase can promote the formation of the mono-particle layer at the oil-water interface, contributing to their better interfacial activities which were investigated comprehensively later.

### 5.2.2 Interfacial Activities of M-Janus Nanoparticles and M-CMC-EC Nanoparticles in Oily Wastewaters

#### 5.2.2.1 Interfacial Tension

**Figure 5-5a** shows the dynamic interfacial tension of the toluene-synthetic seawater interfaces in the presence of different interfacially active materials. The interfacial tension of the clean toluene-synthetic seawater interface was found to be 39.6 ± 0.6 mN/m which is slightly higher than the value of ~ 37.2 ± 0.4 mN/m for a clean toluene-DI water interface. Such difference results from the high concentration of salt in the aqueous phase.[135] For the diluted crude oil-DI water interface, the gradual decrease of the interfacial tension at the initial stage was observed because of the adsorption of asphaltenes in the crude oil at the diluted crude oil-DI water interface. At the final stage, the interfacial tension of the diluted crude oil-DI water interface stabilized at 29.5 ± 0.1 mN/m, in contrast to 26.6 ± 0.1 mN/m for the diluted crude oil-seawater interface. Due to the screening of electrostatic repulsion between charged head groups of asphaltenes, the high concentration of ions in the synthetic seawater could enhance the accumulation of asphaltenes at the crude oil-seawater interface, leading to a lower crude oil-seawater interfacial tension.[256] It is worth noting that, the interfacial tension of the toluene-synthetic seawater interface in the presence of iron oxide nanoparticles (39.6 ± 0.5 mN/m) was almost the same as the case without iron oxide nanoparticles (39.6 ± 0.6 mN/m), suggesting a negligible interfacial inactivity of bare iron oxide nanoparticles (**Figure 5-6a**).

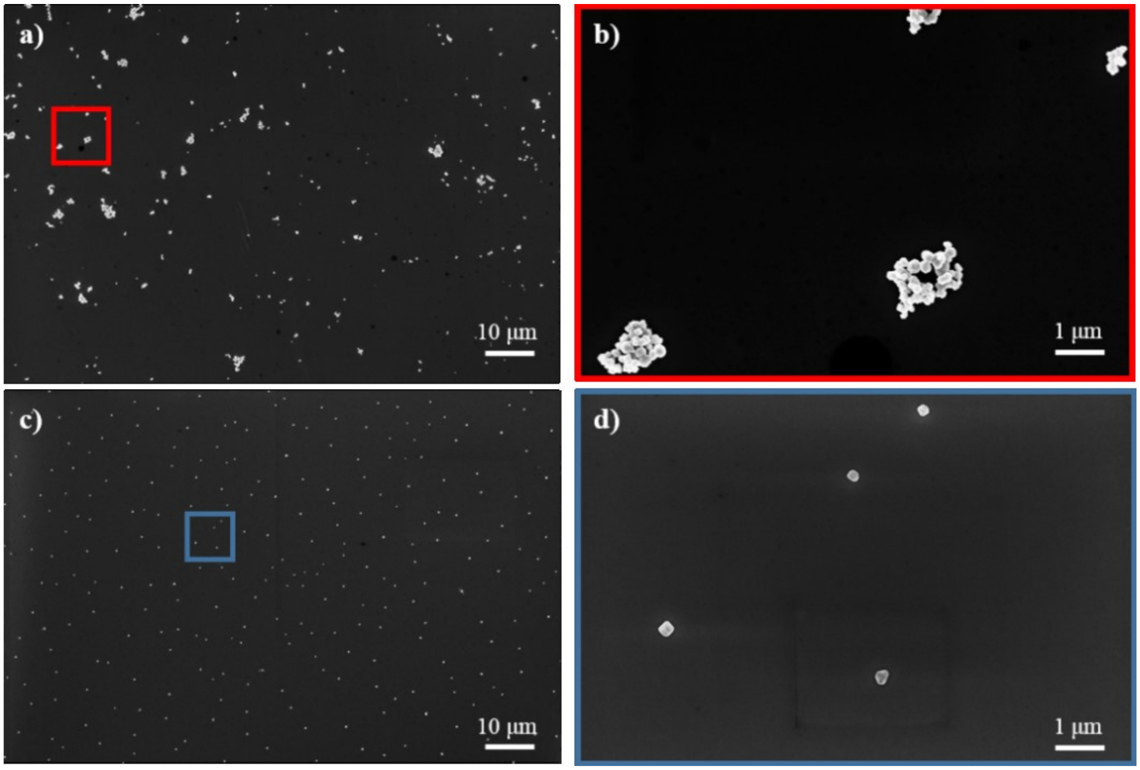

**Figure 5-1.** Field-emission SEM images of 0.1 mg/mL a) M-CMC-EC nanoparticles and c) M-Janus nanoparticles dispersed in aqueous phase, with b) and d) being enlarged view of red zone in a) and blue zone in c), respectively, showing better dispersion of M-Janus nanoparticles than M-CMC-EC nanoparticles in aqueous phase.

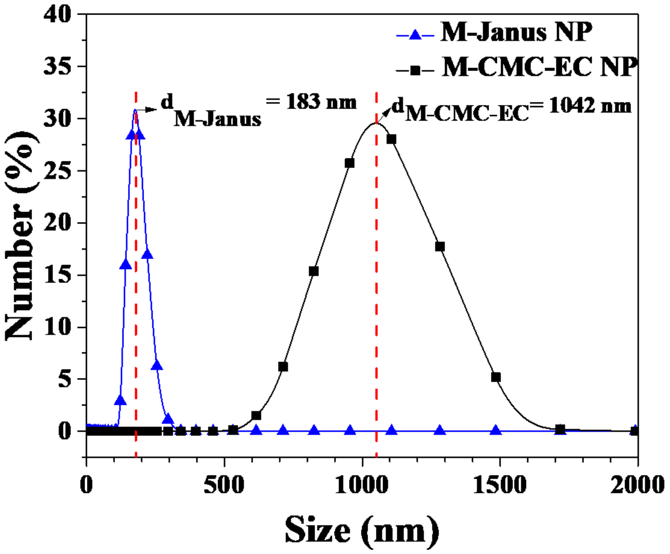

**Figure 5-2.** Size distribution of 0.1 mg/mL M-Janus nanoparticles and M-CMC-EC nanoparticles in deionized water. The experiments were repeated three times, showing a negligible shift in the measured particle size distribution curves.

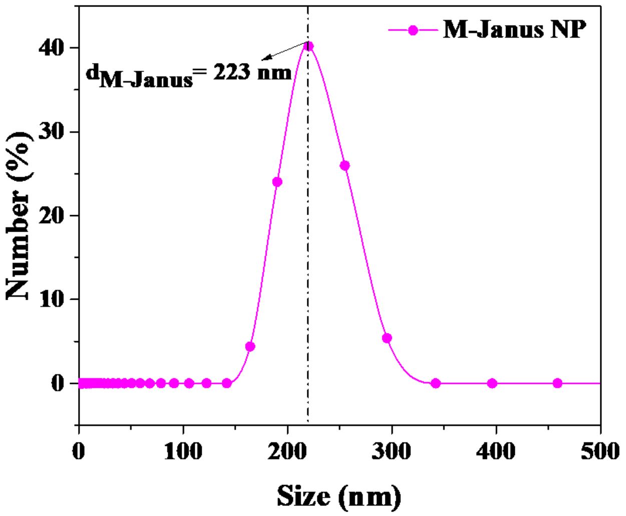

**Figure 5-3.** Size distribution of 0.1 mg/mL M-Janus nanoparticles in synthetic seawater. The experiments were repeated three times, showing a negligible shift in the measured particle size distribution curves to ensure reliability.

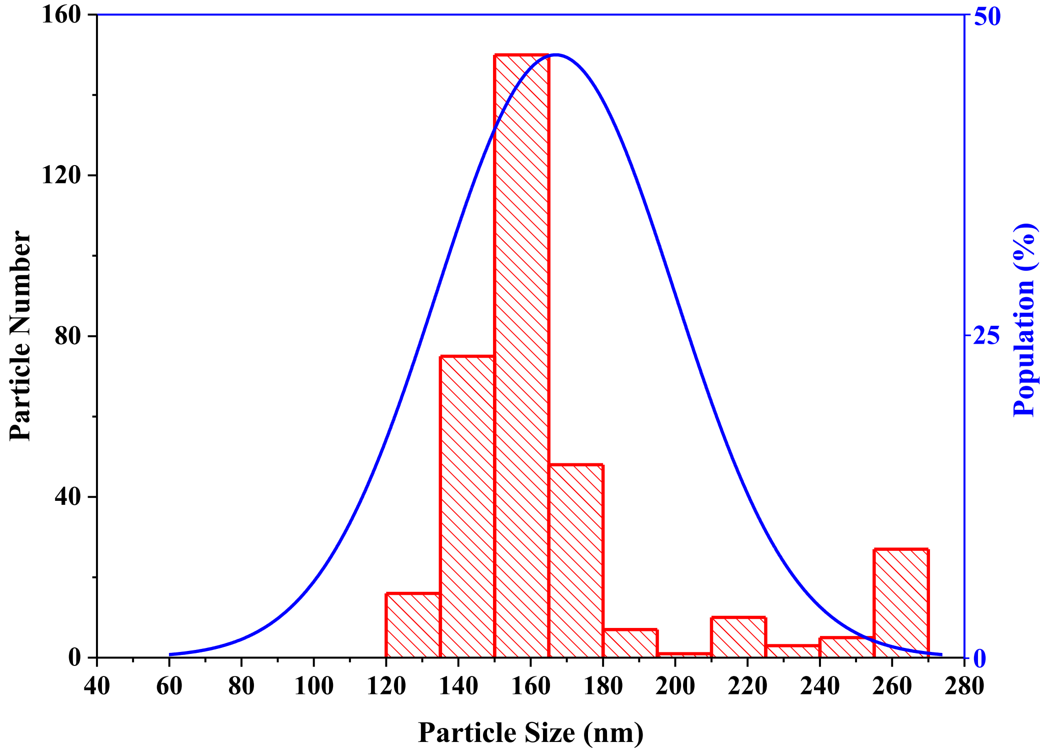

**Figure 5-4.** Size distribution of well-dispersed M-Janus nanoparticles on a silica wafer (analyzed using commercial imaging analysis software Image J).

Compared with the asphaltenes in the crude oil, the M-CMC-EC nanoparticles and the M-Janus nanoparticles were found to be more interfacially active. When the toluene droplet was generated in the suspension of M-CMC-EC nanoparticles in synthetic seawater, the interfacial tension was stabilized at 23.2 ± 0.4 mN/m. In contrast, the dynamic interfacial tension of the toluene-seawater interface in the presence of M-Janus nanoparticles showed a more significant decrease to 22.0 ± 0.2 mN/m, indicating a stronger interfacial activity of M-Janus nanoparticles than M-CMC-EC nanoparticles.

**Figure 5-5b** shows the change of interfacial tensions at the crude oil-seawater interface by the addition of different solutions into the original synthetic seawater. The addition of the pure synthetic seawater was used as a benchmark to indicate a negligible change of the crude oil-seawater interfacial tension with the addition of the pure synthetic seawater. However, the addition of the synthetic seawater with the dispersed M-CMC-EC or M-Janus nanoparticles into the original synthetic seawater led to a significant decrease in the diluted crude oil-synthetic seawater interfacial tension, suggesting the adsorption of these interfacially active nanoparticles onto the diluted crude oil-synthetic seawater interface and the stronger interfacial activities of these interfacially active nanoparticles as compared with the asphaltenes in the crude oil. Compared with the dispersed M-CMC-EC nanoparticles (22.4 ± 0.3 mN/m), the M-Janus nanoparticles (21.5 ± 0.3 mN/m) caused a quicker decrease in the interfacial tension at the initial stage and a lower interfacial tension at the final state, demonstrating superior interfacial activities of the M-Janus nanoparticles.

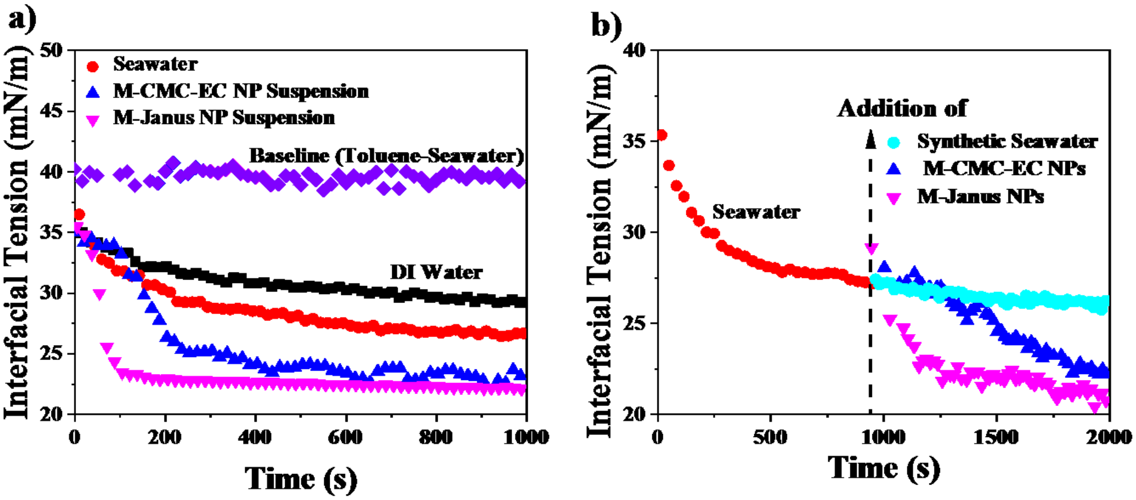

**Figure 5-5.** Dynamic interfacial tension of diluted crude oil and a) water in the presence of different materials (baseline represents toluene-water interface); b) synthetic seawater with subsequent addition as indicated by the dash line of different solutions. Suspensions of nanoparticles are prepared and added in synthetic seawater at 0.1 mg/mL nanoparticles. The experiments were triplicated with a relative experimental error of ± 2%.

**Figure 5-7** shows the effect of the M-Janus nanoparticles, the M-CMC-EC nanoparticles and the detergent on the interfacial tension of the cooking oil-tap water interface. With the adsorption of interfacially active impurities in the cooking oil at the interface, the interfacial tension of the cooking oil-tap water interface finally stabilized at 21.6 ± 0.1 mN/m (**Figure 5-7a**). In contrast, the detergent dissolved in the aqueous phase led to a lower cooking oil-tap water interfacial tension of 18.3 ± 0.2 mN/m, suggesting a more interfacial active nature of the detergent than the impurities in the cooking oil. However, when the cooking oil droplet was generated in the tap water with the dispersed M-Janus (16.5 ± 0.6 mN/m) or M-CMC-EC (17.6 ± 0.2 mN/m) nanoparticles, even lower interfacial tensions were obtained as compared with the interfacial tension of the cooking oil-tap water interface (21.6 ± 0.1 mN/m). Such differences not only demonstrate the effective adsorption of the interfacially active nanoparticles at the cooking oil-tap water interface but also show a superior interfacial activity of the interfacially active nanoparticles when compared with the impurities in the cooking oil.

As shown in **Figure 5-7b**, the addition of tap water caused a slight increase in the interfacial tension of the cooking oil-detergent-containing tap water interface. This increase was most likely caused by the decrease in the concentration of detergent in the bulk aqueous phase with the addition of tap water. In contrast, the addition of the tap water with the dispersed M-Janus or M-CMC-EC nanoparticles into the aqueous phase decreased the interfacial tension of the cooking oil-detergent-containing tap water interface to 15.4 ± 0.4 mN/m and 17.5 ± 0.3 mN/m, respectively. Such a decrease in the interfacial tension clearly shows the adsorption of interfacially active nanoparticles onto the detergent-stabilized cooking oil-tap water interface, with M-Janus nanoparticles being more effective than M-CMC-EC nanoparticles. To better investigate the interfacial activity of M-

Janus nanoparticles and M-CMC-EC nanoparticles, we proceeded with the measurements of interfacial pressure-area isotherms and the measurements of coalescence time.

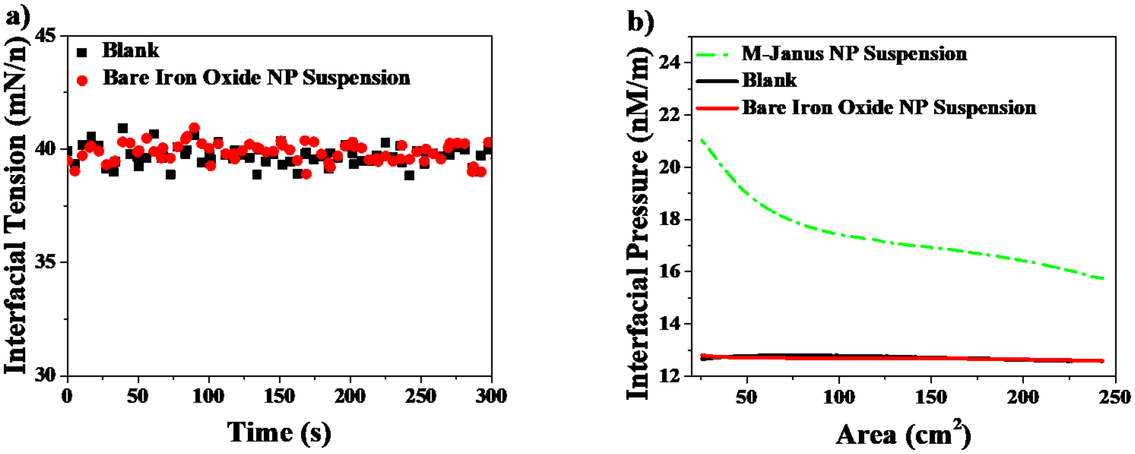

**Figure 5-6.** a) Dynamic interfacial tension of toluene-synthetic seawater interface in the presence or absence (blank) of bare iron oxide nanoparticles and b) interfacial pressure-area isotherm of toluene-synthetic seawater interface in the presence or absence (blank) of bare iron oxide nanoparticles, showing a negligible interfacial activity of bare iron oxide nanoparticles. Suspension contains 0.1 mg/mL bare iron oxide nanoparticles in synthetic seawater. The experiments were triplicated with a relative experimental error of ± 2%.

### 5.2.2.2 Interfacial Pressure-Area ($\pi$-A) Isotherms

To further investigate the interfacial activities of the M-Janus nanoparticles and the M-CMC-EC nanoparticles in the oily wastewaters, the Langmuir-Trough was used to study the interfacial behaviors of the nanoparticles at the toluene-seawater interface. As anticipated, the presence of bare iron oxide nanoparticles would not affect the interfacial pressure of the oil-water interface (**Figure 5-6b**) and therefore we focused on the interfacial activity of M-Janus nanoparticles and M-CMC-EC nanoparticles. As shown in **Figure 5-8a**, the interfacial pressure remained almost the same (12.0 ± 0.4 mN/m) during the compression of the toluene-seawater interface, indicating a clean toluene-seawater interface. In the presence of the interfacially active materials at the toluene-synthetic seawater interface, the interfacial pressure continued to increase with the gradual compression of the interface. Among all the interfacially active materials (crude oil: 18.4 ± 0.2 mN/m and M-CMC-EC nanoparticles: 19.6 ± 0.3 mN/m), the toluene-synthetic seawater interface with the M-Janus nanoparticles reached the highest interfacial pressure (21.0 ± 0.1 mN/m), showing superior interfacial activities of M-Janus nanoparticles.

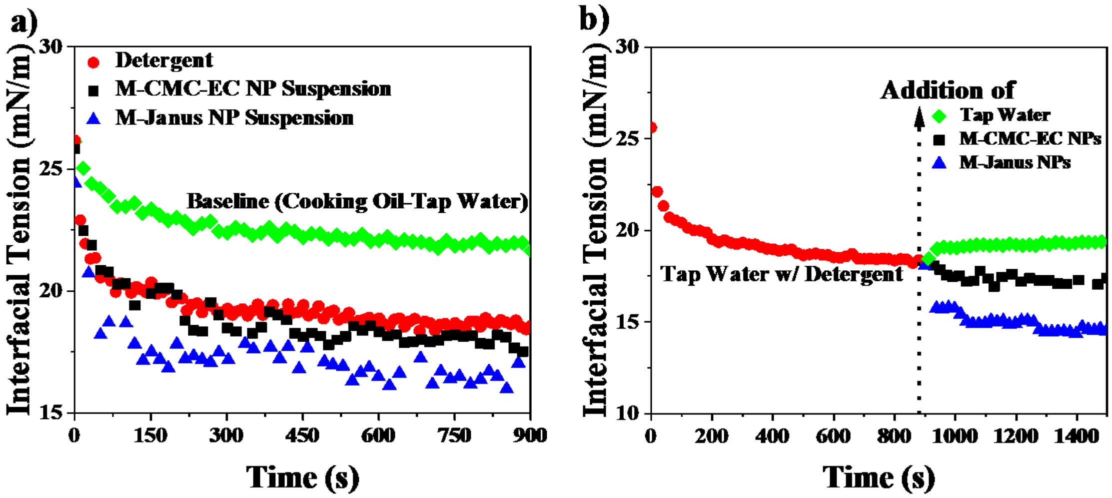

**Figure 5-7.** Dynamic interfacial tension of cooking oil and a) tap water in the presence of different interfacial active materials (baseline represents clean cooking oil-tap water interface) and b) detergent-containing tap water interfaces with subsequent addition as indicated by the dash line of different solutions. Suspensions of nanoparticles in tap water contain 0.1 mg/mL nanoparticles. The experiments were triplicated with a relative experimental error of ± 3%.

**Figure 5-8b** shows the interfacial pressure-area isotherms of the diluted crude oil-synthetic seawater interfaces in the absence and presence of M-Janus nanoparticles or M-CMC-EC nanoparticles. A duration of 15 min was first allowed for the diluted crude oil-synthetic seawater interface to reach equilibrium. The synthetic seawater with the dispersed M-Janus or M-CMC-EC nanoparticles was then carefully injected into the seawater phase with the diluted crude oil-seawater interface at the fully expanded position. The addition of these magnetic nanoparticle suspensions into the original seawater increased the interfacial pressure of diluted crude oil-synthetic seawater interfaces, suggesting the effective adsorption of the interfacially active nanoparticles at the diluted crude oil-seawater interface. The adsorption of M-Janus nanoparticles (27.1 ± 0.4 mN/m) was shown to cause a bigger increase in the interfacial pressure at the diluted crude oil-seawater interface than the adsorption of M-CMC-EC nanoparticles (24.5 ± 0.3 mN/m), confirming superior interfacial activities of the M-Janus nanoparticles.

For the waste cooking oil systems, cooking oil itself, unfortunately, cannot wet the Wilhelmy plate due to its high viscosity. Therefore, we used diluted cooking oil (toluene containing 2 mg/mL cooking oil) as the oil phase to investigate the interfacial activities of M-CMC-EC nanoparticles and M-Janus nanoparticles in the waste cooking oil systems. As shown in **Figure 5-9a**, the interfacial pressure of the toluene-water interface increased continuously with the compression of the trough area, reaching maximum pressure values of 15.8 ± 0.3 mN/m (adsorption of impurities in cooking oil), 18.2 ± 0.3 mN/m (adsorption of M-CMC-EC nanoparticles) and 21.5 ± 0.4 mN/m (adsorption of M-Janus nanoparticles) when the trough area was compressed from 240 cm$^2$ to 25 cm$^2$. Based on these results, the toluene-tap water interface in the presence of M-Janus nanoparticles showed a higher interfacial pressure than that of M-CMC-EC nanoparticles, both being higher than the interfacial pressure of impurities in cooking oil.

**Figure 5-9b** shows a significant impact of M-CMC-EC or M-Janus nanoparticles at the interface on the interfacial pressure of the diluted cooking oil-detergent-containing tap water interface. It is interesting to note that the interfacial pressure of the detergent-stabilized toluene-tap water interface remained almost the same at 16 mN/m during the compression process. It appears that the detergent molecules were reversibly adsorbed at the toluene-tap water interface even though they were more interfacially active as shown by a higher initial interfacial pressure (15.4 ± 0.1 mN/m) when compared with inherent impurities in cooking oil (14.2 ± 0.2 mN/m). The injection of nanoparticle suspensions into the detergent-containing tap water increased interfacial pressures, clearly demonstrating the effective deposition of the interfacially active nanoparticles at the detergent-stabilized cooking oil-water interface. It is worth noting that the highest interfacial pressure was observed for M-Janus nanoparticles (26.2 ± 0.2 mN/m), demonstrating the stronger interfacial activity of the M-Janus nanoparticles as compared with the M-CMC-EC nanoparticles (25.0 ± 0.5 mN/m).

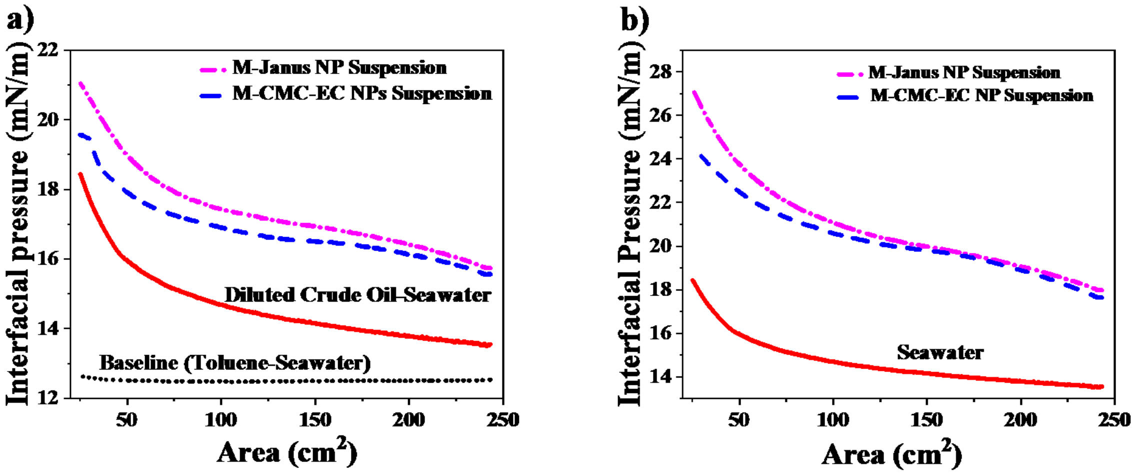

**Figure 5-8.** Interfacial pressure-area isotherms of a) toluene-synthetic seawater interfaces in the presence of M-Janus nanoparticles, M-CMC-EC nanoparticles or interfacially active components in crude oil (baseline represents clean toluene-synthetic seawater interface) and b) diluted crude oil-synthetic seawater interface in the presence of M-Janus nanoparticles and M-CMC-EC nanoparticles. Suspensions of nanoparticles in synthetic seawater contain 0.1 mg/mL nanoparticles. The experiments were triplicated with a relative experimental error of ± 5%.

### 5.2.2.3 Coalescence Time Measurement

The results of the coalescence measurement in **Table 5-1** show an immediate coalescence of the pure toluene droplets in the synthetic seawater upon their contact. However, it took 9.69 ± 2.16 s for two diluted crude oil droplets to coalesce in the synthetic seawater, suggesting stabilization of crude oil-synthetic seawater interface by asphaltenes in the crude oil. The coalescence time of the crude oil droplets in the synthetic seawater suspension of M-CMC-EC nanoparticles increased to 18.47 ± 0.60 s (**Figure 5-10** and **Table 5-1**), indicating enhanced stability of the droplets by M-CMC-EC nanoparticles at the oil droplet surfaces. A further increase in the coalescence time to 38.67 ± 6.60 s was observed for the diluted crude oil droplets stabilized by M-Janus nanoparticles (**Figure 5-10** and **Table 1**), suggesting a much stronger anchoring of M-Janus nanoparticles at the crude oil-synthetic seawater interfaces as compared with M-CMC-EC nanoparticles. With the stronger deposition of M-Janus nanoparticles at the diluted crude oil-synthetic seawater interface, more efficient control of oil droplets stabilized by M-Janus nanoparticles than by M-CMC-EC nanoparticles by an external magnetic field is anticipated.

**Table 5-1.** Coalescence time of two diluted crude oil droplets in different aqueous environments. The measurements of coalescence time were repeated three times and the error range represents one standard deviation of measurements.

| Oil Phase | Aqueous Phase | Coalescence Time (s) |
|---|---|---|
| Pure Toluene | Synthetic Seawater | 0 |
| Diluted Crude Oil | Synthetic Seawater | 9.69 ± 2.16 |
| Diluted Crude Oil | Suspension of 100 ppm M-CMC-EC Nanoparticles in Synthetic Seawater | 18.47 ± 0.60 |
| Diluted Crude Oil | Suspension of 100 ppm M-Janus Nanoparticles in Synthetic Seawater | 38.67 ± 6.60 |

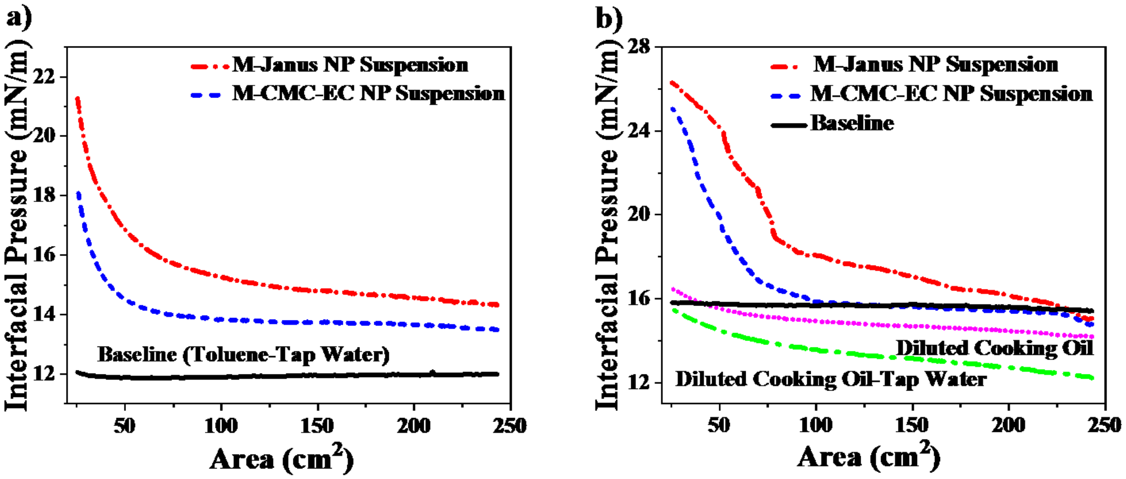

**Figure 5-9.** Interfacial pressure-area isotherms of a) toluene-tap water interfaces in the absence and presence of M-Janus or M-CMC-EC nanoparticles (baseline represents clean toluene-tap water interface) and b) toluene-detergent-containing tap water interface in the absence and presence of M-Janus nanoparticles, M-CMC-EC nanoparticles or cooking oil (baseline represents toluene-detergent-containing tap water). Suspensions of nanoparticles in tap water contain 0.1 mg/mL nanoparticles. The experiments were triplicated with a relative experimental error of ± 4%.

The coalescence processes of the two cooking oil droplets in the different tap water environments are shown in **Figure 5-11** and the results are summarized in **Table 5-2**. The cooking oil droplets required a contact time of 18.67 ± 1.59 s to coalesce in tap water, resulting from the stabilization of the cooking oil-tap water interface by the inherent impurities in the cooking oil. When the cooking oil droplets were contacted in the detergent-containing tap water, the coalescence time of oil droplets increased significantly to 35.07 ± 2.68 s as anticipated. Such increase results from stronger adsorption of interfacially active detergent molecules at the cooking oil-tap water interface. However, the addition of dispersed M-CMC-EC nanoparticles into the aqueous phase caused a further increase in the coalescence time of the cooking oil droplets to 43.60 ± 0.67 s, demonstrating a more interfacially active nature of M-CMC-EC nanoparticles as compared with the remaining detergent in the tap water. An even longer coalescence time of 59.53 ± 3.93 s was observed for cooking oil droplets in tap water containing the same concentration of M-Janus nanoparticles as M-CMC-EC nanoparticles. Such observation indicates a superior interfacial activity of M-Janus nanoparticles as compared with the inherent impurities in the cooking oil, the detergent molecules, and M-CMC-EC nanoparticles. The superior interfacial activity of the M-Janus nanoparticles ensures their effective and firm anchoring on the oil droplet surfaces in the oily wastewater systems, laying the solid foundation for the subsequent removal/recovery of waste oil under an external magnetic field.

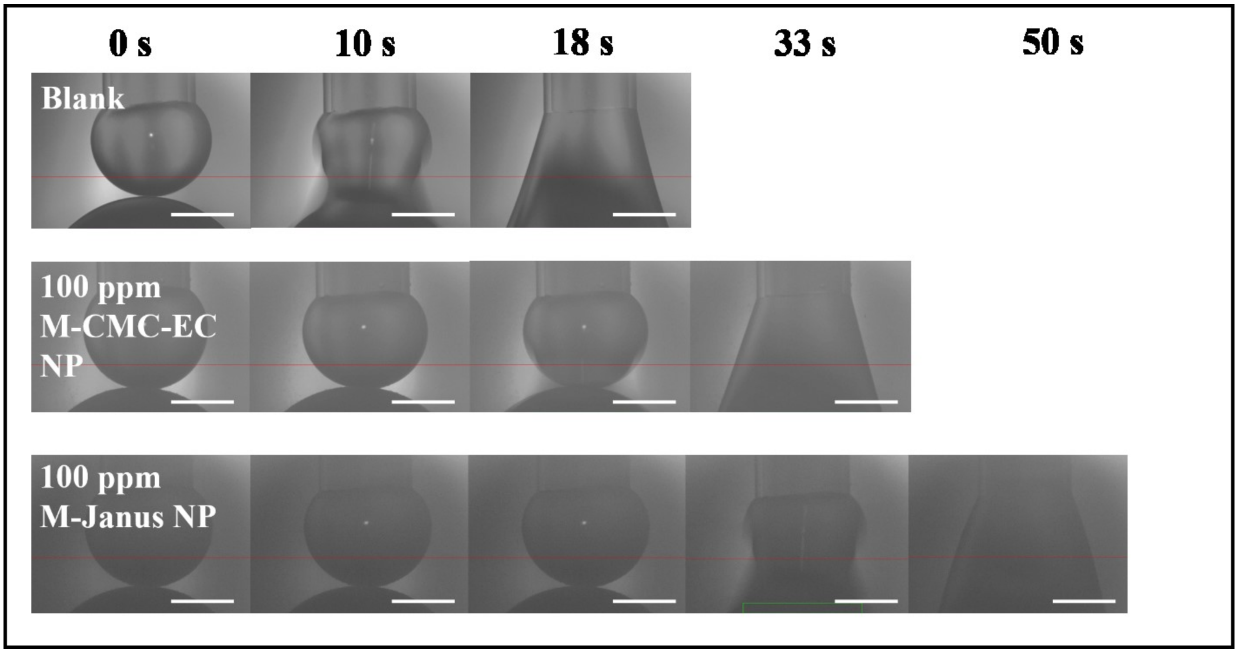

**Figure 5-10.** Snapshots for the coalescence process of diluted crude oil droplets without (blank) or with stabilization by M-CMC-EC or M-Janus nanoparticles in synthetic seawater. The white scale bars in figure are 1 mm. The concentration of nanoparticles in synthetic seawater is 100 ppm.

The results of coalescence time measurements, interfacial pressure-area isotherms measurements and interfacial tension measurements all show the stronger interfacial activities of M-Janus nanoparticles than the other interfacially active components in crude oil or cooking oil, detergent remained in tap water and M-CMC-EC nanoparticles reported previously. With their superior interfacial activities and firmer anchoring at the oil-water interfaces, the M-Janus nanoparticles are anticipated to have promising applications to the oil removal/recovery from the complex oily wastewaters.

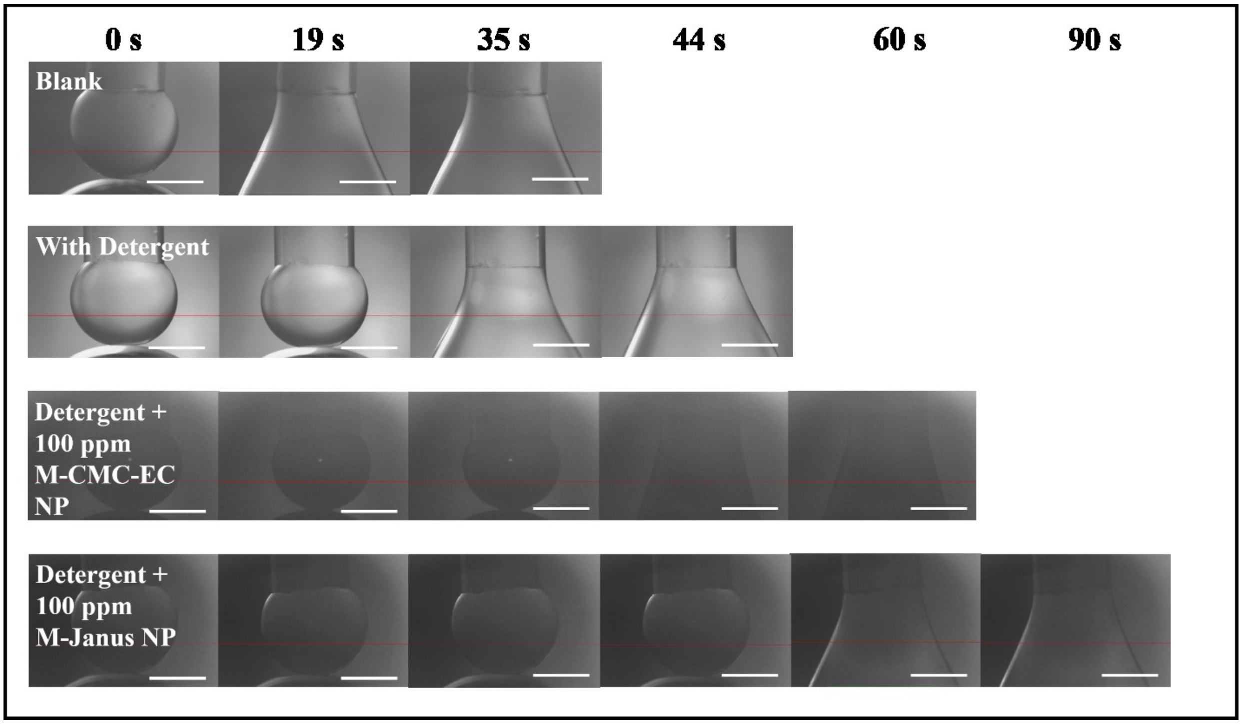

**Figure 5-11.** Snapshots for the coalescence process of cooking oil droplets without or with stabilization by M-CMC-EC or M-Janus nanoparticles in tap water (blank) and detergent-containing tap water. The white scale bars in figure are 1 mm. The concentration of nanoparticles in tap water is 100 ppm.

**Table 5-2.** Coalescence time of two vegetable oil droplets in different aqueous environments. The measurements of coalescence time were repeated three times and the error range represents one standard deviation of measurements.

| Oil Phase | Aqueous Phase | Coalescence Time (s) |
|---|---|---|
| Pure Cooking Oil | Tap Water | 18.67 ± 1.59 |
| Pure Cooking Oil | Tap Water w/Detergent | 35.07 ± 2.68 |
| Pure Cooking Oil | Tap Water w/Detergent + 100 ppm of M-CMC-EC Nanoparticles in Tap Water | 43.60 ± 0.67 |
| Pure Cooking Oil | Tap Water w/Detergent + 100 ppm of M-Janus Nanoparticles in Tap Water | 59.53 ± 3.93 |

### 5.2.3 Concept of M-Janus Nanoparticles for Removing/Recovering Oil from Oily Wastewaters

As shown in **Figure 5-12**, the suspension of M-Janus nanoparticles was prepared by dispersing M-Janus nanoparticles in the tap water or the synthetic seawater (S1) prior to their addition to the oily wastewaters (S2). With their superior interfacial activities, the M-Janus nanoparticles could anchor securely at the oil-water interface. The oil droplets tagged by magnetic M-Janus nanoparticles (schematics above S3) were transported by a strong hand magnet to desired locations and removed/recovered from the oily wastewaters (S3), leading to a clean aqueous phase to be separated for safe disposal (S4 and S5). The M-Janus nanoparticle-tagged oil droplets were attracted firmly to the sidewalls of the vial. Then, the magnet was controlled to move back and forth to strengthen the interactions between the oil droplets, forcing the coalescence of the oil droplets. By repeating the procedures a couple of times, oil droplets stabilized by M-Janus nanoparticles were squeezed out and settling to the bottom of the vial by gravity, achieving the separation of M-Janus nanoparticles and waste oil (S6). The M-Janus nanoparticles separated as such were then collected and cleaned thoroughly by toluene washing as regenerated M-Janus nanoparticles for subsequent applications (S7).

### 5.2.4 Removal/Recovery of Oil from Oily Wastewaters using M-Janus Nanoparticles

**Figure 5-13** shows the process of removing/recovering crude oil or waste cooking oil from synthetic oily wastewaters: crude oil in synthetic seawater (**Figure 5-13a**), crude oil in tap water (**Figure 5-13b**), cooking oil in synthetic seawater (**Figure 5-13c**) and cooking oil in detergent-containing tap water (**Figure 5-13d**) using magnetic M-Janus nanoparticles. The oily wastewaters were prepared by mixing of oil (crude oil or cooking oil) with water (synthetic seawater or tap water) at a volume ratio of 1:9 ($v_{oil}/v_{water}$). After 1-h settling, there was no obvious phase separation in the oily wastewaters, indicating extreme stability of such oily wastewaters if there is no further treatment. To remove/recover waste oil from oily wastewaters, the M-Janus nanoparticles were first dispersed in a small amount of synthetic seawater or tap water to make up different oily wastewater systems. The resulting suspension of M-Janus nanoparticles was then added into the oily wastewaters. Interestingly, despite the stabilization of O/W (oil-in-water) emulsions by M-Janus nanoparticles, the mixture showed a rapid phase separation. The rapid phase separation results most likely from the bridge-flocculation of oil droplets by solvated cellulosic chains of EC on M-Janus nanoparticle surfaces.[239] The dark rim of the oil droplets shown in **Figure 5-14** suggests the anchoring of M-Janus nanoparticles onto the waste oil droplet surfaces. Assisted by a strong hand magnet, oil droplets tagged by M-Janus nanoparticles were attracted to the sidewalls of the vial, leading to a cleaned (clear) aqueous phase. It should be noted that the M-Janus nanoparticle-stabilized oil droplets would interact strongly with each other in an external magnetic field, enhancing the coalescence of oil droplets by magnetic forces (**Figure 5-15**) and resulting in the formation of larger oil droplets. **Figure 5-13** shows that cooking oil-in-water emulsions is more susceptible for magnetic force induced coalescence than crude oil-in-water emulsions, more so for the systems without detergent than with detergent. It appears that for a given magnetic force field, less stable cooking oil-water emulsions are more susceptible for destabilization than more stable crude oil-in-water emulsions as anticipated.

As an example, **Figure 5-16** shows the controlled transport of oil droplets tagged by M-Janus nanoparticles under the external magnetic field, demonstrating the effective magnetic responsiveness of the M-Janus nanoparticle-tagged oil droplets. Such oil droplets showed no obvious coalescence during the transport, suggesting the satisfying stability enhanced by M-Janus nanoparticles. After separating the clean aqueous phase from the oily-rich emulsions, a strong hand magnet was used to remove M-Janus nanoparticles from the oil phase, achieving the effective separation/recovery of oil from the oily wastewaters and showing the potential for the recycle/reuse of the spent M-Janus nanoparticles. Such successful and effective removal/recovery of waste oil from the synthetic wastewaters clearly demonstrates the robust and wide applicability of M-Janus nanoparticles for treating various types of oily wastewaters.

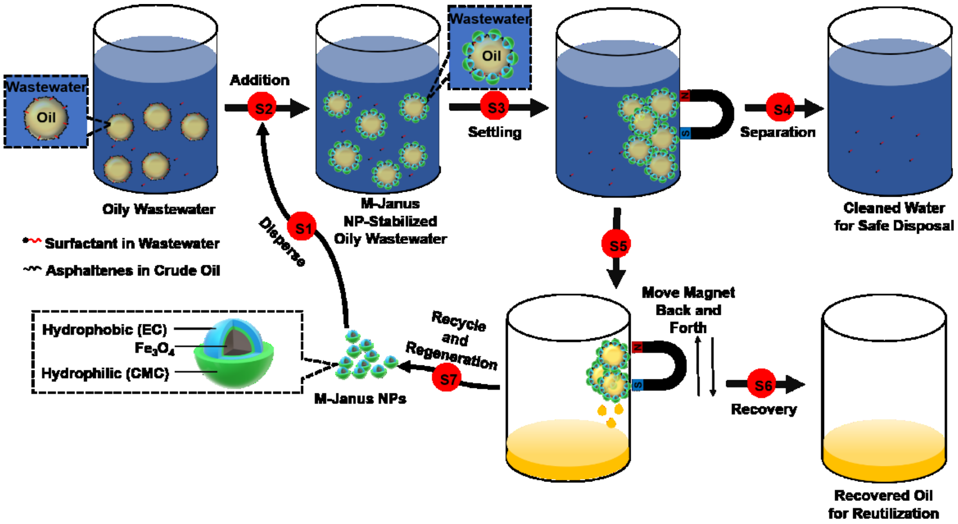

**Figure 5-12.** Schematic illustration of removing/recovering waste oil from oily wastewaters using M-Janus nanoparticles.

### 5.2.5 Efficiency of Removing/Recovering Oil from Oily Wastewaters using M-Janus Nanoparticles

As shown in **Figure 5-17**, by measuring the carbon content of the oily wastewaters before and after oil removal/recovery, an oil removal/recovery efficiency of 87.23 ± 1.68 % and 87.96 ± 2.15 % was obtained by M-CMC-EC nanoparticles for the crude oil/synthetic seawater and crude oil/tap water, respectively. In contrast, the use of M-Janus nanoparticles led to an oil remove/recover efficiency of 95.1 ± 2.31 % and 96.72 ± 1.28 % from synthetic seawater and oily tap water, indicating a more efficient removal/recovery of crude oil from the oily wastewaters by M-Janus nanoparticles than by M-CMC-EC nanoparticles.

With the addition of M-Janus nanoparticles, oil removal/recovery efficiency of 92.67 ± 1.99 % and 91.56 ± 3.51 % was obtained for the cooking oil in synthetic seawater and detergent-containing tap water, respectively, in contrast to 85.77 ± 1.63 % and 84.32 ± 2.27 % obtained with the addition of M-CMC-EC nanoparticles. Such results clearly suggest again more efficient removal/recovery of cooking oil from complex oily wastewaters by M-Janus nanoparticles than by M-CMC-EC nanoparticles. The results of measuring the water content in the recovered oil showed less than 1.6 wt% of the water in the recovered oil-rich phase. With such a low concentration of wastewater, the recovered oil is of satisfying quality for the subsequent refining. It is interesting to note a removing/recovering efficiency of oil from oily wastewaters to be less than 100%, as anticipated due to wetting films of oil remained on hydrophobic sections of M-Janus nanoparticles. This portion of oil will remain in the washing fluids of regeneration that could be further recovered.

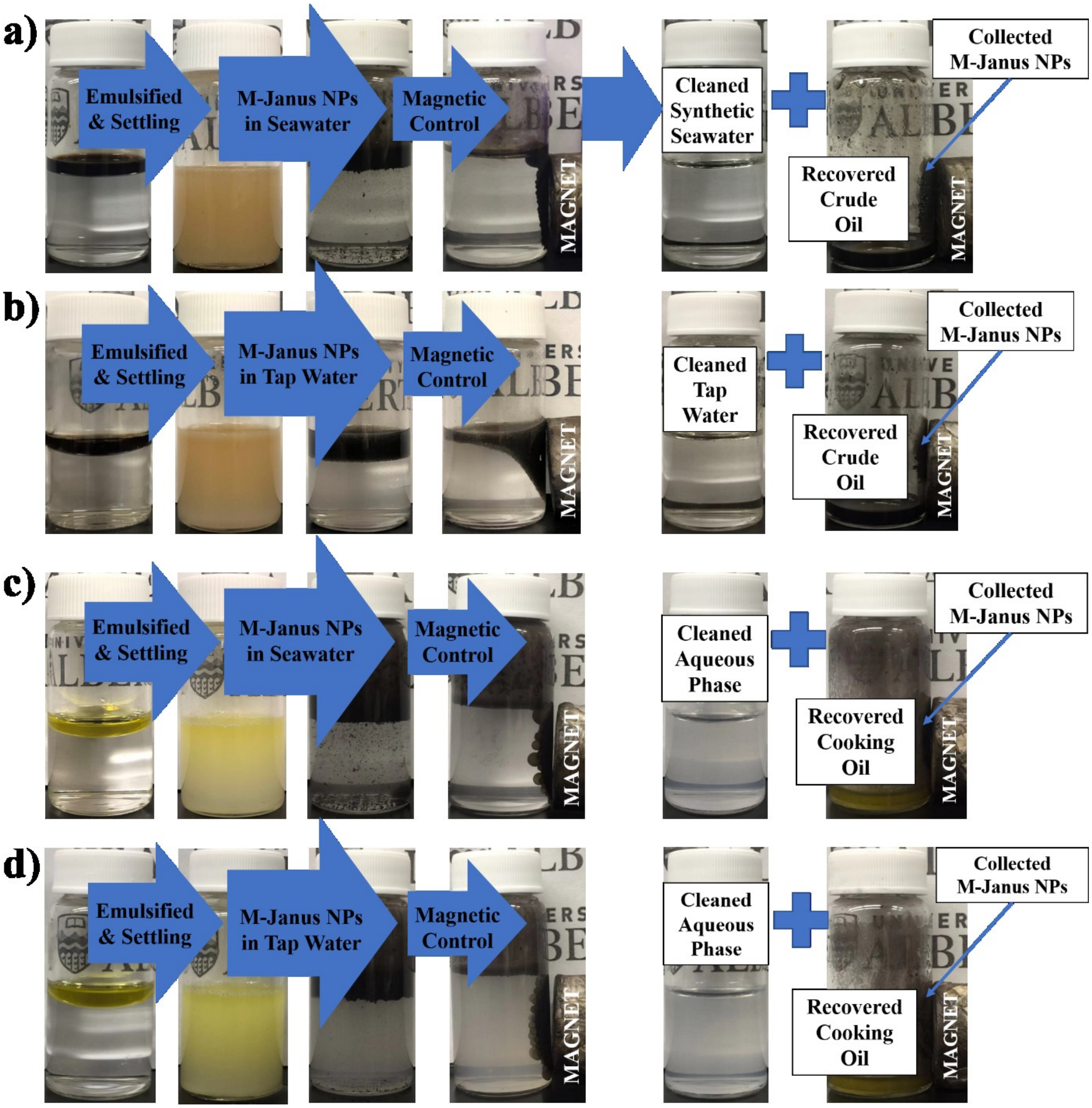

**Figure 5-13.** Demonstration of removing/recovering waste oil from a) diluted crude oil-in-synthetic seawater, b) diluted crude oil-in-tap water, c) cooking oil-in-tap water and d) cooking oil-in-detergent-containing tap water using M-Janus nanoparticles under an external magnetic field. The concentration of M-Janus nanoparticles in aqueous solution is 15 mg/mL.

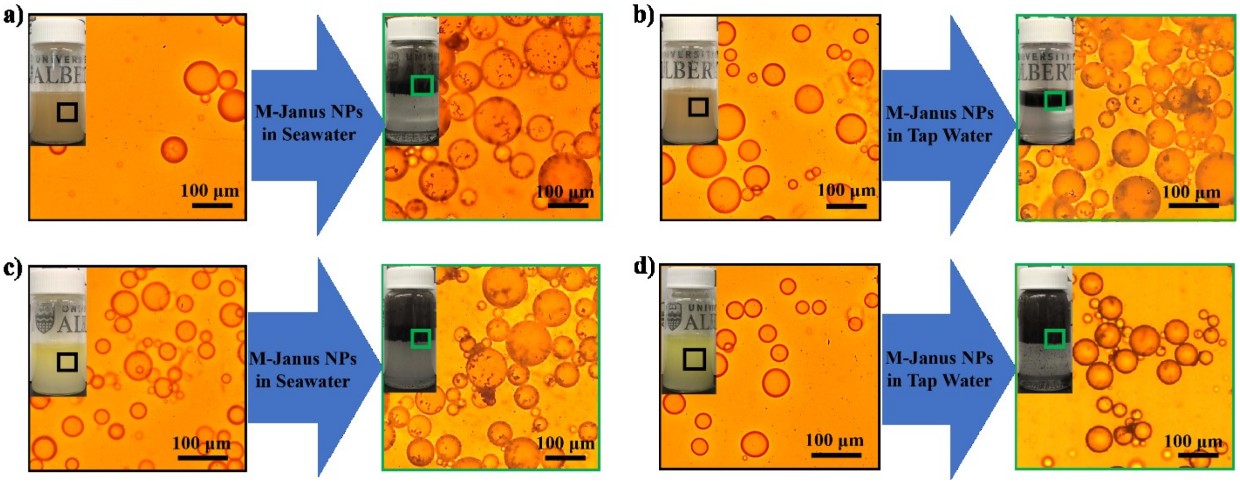

**Figure 5-14.** Microscopy images of a) crude oil-in-synthetic seawater, b) crude oil-in-tap water, c) cooking oil-in-synthetic seawater and d) cooking oil-in-detergent-containing tap water without or with stabilization by M-Janus nanoparticles. The scale bars in figure are 100 µm.

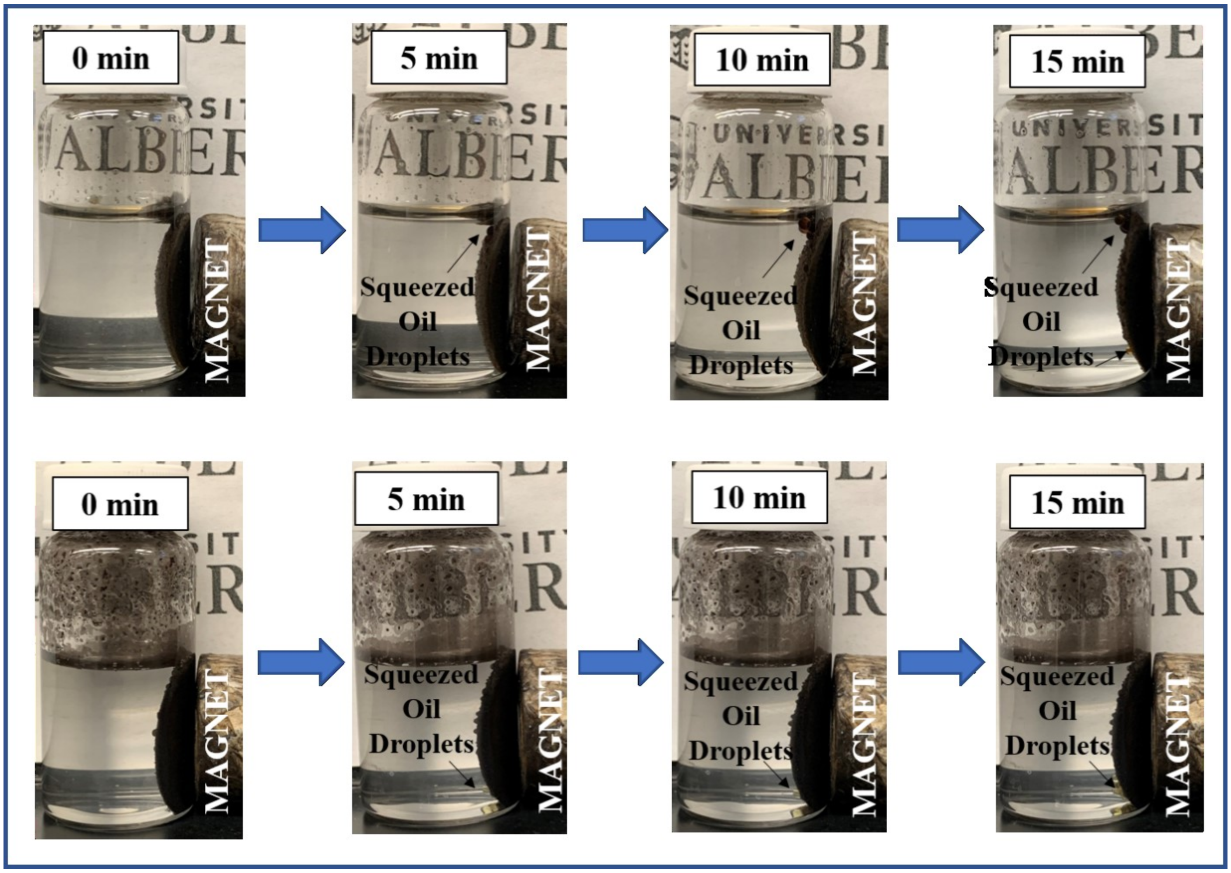

**Figure 5-15.** Formation of large oil droplets during magnetic controlling process.

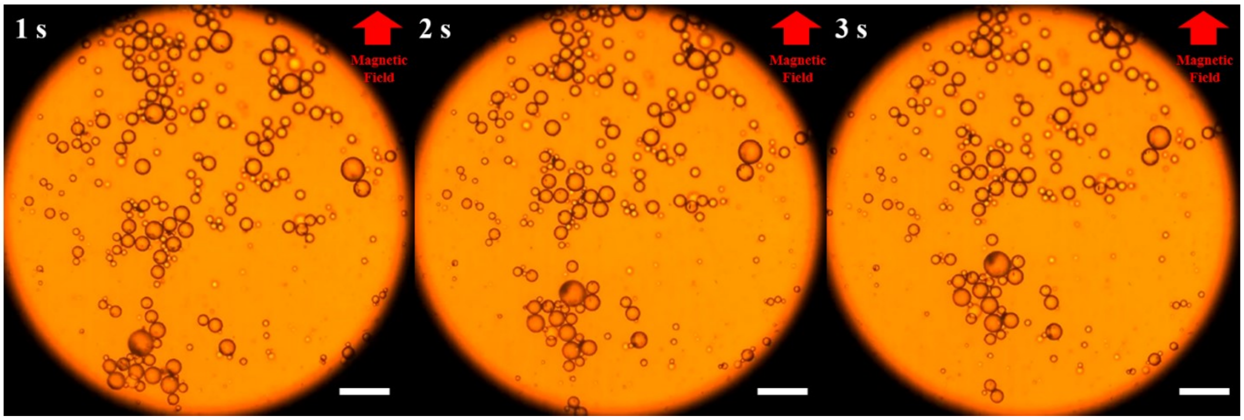

**Figure 5-16.** Magnetic controlling process of M-Janus nanoparticle-stabilized oil droplets. The scale bars in figure are 100 μm.

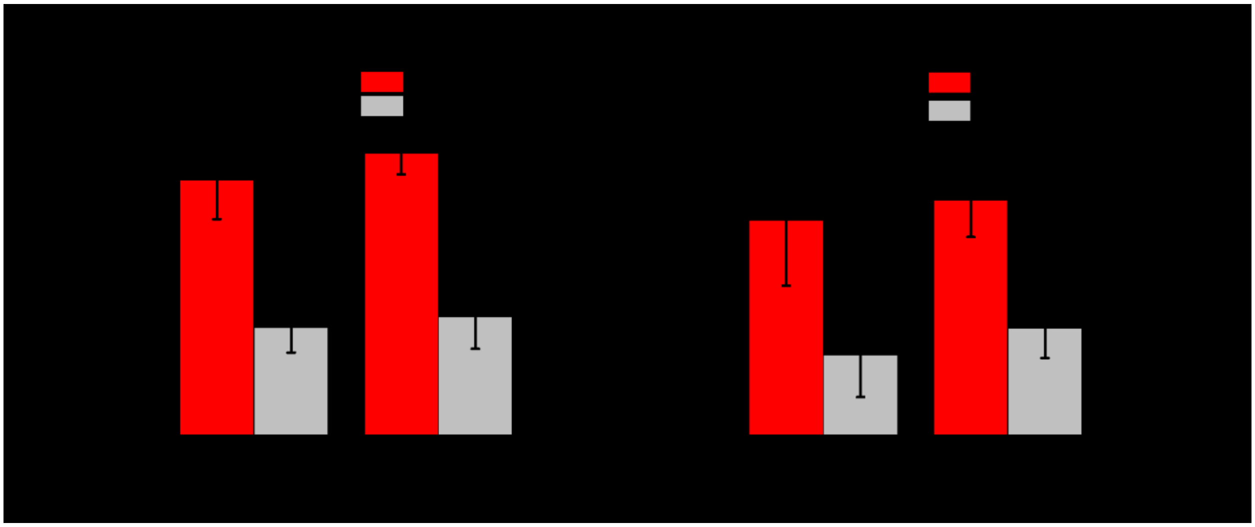

**Figure 5-17.** Oil removal/recovery efficiency using 1.5 wt% M-Janus nanoparticles or M-CMC-EC nanoparticles for a) crude oil and b) cooking oil in oily wastewaters. The experiments of oil removal/recovery were repeated three times with error bars being one standard deviation.

To better understand the relationship between the oil removal/recovery performance of the nanoparticles with their interfacial activities, the mass of nanoparticles which remained in the aqueous phase after oil collection was determined. The results in **Table 5-3** showed fewer M-Janus nanoparticles in the aqueous solutions after oil collection as compared with the M-CMC-EC nanoparticles, suggesting stronger attachment of more M-Janus nanoparticles at the oil-water interface than the M-CMC-EC nanoparticles. This observation correlates well with higher interfacial pressure and much longer coalescence time of oil droplets in suspensions of 100 ppm M-Janus nanoparticles than in 100 ppm M-CMC-EC nanoparticles, illustrating more secure anchoring of M-Janus nanoparticles at the oil-water interface, which led to the observed better oil removal/recovery performance from oily wastewaters by M-Janus nanoparticles than by M-CMC-EC nanoparticles. It is worth noting that the recovered oil-rich phase showed higher turbidity than the original oil. This is because the recovered oil-rich phase contained some remaining M-Janus nanoparticles. The remaining M-Janus nanoparticles in the oil-rich phase may influence the further refinery of the recovered oil. To address this issue, the remaining M-Janus nanoparticles could be separated from the recovered oil via magnetic separating process such as using a magnetic drum separator in practical applications, achieving the highly purified recovered oil phase for the further refinery process.

### 5.2.6 Reusability of M-Janus Nanoparticles for Removing/Recovering Oil from Oily Wastewaters

As discussed above, the M-Janus nanoparticles showed promising applications to removal/recovery of waste oil from oily wastewaters, and it would be extremely attractive if the spent particles could be recycled and reused, reducing not only operating cost but also the generation of secondary wastes.

After removing/recovering oil from the oily wastewaters, the M-Janus nanoparticles were collected and regenerated for the subsequent applications. **Figure 5-18** shows that with simple washing the oil removal/recovery efficiency using the regenerated M-Janus nanoparticles remained high for at least 5 cycles tested. After collecting M-Janus nanoparticles using a strong hand magnet, the collected M-Janus nanoparticles were cleaned by a facile regeneration process (washing with toluene and acetone) to remove possible contaminations (detergents, crude oil and cooking oil) from the recycled M-Janus nanoparticle surfaces. After regeneration, the recycled M-Janus nanoparticles could effectively lower the oil-water interfacial tensions to 21.5 – 23.9 mN/m, which are similar to the interfacial tension (~ 22.2 mN/m) of oil-water interface in the presence of freshly prepared M-Janus nanoparticles, indicating an insignificant contamination of M-Janus nanoparticles after each regeneration by washing with toluene and acetone. The efficiencies of removing/recovering crude oil or cooking oil from synthetic seawater or detergent-containing tap water remained high in all 5 cycles investigated, suggesting the robust nature of M-Janus nanoparticles for the oil removal/recovery from oily wastewaters.

**Table 5-3.** Mass of M-Janus or M-CMC-EC nanoparticles in aqueous phase and estimated mass of corresponding nanoparticles at oil-water interface after oil collection. The experiments of measuring the mass of nanoparticles in aqueous phase were repeated three times and the error range represents one standard deviation of measurements.

| Oily Wastewaters | M-Janus nanoparticles | | M-CMC-EC nanoparticles | |
|---|---|---|---|---|
| | at Oil-Water Interface (mg) [a] | in Aqueous Phase (mg) | at Oil-Water Interface (mg) [a] | in Aqueous Phase (mg) |
| | | Crude Oil | | |
| Synthetic Seawater | 133.2± 2.3 | 16.8 ± 2.3 | 122.6± 2.8 | 27.4 ± 2.8 |
| Tap Water | 137.3± 1.5 | 12.7 ± 1.5 | 126.3± 1.9 | 23.7 ± 1.9 |
| | | Cooking Oil | | |
| Synthetic Seawater | 128.3± 1.7 | 21.7 ± 1.7 | 121.7± 3.5 | 28.3 ± 3.5 |
| Tap Water w/Detergent | 130.7± 3.4 | 19.3 ± 3.4 | 117.1± 2.4 | 32.9 ± 2.4 |

[a] Mass of nanoparticles at oil-water interface = Mass of applied nanoparticles - Mass of nanoparticles in aqueous phase.

**Table 5-4.** Recycle of M-Janus nanoparticles after removing/recovering crude oil from synthetic seawater. The experiments were triplicated and the error range represents one standard deviation of measurements.

| Cycle | 1 | 2 | 3 | 4 | 5 |
|---|---|---|---|---|---|
| Added (mg) | 150.0 | 150.0 | 150.0 | 150.0 | 150.0 |
| Recovered (mg) | 146.6 ± 2.0 | 143.9± 2.2 | 147.1± 1.8 | 145.8± 2.6 | 144.8± 3.1 |
| Recovery of M-Janus nanoparticles (%) | 97.7 ± 1.3 | 95.9 ± 1.5 | 98.1 ± 1.2 | 97.2 ± 1.7 | 96.5 ± 2.1 |

**Table 5-5.** Recycle of M-Janus nanoparticles after removing/recovering crude oil from tap water. The experiments were triplicated and the error range represents one standard deviation of measurements.

| Cycle | 1 | 2 | 3 | 4 | 5 |
|---|---|---|---|---|---|
| Added (mg) | 150.0 | 150.0 | 150.0 | 150.0 | 150.0 |
| Recovered (mg) | 148.7 ± 1.1 | 145.8 ± 1.7 | 146.4 ± 2.2 | 145.2 ± 1.9 | 145.6 ± 2.4 |
| Recovery of M-Janus nanoparticles (%) | 99.1 ± 0.7 | 97.2 ± 1.1 | 97.6 ± 1.5 | 96.8 ± 1.3 | 97.1 ± 1.6 |

**Table 5-6.** Recycle of M-Janus nanoparticles after removing/recovering cooking oil from synthetic seawater. The experiments were triplicated and the error range represents one standard deviation of measurements.

| Cycle | 1 | 2 | 3 | 4 | 5 |
|---|---|---|---|---|---|
| Added (mg) | 150.0 | 150.0 | 150.0 | 150.0 | 150.0 |
| Recovered (mg) | 142.2 ± 2.4 | 144.3 ± 2.7 | 143.4 ± 1.9 | 143.7 ± 2.3 | 144.7 ± 3.3 |
| Recovery of M-Janus nanoparticles (%) | 94.8 ± 1.6 | 96.2 ± 1.8 | 95.6 ± 1.3 | 95.8 ± 1.5 | 96.5 ± 2.2 |

**Table 5-7.** Recycle of M-Janus nanoparticles after removing/recovering cooking oil from detergent-containing tap water. The experiments were triplicated and the error range represents one standard deviation of measurements.

| Cycle | 1 | 2 | 3 | 4 | 5 |
|---|---|---|---|---|---|
| Added (mg) | 150.0 | 150.0 | 150.0 | 150.0 | 150.0 |
| Recovered (mg) | 141.9 ± 2.9 | 139.8 ± 3.5 | 143.7 ± 2.2 | 145.1 ± 1.8 | 140.8 ± 3.4 |
| Recovery of M-Janus nanoparticles (%) | 94.6 ± 1.9 | 93.2 ± 2.3 | 95.8 ± 1.5 | 96.7 ± 1.2 | 93.9 ± 2.3 |

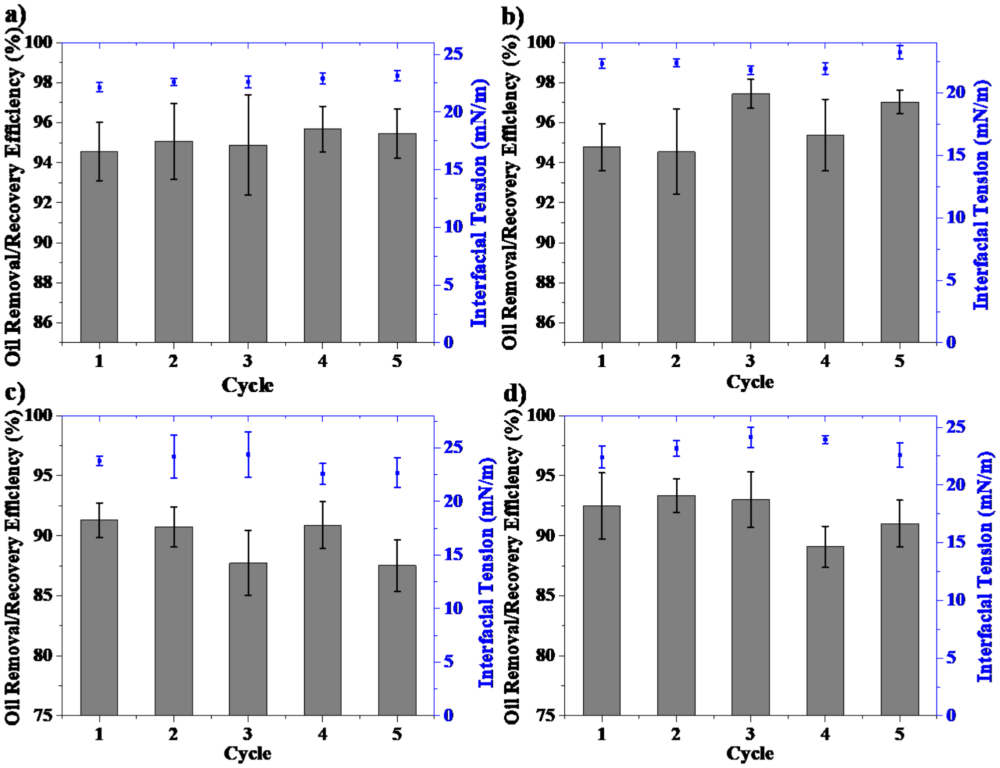

**Figure 5-18.** Removal/recovery efficiency of oil using recycled M-Janus nanoparticles from: a) crude oil-in-synthetic seawater, b) crude oil-in-tap water, c) cooking oil-in-synthetic seawater, and d) cooking oil-in-detergent-containing tap water; and corresponding oil-water interfacial tensions in the presence of M-Janus nanoparticles recycled after each cycle. The experiments were triplicated and the error range represents one standard deviation of measurements.

The recovery of M-Janus nanoparticles in the recycling test is greater than 93.2 % (**Tables 5-4**, **5-5**, **5-6** and **5-7**), demonstrating the successful recycling of M-Janus nanoparticles in a lab-scale batch process. We should note that the recovery of M-Janus nanoparticles in realistic applications could be further improved by using stronger electromagnet or high gradient magnetic separators. The excellent performance of the recycled M-Janus nanoparticles ensures sustainable applications of M-Janus nanoparticles developed in this study for removing/recovery of oil from various types of oily wastewaters.

### 5.3 Conclusions

In this study, magnetic Janus nanoparticles (M-Janus nanoparticles) of asymmetric surface wettability were applied to removing/recovering more effectively of crude oils or waste cooking oils from different oily wastewaters stabilized by natural and/or synthetic surfactants. Despite the stabilization of waste oil by such natural and/or synthetic surfactants, our hypothesis is that the M-Janus nanoparticles of asymmetric wettability as compared with biwettable magnetic nanoparticles of uniform surface wettability could anchor more firmly at the oil-water interface, leading to more effective treatment of oily wastewaters and removal/recovery of waste oil.

Compared with the magnetically responsive and interfacially active nanoparticles (M-CMC-EC nanoparticles) of uniform surface wettability reported previously,[56] the M-Janus nanoparticles of asymmetric surface wettability exhibited superior interfacial activities in the complex oily wastewater systems, including lower oil-water interfacial tension and stronger deposition of M-Janus nanoparticles on droplet surfaces. By anchoring more securely at the waste oil droplet surfaces, the M-Janus nanoparticles showed > 91.5 % oil removal/recovery efficiency in contrast to > 84.3% obtained with the M-CMC-EC nanoparticles. Such results clearly demonstrate the improvement in the oil removal/recovery using Janus nanoparticles of asymmetric surface wettability instead of traditional nanoparticles of uniform surface wettability, confirming our hypothesis. Furthermore, the results from the recycling test after regeneration of spent particles illustrated the reliable and sustainable applications of M-Janus nanoparticles to removing/recovering oil from oily wastewaters under realistic conditions. Compared with other magnetic Janus nanoparticles for oil removal/recovery,[189, 191, 226, 261] our novel M-Janus nanoparticles were facilely synthesized using low-cost, commercially available, biodegradable and naturally available cellulosic materials, leading to applications oily wastewater treatment and oil recovery without generating secondary hazards to the ambient environment.

# Chapter 6 Removal of Emulsified Process Water from Crude Oil Emulsions using Magnetic Janus Nanoparticles

X. He, Q. Liu and Z. Xu, Removal of Emulsified Process Water from Crude Oil Emulsions using Magnetic Janus Nanoparticles, in preparation.

Process water is inevitably emulsified in crude oil during crude oil production processes. The potential catastrophic damage to the downstream equipment by the process water of high electrolyte contents has inspired researchers to develop effective methods to remove the emulsified water from crude oil emulsions prior to their further processing. In this study, novel magnetic Janus nanoparticles of asymmetric surface wettabilities, called M-Janus nanoparticles, were applied for the first time to removing emulsified process water from the crude oil emulsions at room temperature. Despite the presence of other interfacially active components such as natural surfactants and inorganic electrolytes in the process water and asphaltenes in the crude oil, the M-Janus nanoparticles showed stronger interfacial activities that allowed them to anchor more firmly at the diluted crude oil-process water interface than conventional interfacial active nanoparticles (M-CMC-EC nanoparticles) of uniform surface wettabilities. With the addition of 0.75 wt% M-Janus nanoparticles, around 90 wt% emulsified process water was removed from the diluted crude oil, in contrast to the removal of 80 wt% water obtained with the addition of M-CMC-EC nanoparticles at the same dosage. The M-Janus nanoparticles were shown to be more robust in dewatering the crude oil emulsions of different water contents (2.5 wt% - 20 wt%). After dewatering the crude oil emulsions, the M-Janus nanoparticles could be recycled conveniently and reused for the subsequent dewatering process with facile regeneration, retaining excellent interfacial activities and high dewatering efficiency for at least six cycles. The superior interfacial activities, high dewatering efficiency, exceptional recyclability make the M-Janus nanoparticles ideal candidates for dewatering the emulsified process water from crude oil in petroleum production.

## 6.1 Introduction

In petroleum production, process water-in-crude oil emulsions are often inevitably generated.[262-263] The salts such as chlorides and sulfides contained in the process water are harsh hazards to the downstream processing because such salts can cause severe corrosion to the refinery equipment and serious poisoning to the cracking and refining catalysts.[264-265] Removal of the emulsified water from crude oils prior to their downstream processing has been one of the major challenges facing the petroleum industry. In crude oil production, the connate and process water of high salinity is emulsified and stabilized by the formation of an interfacial film at the crude oil-process water interface from the interfacially active components such as asphaltenes, resins and fine particles (waxes and clays).[266-268] The interfacial film of high mechanical strength creates an insurmountable steric barrier between the emulsified water droplets to prevent them from flocculating and coalescing, leading to a process water-in-crude oil emulsion of incredible stability.[196] The intrinsic stability of such emulsions must be broken to remove the emulsified water prior to subsequent processes. The current techniques to break such emulsions include thermal treatment,[269] demulsifier treatment,[195, 239, 270-271] dense carbon dioxide,[272] ionic liquids, and microwave radiation.[154, 273-274] However, these methods have inherent drawbacks, including the high expense of consumed energy, unsatisfying dewatering efficiency, generation of secondary hazards, and inconvenient recycling.

Recently, assisted with an external magnetic field, magnetically responsive and interfacially active nanoparticles have been considered as effective tools to remove emulsified water from crude oil emulsions.[275-276] With the promising interfacial activities, such nanoparticles are capable of anchoring at emulsified water droplet surfaces, leading to the formation of nanoparticle-tagged water droplets. Driven by the responded magnetic force, such water droplets could be attracted and transported to the desired locations, resulting in effective removal of process water from the crude oil emulsions. Compared with the other demulsification technologies, removing process water achieved by magnetically responsive and interfacially active nanoparticles exhibits higher throughput and efficiency, less labor-intensity and consumption of energy, easier recycling of raw materials, and lower cost. A variety of magnetic nanoparticles have been reported to be interfacially active with uniform surface modification by poly(2-demthylaminoethyl methacrylate) (PDMAEMA),[277] oleic acids,[182] polyelectrolytes,[55] polyvinylpyrrolidone, and ethyl cellulose.[56, 58, 183, 220] Such materials on the nanoparticle surfaces can effectively disturb and destroy the stable interfacial film which is the main contribution to the stability of process water-in-crude oil emulsions, resulting in available anchoring sites for the nanoparticles at the water droplet surfaces. With the tagging by the nanoparticles, the process water droplets could be removed under an external magnetic field. However, the nanoparticles may desorb from the water droplet surfaces if the responded magnetic forces are too powerful,[184] leading to unattractable water droplets and hence the ineffective dewatering of the crude oil emulsions. Although a relatively weak magnetic field can avoid the desorption of the nanoparticles from the water droplet surfaces, the responded magnetic forces are feeble at the same time, resulting in slow and inefficient removal of water droplets. Based on these reasons, nanoparticles with more secure anchoring at the oil-water interface are highly desirable for dewatering the crude oil emulsions under the external magnetic field.

Janus nanoparticles have attracted a wide range of interests because of their unique structure and asymmetric surface wettability.[278-279] With two contrasting surface wettability on Janus nanoparticle surfaces, the nanoparticles can possess superior interfacial activities than the nanoparticles of uniform surface wettability.[185, 189] As a result, Janus nanoparticles of asymmetric surface wettability require higher energy to desorb from the oil-water interface than the nanoparticles of uniform surface wettability,[175] representing the stronger anchoring of Janus nanoparticle at the oil-water interface. With the stabilization by such Janus nanoparticles, the Janus nanoparticles-tagged process water droplets are more stable under the external magnetic field and the Janus nanoparticles are anticipated to have better performance on removing water from crude oil emulsions than the nanoparticles of uniform surface wettability. For example, Ali *et al.* reported the interfacially active P(MMA-AA-DVB)/$Fe_3O_4$ Janus nanoparticles, which were applied successfully to removing water from crude oil emulsions at elevated temperature, showing the promising application of Janus nanoparticles to the dewatering of water-in-crude oil emulsions.[191, 226] Recently, we designed a novel magnetic Janus nanoparticle, called M-Janus nanoparticle, which was synthesized via the Pickering emulsion method using hydrophobic ethyl cellulose (EC) and hydrophilic carboxymethyl cellulose (CMC).[194] The M-Janus nanoparticles of asymmetric surface wettability exhibited superior interfacial activities at the clean toluene-water interface than the nanoparticles of uniform surface properties (M-CMC-EC nanoparticles) reported previously.[56, 194] Meanwhile, the M-CMC-EC nanoparticles could dewater the diluted crude oil emulsions at room temperature. Based on these reasons, we anticipate that M-Janus nanoparticles of superior interfacial activities show better performance on dewatering the crude oil emulsions at room temperature than M-CMC-EC nanoparticles.

In this study, the M-Janus nanoparticles were applied for the first time to removing emulsified process water from crude oil emulsions. The M-Janus nanoparticles could anchor securely at the diluted crude oil-process water interface despite the presence of natural surfactants in crude oil and inorganic electrolytes in process water. The M-Janus nanoparticles of asymmetric surface wettability showed superior interfacial activities including lower oil-water interfacial tension and rigidifying oil-water interface than the M-CMC-EC nanoparticles of uniform surface wettability. For dewatering the crude oil emulsions of 5 wt% initial water content, the M-Janus nanoparticles showed a maximum dewatering efficiency of 95%, in contrast to 91% obtained by M-CMC-EC nanoparticles. When the M-Janus nanoparticles were applied to the removal of water from crude oil emulsions of various initial water contents (2.5 wt%-20 wt%), the water contents in the emulsions decreased significantly to less than 1 wt%, showing the robust dewatering ability of M-Janus nanoparticles on treating the diluted crude oil emulsions containing various process water. After the dewatering process, the M-Janus nanoparticles can be recycled and reused without complex regeneration while still retaining high dewatering efficiency and excellent interfacial activities, indicating their promising recyclability and sustainability.

## 6.2 Concept of Dewatering Crude Oil Emulsions using M-Janus Nanoparticles and M-CMC-EC Nanoparticles under External Magnetic Field

**Scheme 6-1** shows the dewatering process water-in-diluted crude oil emulsions using M-Janus nanoparticles and M-CMC-EC nanoparticles. The process water droplets were typically stabilized by the natural surfactants in crude oil. Without proper treatment, the process water droplets of several micrometer sizes were stable and well dispersed in the crude oil emulsion. The suspension of nanoparticles (M-Janus or M-CMC-EC nanoparticles) in organic solvent was prepared by dispersing M-Janus or M-CMC-EC nanoparticles in a tiny amount of heavy. The suspension prepared as such was then added into the process water-in-diluted crude oil emulsion, followed by vigorous mixing. Due to the EC coating on the nanoparticle surface, such interfacially active nanoparticles could effectively break the protective interfacial film and anchor at the water droplet surfaces. A strong hand magnet was then placed by the side of the emulsion to attract the nanoparticles-tagged water droplets, achieving the removal of process water from the bulk diluted crude oil emulsion. Compared with M-CMC-EC nanoparticles of uniform surface wettability, M-Janus nanoparticles of asymmetric surface wettability had superior interfacial activities and anchored more securely at the water droplet surfaces, leading to their more secure anchoring at the process water droplet surfaces. Under the external magnetic field, the M-Janus nanoparticles were more challenging to desorb from the water droplet surfaces than the M-CMC-EC nanoparticles. As a result, the M-Janus nanoparticles-tagged process water droplets were more stable than water droplets tagged by the M-CMC-EC nanoparticles under the external magnetic field, leading to more efficient and effective dewatering of the crude oil emulsion using M-Janus nanoparticles.

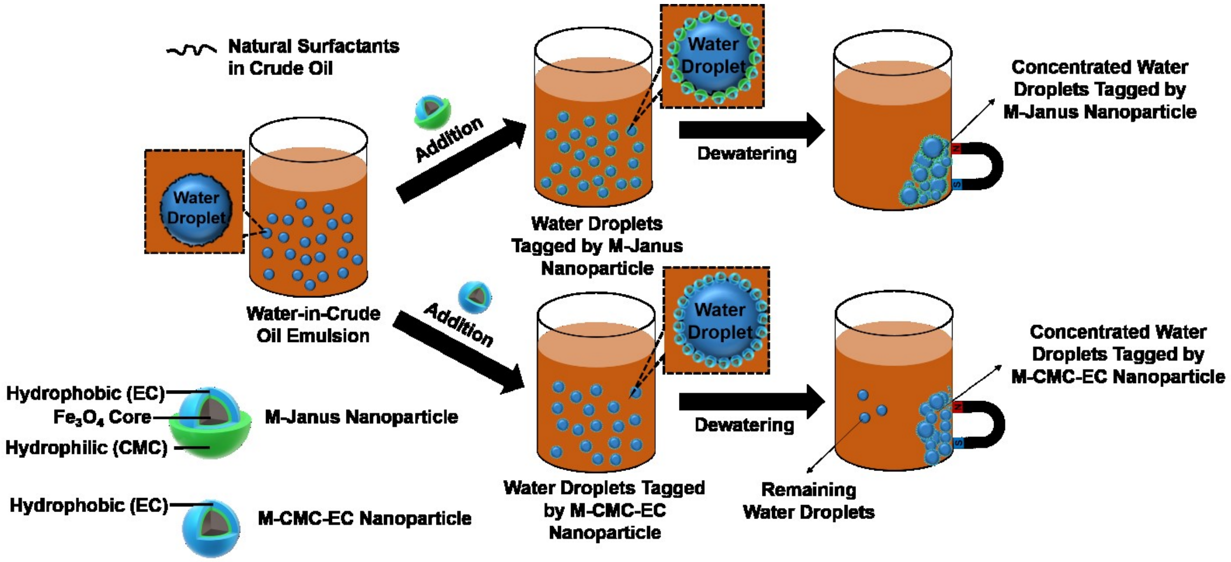

**Scheme 6-1.** Schematic illustration of dewatering process water-in-diluted crude oil emulsions using magnetically responsive and interfacially active nanoparticles.

## 6.3 Results and Discussion

### 6.3.1 Dispersion of M-CMC-EC Nanoparticles and M-Janus Nanoparticles at Oil-Water Interface

**Figure 6-1** shows the dispersion of M-Janus nanoparticles and M-CMC-EC nanoparticles at the oil-water interface. The M-Janus nanoparticles showed better dispersion than the M-CMC-EC nanoparticles, which exhibited severe agglomerations at the oil-water interface. Such a phenomenon results from the stronger electrostatic forces between the M-Janus nanoparticles. Due to the coating of carboxymethyl cellulose, the carboxylate groups on M-Janus nanoparticle surfaces deprotonated in the aqueous phase, leading to the generation of more negative surface charges than the surface charges generated by the ionization of hydroxyl groups on the M-CMC-EC nanoparticle surfaces.[194, 232-233] As a result, the stronger electrostatic repulsion led to better dispersion of M-Janus nanoparticles at the oil-water interface as compared with the M-CMC-EC nanoparticles. The better dispersion at the interface also contributes to more active interfacial behaviors of M-Janus nanoparticles at the diluted crude oil-process water interface, which are comprehensively discussed later.

### 6.3.2 Interfacial Activities of M-CMC-EC Nanoparticles and M-Janus Nanoparticles at Crude Oil-Process Water Interface

#### 6.3.2.1 Interfacial Tension

As shown in **Figure 6-2a**, the interfacial tension of the heavy naphtha-process water interface decreased gradually and stabilized finally at ~ 17.0 mN/m due to the adsorption of the impurities in heavy naphtha onto the heavy naphtha-process water interface. The diluted crude oil-process water interface showed a lower value of interfacial tension than that of the heavy naphtha-process water interface, indicating the more interfacially active properties of the natural surfactants in crude oil than the impurities in heavy naphtha. Compared with the impurities and the natural surfactants in the process water-in-diluted crude oil emulsion, the interfacially active nanoparticles showed stronger interfacial properties indicated by the lower interfacial tension of the heavy naphtha-process water interface in the presence of the nanoparticles. With the adsorption of M-CMC-EC nanoparticles at the interface, the interfacial tension of the heavy naphtha-process water interface stabilized at ~ 12.1 mN/m. As compared, a lower value of ~ 10.3 mN/m was observed for the heavy naphtha-process water interface in the presence of M-Janus nanoparticles, illustrating the superior interfacial activities of M-Janus nanoparticles than M-CMC-EC nanoparticles.

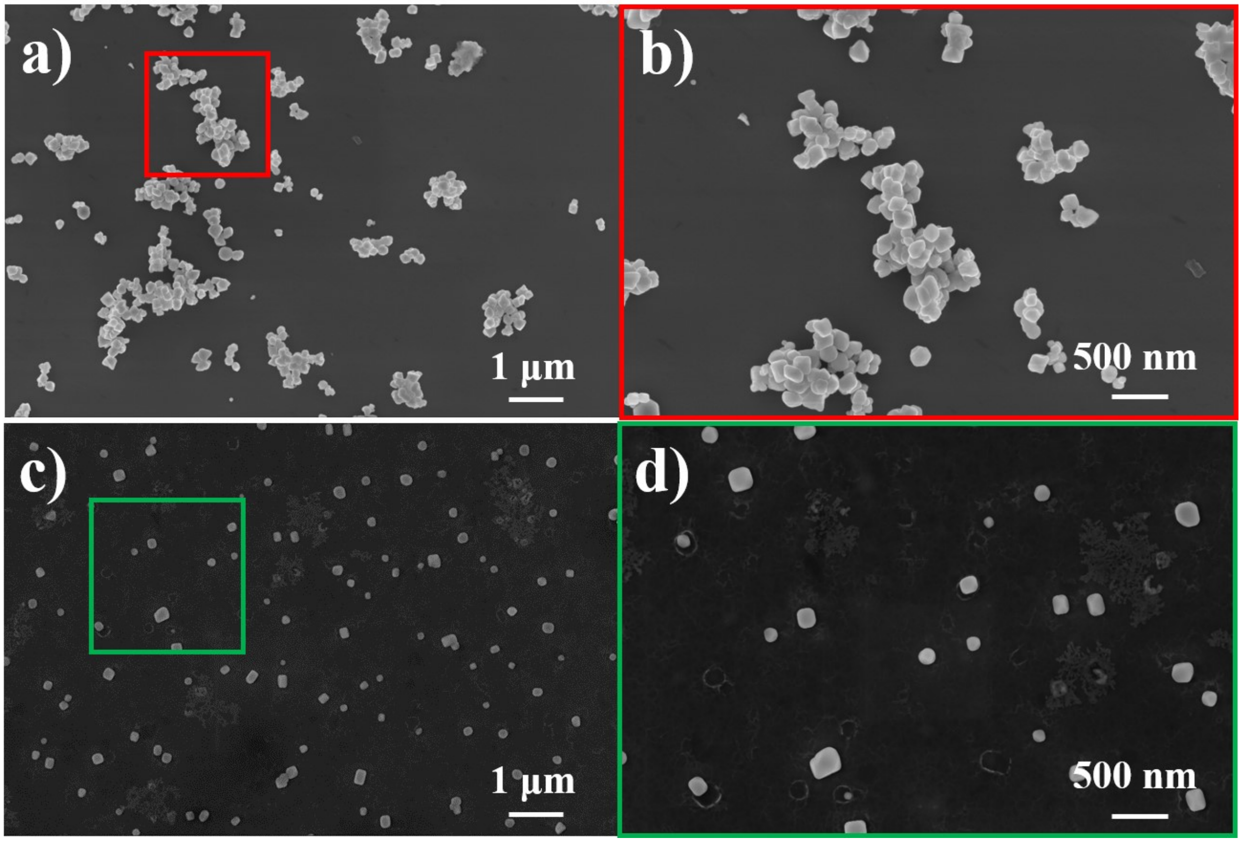

**Figure 6-1.** FE-SEM images of 0.1 mg/mL (a and b) M-CMC-EC nanoparticles and 0.1 mg/mL (c and d) M-Janus nanoparticles at crude oil-process water interface, showing better dispersion of M-Janus nanoparticles than M-CMC-EC nanoparticles at oil-water interface.

**Figure 6-2b** shows the interfacial tension of the diluted crude oil-process water interfaces in the presence of different interfacially active materials. Interestingly, the addition of pure heavy naphtha showed negligible influence on the interfacial tension of the diluted crude oil-process water interface, indicating the irreversible adsorption of natural surfactants in crude oil onto the process water droplet surface. In contrast, the addition of the suspension of M-Janus or M-CMC-EC nanoparticles into the original organic phase resulted in lower interfacial tension of 11.0 mN/m and 13.7 mN/m, respectively, demonstrating the adsorption of the interfacially active nanoparticles at the natural surfactant-stabilized oil-water interface and superior interfacial activities of M-Janus nanoparticles than M-CMC-EC nanoparticles.

#### 6.3.2.2 Interfacial Pressure-Area (π-A) Isotherms

To further investigate and compare the interfacial properties of the M-Janus nanoparticles and the M-CMC-EC nanoparticles in the process water-in-crude oil emulsion, the Langmuir trough was applied to study their interfacial behaviors at the heavy naphtha-process water interface. **Figure 6-3a** shows the gradually increasing interfacial pressure of the heavy naphtha-process water interface under the continuous compression, indicating the adsorption of interfacially active impurities from the process water onto the oil-water interface. In the presence of interfacially active components such as asphaltenes in the crude oil, M-CMC-EC nanoparticles and M-Janus nanoparticles at the heavy naphtha-process water interface, the higher interfacial pressures were observed in contrast to the interfacial pressure of the heavy naphtha-process water interface in the absence of any interfacially active components. Noteworthy, the interface in the presence of M-Janus nanoparticles exhibited the highest interfacial pressure among all the cases, showing the most active interfacial behaviors of M-Janus nanoparticles.

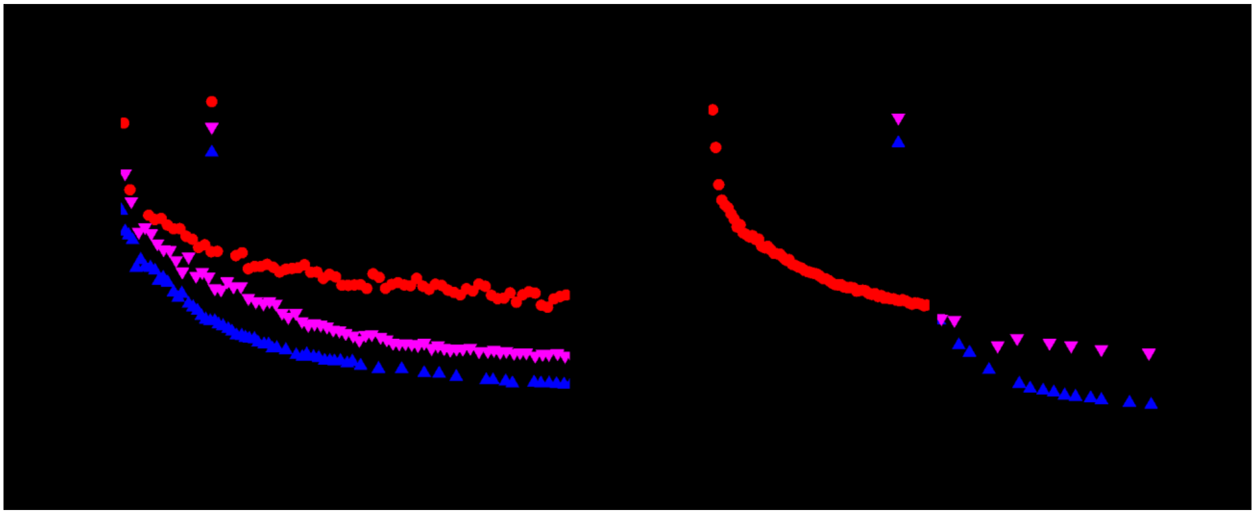

**Figure 6-2.** Dynamic interfacial tension of a) heavy naphtha-process water interface in the presence or absence of crude oil, M-CMC-EC nanoparticles or M-Janus nanoparticles (baseline represents heavy naphtha-process water interface) and b) diluted crude oil-process water interfaces with subsequent addition as indicated by the dash line of different solutions. Suspensions of nanoparticles in heavy naphtha contain 0.1 mg/mL nanoparticles.

**Figure 6-3b** shows the interfacial pressure-area isotherms of the diluted crude oil-process water-interface in the absence or presence of M-Janus nanoparticles or M-CMC-EC nanoparticles. After the original diluted crude oil-process water interface reaching equilibrium, suspension of M-Janus or M-CMC-EC nanoparticles in heavy naphtha was added dropwise into the organic phase without disturbing the original interface. The interface in the presence of M-Janus or M-CMC-EC nanoparticles showed higher interfacial pressure as compared with the previous diluted crude oil-process water interface, indicating the effective adsorption of the interfacially active nanoparticles at the water-oil interface. It is worth noting that the adsorption of M-Janus nanoparticles at the diluted crude oil-process water interface led to a bigger increase in the interfacial pressure than the case of M-CMC-EC nanoparticles, again confirming the superior interfacial properties of M-Janus nanoparticles.

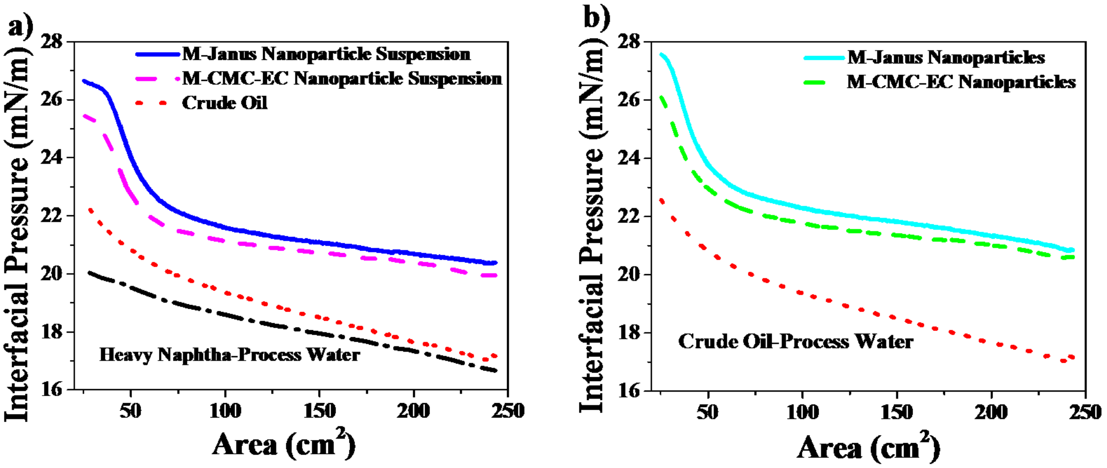

**Figure 6-3.** Interfacial pressure-area ($\pi$-$A$) isotherms of a) heavy naphtha-process water interface in the presence or absence of M-CMC-EC nanoparticles, M-Janus nanoparticles or asphaltenes in crude oil and b) diluted crude oil-process water interface in the presence or absence of M-CMC-EC nanoparticles or M-Janus Janus nanoparticles. Suspensions of nanoparticles in heavy naphtha contain 0.1 mg/mL nanoparticles.

#### 6.3.2.3 Coalescence Time

The results in **Table 6-1** and **Figure 6-4** show that the process water droplets in the heavy naphtha environment required 4.7 ± 1.0 s to coalesce, suggesting the stabilization of the process water droplet by the interfacially active impurities in heavy naphtha. When two process water droplets were contacted in the diluted crude oil, it took an increased time (9.87 ± 2.27 s) for two process water droplets to coalesce, indicating that the natural surfactants in crude oil are more interfacially active than the impurities in heavy naphtha. Interestingly, despite the excellent interfacial activities of M-Janus nanoparticles and M-CMC-EC nanoparticles at the process water-diluted crude oil interface, the addition of nanoparticle suspension into the original diluted crude oil resulted in the immediate coalescence of the process water droplets once contacted. This is because the adsorption of the interfacially active nanoparticles at the process water droplet surfaces can cause displacement of the original protecting interfacial film, resulting in nanoparticle-tagged process water droplets and leading to rupture and voids on the interfacial film. Once contact, such nanoparticle-anchored process water droplets were unstable, leading to immediate coalescence.

**Table 6-1.** Coalescence times of two process water droplets in different organic environments.

| Aqueous Phase | Organic Phase | Coalescence Time (s) |
|---|---|---|
| Process Water | Heavy Naphtha | 4.7 ± 1.0 |
| Process Water | Heavy Naphtha-Diluted Crude Oil | 9.9 ± 2.3 |
| Process Water | Heavy Naphtha-Diluted Crude Oil + 100 ppm of M-CMC-EC Nanoparticles in Heavy Naphtha | Immediate Coalescence |
| Process Water | Heavy Naphtha-Diluted Crude Oil + 100 ppm M-CMC-EC Nanoparticles in Heavy Naphtha | Immediate Coalescence |

### 6.3.3 Dewatering Diluted Crude Oil Emulsions using Different Magnetic Nanoparticles

In this study, 0.5 wt% of different nanoparticles (bare iron oxide nanoparticles, M-CMC-EC nanoparticles, M-CMC-EC nanoparticles, and M-Janus nanoparticles) were added respectively into the crude oil emulsion of 5 wt% initial water content to investigate their dewatering ability. As shown in **Figure 6-5**, the original crude oil emulsion had a water content of 4.9 wt% after settling on the magnet for 15 min, demonstrating the stability of the crude oil emulsion if not properly treated. After the addition of bare iron oxide nanoparticles and M-CMC nanoparticles to the emulsion, the water content in the diluted crude oil emulsion remained almost the same as the blank one, indicating the ineffective dewatering ability of the interfacially inactive nanoparticles. With the addition of 0.5 wt% M-CMC-EC nanoparticles into the emulsion, the water content in the emulsion decreased to 1.9 wt%, showing the effective dewatering achieved by M-CMC-EC nanoparticles. In contrast, with the addition of 0.5 wt% M-Janus nanoparticles, the water content of the diluted crude oil emulsion was found to decrease significantly to 1.1 wt%. Compared with the M-CMC-EC nanoparticles of uniform surface wettability, the M-Janus nanoparticles showed higher dewatering efficiency. Such observation clearly shows that M-Janus nanoparticles could act as a highly effective dewatering tool for the crude oil emulsions, and the unique asymmetric surface wettability helped M-Janus nanoparticle possess better dewatering performance than M-CMC-EC nanoparticles of uniform surface wettability.

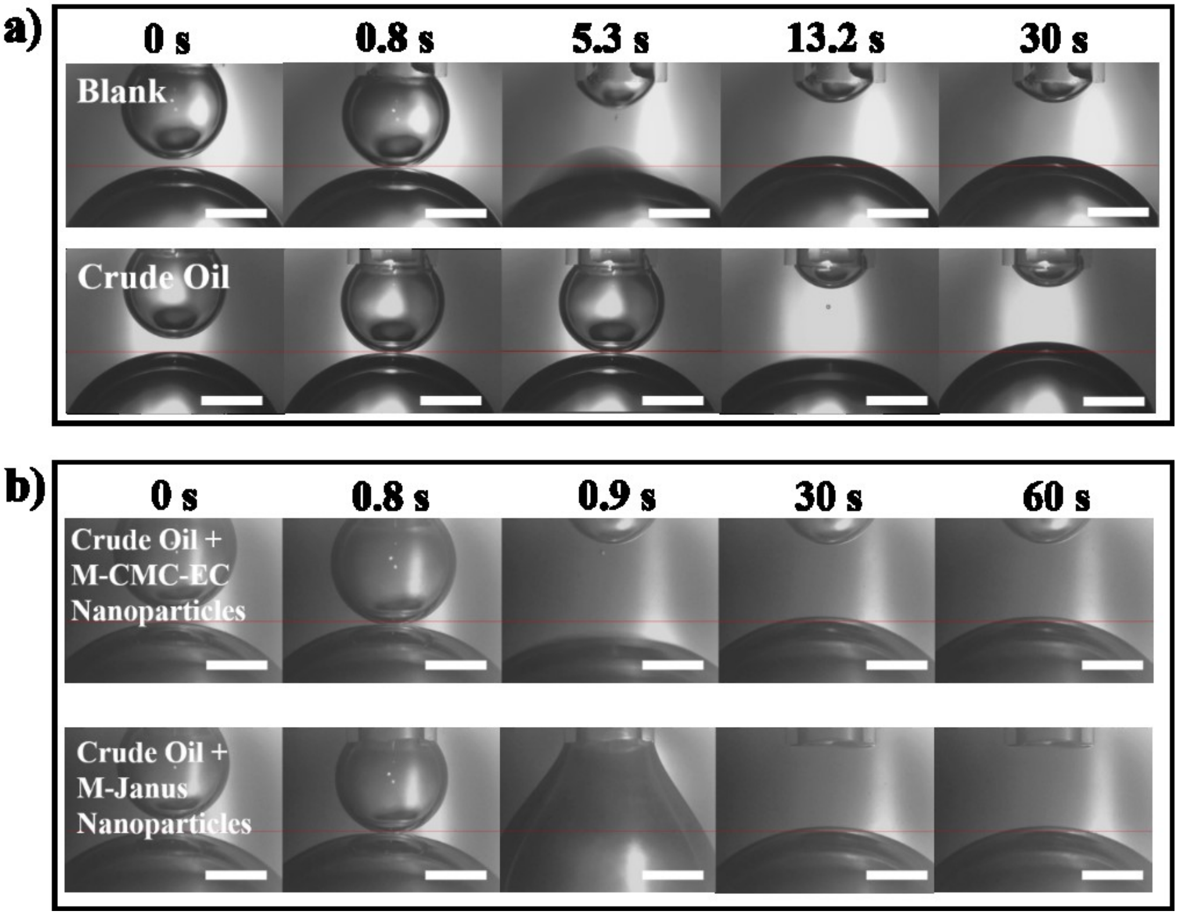

**Figure 6-4.** Snapshots for the coalescence process of process water droplets in a) heavy naphtha without (blank) or with crude oil and b) heavy naphtha-diluted crude oil + 100 ppm M-CMC-EC or M-Janus nanoparticles in heavy naphtha. The scale bars in figure are 1 mm. The concentration of nanoparticles in heavy naphtha is 100 ppm.

### 6.3.4 Dewatering Diluted Crude Oil Emulsions using M-Janus Nanoparticles and M-CMC-EC Nanoparticles at Different Dosages

The initial water content of the diluted crude oil emulsions was measured as 5 wt%. Without the addition of the nanoparticles, the water content of the emulsion showed negligible change after settling for 30 min, indicating the remarkable stability of the process water-in-diluted crude oil emulsion. As shown in **Figure 6-6**, when treated with 0.05 wt% M-Janus nanoparticles, the water content of the diluted crude oil emulsion decreased slightly from 5 wt% to 4.2 wt%, corresponding to a dewatering efficiency of ~ 7.8 %. When the addition of M-Janus nanoparticles increased to 0.25 wt%, the dewatering efficiency was enhanced dramatically to ~ 52.3 %, indicating the enhanced dewatering achieved by M-Janus nanoparticles at a higher dosage under the external magnetic field. With the addition of 1.0 wt% M-Janus nanoparticles into the emulsions, it is observed that the dewatering efficiency achieved by M-Janus nanoparticles reached ~ 95.2 %, indicating nearly complete removal of process water from the diluted crude oil emulsion. Further increase in the dosage of the applied M-Janus nanoparticles showed a marginal increase in their dewatering efficiencies. When compared with the M-CMC-EC nanoparticles, the M-Janus nanoparticles showed better dewatering performance at all applied dosages. Such observation clearly demonstrates that M-Janus nanoparticles of asymmetric surface wettability can achieve better dewatering performance than M-CMC-EC nanoparticles of uniform surface wettability. We should note that despite the removal of 90 wt% process water from the crude oil emulsions, a small amount of water (10 wt%) was still in the bulk crude oil emulsions. This is because the remaining water in the crude oil emulsions is in the form of the tiny droplets with nanometer sizes. Due to the size effect of the M-Janus nanoparticles (~ 100-200 nm) used for dewatering, the nanoparticles cannot effectively adsorb onto the tiny water droplet surfaces, resulting in incomplete dewatering for the water-in-crude oil emulsions under the external magnetic field. To address this concern, we can apply the magnetic Janus nanoparticles of smaller sizes to the dewatering of the crude oil emulsions. Also, in the practical applications, we can apply the demulsification methods such as thermal heating to destabilize the crude oil emulsions to decrease the percentage of the nano-sized water droplets in the crude oil emulsions prior to the treatment using magnetic Janus nanoparticles.

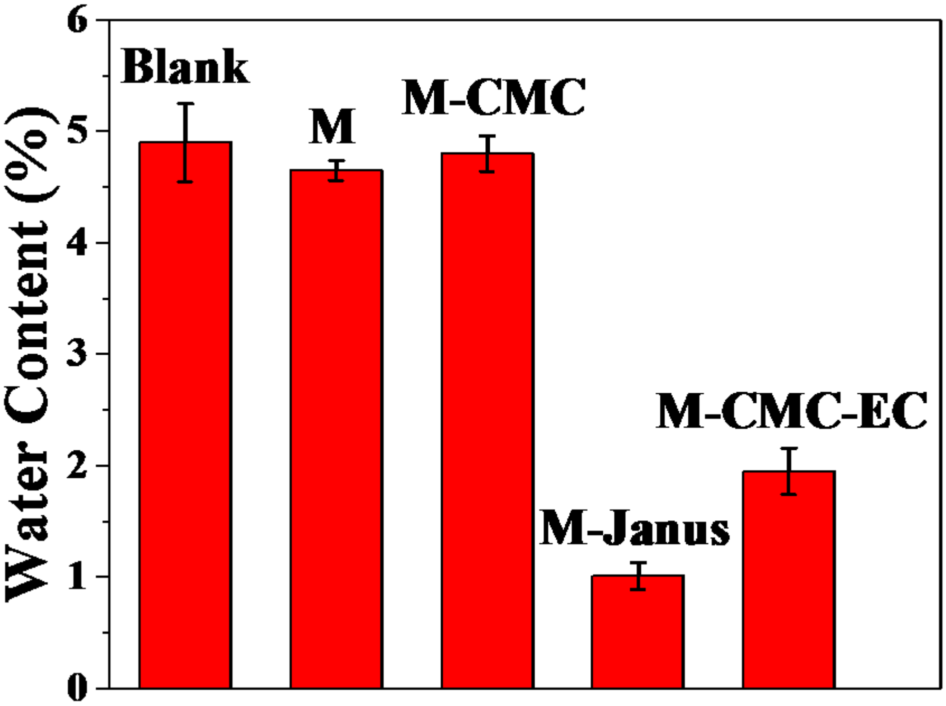

**Figure 6-5.** Dewatering diluted crude oil emulsions using 0.5 wt% bare iron oxide (M) nanoparticles, M-CMC nanoparticles, M-CMC-EC nanoparticles and M-Janus nanoparticles, showing better dewatering performance of M-Janus nanoparticles than M-CMC-EC nanoparticles.

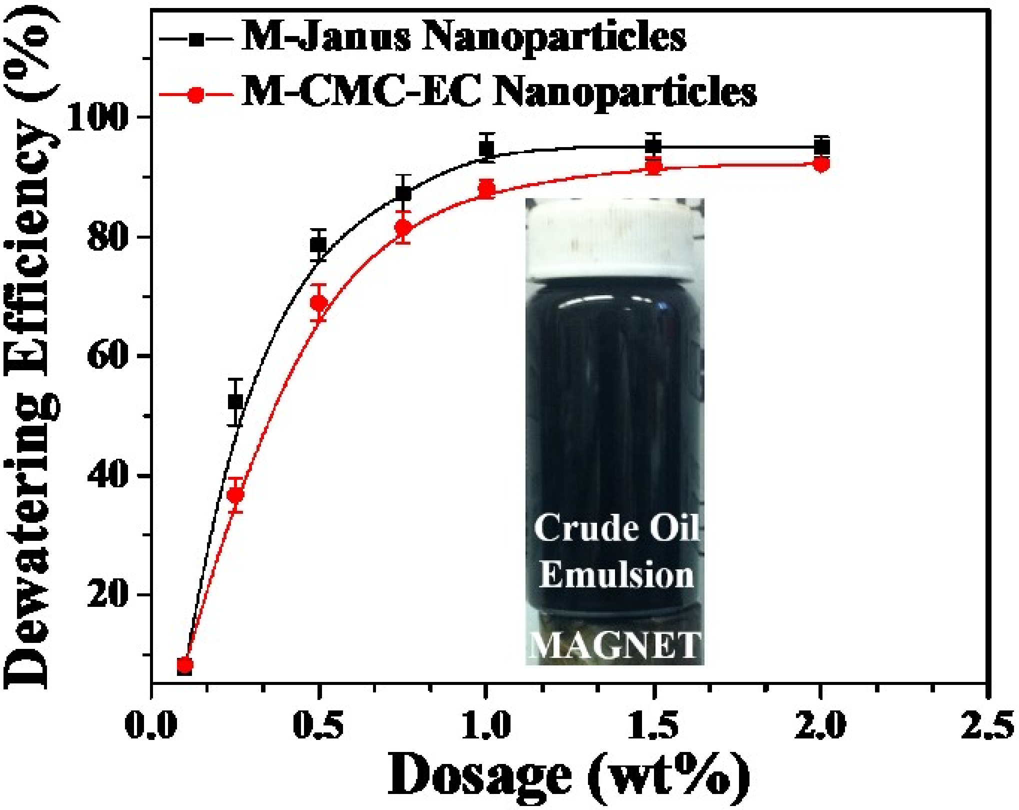

**Figure 6-6.** Dewatering diluted crude oil emulsions of 5 wt% initial water content using M-Janus nanoparticles and M-CMC-EC nanoparticles at different particle dosages.

### 6.3.5 Dewatering Diluted Crude Oil Emulsions of Different Initial Water Contents using M-Janus Nanoparticles

The M-Janus nanoparticles showed promising dewatering efficiency for the diluted crude oil emulsions of 5 wt% initial water content. However, the water content of the crude oil emulsions varies according to the different realistic conditions. Therefore, it is essential to investigate the performance of M-Janus nanoparticles in dewatering the diluted crude oil emulsions of different initial water contents.

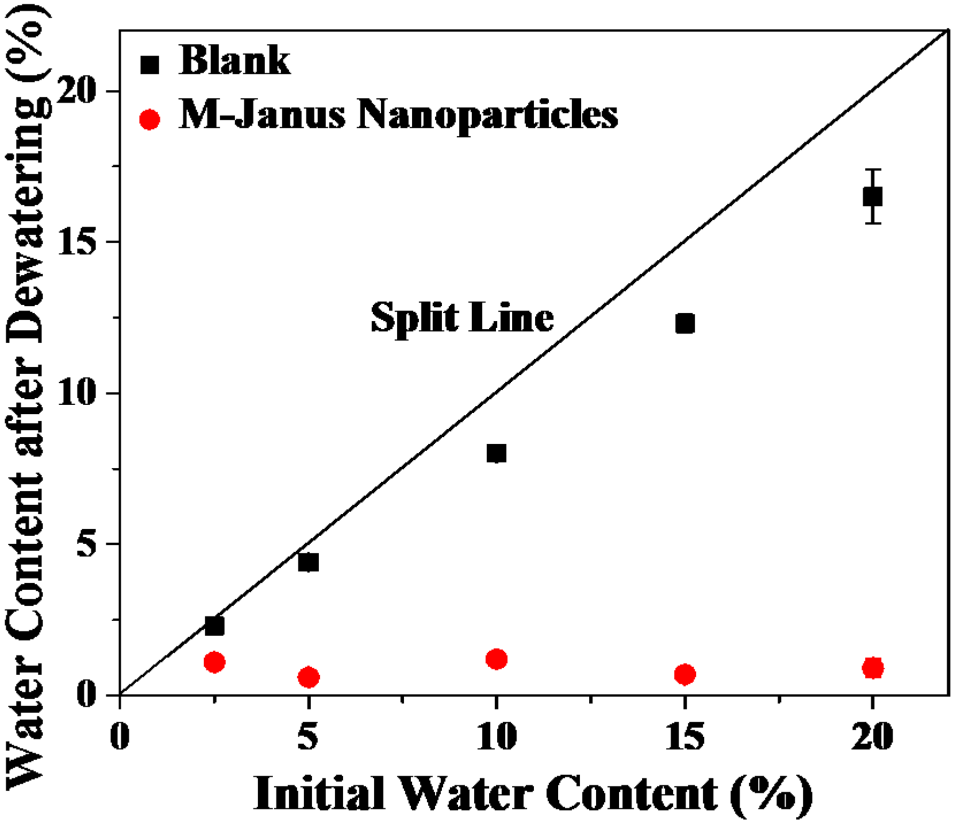

**Figure 6-7.** Dewatering diluted crude oil emulsions of different initial water contents without (blank) or with 1.0 wt% M-Janus nanoparticles.

As shown in **Figure 6-7**, without the addition of M-Janus nanoparticles, the diluted crude oil emulsions of 2.5 wt% and 5 wt% initial water contents showed a negligible decrease in their water contents after settling by gravity for 15 min, indicating the stability of the crude oil emulsions at relatively low initial water contents. However, for the diluted crude oil emulsions of 10 wt%, 15 wt% and 20 wt% initial water contents, around 3-5 wt% of process water could be settled to the bottom of the emulsions after a short-time settling by gravity only, showing the intrinsic instability of the diluted crude oil emulsions at higher initial water content. Such instability results from the reason that crude oil emulsion of a higher water content has more coalesced and aggregated water droplets, leading to quicker removal of water droplets by gravity-driven settling. As shown in **Figure 6-8**, the water droplets with larger sizes were monitored frequently in the diluted crude oil emulsions of higher initial water contents (10 wt%, 15 wt%, and 20 wt%). In contrast, the water droplets with smaller sizes in the emulsions of lower initial water contents (2.5 wt% and 5 wt%) showed better dispersion state (**Figure 6-9a** and **9b**), leading to more stable emulsions under gravity-driven settling only.

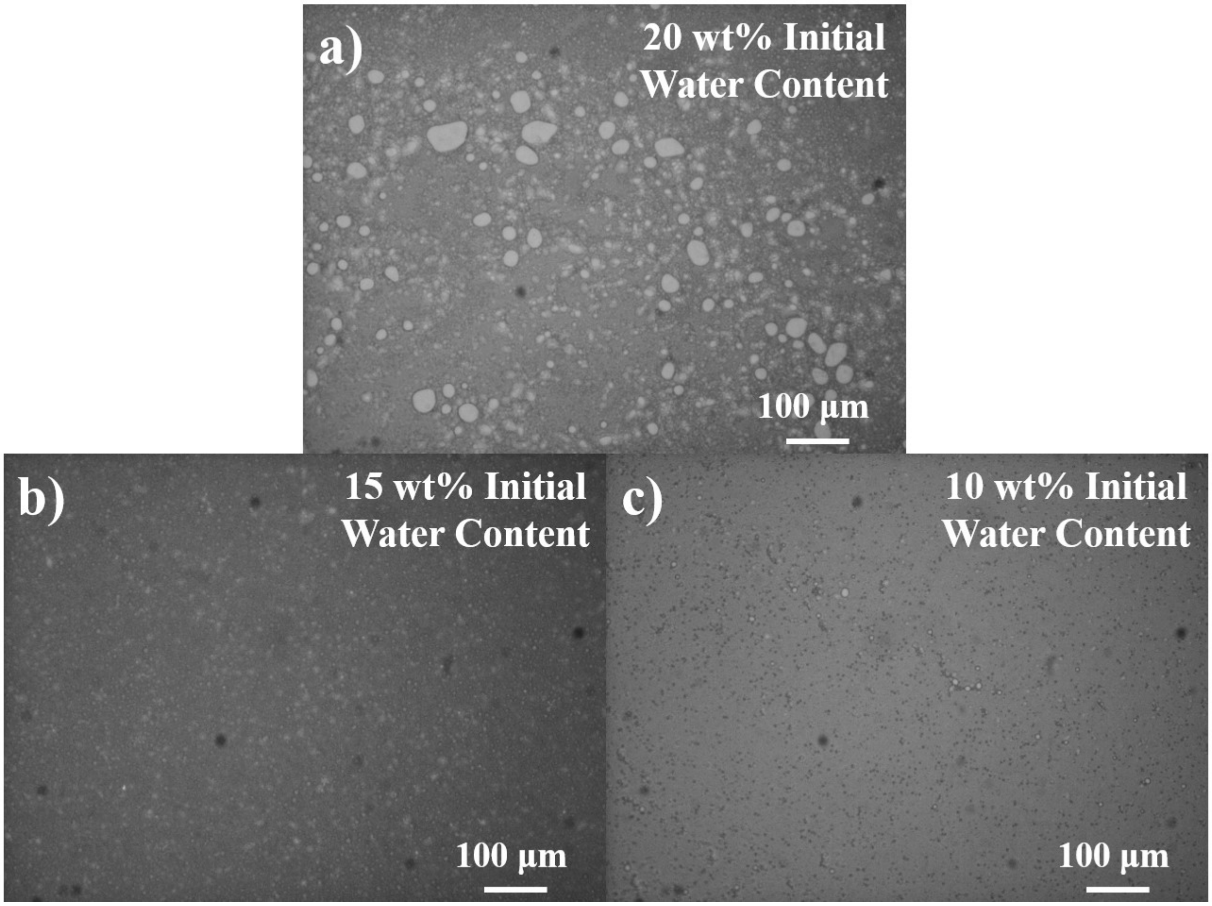

**Figure 6-8.** Micrographs of water droplets in diluted crude oil emulsions of a) 20 wt%, b) 15 wt%, or c) 10 wt% initial water contents. The scale bars in figure are 100 µm.

With the addition of 1.0 wt% M-Janus nanoparticles, the water contents of all the diluted crude oil emulsions decreased significantly to around 1.0 wt%, showing the excellent dewatering ability of M-Janus nanoparticles on treating diluted crude oil emulsions of different initial water contents.

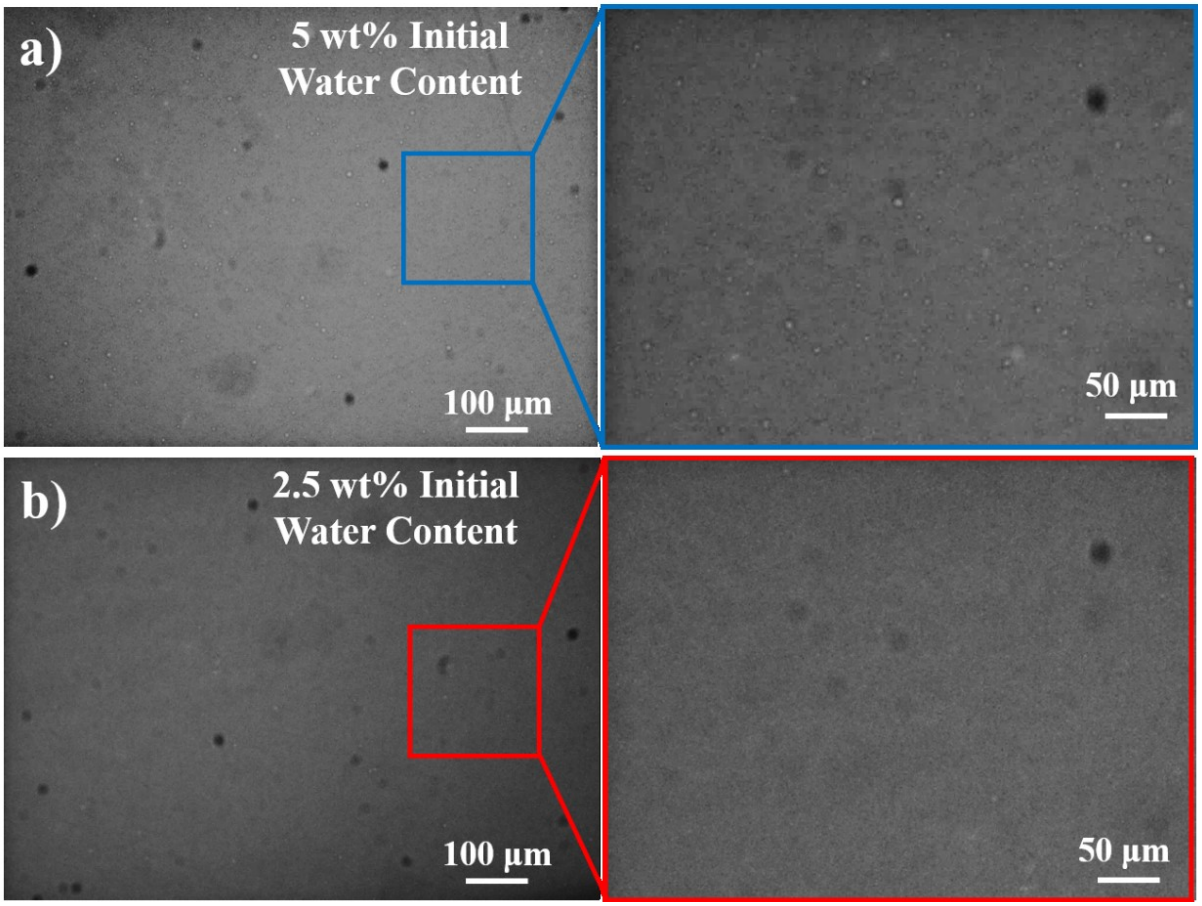

**Figure 6-9.** Micrographs of water droplets in diluted crude oil emulsions of a) 5 wt% or b) 2.5 wt% initial water contents. The scale bars in figure are 100 µm.

### 6.3.6 Water Contents at Different Depths of Diluted Crude Oil Emulsions after Dewatering

To investigate the dynamic dewatering process achieve by M-Janus nanoparticles under the external magnetic field, the water contents at different depths of the emulsion were measured after dewatering. As shown in **Figure 6-10**, without any addition of M-Janus nanoparticles, the diluted crude oil emulsion showed almost constant water contents (4.6 wt% - 4.8 wt%) through the whole test vial, indicating the negligible oil/water separation under gravity-driven and emphasizing the stability of the process water-diluted crude oil emulsions. After the addition of 1.0 wt% M-Janus nanoparticles, followed by settling on a strong hand magnet for 15 min, the water contents in the top 2 cm of the diluted crude oil emulsion were found less than 0.5 wt%, indicating nearly complete removal of process water from the bulk crude oil emulsion. In contrast, at the bottom of the vial, the water content sharply increased to over 25 wt%, indicating that more than 95 wt% of the process water was settled to the bottom position of the emulsion. Such results clearly show the excellent dewatering ability of M-Janus nanoparticles on the process water-in-crude oil emulsions.

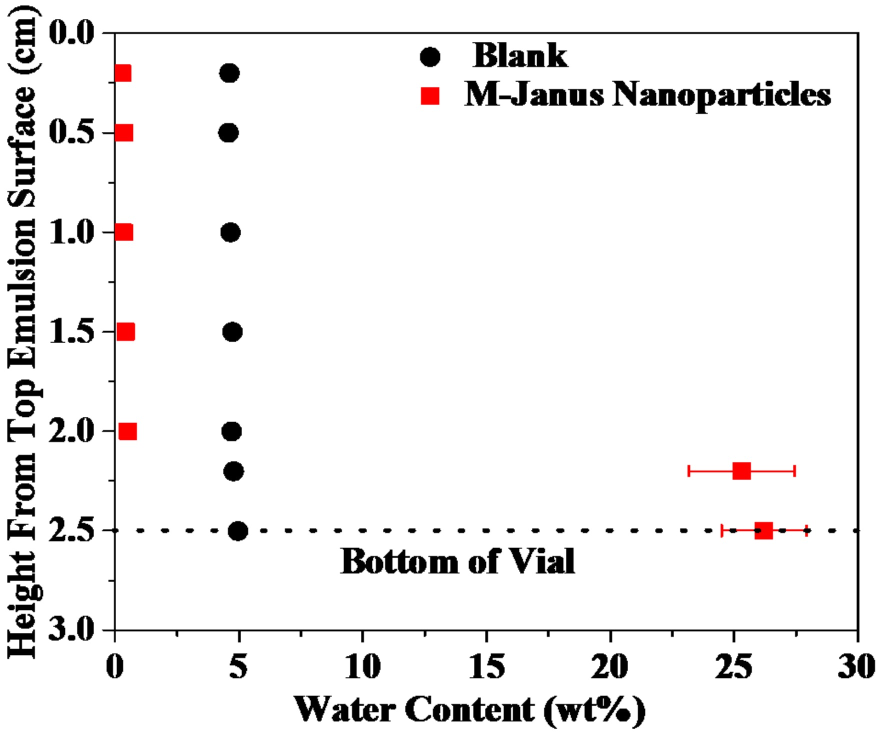

**Figure 6-10.** Water contents at different depths of diluted crude oil emulsions dewatered without (blank) or with addition of 1.0 wt% M-Janus nanoparticles under external magnetic field.

### 6.3.7 Effect of Magnetic Field on Dewatering Efficiency using M-Janus Nanoparticles

To remove process water efficiently from the diluted crude oil emulsions, the effective responsiveness to the external magnetic field is of great importance for magnetically responsive and interfacially active nanoparticles. The effect of the magnetic property of M-Janus nanoparticles on the dewatering performance was investigated by measuring the water content of crude oil emulsion after dewatering using M-Janus nanoparticles without (JGS) or with (JMS) an external magnetic field. The diluted crude oil emulsion treated by gravity-driven settling (GMS) was used as a benchmark for comparison. **Figure 6-11** shows that the water content decreased from 5.64 % to 5.14 % after 2-days settling, indicating the extreme stability of the diluted crude oil emulsion. With the addition of 1 wt% M-Janus nanoparticles, the water content in the diluted crude oil emulsion decreased gradually along with the settling time even without the external magnetic field. Such a phenomenon results from the enhanced coalescence and aggregation of the water droplets achieved by M-Janus nanoparticles, leading to quicker settling of the water droplets. In contrast, after settling on a strong magnet, the water content of the diluted crude oil emulsion can be effectively reduced to ~ 0.5 % in only 5 min, showing the importance of the magnetic responsiveness of M-Janus nanoparticles to the efficient dewatering performance on the diluted crude oil emulsion.

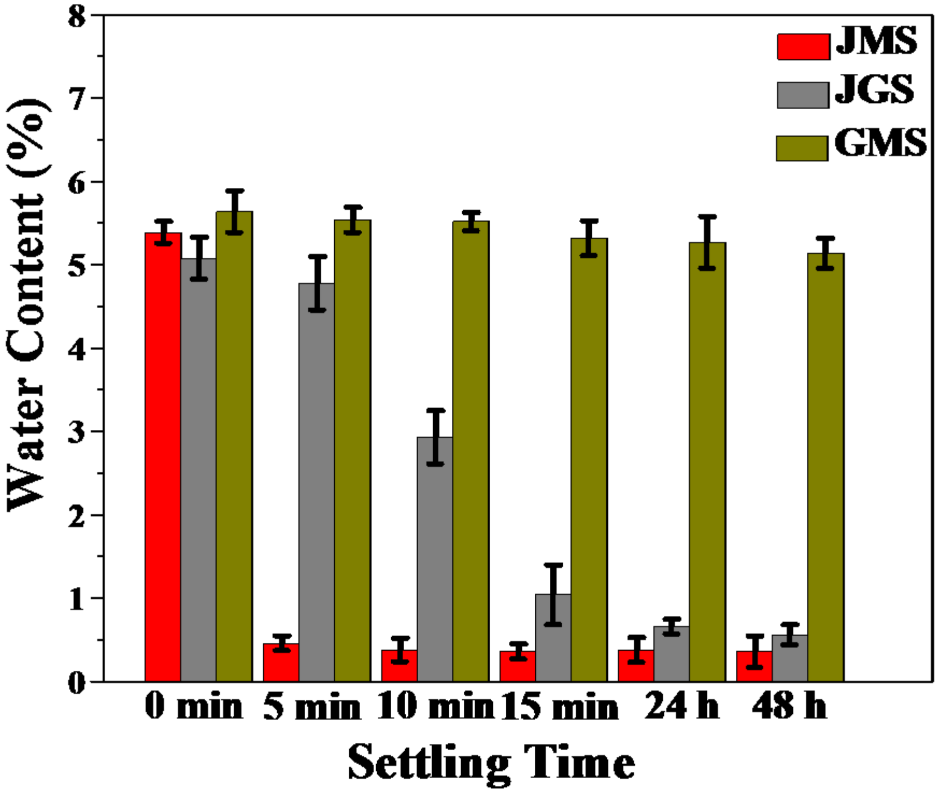

**Figure 6-11.** Dewatering diluted crude oil emulsions with gravity-driven settling (GMS) or using 1.0 wt% M-Janus nanoparticles without (JGS) or with (JMS) an external magnetic field.

### 6.3.8 Micrographs of Diluted Crude Oil Emulsions in Dewatering Process

**Figures 6-12a** and **12b** show the micrographs of the process water droplets before dewatering. It is observed that the process water droplets of several micrometer sizes were homogeneously dispersed in the top and bottom positions of the emulsion and the water droplets showed no obvious coalescence and flocculation even after settling for 24 h. Such observation clearly demonstrates the stability of the water droplets in the diluted crude oil emulsion. **Figures 6-12c** and **12d** show that with the addition of 1.0 wt% M-Janus nanoparticles into the emulsion, followed by settling on a strong magnet, the emulsion showed clear oil/water separation. In the top position of the emulsion (**Figure 6-12c**), no obvious water droplets were observed, indicating the successful removal of process water from the top position of the crude oil emulsion using M-Janus nanoparticles under an external magnetic field. While the water droplets with sizes ranging from 10 μm to 100 μm were detected in the bottom of the emulsion, demonstrating the enhanced coalescence and resulting settling of the water droplets. Figure 11d shows the obvious black rim at the water droplet surfaces, indicating the tagging of the water droplets by M-Janus nanoparticles. The anchoring of M-Janus nanoparticles at the diluted crude oil-process water interface indicates the interfacial activity of the magnetic Janus nanoparticles in turn. It is worth noting that some small water droplets formed flocculation other than coalescence, which also accelerates the settling of the water droplets. Such phenomena possibly resulted from the bridging flocculation effect by the loops and tails of EC on M-Janus nanoparticle surfaces.[127] The different situations of water droplets at the top and the bottom of the emulsions suggest the successful and effective dewatering of the diluted crude oil emulsions using M-Janus nanoparticles under an external magnetic field.

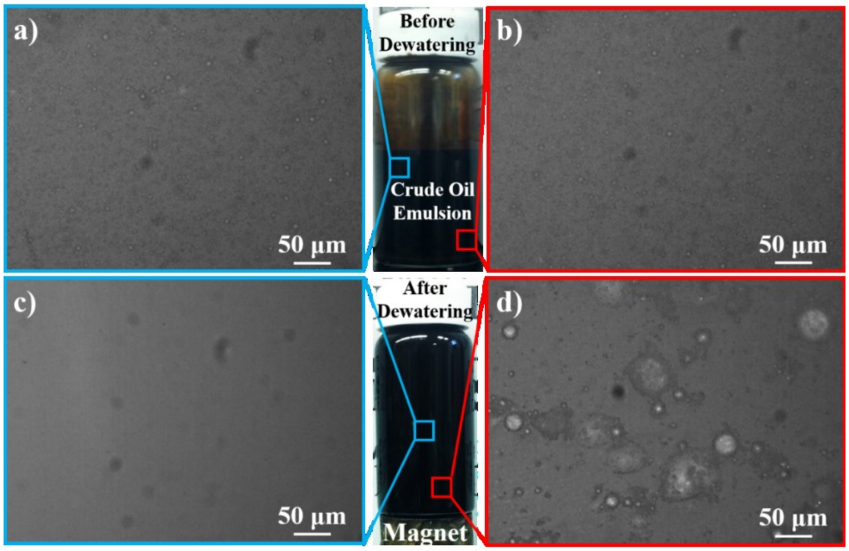

**Figure 6-12.** Morphology of water droplets in diluted crude oil emulsions of 5 wt% initial water content before (a and b) and after (c and d) dewatering using 1.0 wt% M-Janus nanoparticles. The scale bars in figure are 50 μm.

### 6.3.9 Recyclability and Reusability of M-Janus Nanoparticles for Dewatering Diluted Crude Oil Emulsions

In order to investigate the recyclability of M-Janus nanoparticles, the M-Janus nanoparticles were collected using a strong hand magnet after the dewatering process. The M-Janus nanoparticles collected as such were then regenerated by washing with acetone and toluene three times to remove impurities on the M-Janus nanoparticle surfaces. The cleaned M-Janus nanoparticles were dried in a vacuum oven and then applied to dewatering the freshly prepared process water-in-diluted crude oil emulsion in several cycles. After the dewatering process, the M-Janus nanoparticles were collected and regenerated for the subsequent dewatering processes.

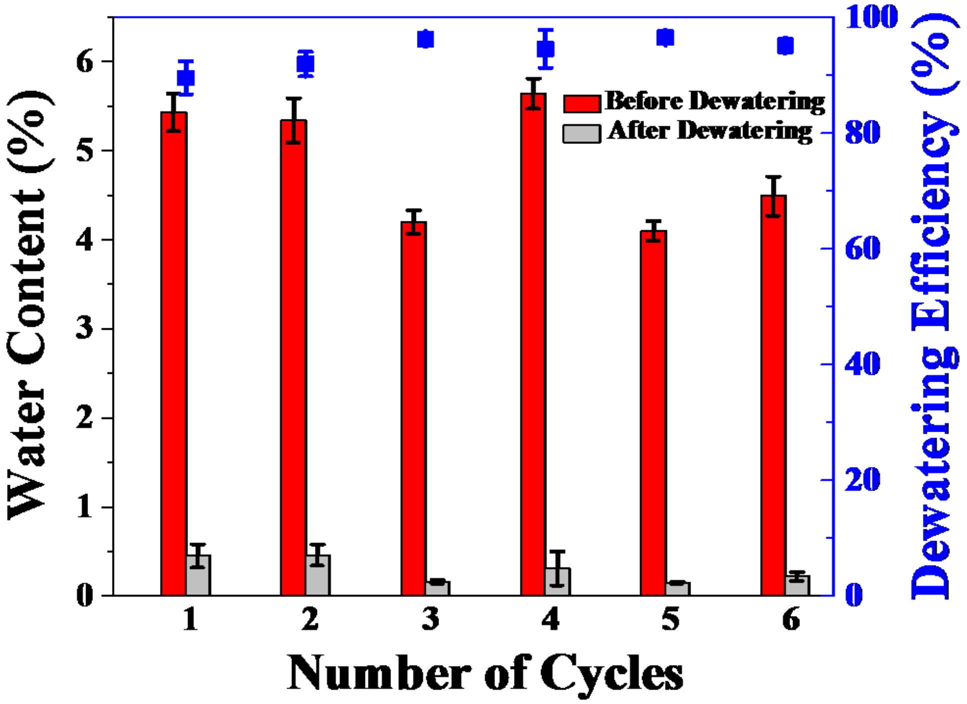

**Figure 6-13.** Dewatering efficiency of diluted crude oil emulsions using recycled M-Janus nanoparticles, and corresponding oil-water interfacial tensions in the presence of recycled M-Janus nanoparticles.

As shown in **Figure 6-13**, the recycled M-Janus nanoparticles showed high dewatering efficiencies of over 90% in all dewatering cycles, demonstrating their sustainable dewatering ability and promising recyclability. Although only six dewatering cycles were conducted to investigate the recyclability of M-Janus nanoparticles, the nearly constant dewatering efficiencies in these cycles indicate the excellent performance of M-Janus nanoparticles in the subsequent dewatering processes.

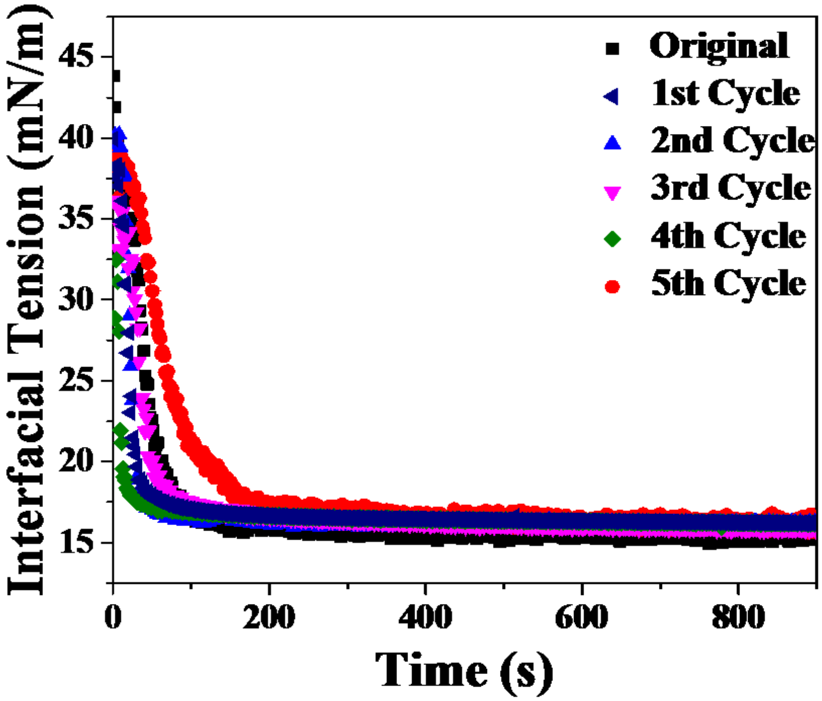

**Figure 6-14.** Dynamic interfacial tension of toluene-DI water interfaces in the presence of pristine M-Janus nanoparticles or M-Janus nanoparticles recycled and regenerated from each dewatering cycle.

The M-Janus nanoparticles collected from each recycling test were simply regenerated by washing with toluene and acetone three times, followed by drying in a vacuum oven at 80 ºC for 12h. The interfacial activities of the recycled M-Janus nanoparticles were measured using a Theta Optical Tensiometer via the pendant drop method. The results shown in **Figure 6-14** illustrate that the recycled M-Janus nanoparticle can anchor effectively at the toluene-water interface and lower the interfacial tension of the toluene-water interface. It is worth to note that the recycled M-Janus nanoparticles still remained highly interfacially active, indicating the excellent stability and sustainability of the recycled M-Janus nanoparticles.

## 6.4 Conclusions

In this study, the magnetically responsive and interfacially active Janus nanoparticles were applied for the first time to the removal of emulsified process water from the crude oil emulsions. The M-Janus nanoparticle could anchor securely at the process water droplet surfaces despite the presence of natural surfactants in crude oil, impurities in heavy naphtha and inorganic electrolytes in the process water. Compared with the M-CMC-EC nanoparticles of uniform surface wettability, M-Janus nanoparticles of asymmetric surface wettability exhibited more active interfacial behaviors at process water-crude oil interface. In the application part, the M-Janus nanoparticles could remove over 90 % of process water from the diluted crude oil emulsion when the dosage of the added nanoparticles was higher than 0.75 wt%, showing the excellent dewatering ability of M-Janus nanoparticles. Compared with M-CMC-EC nanoparticles, the M-Janus nanoparticles showed higher dewatering efficiency at all applied particle dosages. With the addition of M-Janus nanoparticles, no obvious water droplets were observed at the top of the diluted crude oil emulsion, demonstrating the successful dewatering achieved by M-Janus nanoparticles under the external magnetic field. The presence of process water droplets of large sizes at the bottom of the emulsion indicated the enhanced coalescence of water droplets by M-Janus nanoparticles. Assisted with the external magnetic field, the M-Janus nanoparticles could achieve more rapid removal of process water and higher dewatering efficiency than the dewatering without the external magnetic field. After removing process water from the diluted crude oil emulsion, the M-Janus nanoparticles could be conveniently recycled and facilely regenerated while remaining high interfacial activities and promising dewatering efficiency. The superior interfacial activities, excellent dewatering ability, promising recyclability and high magnetic responsiveness make M-Janus nanoparticles potential candidates for removing emulsified process water droplets from crude oil emulsions.

# Chapter 7 Conclusions and Future Perspectives of the Work

The conclusions of this thesis and future perspectives are summarized in this chapter.

## 7.1 Conclusions

Ever-increasing volumes of W/O emulsions and O/W emulsions have been generated along as a result of the prosperous development of industry and explosive population. However, due to the lack of environmental awareness and the lag of effective management, most of the generated emulsions were directly discharged to the natural environment, resulting in serious environmental issues. Recently, there is a wide range of interests in using magnetically responsive and interfacially active nanoparticles for the treatment of W/O or O/W emulsions. In this thesis, we designed and synthesized novel magnetic Janus nanoparticles of asymmetric surface properties for treating oily wastewaters and water-in-crude oil emulsions. Such Janus nanoparticles showed superior interfacial activities and better performance on oil/water separation as compared with conventional magnetic nanoparticles of uniform surface properties. The main conclusions derived from this study are summarized as follows:

Novel magnetically responsive Janus (M-Janus) nanoparticles were synthesized using the Pickering emulsion method by sequential adsorption of cellulosic materials with contrasting wettabilities: hydrophobic ethyl cellulose (EC) and hydrophilic carboxymethyl cellulose (CMC) on the opposite sides of bare iron oxide ($Fe_3O_4$) nanoparticles. The M-Janus nanoparticles were confirmed to feature asymmetric coatings. The EC coated nanoparticle surfaces showed a more hydrophobic nature than the nanoparticle surfaces coated with hydrophilic CMC. Compared with conventional nanoparticles (M-CMC-EC nanoparticles) of uniform surface properties, the M-Janus nanoparticles of asymmetric surface properties exhibited superior interfacial activities at a clean toluene-water interface, including quicker adsorption onto oil-water interface, lower interfacial tension, more rigid oil-water interface and better prevention of the emulsified phase from coalescing. In addition, such Janus nanoparticles not only showed excellent capability and high efficiency in separating emulsified water from water-in-crude oil emulsions and the oil from oily wastewaters under an external magnetic field, but also retained high interfacial activity and hence desirable separation efficiency after five cycles of applications. Moreover, because of the environmentally friendly and biodegradable cellulosic materials used in the synthesis, the M-Janus nanoparticle can process effective oil/water phase separation without causing further pollution to the continuous phase.

Due to their excellent interfacial activity, magnetic Janus nanoparticles are considered to be a great vehicle to develop a viable technology for treating large volumes of various types of oily wastewaters and sludges. The M-Janus nanoparticles were applied for the first time to removal or recovery of crude oil or waste cooking oil from oily wastewaters under mimetically realistic conditions. The M-Janus nanoparticles of superior interfacial activities could anchor securely at the oil-water interface of emulsified oil droplets despite the presence of other interfacially active components such as asphaltenes, natural and/or synthetic surfactants in cooking oil and remaining detergents in the studied oily wastewaters. Compared with the interfacially active nanoparticles of uniform surface properties reported previously, the M-Janus nanoparticles showed stronger interfacial activities such as lower oil-water interfacial tension and firmer deposition at the oil-water interface of the different oily wastewater systems. With the tagging of emulsified oil droplets by M-Janus nanoparticles, followed by magnetic separation, an oil removal or recovery efficiency of greater than 91% was achieved for treating different oily wastewaters. The oil recovered as such contained less than 1.6 wt% of water, showing its high quality for the subsequent oil refining. Furthermore, the M-Janus nanoparticles could be recycled and reused at a high oil recovery and removal efficiency in the subsequent applications without complex regeneration. The superior interfacial activity, high efficiency and exceptional robustness of M-Janus nanoparticles make them an excellent candidate for treating various types of oily wastewaters such as oil spills in seawater, produced wastewater in the oil field or domestic sewage of waste cooking oils.

We further applied M-Janus nanoparticles to removing process water from the diluted crude oil emulsions at room temperature. Despite the presence of interfacially active components such as natural surfactants in the process water and asphaltenes in the crude oil, the M-Janus showed superior interfacial behaviors and anchored more stably at the process water-diluted crude oil interface as compared with the nanoparticles of uniform surface modification by EC (M-CMC-EC nanoparticles). With the addition of 0.75 wt% M-Janus nanoparticles, around 90 wt% of process water was removed from the diluted bitumen emulsions, in contrast to 80 wt% of water removal obtained with the addition of M-CMC-EC nanoparticles at the same dosage. The M-Janus nanoparticles showed robust dewatering ability for the diluted crude oil emulsions of different initial water contents (2.5 wt% ~ 20 wt%). After dewatering the diluted crude oil emulsions, the M-Janus nanoparticles could be recycled and reused for the subsequent dewatering process with facile regeneration. Furthermore, the recycled M-Janus nanoparticles could still retain high dewatering efficiency and excellent interfacial activities at least for six cycles. With their superior interfacial activities, high dewatering efficiency, and exceptional recyclability, the M-Janus nanoparticles are anticipated to be applied to dewatering the process water-in-diluted crude oil emulsions.

## 7.2 Future Perspectives of the Work

Future work should address the following issues:

1. In Chapter 4, the bare iron oxide nanoparticles were bought from Sigma-Aldrich and their shapes were irregular. Such a drawback led to difficulties in calculating the desorption energy from the oil-water interface. Future work should address this problem by synthesizing spherical bare iron oxide nanoparticles and calculate the desorption energy of the nanoparticles.

2. In Chapter 3, the adsorption of EC on CMC layers and CMC on the EC layer was investigated in detail using quartz crystal microbalance with dissipation monitoring (QCM-D). However, the reasons contributing to the strong interactions between the EC and CMC are not clear. To address this problem, techniques such as simulation and atomic force microscope (AFM) should be applied to clearing the mechanism of the interactions between these two cellulosic materials.

3. In Chapters 4 and 5, we compared the interfacial behaviors of M-Janus nanoparticles and M-CMC-EC nanoparticles at the oil-water interface in the presence of other interfacially active components. However, it would be more appealing to compare their interfacial behaviors in more fundamental ways. Future work should address this problem by measuring and comparing the force they need to desorb from the interface or the attractive forces they need to anchor at the interface using an atomic force microscope (AFM).

4. In our current study, we used 1 wt% EC/toluene for synthesizing M-Janus nanoparticles. It would be more interesting to change the concentration of EC/toluene to control the mass of the EC layer adsorbed on the M-Janus nanoparticle surfaces, which would affect the interfacial activities of the synthesized M-Janus nanoparticles.

# Bibliography

1. Milz, E., Evaluating oil spill control equipment and techniques. *Ocean Ind.,* **1970,** *5* (7).

2. Wilson, D. L.; Trippe, J. C., Device for skimming oil from water, Google Patents, **1990**.

3. Abu Amro, M.; Sprenger, F.; Berlin, T., An innovative offshore oil Skimming System for operations in harsh Seas. *Ship Technol. Res.,* **2008**, *55* (4), 147-156.

4. Ayers, R.; Barnett, A. In *SOCK*—an oil skimming kit for vessels of convenience, International Oil Spill Conference, American Petroleum Institute, **1977**, pp 361-366.

5. Prendergast, D. P.; Gschwend, P. M., Assessing the Performance and Cost of Oil Spill Remediation Technologies. *J. Cleaner Production,* **2014,** *78*, 233-242.

6. Banerjee, S. S.; Joshi, M. V.; Jayaram, R. V., Treatment of oil spill by sorption technique using fatty acid grafted sawdust. *Chemosphere,* **2006,** *64* (6), 1026-1031.

7. Ji, F.; Li, C.; Dong, X.; Li, Y.; Wang, D., Separation of oil from oily wastewater by sorption and coalescence technique using ethanol grafted polyacrylonitrile. *J. Hazard. Mater.,* **2009,** *164* (2-3), 1346-1351.

8. Wang, J.; Zheng, Y.; Wang, A., Superhydrophobic kapok fiber oil-absorbent: Preparation and high oil absorbency. *Chem. Eng. J.,* **2012,** *213*, 1-7.

9. Nwadiogbu, J.; Ajiwe, V.; Okoye, P., Removal of crude oil from aqueous medium by sorption on hydrophobic corncobs: equilibrium and kinetic studies. *J. Taibah Univ. Sci.,* **2016,** *10* (1), 56-63.

10. Banerjee, S. S.; Joshi, M. V.; Jayaram, R. V., Treatment of oil spills using organo-fly ash. *Desalination,* **2006,** *195* (1-3), 32-39.

11. Pouet, M.-F.; Grasmick, A., Urban wastewater treatment by electrocoagulation and flotation. *Water Sci. Technol.* **1995,** *31* (3-4), 275-283.

12. Holt, P.; Barton, G.; Mitchell, C., Electrocoagulation as a wastewater treatment. *The Third Annual Australian Environ. Eng. Res. Event,* **1999,** *1000*, 41-46.

13. Mollah, M. Y. A.; Schennach, R.; Parga, J. R.; Cocke, D. L., Electrocoagulation (EC)—science and applications. *J. Hazard. Mater.,* **2001,** *84* (1), 29-41.

14. Xu, X.; Zhu, X., Treatment of refectory oily wastewater by electro-coagulation process. *Chemosphere,* **2004,** *56* (10), 889-894.

15. Inan, H.; Dimoglo, A.; Şimşek, H.; Karpuzcu, M., Olive oil mill wastewater treatment by means of electro-coagulation. *Sep. Purif. Technol.,* **2004,** *36* (1), 23-31.

16. Can, O.; Kobya, M.; Demirbas, E.; Bayramoglu, M., Treatment of the textile wastewater by combined electrocoagulation. *Chemosphere,* **2006,** *62* (2), 181-187.

17. Chen, X.; Chen, G.; Yue, P. L., Separation of pollutants from restaurant wastewater by electrocoagulation. *Sep. Purif. Technol.,* **2000,** *19* (1-2), 65-76.

18. Kota, A. K.; Kwon, G.; Choi, W.; Mabry, J. M.; Tuteja, A., Hygro-responsive membranes for effective oil–water separation. *Nat. Commun.,* **2012,** *3* (1), 1-8.

19. Gao, P.; Liu, Z.; Sun, D. D.; Ng, W. J., The efficient separation of surfactant-stabilized oil–water emulsions with a flexible and superhydrophilic graphene–TiO 2 composite membrane. *J. Mater. Chem. A.,* **2014,** *2* (34), 14082-14088.

20. Huotari, H. M.; Huisman, I. H.; Trägårdh, G., Electrically enhanced crossflow membrane filtration of oily waste water using the membrane as a cathode. *J. Membr. Sci.,* **1999,** *156* (1), 49-60.

21. Wu, C.; Li, A.; Li, L.; Zhang, L.; Wang, H.; Qi, X.; Zhang, Q., Treatment of oily water by a poly (vinyl alcohol) ultrafiltration membrane. *Desalination,* **2008,** *225* (1-3), 312-321.

22. Monfared, M. A.; Kasiri, N.; Mohammadi, T., Microscopic modeling of critical pressure of permeation in oily waste water treatment via membrane filtration. *RSC adv.,* **2016,** *6* (75), 71744-71756.

23. Tanudjaja, H. J.; Hejase, C. A.; Tarabara, V. V.; Fane, A. G.; Chew, J. W., Membrane-based separation for oily wastewater: A practical perspective. *Water Res.,* **2019**.

24. Zhu, Z.; Wang, W.; Qi, D.; Luo, Y.; Liu, Y.; Xu, Y.; Cui, F.; Wang, C.; Chen, X., Calcinable Polymer Membrane with Revivability for Efficient Oily-Water Remediation. *Adv. Mater.,* **2018,** *30* (30), 1801870.

25. He, Z.; Miller, D. J.; Kasemset, S.; Paul, D. R.; Freeman, B. D., The effect of permeate flux on membrane fouling during microfiltration of oily water. *J. Membr. Sci.,* **2017,** *525*, 25-34.

26. Huang, S.; Ras, R. H.; Tian, X., Antifouling membranes for oily wastewater treatment: Interplay between wetting and membrane fouling. *Curr. Opin. Colloid Interface Sci.,* **2018,** *36*, 90-109.

27. Huang, X.; Wang, W.; Liu, Y.; Wang, H.; Zhang, Z.; Fan, W.; Li, L., Treatment of oily waste water by PVP grafted PVDF ultrafiltration membranes. *Chem. Eng. J.,* **2015,** *273*, 421-429.

28. Saththasivam, J.; Loganathan, K.; Sarp, S., An overview of oil–water separation using gas flotation systems. *Chemosphere,* **2016,** *144*, 671-680.

29. Rajak, V.; Relish, K.; Kumar, S.; Mandal, A., Mechanism and kinetics of separation of oil from oil-in-water emulsion by air flotation. *Petro. Sci. Technol.,* **2015,** *33* (23-24), 1861-1868.

30. Etchepare, R.; Oliveira, H.; Azevedo, A.; Rubio, J., Separation of emulsified crude oil in saline water by dissolved air flotation with micro and nanobubbles. *Sep. Purif. Technol.,* **2017,** *186*, 326-332.

31. Sikes, C. S.; Sikes, T. D.; Hochwalt, M. A., Flotation and separation of flocculated oils and solids from waste waters, Google Patents, **2016**.

32. Chen, S.; Wang, S.; Li, L.; Qu, J.; Tao, X.; He, H., Exploration on the mechanism of enhancing low-rank coal flotation with cationic surfactant in the presence of oily collector. *Fuel,* **2018,** *227*, 190-198.

33. Radzuan, M. A.; Belope, M. A.-B.; Thorpe, R., Removal of fine oil droplets from oil-in-water mixtures by dissolved air flotation. *Chem. Eng. Res. Des.,* **2016,** *115*, 19-33.

34. Jamaly, S.; Giwa, A.; Hasan, S. W., Recent improvements in oily wastewater treatment: Progress, challenges, and future opportunities. *J. Environ. Sci.,* **2015,** *37*, 15-30.

35. Liu, R.; Gao, Y.; Ji, Y.; Zhang, Y.; Yang, M., Characteristics of hydrocarbon hydroxylase genes in a thermophilic aerobic biological system treating oily produced wastewater. *Water Sci. Technol.,* **2015,** *71* (1), 75-82.

36. Zhang, M.; Wang, J.; Zhang, Z.; Song, Z.; Zhang, Z.; Zhang, B.; Zhang, G.; Wu, W.-M., A field pilot-scale study of biological treatment of heavy oil-produced water by biological filter with airlift aeration and hydrolytic acidification system. *Environ. Sci. Pollut. Res.,* **2016,** *23* (5), 4919-4930.

37. Camarillo, M. K.; Stringfellow, W. T., Biological treatment of oil and gas produced water: a review and meta-analysis. *Clean Technol. Envir.,* **2018,** *20* (6), 1127-1146.

38. Jones, T.; Neustadter, E.; Whittingham, K., Water-in-crude oil emulsion stability and emulsion destabilization by chemical demulsifiers. *J. Can. Petrol. Technol.,* **1978,** *17* (02).

39. Peña, A. A.; Hirasaki, G. J.; Miller, C. A., Chemically Induced Destabilization of Water-in-Crude Oil Emulsions. *Ind. Eng. Chem. Res.,* **2005,** *44* (5), 1139-1149.

40. Feng, X.; Mussone, P.; Gao, S.; Wang, S.; Wu, S.-Y.; Masliyah, J. H.; Xu, Z., Mechanistic study on demulsification of water-in-diluted bitumen emulsions by ethylcellulose. *Langmuir,* **2010,** *26* (5), 3050-3057.

41. Feng, X.; Xu, Z.; Masliyah, J., Biodegradable Polymer for Demulsification of Water-in-Bitumen Emulsions. *Energ. Fuel,* **2009,** *23* (1), 451-456.

42. Feng, X.; Wang, S.; Hou, J.; Wang, L.; Cepuch, C.; Masliyah, J.; Xu, Z., Effect of Hydroxyl Content and Molecular Weight of Biodegradable Ethylcellulose on Demulsification of Water-in-Diluted Bitumen Emulsions. *Ind. Eng. Chem. Res.,* **2011,** *50* (10), 6347-6354.

43. Hou, J.; Feng, X.; Masliyah, J.; Xu, Z., Understanding interfacial behavior of ethylcellulose at the water–diluted bitumen interface. *Energ. Fuel,* **2012,** *26* (3), 1740-1745.

44. Akbari, S.; Nour, A.; Jamari, S.; Rajabi, A., Demulsification of water-in-crude oil emulsion via conventional heating and microwave heating technology in their optimum conditions. *Aust. J. Basic. Appl. Sci.,* **2016,** *10* (4), 66-74.

45. Kar, T.; Hascakir, B., The role of resins, asphaltenes, and water in water–oil emulsion breaking with microwave heating. *Energ. Fuel,* **2015,** *29* (6), 3684-3690.

46. Abdurahman, N.; Yunus, R.; Azhari, N.; Said, N.; Hassan, Z., The potential of microwave heating in separating water-in-oil (w/o) emulsions. *Energy Procedia,* **2017,** *138*, 1023-1028.

47. Santos, D.; da Rocha, E. C.; Santos, R. L.; Cancelas, A. J.; Franceschi, E.; Santos, A. F.; Fortuny, M.; Dariva, C., Demulsification of water-in-crude oil emulsions using single mode and multimode microwave irradiation. *Sep. Purif. Technol.,* **2017,** *189*, 347-356.

48. Noik, C.; Chen, J.; Dalmazzone, C. S., In electrostatic demulsification on crude oil: A state-of-the-art review, *International Oil & Gas Conference and Exhibition in China*, Society of Petroleum Engineers, **2006**.

49. Hirato, T.; Koyama, K.; Tanaka, T.; Awakura, Y.; Majima, H., Demulsification of water-in-oil emulsion by an electrostatic coalescence method. *Mater. Trans.,* **1991,** *32* (3), 257-263.

50. Kim, B.-Y.; Moon, J. H.; Sung, T.-H.; Yang, S.-M.; Kim, J.-D., Demulsification of water-in-crude oil emulsions by a continuous electrostatic dehydrator. *Sep. Sci. Technol.,* **2002,** *37* (6), 1307-1320.

51. Zolfaghari, R.; Fakhru'l-Razi, A.; Abdullah, L. C.; Elnashaie, S. S.; Pendashteh, A., Demulsification techniques of water-in-oil and oil-in-water emulsions in petroleum industry. *Sep. Purif. Technol.,* **2016,** *170*, 377-407.

52. Mirshahghassemi, S.; Lead, J. R., Oil Recovery from Water under Environmentally Relevant Conditions Using Magnetic Nanoparticles. *Environ. Sci. Technol.,* **2015,** *49* (19), 11729-36.

53. Palchoudhury, S.; Lead, J. R., A facile and cost-effective method for separation of oil-water mixtures using polymer-coated iron oxide nanoparticles. *Environ. Sci. Technol.,* **2014,** *48* (24), 14558-63.

54. Wang, X.; Shi, Y.; Graff, R. W.; Lee, D.; Gao, H., Developing recyclable pH-responsive magnetic nanoparticles for oil–water separation. *Polymer,* **2015,** *72*, 361-367.

55. Mao, X.; Gong, L.; Xie, L.; Qian, H.; Wang, X.; Zeng, H., Novel Fe3O4 based superhydrophilic core-shell microspheres for breaking asphaltenes-stabilized water-in-oil emulsion. *Chem. Eng. J.,* **2019,** *358*, 869-877.

56. Liang, C.; He, X.; Liu, Q. X.; Xe, Z. H., Adsorption-Based Synthesis of Magnetically Responsive and Interfacially Active Composite Nanoparticles for Dewatering of Water-in-Diluted Bitumen Emulsions. *Energ. Fuel,* **2018,** *32* (8), 8078-8089.

57. Peng, J.; Liu, Q.; Xu, Z.; Masliyah, J., Synthesis of Interfacially Active and Magnetically Responsive Nanoparticles for Multiphase Separation Applications. *Adv. Func. Mater.,* **2012,** *22* (8), 1732-1740.

58. Peng, J.; Liu, Q.; Xu, Z.; Masliyah, J., Novel Magnetic Demulsifier for Water Removal from Diluted Bitumen Emulsion. *Energ. Fuel,* **2012,** *26* (5), 2705-2710.

59. Dickinson, E., Emulsions and droplet size control: Controlled particle, droplet and bubble formation*,* **1994**, 189-216.

60. Masliyah, J. H.; Xu, Z.; Czarnecki, J. A., Handbook on theory and practice of bitumen recovery from Athabasca oil sands. Kingsley Knowledge Pub.: 2011.

61. Binks, B. P.; Murakami, R., Phase inversion of particle-stabilized materials from foams to dry water. *Nat. Mater.,* **2006,** *5* (11), 865.

62. Tadros, T. F., Emulsion formation, stability, and rheology, **2013,** *1*, 1-75.

63. Ruckenstein, E., The origin of thermodynamic stability of microemulsions. *Chem. Phys. Lett.,* **1978,** *57* (4), 517-521.

64. Binks, B. P., Particles as surfactants—similarities and differences. *Curr. Opin. Colloid Interface Sci.,* **2002,** *7* (1-2), 21-41.

65. Pickering, S. U., Cxcvi., Emulsions. *J. Chem. Soc.,* **1907,** *91*, 2001-2021.

66. Aveyard, R.; Binks, B. P.; Clint, J. H., Emulsions stabilised solely by colloidal particles. *Adv. Colloid Interface Sci.,* **2003,** *100*, 503-546.

67. Binks, B. P.; Lumsdon, S. O., Pickering Emulsions Stabilized by Monodisperse Latex Particles: Effects of Particle Size. *Langmuir,* **2001,** *17* (15), 4540-4547.

68. Binks, B. P.; Lumsdon, S. O., Influence of particle wettability on the type and stability of surfactant-free emulsions. *Langmuir,* **2000,** *16* (23), 8622-8631.

69. Wu, J.; Ma, G. H., Recent Studies of Pickering Emulsions: Particles Make the Difference. *Small,* **2016,** *12* (34), 4633-48.

70. Rio, E.; Drenckhan, W.; Salonen, A.; Langevin, D., Unusually stable liquid foams. *Adv. Colloid Interface Sci.,* **2014,** *205*, 74-86.

71. Leunissen, M. E.; van Blaaderen, A.; Hollingsworth, A. D.; Sullivan, M. T.; Chaikin, P. M., Electrostatics at the oil-water interface, stability, and order in emulsions and colloids. *Proc. Natl. Acad. Sci. U. S. A.,* **2007,** *104* (8), 2585-90.

72. Wang, H.; Singh, V.; Behrens, S. H., Image Charge Effects on the Formation of Pickering Emulsions. *J. Phys. Chem. Lett.,* **2012,** *3* (20), 2986-90.

73. Abend, S.; Bonnke, N.; Gutschner, U.; Lagaly, G., Stabilization of emulsions by heterocoagulation of clay minerals and layered double hydroxides. *Colloid Polym. Sci.,* **1998,** *276* (8), 730-737.

74. Abend, S.; Lagaly, G., Bentonite and double hydroxides as emulsifying agents. *Clay Miner.,* **2018,** *36* (4), 557-570.

75. Berland, K.; Cooper, V. R.; Lee, K.; Schröder, E.; Thonhauser, T.; Hyldgaard, P.; Lundqvist, B. I., van der Waals forces in density functional theory: a review of the vdW-DF method. *Rep. Prog. Phys.,* **2015,** *78* (6), 066501.

76. Rajter, R. F.; Podgornik, R.; Parsegian, V. A.; French, R. H.; Ching, W. Y., van der Waals–London dispersion interactions for optically anisotropic cylinders: Metallic and semiconducting single-wall carbon nanotubes. *Phys. Rev. B.,* **2007,** *76* (4).

77. Adair, J. H.; Suvaci, E.; Sindel, J., Surface and Colloid Chemistry. **2001**, 1-10.

78. Napper, D. H., Steric stabilization. *J. Colloid Interface Sci.,* **1977,** *58* (2), 390-407.

79. Piirma, I., Polymeric surfactants. CRC Press, **2012**.

80. Kleshchanok, D.; Tuinier, R.; Lang, P. R., Direct measurements of polymer-induced forces. *J. Phys. Conden. Matt.,* **2008,** *20* (7), 073101.

81. Biggs, S., Steric and Bridging Forces between Surfaces Bearing Adsorbed Polymer: An Atomic Force Microscopy Study. *Langmuir,* **1995,** *11* (1), 156-162.

82. Christenson, H. K., Non-Dlvo Forces between Surfaces -Solvation, Hydration and Capillary Effects. *J. Dispers. Sci. Technol.,* **1988,** *9* (2), 171-206.

83. Xu, Z.; Yoon, R.-H., A study of hydrophobic coagulation. *J. Colloid Interface Sci.* **1990,** *134* (2), 427-434.

84. Al-mulali, U., Oil consumption, CO2 emission and economic growth in MENA countries. *Energy,* **2011,** *36* (10), 6165-6171.

85. Yu, L.; Han, M.; He, F., A review of treating oily wastewater. *Arab. J. Chem.,* **2017,** *10*, S1913-S1922.

86. Li, Y. S.; Yan, L.; Xiang, C. B.; Hong, L. J., Treatment of oily wastewater by organic–inorganic composite tubular ultrafiltration (UF) membranes. *Desalination,* **2006,** *196* (1-3), 76-83.

87. Xu, X.; Zhu, X., Treatment of refectory oily wastewater by electro-coagulation process. *Chemosphere,* **2004,** *56* (10), 889-94.

88. Karlapudi, A. P.; Venkateswarulu, T. C.; Tammineedi, J.; Kanumuri, L.; Ravuru, B. K.; Dirisala, V. r.; Kodali, V. P., Role of biosurfactants in bioremediation of oil pollution-a review. *Petrol.,* **2018,** *4* (3), 241-249.

89. Sarbatly, R.; Krishnaiah, D.; Kamin, Z., A review of polymer nanofibres by electrospinning and their application in oil-water separation for cleaning up marine oil spills. *Mar. Pollut. Bull.,* **2016,** *106* (1-2), 8-16.

90. Pavia-Sanders, A.; Zhang, S.; Flores, J. A.; Sanders, J. E.; Raymond, J. E.; Wooley, K. L., Robust magnetic/polymer hybrid nanoparticles designed for crude oil entrapment and recovery in aqueous environments. *ACS Nano,* **2013,** *7* (9), 7552-61.

91. Allan, S. E.; Smith, B. W.; Anderson, K. A., Impact of the deepwater horizon oil spill on bioavailable polycyclic aromatic hydrocarbons in Gulf of Mexico coastal waters. *Environ. Sci. Technol.,* **2012,** *46* (4), 2033-9.

92. Lin, Q.; Mendelssohn, I. A., Impacts and recovery of the Deepwater Horizon oil spill on vegetation structure and function of coastal salt marshes in the northern Gulf of Mexico. *Environ. Sci. Technol.,* **2012,** *46* (7), 3737-43.

93. McCrea-Strub, A.; Kleisner, K.; Sumaila, U. R.; Swartz, W.; Watson, R.; Zeller, D.; Pauly, D., Potential Impact of theDeepwater HorizonOil Spill on Commercial Fisheries in the Gulf of Mexico. *Fisheries,* **2011,** *36* (7), 332-336.

94. Gossen, L. P.; Velichkina, L. M., Environmental problems of the oil-and-gas industry (Review). *Petrol. Chem.,* **2006,** *46* (2), 67-72.

95. Hayat, S.; Ahmad, I.; Azam, Z. M.; Ahmad, A.; Inam, A.; Samiullah, Effect of long-term application of oil refinery wastewater on soil health with special reference to microbiological characteristics. *Bio. Technol.,* **2002,** *84* (2), 159-163.

96. Takht Ravanchi, M.; Kaghazchi, T.; Kargari, A., Application of membrane separation processes in petrochemical industry: a review. *Desalination,* **2009,** *235* (1-3), 199-244.

97. Rajter, R. F.; Podgornik, R.; Parsegian, V. A.; French, R. H.; Ching, W. Y., van der Waals–London dispersion interactions for optically anisotropic cylinders: Metallic and semiconducting single-wall carbon nanotubes. *Phys. Rev. B.,* **2007,** *76* (4).

98. Bowen, W. R.; Jenner, F., Theoretical descriptions of membrane filtration of colloids and fine particles: An assessment and review. *Adv. Colloid Interface Sci.,* **1995,** *56*, 141-200.

99. Zularisam, A. W.; Ismail, A. F.; Salim, R., Behaviours of natural organic matter in membrane filtration for surface water treatment — a review. *Desalination,* **2006,** *194* (1-3), 211-231.

100. Luo, C.; Liu, Q., Oxidant-Induced High-Efficient Mussel-Inspired Modification on PVDF Membrane with Superhydrophilicity and Underwater Superoleophobicity Characteristics for Oil/Water Separation. *ACS Appl. Mater. Interfaces,* **2017,** *9* (9), 8297-8307.

101. Tian, D.; Zhang, X.; Wang, X.; Zhai, J.; Jiang, L., Micro/nanoscale hierarchical structured ZnO mesh film for separation of water and oil. *Phys. Chem. Chem. Phys.,* **2011,** *13* (32), 14606-10.

102. Maartens, A.; Jacobs, E. P.; Swart, P., UF of pulp and paper effluent: membrane fouling-prevention and cleaning. *J. Membr. Sci.* **2002,** *209* (1), 81-92.

103. Van der Bruggen, B., Microfiltration, ultrafiltration, nanofiltration, reverse osmosis, and forward osmosis. **2018**, 25-70.

104. Lin, L.; Liu, M.; Chen, L.; Chen, P.; Ma, J.; Han, D.; Jiang, L., Bio-inspired hierarchical macromolecule-nanoclay hydrogels for robust underwater superoleophobicity. *Adv. Mater.,* **2010,** *22* (43), 4826-30.

105. Guo, W.; Ngo, H. H.; Li, J., A mini-review on membrane fouling. *Bioresour. Technol.,* **2012,** *122*, 27-34.

106. Baker, R. W., Membrane technology and applications. John Wiley & Sons, **2012**.

107. Rubio, J.; Souza, M. L.; Smith, R. W., Overview of flotation as a wastewater treatment technique. *Miner. Engineer.,* **2002,** *15* (3), 139-155.

108. Moosai, R.; Dawe, R. A., Gas attachment of oil droplets for gas flotation for oily wastewater cleanup. *Sep. Purif. Technol.,* **2003,** *33* (3), 303-314.

109. Yang, C., Electrochemical coagulation for oily water demulsification. *Sep. Purif. Technol.,* **2007,** *54* (3), 388-395.

110. Ahmad, A. L.; Sumathi, S.; Hameed, B. H., Coagulation of residue oil and suspended solid in palm oil mill effluent by chitosan, alum and PAC. *Chem. Eng. J.,* **2006,** *118* (1-2), 99-105.

111. Menezes, F. M.; Amal, R.; Luketina, D., Removal of particles using coagulation and flocculation in a dynamic separator. *Powder Technol.,* **1996,** *88* (1), 27-31.

112. Zeng, Y.; Yang, C.; Zhang, J.; Pu, W., Feasibility investigation of oily wastewater treatment by combination of zinc and PAM in coagulation/flocculation. *J. Hazard. Mater.,* **2007,** *147* (3), 991-6.

113. Vik, E. A.; Carlson, D. A.; Eikum, A. S.; Gjessing, E. T., Electrocoagulation of potable water. *Water Res.,* **1984,** *18* (11), 1355-1360.

114. Kuokkanen, V.; Kuokkanen, T.; Rämö, J.; Lassi, U., Recent Applications of Electrocoagulation in Treatment of Water and Wastewater—A Review. *Green Sustain. Chem.,* **2013,** *03* (02), 89-121.

115. Mollah, M. Y. A.; Schennach, R.; Parga, J. R.; Cocke, D. L., Electrocoagulation (EC) — science and applications. *J. Hazard. Mater.,* **2001,** *84* (1), 29-41.

116. Kriipsalu, M.; Marques, M.; Nammari, D. R.; Hogland, W., Bio-treatment of oily sludge: the contribution of amendment material to the content of target contaminants, and the biodegradation dynamics. *J. Hazard. Mater.,* **2007,** *148* (3), 616-22.

117. Sirianuntapiboon, S.; Ungkaprasatcha, O., Removal of Pb2+ and Ni2+ by bio-sludge in sequencing batch reactor (SBR) and granular activated carbon-SBR (GAC-SBR) systems. *Bioresour. Technol.,* **2007,** *98* (14), 2749-57.

118. Ottengraf, S. P.; Van Den Oever, A. H., Kinetics of organic compound removal from waste gases with a biological filter. *Biotechnol. Bioeng.,* **1983,** *25* (12), 3089-102.

119. De Gisi, S.; Galasso, M.; De Feo, G., Treatment of tannery wastewater through the combination of a conventional activated sludge process and reverse osmosis with a plane membrane. *Desalination,* **2009,** *249* (1), 337-342.

120. Walker, G., Biological activated carbon treatment of industrial wastewater in stirred tank reactors. *Chem. Eng. J.,* **1999,** *75* (3), 201-206.

121. Neyens, E.; Baeyens, J.; Dewil, R.; De heyder, B., Advanced sludge treatment affects extracellular polymeric substances to improve activated sludge dewatering. *J. Hazard. Mater.,* **2004,** *106* (2-3), 83-92.

122. Nguyen, S. T.; Roddick, F. A., Effects of ozonation and biological activated carbon filtration on membrane fouling in ultrafiltration of an activated sludge effluent. *J. Membr. Sci.,* **2010,** *363* (1-2), 271-277.

123. Ventikos, N. P.; Vergetis, E.; Psaraftis, H. N.; Triantafyllou, G., A high-level synthesis of oil spill response equipment and countermeasures. *J. Hazard. Mater.,* **2004,** *107* (1-2), 51-8.

124. Broje, V.; Keller, A. A., Improved mechanical oil spill recovery using an optimized geometry for the skimmer surface. *Environ. Sci. Technol.,* **2006,** *40* (24), 7914-8.

125. Bhardwaj, A.; Hartland, S., Dynamics of emulsification and demulsification of water in crude oil emulsions. *Ind. Eng. Chem. Res.,* **1994,** *33* (5), 1271-1279.

126. Obah, B., The Chemical Demulsification of Crude Oil Emulsion: Problem in a Niger Delta Oil Terminal. *Erdohl, Kohle, Erdgas Petrochem,* **1988,** *41* (2), 71-74.

127. Feng, X.; Mussone, P.; Gao, S.; Wang, S.; Wu, S. Y.; Masliyah, J. H.; Xu, Z., Mechanistic study on demulsification of water-in-diluted bitumen emulsions by ethylcellulose. *Langmuir,* **2010,** *26* (5), 3050-7.

128. Asaoka, S.; Nakata, S.; Shiroto, Y.; Takeuchi, C., Asphaltene cracking in catalytic hydrotreating of heavy oils. 2. Study of changes in asphaltene structure during catalytic hydroprocessing. *Ind. Eng. Chem. Process Des. Dev.,* **1983,** *22* (2), 242-248.

129. Kokal, S. L.; Sayegh, S. G. In asphaltenes: the cholesterol of petroleum, *Middle East Oil Show*, Society of Petroleum Engineers, **1995**.

130. Ferworn, K. A.; Svrcek, W. Y., Characterization and phase behavior of asphaltenic crude oils. In Structures and Dynamics of Asphaltenes, Springer: **1998**; pp 227-246.

131. Liu, H.; Liu, Z.; Guo, A.; Chen, K.; Sun, S.; Wang, Z., Peptizing Effect of the Native Heavy Resin Fraction on Asphaltenes. *Energ. Fuel,* **2018,** *32* (3), 3380-3390.

132. Groenzin, H.; Mullins, O. C., Asphaltene molecular size and weight by time-resolved fluorescence depolarization. In Asphaltenes, heavy oils, and petroleomics, Springer, **2007**; pp 17-62.

133. Strausz, O. P.; Mojelsky, T. W.; Lown, E. M., The molecular structure of asphaltene: an unfolding story. *Fuel,* **1992,** *71* (12), 1355-1363.

134. Groenzin, H.; Mullins, O. C., Asphaltene molecular size and weight by time-resolved fluorescence depolarization. **2007**, 17-62.

135. Masliyah J. H., Czarnecki J., Xu Z.X., Handbook on theory and practice of bitumen recovery from Athabasca Oil Sands: Theoretical Basis. 1st ed.; Kingsley Knowledge Publishing, Canada, **2011**; Vol. 1, p 25-26.

136. Langevin, D.; Argillier, J.-F., Interfacial behavior of asphaltenes. *Adv. Colloid Interface Sci.,* **2016,** *233*, 83-93.

137. Ekott, E. J.; Akpabio, E. J., A review of water-in-crude oil emulsion stability, destabilization and interfacial rheology. *J. Eng. Appl. Sci.,* **2010,** *5* (6), 447-452.

138. Jeribi, M.; Almir-Assad, B.; Langevin, D.; Henaut, I.; Argillier, J., Adsorption kinetics of asphaltenes at liquid interfaces. *J. Colloid Interface Sci.,* **2002,** *256* (2), 268-272.

139. Dabros, T.; Yeung, A.; Masliyah, J.; Czarnecki, J., Emulsification through Area Contraction. *J. Colloid Interface Sci.,* **1999,** *210* (1), 222-224.

140. Singh, B. P., Performance of Demulsifiers: Prediction Based on Film Pressure-Area Isotherms and Solvent Properties. *Energy Sources,* **2007,** *16* (3), 377-385.

141. Zhang, L. Y.; Xu, Z.; Masliyah, J. H., Langmuir and Langmuir−Blodgett Films of Mixed Asphaltene and a Demulsifier. *Langmuir,* **2003,** *19* (23), 9730-9741.

142. Urdahl, O.; MØvik, A. E.; Sjöblom, J., Water-in-crude oil emulsions from the Norwegian continental shelf 8. Surfactant and macromolecular destabilization. *Colloids Surface. A.,* **1993,** *74* (2-3), 293-302.

143. Shetty, C. S.; Nikolov, A. D.; Wasan, D. T.; Bhattacharyya, B. R., Demulsification of Water in Oil Emulsions Using Water Soluble Demulsifiers. *J. Disp. Sci. Technol.,* **2007,** *13* (2), 121-133.

144. Sjoblom, J., Encyclopedic handbook of emulsion technology. CRC Press, **2001**.

145. Zaki, N.; Abdel-Raouf, M.; Abdel-Azim, A.-A., Propylene oxide-ethylene oxide block copolymers as demulsifiers for water-in-oil emulsions, I. Effect of molecular weight and hydrophilic-lipophylic balance on the demulsification efficiency. *Monatshefte für Chemie/Chemical Monthly,* **1996,** *127* (6-7), 621-629.

146. Wang, C.; Fang, S.; Duan, M.; Xiong, Y.; Ma, Y.; Chen, W., Synthesis and evaluation of demulsifiers with polyethyleneimine as accepter for treating crude oil emulsions. *Polym. Adv. Technol.,* **2015,** *26* (5), 442-448.

147. Wu, J.; Xu, Y.; Dabros, T.; Hamza, H., Effect of Demulsifier Properties on Destabilization of Water-in-Oil Emulsion. *Energ. Fuel,* **2003,** *17* (6), 1554-1559.

148. Evdokimov, I. N.; Losev, A. P., Microwave treatment of crude oil emulsions: Effects of water content. *J. Petrol. Sci. Eng.,* **2014,** *115*, 24-30.

149. Wolf, N. O., Use of microwave radiation in separating emulsions and dispersions of hydrocarbons and water. Google Patents, **1986**.

150. Fang, C. S.; Chang, B. K. L.; Lai, P. M. C.; Klaila, W. J., Microwave Demulsification. *Chem. Eng. Commun.,* **2009,** *73* (1), 227-239.

151. Chan, C.-C.; Chen, Y.-C., Demulsification of W/O Emulsions by Microwave Radiation. *Sep. Sci. Technol.* **2007,** *37* (15), 3407-3420.

152. Xia, L.-X.; Lu, S.-W.; Cao, G.-Y., Salt-Assisted Microwave Demulsification. *Chem. Eng. Commun.,* **2004,** *191* (8), 1053-1063.

153. Lemos, R. C. B.; da Silva, E. n. B.; dos Santos, A. l.; Guimarães, R. C. L.; Ferreira, B. M. S.; Guarnieri, R. A.; Dariva, C. u.; Franceschi, E.; Santos, A. F.; Fortuny, M., Demulsification of Water-in-Crude Oil Emulsions Using Ionic Liquids and Microwave Irradiation. *Energ. Fuel,* **2010,** *24* (8), 4439-4444.

154. Fortuny, M.; Oliveira, C. B. Z.; Melo, R. L. F. V.; Nele, M.; Coutinho, R. C. C.; Santos, A. F., Effect of Salinity, Temperature, Water Content, and pH on the Microwave Demulsification of Crude Oil Emulsions. *Energ. Fuel,* **2007,** *21* (3), 1358-1364.

155. Xia, L.; Lu, S.; Cao, G., Stability and demulsification of emulsions stabilized by asphaltenes or resins. *J. Colloid Interface Sci.,* **2004,** *271* (2), 504-6.

156. Mutyala, S.; Fairbridge, C.; Paré, J. R. J.; Bélanger, J. M. R.; Ng, S.; Hawkins, R., Microwave applications to oil sands and petroleum: A review. *Fuel Process. Technol.,* **2010,** *91* (2), 127-135.

157. Eow, J., Electrostatic enhancement of coalescence of water droplets in oil: a review of the technology. *Chem. Eng. J.,* **2002,** *85* (2-3), 357-368.

158. Cottrell, F. G.; Speed, J. B., Separating and collecting particles of one liquid suspended in another liquid. Google Patents: **1911**.

159. Cottrell, F. G., Process for collecting particles suspended in another liquid. Google Patents: **1912**.

160. Eow, J. S.; Ghadiri, M.; Sharif, A. O.; Williams, T. J., Electrostatic enhancement of coalescence of water droplets in oil: a review of the current understanding. *Chem. Eng. J.,* **2001,** *84* (3), 173-192.

161. Bhardwaj, A.; Hartland, S., Kinetics of Coalescence of Water Droplets in Water-in-Crude Oil Emulsions. *J. Dispers. Sci. Techno.,* **1994,** *15* (2), 133-146.

162. Isaacs, E.; Chow, R., Practical aspects of emulsion stability. *Adv. Chem. Series.,* **1992,** (231), 51-77.

163. Zhang, X.; Basaran, O. A.; Wham, R. M., Theoretical prediction of electric field-enhanced coalescence of spherical drops. *AIChE J.,* **1995,** *41* (7), 1629-1639.

164. Pohl, H. A., Some Effects of Nonuniform Fields on Dielectrics. *J. Appl. Phys.,* **1958,** *29* (8), 1182-1188.

165. Pohl, H. A., The Motion and Precipitation of Suspensoids in Divergent Electric Fields. *J.Appl. Phys.,* **1951,** *22* (7), 869-871.

166. Taylor, S. In conductivity and coalescence of water-in-crude oil emulsions under high electric-fluids, Institute of Physics Conference Series, IOP Publishing LTD, **1991**; pp 185-190.

167. Zhou, J.; Qiao, X.; Binks, B. P.; Sun, K.; Bai, M.; Li, Y.; Liu, Y., Magnetic Pickering emulsions stabilized by Fe3O4 nanoparticles. *Langmuir,* **2011,** *27* (7), 3308-16.

168. Ramsden, W., Separation of Solids in the Surface-Layers of Solutions and 'Suspensions' (Observations on Surface-Membranes, Bubbles, Emulsions, and Mechanical Coagulation). -- Preliminary Account. *Proc. R. Soc. Lond.,* **1903,** *72* (477-486), 156-164.

169. Dickinson, E., Food emulsions and foams: Stabilization by particles. *Curr. Opin. Colloid Interface Sci.,* **2010,** *15* (1-2), 40-49.

170. Chen, T.; Colver, P. J.; Bon, S. A., Organic–Inorganic Hybrid Hollow Spheres Prepared from $TiO_2$-Stabilized Pickering Emulsion Polymerization. *Adv. Mater.,* **2007,** *19* (17), 2286-2289.

171. Lecomte-Nana, G. L.; Niknam, V.; Aimable, A.; Bieniab, M.; Kpogbemabou, D.; Robert-Arnouila, J.-C.; Lajmi, A., Microcapsules from Pickering emulsions stabilized by clay particles. **2015**, 107-124.

172. Chevalier, Y.; Bolzinger, M.-A., Emulsions stabilized with solid nanoparticles: Pickering emulsions. *Colloids Surface. A.,* **2013,** *439*, 23-34.

173. Li, Q.; Huang, Y.; Xi, S.; Yang, Q.; Li, G., Double emulsions of immiscible polymer blends stabilized by interfacially active nanoparticles. *AIChE J.,* **2013,** *59* (11), 4373-4382.

174. Ondarçuhu, T.; Fabre, P.; Raphaël, E.; Veyssié, M., Specific properties of amphiphilic particles at fluid interfaces. *J. Phys.,* **1990,** *51* (14), 1527-1536.

175. Binks, B. P.; Fletcher, P. D. I., Particles adsorbed at the oil−water iInterface: a theoretical comparison between spheres of uniform wettability and "Janus" particles. *Langmuir,* **2001,** *17* (16), 4708-4710.

176. Johannes, M. D.; Mazin, I. I., Microscopic origin of magnetism and magnetic interactions in ferropnictides. *Phys. Rev. B.,* **2009,** *79* (22).

177. Xu, H.; Jia, W.; Ren, S.; Wang, J., Novel and recyclable demulsifier of expanded perlite grafted by magnetic nanoparticles for oil separation from emulsified oil wastewaters. *Chem. Eng. J.,* **2018,** *337*, 10-18.

178. Fouad, R. R.; Aljohani, H. A.; Shoueir, K. R., Biocompatible poly(vinyl alcohol) nanoparticle-based binary blends for oil spill control. *Mar. Pollut. Bull.,* **2016,** *112* (1-2), 46-52.

179. Mohamed, M.; Ouki, S., Removal mechanisms of toluene from aqueous solutions by chitin and chitosan. *Ind. Eng. Chem. Res.,* **2011,** *50* (16), 9557-9563.

180. Liang, C.; Liu, Q.; Xu, Z., Surfactant-free switchable emulsions using $CO_2$-responsive particles. *ACS Appl. Mater. Interfaces,* **2014,** *6* (9), 6898-904.

181. Ojala, J.; Sirviö, J. A.; Liimatainen, H., Nanoparticle emulsifiers based on bifunctionalized cellulose nanocrystals as marine diesel oil–water emulsion stabilizers. *Chem. Eng. J.,* **2016,** *288*, 312-320.

182. Liang, J.; Du, N.; Song, S.; Hou, W., Magnetic demulsification of diluted crude oil-in-water nanoemulsions using oleic acid-coated magnetite nanoparticles. *Colloids Surface. A.,* **2015,** *466*, 197-202.

183. Shao; Li; Lü; Qi; Zhang; Zhao, Removal of emulsified oil from aqueous environment by using polyvinylpyrrolidone-coated magnetic nanoparticles. *Water,* **2019,** *11* (10), 1993.

184. Melle, S.; Lask, M.; Fuller, G. G., Pickering emulsions with controllable stability. *Langmuir,* **2005,** *21* (6), 2158-62.

185. Walther, A.; Muller, A. H., Janus particles: synthesis, self-assembly, physical properties, and applications. *Chem. Rev.,* **2013,** *113* (7), 5194-261.

186. Hu, J.; Zhou, S.; Sun, Y.; Fang, X.; Wu, L., Fabrication, properties and applications of Janus particles. *Chem. Soc. Rev.,* **2012,** *41* (11), 4356-78.

187. Takahara, Y. K.; Ikeda, S.; Ishino, S.; Tachi, K.; Ikeue, K.; Sakata, T.; Hasegawa, T.; Mori, H.; Matsumura, M.; Ohtani, B., Asymmetrically modified silica particles: a simple particulate surfactant for stabilization of oil droplets in water. *J. Am. Chem. Soc.,* **2005,** *127* (17), 6271-5.

188. Wang, Z.; Wang, Y., Tuning amphiphilicity of particles for controllable Pickering emulsion. *Mater.,* **2016,** *9* (11).

189. Song, Y.; Zhou, J.; Fan, J.-B.; Zhai, W.; Meng, J.; Wang, S., Hydrophilic/Oleophilic magnetic Janus particles for the rapid and efficient oil-water separation. *Adv. Func. Mater.,* **2018**, 1802493.

190. Ali, N.; Zhang, B.; Zhang, H.; Li, W.; Zaman, W.; Tian, L.; Zhang, Q., Novel Janus magnetic micro particle synthesis and its applications as a demulsifier for breaking heavy crude oil and water emulsion. *Fuel,* **2015,** *141*, 258-267.

191. Ali, N.; Zhang, B.; Zhang, H.; Zaman, W.; Li, X.; Li, W.; Zhang, Q., Interfacially active and magnetically responsive composite nanoparticles with raspberry like structure; synthesis and its applications for heavy crude oil/water separation. *Colloid Surface. A.,* **2015,** *472*, 38-49.

192. Chen, T.; Colver, P. J.; Bon, S. A., Organic–Inorganic Hybrid Hollow Spheres Prepared from $TiO_2$-Stabilized Pickering Emulsion Polymerization. *Adv. Mater.,* **2007,** *19* (17), 2286-2289.

193. Zhou, Y.-B.; Tang, X.-Y.; Hu, X.-M.; Fritschi, S.; Lu, J., Emulsified oily wastewater treatment using a hybrid-modified resin and activated carbon system. *Sep. Purif. Technol.,* **2008,** *63* (2), 400-406.

194. He, X.; Liang, C.; Liu, Q.; Xu, Z., Magnetically responsive Janus nanoparticles synthesized using cellulosic materials for enhanced phase separation in oily wastewaters and water-in-crude oil emulsions. *Chem. Eng. J.,* **2019**, 122045.

195. Lin, F.; He, L.; Hou, J.; Masliyah, J.; Xu, Z. H., Role of ethyl cellulose in bitumen extraction from oil sands ores using an aqueous-nonaqueous hybrid process. *Energ. Fuel,* **2016,** *30* (1), 121-129.

196. Yan, Z.; Elliott, J. A.; Masliyah, J. H., Roles of various bitumen components in the stability of water-in-diluted bitumen emulsions. *J. Colloid Interface Sci.,* **1999,** *220* (2), 329-337.

197. Yan, L.; Hong, S.; Li, M. L.; Li, Y. S., Application of the Al2O3–PVDF nanocomposite tubular ultrafiltration (UF) membrane for oily wastewater treatment and its antifouling research. *Sep. Purif. Technol.,* **2009,** *66* (2), 347-352.

198. Jamaly, S.; Giwa, A.; Hasan, S. W., Recent improvements in oily wastewater treatment: Progress, challenges, and future opportunities. *J. Environ. Sci.,* **2015,** *37*, 15-30.

199. Ji, F.; Li, C.; Dong, X.; Li, Y.; Wang, D., Separation of oil from oily wastewater by sorption and coalescence technique using ethanol grafted polyacrylonitrile. *J. Hazard. Mater.,* **2009,** *164* (2-3), 1346-51.

200. Yue, X.; Zhang, T.; Yang, D.; Qiu, F.; Rong, J.; Xu, J.; Fang, J., The synthesis of hierarchical porous $Al_2O_3$/acrylic resin composites as durable, efficient and recyclable absorbents for oil/water separation. *Chem. Eng. J.,* **2017,** *309*, 522-531.

201. Kong, L.; Li, Y.; Qiu, F.; Zhang, T.; Guo, Q.; Zhang, X.; Yang, D.; Xu, J.; Xue, M., Fabrication of hydrophobic and oleophilic polyurethane foam sponge modified with hydrophobic $Al_2O_3$ for oil/water separation. *J. Ind. Eng. Chem.,* **2018,** *58*, 369-375.

202. Karakulski, K.; Kozlowski, A.; Morawski, A. W., Purification of oily wastewater by ultrafiltration. *Sep. Technol.,* **1995,** *5* (4), 197-205.

203. Kong, J.; Li, K., Oil removal from oil-in-water emulsions using PVDF membranes. *Sep. Purif. Technol.,* **1999,** *16* (1), 83-93.

204. Fouad, Y. O., Separation of cottonseed oil from oil–water emulsions using electrocoagulation technique. *Alex. Eng. J.,* **2014,** *53* (1), 199-204.

205. Karatum, O.; Steiner, S. A., 3rd; Griffin, J. S.; Shi, W.; Plata, D. L., Flexible, Mechanically Durable Aerogel Composites for Oil Capture and Recovery. *ACS Appl. Mater. Interfaces,* **2016,** *8* (1), 215-24.

206. Zhou, Y. B.; Chen, L.; Hu, X. M.; Lu, J., Modified resin coalescer for oil-in-water emulsion treatment: effect of operating conditions on oil removal performance. *Ind. Eng. Chem. Res.,* **2009,** *48* (3), 1660-1664.

207. Zhao, H.; Li, G., Application of fibrous coalescer in the treatment of oily wastewater. *Proc. Environ. Sci.,* **2011,** *10*, 158-162.

208. Hosny, A. Y., Separating oil from oil-water emulsions by electroflotation technique. *Sep. Technol.,* **1996,** *6* (1), 9-17.

209. Ichikawa, T., Electrical demulsification of oil-in-water emulsion. *Colloid Surface. A.,* **2007,** *302* (1-3), 581-586.

210. Nour, A. H., R. Mohd Yunus, and H. Anwaruddin, Water-in-crude oil emulsions: its stabilization and demulsification. *J. Appl. Sci.,* **2007,** *7* (22), 3512-3517.

211. Yang, F.; Tchoukov, P.; Pensini, E.; Dabros, T.; Czarnecki, J.; Masliyah, J.; Xu, Z., Asphaltene subfractions responsible for stabilizing water-in-crude oil emulsions. Part 1: interfacial behaviors. *Energ. Fuel,* **2014,** *28* (11), 6897-6904.

212. Tchoukov, P.; Yang, F.; Xu, Z.; Dabros, T.; Czarnecki, J.; Sjoblom, J., Role of asphaltenes in stabilizing thin liquid emulsion films. *Langmuir,* **2014,** *30* (11), 3024-33.

213. Zhang, Z.; Xu, G. Y.; Wang, F.; Dong, S. L.; Li, Y. M., Characterization and demulsification of poly(ethylene oxide)-block-poly(propylene oxide)-block-poly(ethylene oxide) copolymers. *J. Colloid Interface Sci.,* **2004,** *277* (2), 464-70.

214. Brugger, B.; Richtering, W., Magnetic, Thermosensitive microgels as stimuli-responsive emulsifiers allowing for remote control of separability and stability of oil-in-water emulsions. *Adv. Mater.,* **2007,** *19* (19), 2973-2978.

215. Marzougui, Z.; Damak, M.; Bitar, A.; Augsti, G.; Lelong, Q.; Elleuch, B.; Elaissari, A., Carboxylic magnetic latex particles using seeded emulsion polymerization for wastewater Treatment. **2018**, 179-182.

216. Chen, H. J.; Hang, T.; Yang, C.; Liu, G.; Lin, D. A.; Wu, J.; Pan, S.; Yang, B. R.; Tao, J.; Xie, X., Anomalous dispersion of magnetic spiky particles for enhanced oil emulsions/water separation. *Nanoscale,* **2018,** *10* (4), 1978-1986.

217. Fenoll, J.; Garrido, I.; Pastor-Belda, M.; Campillo, N.; Viñas, P.; Yañez, M. J.; Vela, N.; Navarro, S., Solar detoxification of water polluted with fungicide residues using ZnO-coated magnetic particles. *Chem. Eng. J.,* **2017,** *330*, 71-81.

218. Raza, S.; Yong, X.; Raza, M.; Deng, J., Synthesis of biomass trans-anethole based magnetic hollow polymer particles and their applications as renewable adsorbent. *Chem. Eng. J.,* **2018,** *352*, 20-28.

219. Lin, Y.; Xu, S.; Li, J., Fast and highly efficient tetracyclines removal from environmental waters by graphene oxide functionalized magnetic particles. *Chem. Eng. J.,* **2013,** *225*, 679-685.

220. Peng, J. X.; Liu, Q. X.; Xu, Z. H.; Masliyah, J., Synthesis of interfacially active and magnetically responsive nanoparticles for multiphase separation applications. *Adv. Func. Mater.,* **2012,** *22* (8), 1732-1740.

221. Pensini, E.; Yip, C. M.; O'Carroll, D.; Sleep, B. E., Carboxymethyl cellulose binding to mineral substrates: characterization by atomic force microscopy-based force spectroscopy and quartz-crystal microbalance with dissipation monitoring. *J. Colloid Interface Sci.,* **2013,** *402*, 58-67.

222. Ghosh, S.; Tran, T.; Rousseau, D., Comparison of Pickering and network stabilization in water-in-oil emulsions. *Langmuir,* **2011,** *27* (11), 6589-6597.

223. Destribats, M.; Lapeyre, V.; Wolfs, M.; Sellier, E.; Leal-Calderon, F.; Ravaine, V.; Schmitt, V., Soft microgels as Pickering emulsion stabilisers: role of particle deformability. *Soft Matter.,* **2011,** *7* (17), 7689-7698.

224. Kumar, A.; Park, B. J.; Tu, F. Q.; Lee, D., Amphiphilic Janus particles at fluid interfaces. *Soft Matter.,* **2013,** *9* (29), 6604-6617.

225. Fujimoto, K.; Nakahama, K.; Shidara, M.; Kawaguchi, H., Preparation of unsymmetrical microspheres at the interfaces. *Langmuir,* **1999,** *15* (13), 4630-4635.

226. Ali, N.; Zhang, B. L.; Zhang, H. P.; Li, W.; Zaman, W.; Tian, L.; Zhang, Q. Y., Novel Janus magnetic micro particle synthesis and its applications as a demulsifier for breaking heavy crude oil and water emulsion. *Fuel,* **2015,** *141*, 258-267.

227. Wang, S.; Segin, N.; Wang, K.; Masliyah, J. H.; Xu, Z., Wettability control mechanism of highly contaminated hydrophilic silica/alumina surfaces by ethyl cellulose. *J. Phys. Chem. C.,* **2011,** *115* (21), 10576-10587.

228. Rodahl, M.; Hook, F.; Fredriksson, C.; Keller, C. A.; Krozer, A.; Brzezinski, P.; Voinova, M.; Kasemo, B., Simultaneous frequency and dissipation factor QCM measurements of biomolecular adsorption and cell adhesion. *Faraday Discuss.,* **1997,** (107), 229-46.

229. Voinova, M. V.; Rodahl, M.; Jonson, M.; Kasemo, B., Viscoelastic acoustic response of layered polymer films at fluid-solid interfaces: continuum mechanics approach. *Phys. Scripta.,* **1999,** *59* (5), 391-396.

230. Liu, S. X.; Kim, J.-T., Application of Kevin–Voigt model in quantifying whey protein adsorption on polyethersulfone using QCM-D. *J. Lab. Autom.,* **2009,** *14* (4), 213-220.

231. Schwegmann, H.; Feitz, A. J.; Frimmel, F. H., Influence of the zeta potential on the sorption and toxicity of iron oxide nanoparticles on S. cerevisiae and E. coli. *J. Colloid Interface Sci.,* **2010,** *347* (1), 43-8.

232. Jin, H.; Zhou, W.; Cao, J.; Stoyanov, S. D.; Blijdenstein, T. B. J.; de Groot, P. W. N.; Arnaudov, L. N.; Pelan, E. G., Super stable foams stabilized by colloidal ethyl cellulose particles. *Soft Matter,* **2012,** *8* (7), 2194-2205.

233. Marinova, K. G.; Alargova, R. G.; Denkov, N. D.; Velev, O. D.; Petsev, D. N.; Ivanov, I. B.; Borwankar, R. P., Charging of oil−water interfaces due to spontaneous adsorption of hydroxyl ions. *Langmuir,* **1996,** *12* (8), 2045-2051.

234. Zhou, Y.; Wang, S.; Ding, B.; Yang, Z., Modification of magnetite nanoparticles via surface-initiated atom transfer radical polymerization (ATRP). *Chem. Eng. J.,* **2008,** *138* (1-3), 578-585.

235. Aulin, C.; Ahola, S.; Josefsson, P.; Nishino, T.; Hirose, Y.; Osterberg, M.; Wagberg, L., Nanoscale cellulose films with different crystallinities and mesostructures--their surface properties and interaction with water. *Langmuir,* **2009,** *25* (13), 7675-85.

236. Tammelin, T.; Abburi, R.; Gestranius, M.; Laine, C.; Setala, H.; Osterberg, M., Correlation between cellulose thin film supramolecular structures and interactions with water. *Soft Matter,* **2015,** *11* (21), 4273-82.

237. Gao, S.; Moran, K.; Xu, Z.; Masliyah, J., Role of bitumen components in stabilizing water-in-diluted oil emulsions. *Energ. Fuel,* **2009,** *23* (5), 2606-2612.

238. Asekomhe, S. O.; Chiang, R.; Masliyah, J. H.; Elliott, J. A. W., Some observations on the contraction behavior of a water-in-oil drop with attached solids. *Ind. Eng. Chem. Res.,* **2005,** *44* (5), 1241-1249.

239. Chen, Z.; Peng, J.; Ge, L.; Xu, Z., Demulsifying water-in-oil emulsions by ethyl cellulose demulsifiers studied using focused beam reflectance measurement. *Chem. Eng. Sci.,* **2015,** *130*, 254-263.

240. Zhang, S.; Wang, P.; Fu, X.; Chung, T. S., Sustainable water recovery from oily wastewater via forward osmosis-membrane distillation (FO-MD). *Water Res.,* **2014,** *52*, 112-21.

241. Kulkarni, M. G.; Dalai, A. K., Waste cooking oil as an economical source for biodiesel: a review. *Ind. Eng. Chem. Res.,* **2006,** *45* (9), 2901-2913.

242. Yu, K.; Wang, Z.; Jin, Y.; Sun, Z.; Liu, Y.; Yang, J.; Cai, Y., Single- and multi-stage counter-current solvent extractions of bitumen from Xinjiang oil Sands. *Energ. Fuel,* **2013,** *27* (11), 6491-6500.

243. Li, F.; Bhushan, B.; Pan, Y.; Zhao, X., Bioinspired superoleophobic/superhydrophilic functionalized cotton for efficient separation of immiscible oil-water mixtures and oil-water emulsions. *J. Colloid Interface Sci.,* **2019,** *548*, 123-130.

244. Teas, C.; Kalligeros, S.; Zanikos, F.; Stournas, S.; Lois, E.; Anastopoulos, G., Investigation of the effectiveness of absorbent materials in oil spills clean up. *Desalination,* **2001,** *140* (3), 259-264.

245. Beshkar, F.; Khojasteh, H.; Salavati-Niasari, M., Recyclable magnetic superhydrophobic straw soot sponge for highly efficient oil/water separation. *J. Colloid Interface Sci.,* **2017,** *497*, 57-65.

246. Pendergast, M. M.; Hoek, E. M. V., A review of water treatment membrane nanotechnologies. *Energ. Environ. Sci.,* **2011,** *4* (6), 1946.

247. Hoek, E. M. V.; Pendergast, M. T. M.; Ghosh, A. K., Nanotechnology-based membranes for water purification. **2014**, 133-154.

248. Zhang, M.; Ma, W.; Wu, S.; Tang, G.; Cui, J.; Zhang, Q.; Chen, F.; Xiong, R.; Huang, C., Electrospun frogspawn structured membrane for gravity-driven oil-water separation. *J. Colloid Interface Sci.,* **2019,** *547*, 136-144.

249. Yuan, R.; Liu, J.; Li, Z.; Chen, Y.; Wang, Z.; Liu, Z.; Jing, G.; Zhu, Y.; Wang, H., Ultrahigh-flux (>190,000L.m$^{-2}$h$^{-1}$) separation of oil and water by a robust and durable $Cu(OH)_2$ nanoneedles mesh with inverse wettability. *J. Colloid Interface Sci.,* **2019,** *555*, 569-582.

250. Zhang, H.; Wang, Z.; Shen, Y.; Mu, P.; Wang, Q.; Li, J., Ultrathin 2D $Ti_3C_2Tx$ MXene membrane for effective separation of oil-in-water emulsions in acidic, alkaline, and salty environment. *J. Colloid Interf Sci.,* **2019**.

251. Liu, W.; Cui, M.; Shen, Y.; Zhu, G.; Luo, L.; Li, M.; Li, J., Waste cigarette filter as nanofibrous membranes for on-demand immiscible oil/water mixtures and emulsions separation. *J. Colloid Interface Sci.,* **2019,** *549*, 114-122.

252. Beltran, F. J.; Alvarez, P. M.; Rodriguez, E. M.; Garcia-Araya, J. F.; Rivas, J., Treatment of high strength distillery wastewater (cherry stillage) by integrated aerobic biological oxidation and ozonation. *Biotechnol. Prog.,* **2001,** *17* (3), 462-7.

253. Cheng, H.; Li, Z.; Li, Y.; Shi, Z.; Bao, M.; Han, C.; Wang, Z., Multi-functional magnetic bacteria as efficient and economical Pickering emulsifiers for encapsulation and removal of oil from water. *J. Colloid Interface Sci.,* **2019**.

254. Ngai, T.; Bon, S. A., Particle-stabilized emulsions and colloids: formation and applications. Royal Society of Chemistry, **2014**.

255. Li, Z.; Ming, T.; Wang, J.; Ngai, T., High internal phase emulsions stabilized solely by microgel particles. *Angew. Chem.,* **2009,** *121* (45), 8642-8645.

256. Farooq, U.; Simon, S.; Tweheyo, M. T.; Øye, G.; Sjöblom, J., Interfacial Tension Measurements Between Oil Fractions of a Crude Oil and Aqueous Solutions with Different Ionic Composition and pH. *J. Disper. Sci. Technol.,* **2013,** *34* (5), 701-708.

257. Wu, Z.; Zhang, J.; Li, Z.; Xie, J.; Mujumdar, A. S., Production of a solid fuel using sewage sludge and spent cooking oil by immersion frying. *J. Hazard. Mater.,* **2012,** *243*, 357-63.

258. Lam, M. K.; Lee, K. T.; Mohamed, A. R., Homogeneous, heterogeneous and enzymatic catalysis for transesterification of high free fatty acid oil (waste cooking oil) to biodiesel: a review. *Biotechnol. Adv.,* **2010,** *28* (4), 500-18.

259. Hou, Y.; Li, Y.; Wang, L.; Chen, D.; Bao, M.; Wang, Z., Amphiphilic Janus particles for efficient dispersion of oil contaminants in seawater. *J. Colloid Interface Sci.,* **2019,** *556*, 54-64.

260. Razavi, S.; Hernandez, L. M.; Read, A.; Vargas, W. L.; Kretzschmar, I., Surface tension anomaly observed for chemically-modified Janus particles at the air/water interface. *J. Colloid Interface Sci.,* **2020,** *558*, 95-99.

261. Pan, D.; Mou, F.; Li, X.; Deng, Z.; Sun, J.; Xu, L.; Guan, J., Multifunctional magnetic oleic acid-coated MnFe2O4/polystyrene Janus particles for water treatment. *J. Mater. Chem. A.,* **2016,** *4* (30), 11768-11774.

262. Anton Walker, T. D., Jianmin Kan, Yicheng Long. Process for treating heavy oil emulsions using a light aliphatic solvent–naphtha mixture. 2005.

263. He, L.; Lin, F.; Li, X.; Sui, H.; Xu, Z., Interfacial sciences in unconventional petroleum production: from fundamentals to applications. *Chem. Soc. Rev.,* **2015,** *44* (15), 5446-94.

264. Wu, X., Investigating the stability mechanism of water-in-diluted bitumen emulsions through isolation and characterization of the stabilizing materials at the interface. *Energ. Fuel,* **2003,** *17* (1), 179-190.

265. Sztukowski, D. M.; Yarranton, H. W., Characterization and interfacial behavior of oil sands solids implicated in emulsion stability. *J. Disper. Sci. Technol.,* **2004,** *25* (3), 299-310.

266. Yan, Z. L.; Elliott, J. A. W.; Masliyah, J. H., Roles of various bitumen components in the stability of water-in-diluted-bitumen emulsions. *J. Colloid Interface Sci.,* **1999,** *220* (2), 329-337.

267. Stark, J. L.; Asomaning, S., Synergies between asphaltene stabilizers and demulsifying agents giving improved demulsification of asphaltene-stabilized emulsions. *Energ. Fuel,* **2005,** *19* (4), 1342-1345.

268. Poindexter, M. K.; Marsh, S. C., Inorganic solid content governs water-in-crude oil emulsion stability predictions. *Energ. Fuel,* **2009,** *23* (3), 1258-1268.

269. Ohsol, E. O.; Pinkerton, J. W.; Gillespie, T. E.; Laity, T. H., Process for upgrading heavy crude oil production. Google Patents, **1999**.

270. Zaki, N. N.; Abdel-Raouf, M. E.; Abdel-Azim, A. A. A., Polyoxyethylenated bisphenol-A for breaking water-in-oil emulsions. *Polym. Adv. Technol.,* **1996,** *7* (10), 805-808.

271. Zhang, Z.; Xu, G.; Wang, F.; Dong, S.; Chen, Y., Demulsification by amphiphilic dendrimer copolymers. *J. Colloid Interface Sci.,* **2005,** *282* (1), 1-4.

272. Zaki, N. N.; Carbonell, R. G.; Kilpatrick, P. K., A novel process for demulsification of water-in-crude oil emulsions by dense carbon dioxide. *Ind. Eng. Chem. Res.,* **2003,** *42* (25), 6661-6672.

273. Nour, A. H.; Yunus, R. M.; Anwaruddin, H., Water-in-crude oil emulsions: its stabilization and demulsification. *J. Appl. Sci.,* **2007,** *7* (22), 3512-3517.

274. Guzmán-Lucero, D.; Flores, P.; Rojo, T.; Martínez-Palou, R., Ionic liquids as demulsifiers of water-in-crude oil emulsions: study of the microwave effect. *Energ. Fuel,* **2010,** *24* (6), 3610-3615.

275. Laurent, S.; Forge, D.; Port, M.; Roch, A.; Robic, C.; Vander Elst, L.; Muller, R. N., Magnetic iron oxide nanoparticles: synthesis, stabilization, vectorization, physicochemical characterizations, and biological applications. *Chem. Rev.,* **2008,** *108* (6), 2064-110.

276. Maity, D.; Agrawal, D. C., Synthesis of iron oxide nanoparticles under oxidizing environment and their stabilization in aqueous and non-aqueous media. *J. Magn. Magn. Mater.,* **2007,** *308* (1), 46-55.

277. Tang, J.; Quinlan, P. J.; Tam, K. C., Stimuli-responsive Pickering emulsions: recent advances and potential applications. *Soft Matter,* **2015,** *11* (18), 3512-29.

278. Yang Z, M. A., Xu C, Jiang S, Granick S, Schneider H, et al, Janus particle synthesis, self-assembly, and applications. 1st ed.; **2012**.

279. Wang, Y.; Zhang, C.; Tang, C.; Li, J.; Shen, K.; Liu, J.; Qu, X.; Li, J.; Wang, Q.; Yang, Z., Emulsion interfacial synthesis of asymmetric Janus particles. *Macromolecules.,* **2011,** *44* (10), 3787-3794.